NTNU

Norwegian University of
Science and Technology

Energy Efficient and Environmental Friendly Snow Production by Refrigeration systems

Kaja Wright Bergwitz-
Larsen

Master of Energy and Environmental Engineering
Submission date: June 2017
Supervisor: Trygve Magne Eikevik, EPT

Norwegian University of Science and Technology
Department of Energy and Process Engineering

NTNU

Norwegian University
of Science and Technology

Department of Energy
and Process Engineering

EPT-M-2017-11

MASTER THESIS

for

Student Kaja Bergwitz-Larsen

Spring 2017

Energy Efficient and Environmental Friendly Snow Production by Refrigeration systems

Energieffektiv og miljøvennlig snøproduksjon ved hjelp av kuldetekniske systemer

Background and objective

In the perspective of increasing global temperatures, there is a challenge having available snow close to the cities and villages in the mountain for a reasonable winter season. The periods of natural snow is shorter and in some areas, the snow in the winter is disappearing. In Europe the facilities is moving to higher locations to be able to arrange winter games.

In the Nordic countries, it is also a tradition for doing winter activities in snow like kinder gardens, schools and for the families to go skiing in weekends and holidays. If the trend with milder winters is going on, the distance the individual have to go from the homes to areas with snow will grow. To be able to maintain the snow activity close to the cities it will be of importance to produce snow at temperatures above 0°C. Since this is an energy consuming process, the energy efficiency of the equipment is of importance and the possibility to utilize the heat for space heating or hot tap water, with emphasize on reducing the operational costs. There is an antagonism between the need of heat and the need of snow. This will imply the need of storing the snow in periods.

The project work and master thesis will be in close cooperation with Trondheim Kommune and the Norwegian Ski Association within the scope of "Snow for the future". Trondheim Kommune will in the near future build a center in Granåsen that will give possibilities for future winter games and give the people possibility to enjoy the winter activity in the period from November to March.

The following tasks are to be considered:

1. Literature review of indoor and outdoor snow making systems
2. Investigate the air cycle refrigeration system (Reversed Brayton cycle) for indoor snow production, and compare with traditional refrigeration system
3. Further development of the EES model for the CO2 refrigeration system for 100 ton snow production per day.
4. Describe different strategies for energy efficient snow production to utilize the heat from the system, combined with models for snow melting analysis, climatic impact on production rates.
5. Make a draft scientific paper with the main results for the thesis
6. Make proposal for further work

-- " --

Within 14 days of receiving the written text on the master thesis, the candidate shall submit a research plan for his project to the department.

When the thesis is evaluated, emphasis is put on processing of the results, and that they are presented in tabular and/or graphic form in a clear manner, and that they are analyzed carefully.

The thesis should be formulated as a research report with summary both in English and Norwegian, conclusion, literature references, table of contents etc. During the preparation of the text, the candidate should make an effort to produce a well-structured and easily readable report. In order to ease the evaluation of the thesis, it is important that the cross-references are correct. In the making of the report, strong emphasis should be placed on both a thorough discussion of the results and an orderly presentation.

The candidate is requested to initiate and keep close contact with his/her academic supervisor(s) throughout the working period. The candidate must follow the rules and regulations of NTNU as well as passive directions given by the Department of Energy and Process Engineering.

Risk assessment of the candidate's work shall be carried out according to the department's procedures. The risk assessment must be documented and included as part of the final report. Events related to the candidate's work adversely affecting the health, safety or security, must be documented and included as part of the final report. If the documentation on risk assessment represents a large number of pages, the full version is to be submitted electronically to the supervisor and an excerpt is included in the report.

Pursuant to "Regulations concerning the supplementary provisions to the technology study program/Master of Science" at NTNU §20, the Department reserves the permission to utilize all the results and data for teaching and research purposes as well as in future publications.

The final report is to be submitted digitally in DAIM. An executive summary of the thesis including title, student's name, supervisor's name, year, department name, and NTNU's logo and name, shall be submitted to the department as a separate pdf file. The final report in Word and PDF format, scientific paper and all other material and documents should be given to the academic supervisor in digital format on a DVD/CD-rom or a memory stick at the time of delivery of the Master Thesis.

☐ Work to be done in lab (Water power lab, Fluids engineering lab, Thermal engineering lab)
☐ Field work

Department of Energy and Process Engineering, 15. January 2017

Prof. Trygve M. Eikevik
Academic Supervisor
e–mail: trygve.m.eikevik@ntnu.no

Research Advisor:
Dr. Ignat Tolstorebrov, NTNU, e-mail: ignat.tolstorebrov@ntnu.no

In agreement with supervisor, Trygve M. Eikevik, the description of tasks has been adapted. Instead of developing models for snow melting and climatic impact on production rates, trends are only discussed briefly. As an additional point, the flake ice machine is studied more in depth; by improving the COMSOL model of the snow making system to operate with a production of 100 tons snow per day and two-phase refrigerant flow.

1/6 - 2017 —

Preface

This master thesis was performed at NTNU during the spring 2017. The thesis is within the scope of the project "Snow for the future", and is written in coordination with Trondheim Kommune, the Norwegian Ski Association, SINTEF and NTNU. This thesis investigates snow production equipment by refrigeration systems operating at ambient temperatures above 0 °C, in combination with corresponding coupled heat recovery strategies. It is an extension of the topic from two previous master theses written within the same project.

It should be mentioned that this thesis uses results from (Bergwitz-Larsen, 2016), which was a pre-study for the master thesis, available at the Department of Energy and Process Engineering at NTNU. The thesis uses a flake ice model developed in that work, and parts of the literature, definitions and results are taken directly from it. Because this pre-work and its resulting simulation model was based on flake ice technology for snow production, the system has somewhat more focus than the indoor snow production models evaluated in this thesis.

I would like to thank my academic supervisor Professor Trygve M. Eikevik for great guidance and dedication to the project during the work. Special thanks also to Professor Armin Hafner and Professor Erling Næss for helpful discussion and advice on the way. Thanks to my co-supervisor Dr. Ignat Tolestorebrov, Application Engineer and Dr. Bertil Nistad for great advice with COMSOL, and Senior Engineer Eugen Uthaug for help with software and programming. Senior Engineer Kazuhiro at Mayekawa and CEO Hannu Pesonen at SnowTek shall have great thanks for supplied information and data.

Trondheim, June 11, 2017

Kaja Bergwitz-Larsen

Abstract

In the light of increasing global temperatures, the winters tend to be shorter and milder, with the periods of natural snow being drastically reduced. In order to counter the challenges of climate changes and maintaining good skiing conditions in the winters to come, snow production equipment that can operate in ambient temperatures above 0 °C will be important for future applications. Such technology exists today, but it is expensive and highly energy-intensive; with an excessive amount of surplus heat that is released to the surroundings and thus wasted. In this thesis, methods to increase the energy efficiency of the snow producing equipment is explored; by integrating different snowmaking technologies with combined refrigeration and heat recovery systems. Use of environmental friendly refrigerants is highlighted.

An outdoor flake ice system with a production of 100 tons/day is modelled in EES and implemented with a transcritical CO_2 process for heat recovery. By optimizing the gas cooler pressure, the heat recovery potential is increased compared to the pre-study. Integration of a coaxial heat exchanger yields the best thermodynamic performance; with maximized COP and close temperature approach. This approach offers the possibility of reduced demand of the intercooler and suction gas heat exchanger. The calculations in COMSOL validates the assumptions in EES. It emphasizes the importance of correct design of the flake ice drum and points to the need of an optimization process; in order to ensure efficient heat transfer characteristics.

Analysis shows that an air refrigeration cycle is unsuitable for indoor snow production. Simultaneous design for a large refrigeration load, high temperature and high relative humidity, yields an extensive mass flow and saturation below the freezing point, and icing in the expander cannot be avoided. An indoor transcritical CO_2 cycle is seen to have superior thermodynamic performance at the dimensioning conditions. The system is easily adaptable, and provides highly energy efficient refrigeration and heating, without a simultaneous drop in the efficiency of the snowmaking process. While two-stage compression is required for the flake ice system due to the low evaporation temperature, one-stage compression can be applied to obtain the same heat duty in an indoor system. The flake ice drum suffers from the influence of melting of the snow in the pile during production, while this feature is negligible when production occurs in an indoor controlled environment. Indoor snowmaking is considered more space demanding and expensive, but with a better thermodynamic performance of the combined heating and refrigeration system.

The thermodynamic analysis points to indoor snow production combined with the transcritical CO_2 refrigeration cycle and heat recovery by DHW heating as the best solution for the site. I have reviewed previous relevant studies and models developed at NTNU. The theories, conclusions and models developed through my work make it possible to approach a practical application for “energy efficient and environmental friendly snow production” – and thereby fulfill the ambitions within the scope of “Snow for the future”. Some further analysis is however required before drawing a final conclusion, and the results should be seen in combination with total costs and models for snow melting and climatic impact on production rates.

Sammendrag

I lys av økende globale temperaturer, blir vintrene stadig mildere, samtidig som perioden med naturlig snø blir betydelig kortere. For å møte denne utviklingen og skaffe gode snøforhold i vintrene fremover, er det viktig å kunne produsere snø ved temperaturer over 0 °C. Slik teknologi finnes i dag, men produksjonsprosessen er svært dyrt og energikrevende, med en betydelig mengde uutnyttet overskuddsvarme. I denne oppgaven studeres metoder for å øke energieffektiviteten til utstyret; ved å evaluere ulike snøproduksjonsteknologier med kombinerte kjøle- og varmegjenvinningssystemer. Bruk av miljøvennlige kjølemidler står sentralt.

En utendørs flakismaskin med en produksjonskapasitet på 100 tonn/dag er modellert i EES og implementert med en transkritisk CO_2-prosess for varmegjenvinning. Ved å optimalisere gasskjølertrykket øker varmegjenvinningspotensialet sammenlignet med modellen i forarbeidet. Integrasjon av en koaksialvarmeveksler gir den beste termodynamiske ytelsen; med maksimal COP og god temperaturtilpasning. Dette gir mulighet for å redusere ytelsen til mellomkjøleren og sugegassvarmeveksleren. Beregningene i COMSOL validerer antagelsene i EES, og de understreker viktigheten av tilpasset design og optimalisering av flakistrommelen for å sikre god varmeovergang.

Analysene viser at et luftbasert kjølesystem er uegnet for innendørs snøproduksjon. Samtidig dimensjonering for høy kjøleeffekt, temperatur og luftfuktighet gir påfølgende stor massestrøm og metning under frysepunktet; med utfelling av is i turbinen. Et innendørs transkritisk CO_2-system vil derimot unngå driftsproblemer, og gi overlegen COP ved det gitte dimensjoneringspunktet. Systemet er lett å tilpasse, og det er fleksibelt og pålitelig. Dette gir effektive kjøle- og varmegjenvinningsegenskaper, samtidig som det ikke går på bekostning av virkningsgraden til snøproduksjonsutstyret. Mens totrinnskompresjon er nødvendig for flakissystemet på grunn av den lave fordampningstemperaturen, er kompresjon i ett steg tilstrekkelig for å oppnå samme varmeeffekt for et innendørs system. En ulempe med flakistrommelen er at produksjonen foregår utendørs hvor smeltingsraten ikke kan kontrolleres, hvilket øker produksjonstiden sammenlignet med innendørs produksjonsmetoder. Innendørs snøanlegg er dyrere og tar mer plass, men gir bedre termodynamisk ytelse for det kombinerte varme- og kjølesystemet.

Analysene viser at innendørs snøproduksjon basert på lanser; kombinert med en transkritisk CO_2-prosess for kjøling og varmegjenvinning i form av varmtvannsoppvarming, gir den best egnete løsningen for skianlegget i Granåsen. Jeg har gått gjennom tidligere relevante studier og modeller utarbeidet ved NTNU. Teoriene, konklusjonene og modellene utviklet gjennom mitt arbeid gjør det mulig å komme nærmere en praktisk anvendelse for «energieffektiv og miljøvennlig snøproduksjon» - og sånn sett oppfylle ambisjonene innenfor «Snow for the future» programmet. Videre og mer omfattende analyse er likevel nødvendig før en endelig konklusjon kan bli gitt, og resultatene bør sees i sammenheng med optimalisering av samlede kostnader, og klimaanalyser for snøsmelting på produksjonsraten.

Contents

List of Figures

List of Tables

Nomenclature

Latin letters

A	Area	[m^2]
B	Constant, water heat transfer	[-]
c_p	Specific heat capacity	[kJ/kgK]
C	Chisholm parameter	[-]
d	Diameter	[m]
E	Energy	[kW]
f	Friction factor	[-]
F	Correction factor for evaporation of CO_2	[-]
g	Gravitational constant	[m/s^2]
G	Mass flux	[kg/m^2s]
h	Enthalpy	[kJ/kg]
H	Height	[m]
H_i	Inter-plate channel height	[m]
k	Thermal conductivity	[W/mK]
L	Length	[m]
m	Mass	[kg]
$\dot{m}$	Mass flow rate	[kg/s]
M	Molecular weight	[kg/kmol]
n	Counting number	[-]
N_{ch}	Number of plate pairs	[-]
p	Wetted perimeter	[m]
P	Pressure	[Pa]
q	Heat flux	[kW/m^2]
Q	Heat transfer	[kW]
R	Thermal resistance	[m^2K/W]
$\overline{R}$	Universal gas constant	[kJ/kmolK]
S	Nucleate boiling suppression factor	[-]
T	Temperature	[K]
u	Velocity	[m/s]
U	U-value, overall heat transfer coefficient	[W/m^2K]
V	Volume	[m^3]
$\dot{V}$	Volumetric flow rate	[m^3/s]
w	Width	[m]
W	Work	[kW]
x	Distance	[m]
X_{tt}	Lockhart Martinelli parameter	[-]
y	Mole fraction	[-]
z	Gas quality	[-]

Abbreviations

Bo	Boiling number	[-]
CFC	Chlorofluorocarbon	[-]
CFD	Computational fluid dynamics	[-]

COP	Coefficient of performance	[-]
De	Dean number	[-]
DHW	Domestic hot water	[-]
EES	Engineering equation solver	[-]
EVR	Energy-volume ratio	[kWh/m^3]
F-gases	Fluorinated greenhouse gases	[-]
FID	Flake ice drum	[-]
GWP	Global warming potential	[-]
HCFC	Hydrochlorofluorocarbon	[-]
HFC	Halofluorocarbon	[-]
HVAC	Heating, ventilation and air conditioning	[-]
ICS	Infinite crystals snowmaking	[-]
LED	Light-emitting diode	[-]
ln	Natural logarithm	[-]
log	Logarithmic	[-]
MAWP	Maximum allowable working pressure	[-]
NDA	Non-disclosure agreement	[-]
NOK	Norwegian krone	[-]
Nu	Nusselt number	[-]
ODP	Ozone depletion potential	[-]
OEEP	Overall energy efficiency of plant	[-]
P-h	Pressure-enthalpy	[-]
PHE	Plate heat exchanger	[-]
Pr	Prandtl number	[-]
PR	Pressure ratio	[-]
RANS	Reynolds-averaged Navier Stokes	[-]
Re	Reynolds number	[-]
RH	Relative humidity	[-]
SGHX	Suction gas heat exchanger	[-]
SPF	Seasonal performance factor	[-]
SUS	Steel use stainless	[-]
TDS	Temperature dependent snowmaking	[-]
T-h	Temperature-enthalpy	[-]
TIS	Temperature independent snowmaking	[-]
T-s	Temperature-entropy	[-]
T-v	Temperature-volume	[-]
UTS	Ultimate tensile strength	[-]
VIM	Vacuum ice maker	[-]

Greek letters

α	Heat transfer coefficient	[W/m^{2}K]
β	Chevron angle	[°]
γ	Circulation rate	[-]
δ	Thickness of wall/plate section	[m]
ε	Surface roughness	[-]
η	Efficiency	[-]
θ	Smoothed function	[-]
λ	Volumetric efficiency	[-]

μ	Dynamic viscosity	[kg/ms]
ν	Kinematic viscosity	[m^2/s]
ξ	Empirical parameter	[-]
ρ	Density	[kg/m^3]
σ	Surface tension	[N/m]
φ	Surface enhancement factor	[-]
φ^2	Two-phase frictional multiplier	[-]
ω	Absolute humidity	[kg vapour/kg dry air]

Subscripts

a	Dry air	[-]
A	Approach	[-]
acc	Acceleration	[-]
amb	Ambient	[-]
b	Boundary	[-]
c	Cross-sectional	[-]
ch	Channel	[-]
C	Cold	[-]
comp	Compressor	[-]
cond	Condensation	[-]
crit	Critical	[-]
diff	Difference	[-]
e	Equivalent	[-]
evap	Evaporation	[-]
f	Fluid	[-]
fg	Liquid-gas phase transition	[-]
fric	Friction	[-]
g	Saturated gas	[-]
gc	Gas cooler	[-]
gr	Gravity	[-]
h	Hydraulic	[-]
H	Hot	[-]
is	Isentropic	[-]
l	Saturated liquid	[-]
L	Low	[-]
LM	Logarithmic mean	[-]
m	Mean	[-]
man	Manifold	[-]
max	Maximum	[-]
nb	Nucleate boiling	[-]
opt	Optimal	[-]
p	Port	[-]
prod	Product	[-]
r	Reduced	[-]
ref	Refrigeration	[-]
R	Refrigerant	[-]
s	Isentropic state point	[-]

sat	Saturation	[-]
sc	Subcooling	[-]
SGHX	Suction gas heat exchanger	[-]
sh	Superheat	[-]
tot	Total	[-]
trans	Transmission	[-]
v	Water vapour	[-]
w	Water	[-]
W	Wall	[-]

1 Introduction

1.1 Background

In the light of increasing global temperatures, there is a challenge having available snow close to the cities and villages in the mountain for a reasonable winter season. The trend is shorter and milder winters; with the periods of natural snow being drastically reduced. In some areas, the snow in the winter is disappearing, and in Europe the facilities are moving to higher locations to be able to arrange winter games.

In Norway, the winter traditionally has been associated with good snow conditions, and skiing is by many considered the national sport. It is a tradition for doing winter activities both in kinder gardens, schools and for the families to go skiing in weekends and holidays; even in the densely-populated areas. If the trend with milder winters continues, the distance the individuals have to go from the home to areas with acceptable snow conditions will increase. In order to counter the challenges of climate changes and maintain snow activity close to the cities, it is important to develop technology that can provide snow at temperatures above 0 °C. This requires increased competence, and technology that is applicable under marginal conditions (Gjerland and Olsen, 2014). Such technology exists today, but as it is an energy consuming process, it is not widely utilized. The focus of this thesis will be on implementing such equipment at a ski arena located in Trondheim. Trondheim Kommune will in the near future build a centre in Granåsen that will give possibilities for future winter games, and for people to enjoy winter activity in the period from November to March.

Since snowmaking is an energy consuming process, methods to increase the efficiency of the equipment are important. In this thesis, combined heating and refrigeration systems for different snowmaking technologies will be evaluated. If the surplus heat from the snow production can be utilized, the overall energy efficiency of the system will increase; which might justify the extensive investment and operating costs of such technology.

1.2 Objective

The objective of this thesis is to get an overview of available snow and ice producing equipment. Based on this, refrigeration systems and heat recovery strategies for different production methods will be evaluated; in order to find the best suitable solution for the site, given the geographic and climatic conditions. The EES model of the outdoor flake ice system from the pre-study will be further developed, and it is compared with simulation models of air cycle and CO_2 refrigeration systems for indoor snow production. The performances of these systems are compared with the results from the previous master assignments of Dieseth (2016) and Vagle (2016). A final recommendation for the direction and focus of further work will be proposed. The main results from the flake ice model will be highlighted in a scientific paper.

1.3 Limitation of scope

The snow from the production equipment is intended to be used outdoors. Indoor skiing halls will consequently not be considered in this thesis, although production may occur indoors. The results obtained from the analyses are not fixed. They are supposed to serve as a reasonable first estimate; appropriate for an even-handed decision basis. Any assumption made to simplify the analysis will be stated. The aim of this thesis is not to come up with a definite conclusion, but rather to draw a picture of the feasibility of combining different production technologies, refrigeration systems and heat recovery strategies. The main focus is on the thermodynamic performance. Costs and models for snow melting and climatic impact on production rates are excluded. The analyses have limited focus on snow quality, ice crushing devices, water spray arrangements and distribution.

1.4 Outline of thesis

Chapter 2 gives a presentation of temperature dependent snowmaking. Current available and conventional snow production technologies at ambient temperatures below 0 °C are described.

Chapter 3 presents temperature independent snowmaking and describes different methods for producing ice at temperatures above 0 °C. The main focus is on flake ice production.

Chapter 4 presents the main principles of indoor snowmaking. Both conventional refrigeration and air cycle refrigeration systems are outlined.

Chapter 5 describes different system configurations and product data for the technologies described in Chapter 2 - 4. It gives an overview of different manufacturers of temperature independent snowmaking equipment, and machines with equal production capacity of 100 tons/day are compared. A presentation of the capacity and dimensions for two indoor skiing halls are given. Product data for a commercial air refrigeration system is provided.

Chapter 6 gives a brief discussion on the snow quality aspect; with respect to the different production technologies.

Chapter 7 presents theory relevant for the simulations models.

Chapter 8 presents the adapted EES model and the flake ice system. Correlations and procedure are described, and relevant assumptions are stated. The results from the simulation are evaluated and discussed, and they are compared with results from the original model.

Chapter 9 describes the simulation of the flake ice system in COMSOL. Design of the flake ice drum and assumptions from the EES model are evaluated, and the results are discussed.

Chapter 10 presents the simulation models for indoor production, with basis in temperature dependent snowmaking. The set-up and assumptions of the indoor production hall are outlined. The performance of an air cycle refrigeration system is compared with a transcritical CO_2 refrigeration cycle. Strategies for integrated heat recovery are evaluated and discussed.

Chapter 11 gives a comparison of the performance of the different refrigeration and heat recovery systems evaluated in this thesis. Lines are drawn to the pre-study and the previous master assignments. A final recommendation of the best suitable system is proposed.

Chapter 12 outlines sources of error. Limitations with regard to the validity of the results and the assumptions of the simulation models are discussed.

Chapter 13 comprises the conclusion and suggestions for further work.

2 Temperature dependent snowmaking

Temperature dependent snowmaking (TDS), commonly known as *artificial* snow production, is characterized by being highly dependent on ambient air temperatures and local climatic conditions. Since the first TDS machines came into the market in the early fifties, the technology has improved considerably (Fauve and Rhyner, 2004). Today there are various methods for producing snow using the jet technique in snow guns. However, they all share the basic principle of combining air and water to form snow. The water droplets produced in a snow gun should freeze in the air before reaching the ground. Machine parameters, such as water flow and operating pressure, can be adapted to meteorological conditions in order to optimize the snow quality. To be able to reduce costs, improve snow quality and produce more snow under marginal conditions, one can expect development and innovation of new cannon types, techniques and optimization of existing products for a long time to come (Gjerland and Olsen, 2014). There are three main production technologies that prevail on the market. These can be used both in stationary and mobile systems.

2.1 Types of TDS

2.1.1 High-pressure towers (air/water snowmakers)

Using this technique, pressurized water is mixed together with a large amount of compressed air through nozzles, before being atomized (Fauve and Rhyner, 2004). Since the amount of both water and compressed air can be adjusted precisely, the system tends to be working well in marginal temperatures (Roundtop Mountain Resort, 2016). The production rate is quite good, but the energy consumption is very high; due to the large amount of pressurized air that is needed to run the snowmaker (Gjerland and Olsen, 2014). Due to a high energy consumption and noise level, these snowmakers are being phased out of the market. A schematic is shown in Figure 1 (Ratnik Industries Inc., 2015).

Figure 1. Air/water snowmaker

2.1.2 Low-pressure snow guns (lances)

The working principle of this technology is similar to that of the air/water snowmakers, except that a lance use 70-80 % less compressed air (Ratnik Industries Inc., 2015). This results in a system with low energy consumption and low noise level. Lances are simple in operation, and with little need for maintenance during operation. However, they have less options for adjusting

the snow quality (Gjerland and Olsen, 2014). The reduced amount of compressed air results in a lower droplet speed out of the nozzles, which requires the snowmakers to be mounted in towers; to ensure that the droplets have enough time in the air for freezing (SMI Snowmakers, 2012). The production rate is quite low compared to other techniques. They have a limited throw and are very sensitive to wind. A schematic is shown in Figure 2 (Demaklenko, 2016).

Figure 2. Snow lance

2.1.3 Fan guns (airless snow guns)

In these low-pressure snow guns, pressurized water is sprayed through nozzles into an air jet formed by a fan (Fauve and Rhyner, 2004). They differ from the two other techniques in that they use a fan to blow the snow; leading to a very high production rate. The fan guns are characterized by having a long snow projection and throw, high capacity in all weather conditions, low sensitivity to wind and an overall good performance (SMI Snowmakers, 2012). A schematic is shown in Figure 3 (Demaklenko, 2016). They have a low energy consumption, relatively low noise level, and provide snow of good quality (Gjerland and Olsen, 2014). However, they suffer from being quite large and heavy, relatively expensive and difficult to transport. Also, this technology requires much maintenance over time.

Figure 3. Fan gun

2.2 Basic principles

Production of artificial snow is a complex dynamic and thermodynamic process which consists of two stages: (1) generation and propulsion of water droplets, and (2) freezing of the droplets (Fauve and Rhyner, 2004). To ensure that small enough droplets are obtained, water is sprayed at high pressures through special small diameter nozzles into the air at atmospheric pressure. The pressure difference between the atmospheric air and the pressurized water will accelerate the water. At sufficiently high water pressures, high speeds will cause turbulence that breaks

the water jet and creates water droplets, which then enters the surrounding air. The droplets formed in the jet will freeze if the following three conditions are satisfied:

1. There is sufficient energy exchange to freeze the volume of water. This means there must be a thermal balance between the wet-bulb temperature of the air, the humidity and the water temperature.
2. Sufficient amount of freezing nuclei present, which will trigger the freezing process.
3. Sufficient flight time in the air to allow for complete freezing of the droplets.

The water temperature is decreased by heat and mass exchange; by convection and evaporation between the water droplets and the air. Convection is the dominating process; depending on the temperature difference between the water and the air. Evaporation at the surface of the droplets will accelerate the cooling process. When water evaporates, energy in the form of latent heat is released; reducing the temperature of the remaining droplets. This phenomenon is known as *evaporative cooling*, and it is an ongoing process until the air is saturated with water vapour. The water temperature will continue to fall until it reaches nucleation temperature; the point where phase change begins, illustrated as point B in Figure 4 (Fauve and Rhyner, 2004).

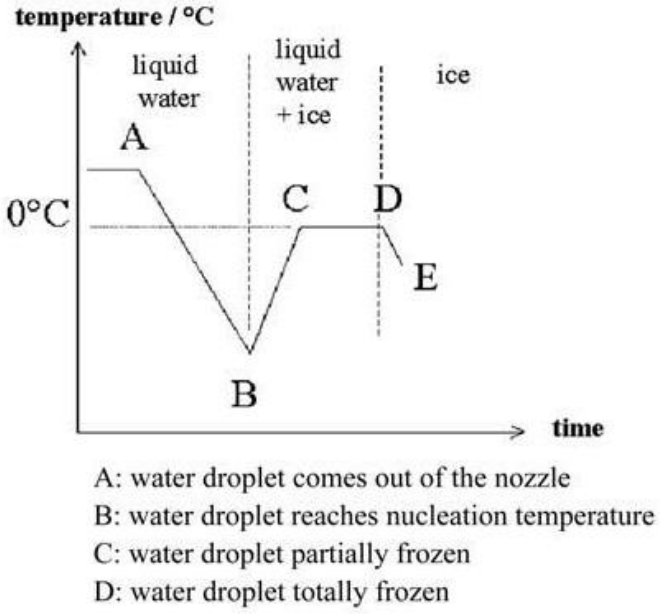

Figure 4. Temperature of water droplet during the nucleation process

To start the freezing process, there has to be formed a nucleus (Gjerland and Olsen, 2014). The water quality of the droplets is important in this process. Chemically pure water can remain in liquid state at temperatures down to -45 °C. However, by adding a nucleating agent, the freezing process may occur at higher temperatures. Commercial nucleating agents will trigger the freezing process by forming a nucleus at higher temperature; thereby providing better water-to-snow conversion. This way, it is possible to create nuclei at wet-bulb temperatures up to -3 °C (Fauve and Rhyner, 2004). When the nucleation temperature is reached, the freezing process starts and heat is released; thereby increasing the temperature of the ice/water mixture. When the droplet is completely frozen, its temperature will decrease.

Artificial snow production is characterized by rapid freezing of water droplets from the surface to the nucleus (inner core), as shown in Figure 5 (Fauve and Rhyner, 2004). This procedure is different from the formation of natural snow; where the crystals grow by condensation of water vapour on snow grains, when small water droplets fall through several layers of air in the atmosphere. The way of formation influences on the shape and properties of the snow. Artificial snow particles are characterized by a spherical shape, often containing air pockets, bulges at the surface and fraction of the grains. This is seen in contrast to the regular hexagonal shape of natural snow crystals. The aim is that the artificial snow should feel and look much the same as natural snow when using it for skiing purposes. Experience shows that artificial snow can withstand long periods of mild weather and wear better than natural snow (Gjerland and Olsen, 2014).

Figure 5. Stages of the nucleation process

The evaporative cooling process is strongly dependent on temperature and humidity. The term *wet-bulb* is commonly used in association with snowmaking, and it is a combination of the *dry-bulb* temperature and the relative humidity (RH) of the air (Moran et al., 2012c). The dry-bulb temperature simply refers to the air temperature that would be measured by a thermometer protected from radiation; thereby not affected by the moisture in the air. The RH is defined as the ratio of the water content in a moist air sample to the water content in a saturated moist air sample, at the same mixture temperature and pressure (Equation (7.10)). The lower the temperature and pressure, the less water the air can contain. If the RH is 100 %, the air cannot absorb more water and is said to be *saturated*. The wet-bulb temperature decreases with decreasing RH. It will always be lower than or equal to the dry-bulb temperature.

When the outdoor air is dry, there is a large potential of absorbing water from the jet. More water will evaporate the drier the air is, and more energy will consequently be dissipated for lowering the water temperature (Fauve and Rhyner, 2004). Snowmaking is seen to be most efficient and with best quality when the wet-bulb temperature is well below the freezing point (Gjerland and Olsen, 2014). Despite this, it is still possible to make snow in marginal temperatures if the air is sufficiently dry. This is illustrated in Figure 6 (SNOWatHOME, 2016), which shows a relationship between the dry- and wet-bulb temperatures, the humidity ratio and the conditions where temperature dependent snowmaking is possible. At too high temperatures and/or RH's, snowmaking will not be possible, and TDS is seen to be limited to a certain production range. This is a drawback concerning the trend of shorter and milder winters.

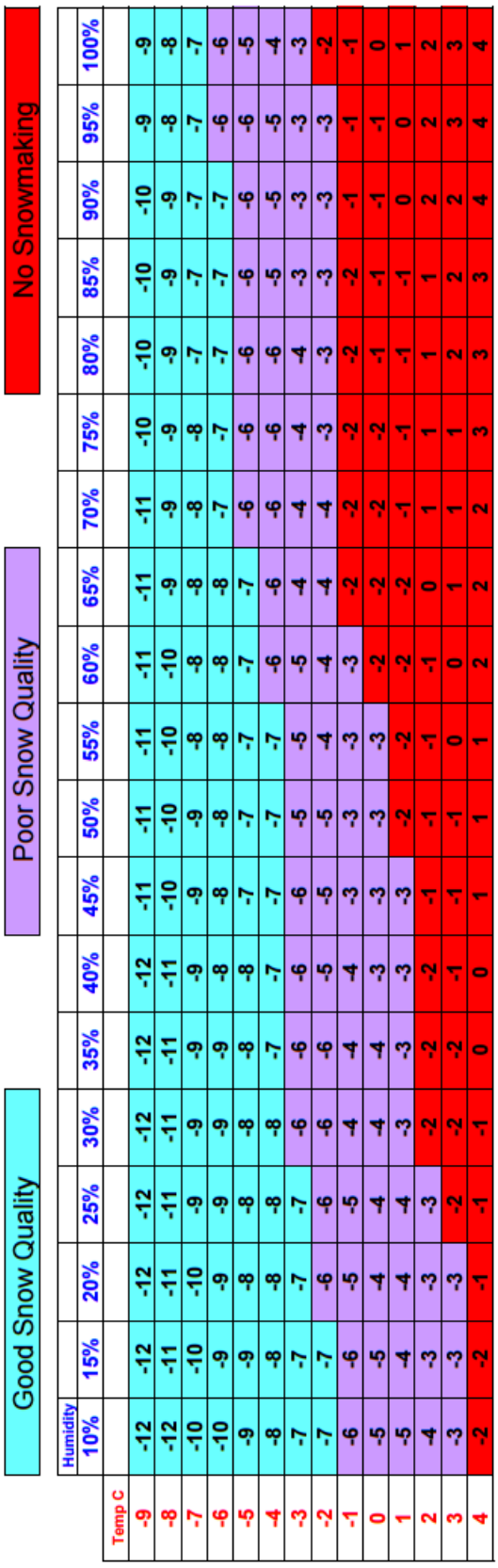

Figure 6. Snowmaking chart. Dry-bulb temperatures are shown on the vertical axis and RH's at the horizontal axis. Temperatures provided in the chart are defined as wet-bulb.

3 Temperature independent snowmaking

A temperature independent snowmaking (TIS) machine uses technology that makes it possible to produce snow above 0 °C, independent of the ambient temperature (Gjerland and Olsen, 2014). The snow produced by these machines is not snow as we know it in its natural form, but rather small ice particles. Today there are at least four known manufacturers of TIS equipment. The production is based on different techniques, which provides different types of ice; flake ice, plate ice or ice slurry. Dependent on which production method is used, the ice will contain different amount of water and exhibit different thermodynamic properties.

3.1 Flake ice production

This type of machine forms ice on the surface of a cooled cylindrical heat exchanger. The ice is harvested as dry subcooled flakes, usually 2-3 mm thick, and collected by a scraper on the inner surface (Graham et al., 1993). There are mainly two different configurations. In some models, the cylinder drum rotates while the scraper on the surface of the cylinder remains stationary. Usually, the drum rotates about a vertical axis. In other models, the drum remains stationary while the scraper rotates and removes the ice. One significant advantage of using a rotating drum, is that maintenance is quite easy. Because the ice release mechanism and ice-forming surfaces are exposed to the ambient, the operator can observe whether the ice plant is operating satisfactorily. The main advantage with using a stationary drum is that it does not require a rotating seal on the refrigerant supply and pipelines. Nevertheless, in modern machines this seal has been developed with a high degree of reliability.

In the flake ice machine water will enter at the top of the cylindrical evaporator, through a series of distribution tubes. The water is sprinkled onto the inner surface of the evaporator, where it is rapidly cooled to form ice. Any water not frozen is allowed to fall into a collection dish, from where it is removed. When the ice is collected, it is subcooled. The degree of subcooling depends on various factors; where the temperature of the refrigerant and the time for subcooling of the ice are the most important. In the subcooling region, located immediately before the scraper, no water is added and the ice temperature is reduced. This ensures only dry, subcooled ice to fall from the walls into the collector space in an opening at the bottom of the machine. The ice must be further processed by utilizing an ice crusher and a distribution system to obtain snow of smaller particle sizes and optimal quality. A schematic diagram of a flake ice drum (FID) is shown in Figure 7 (Cao et al., 2015).

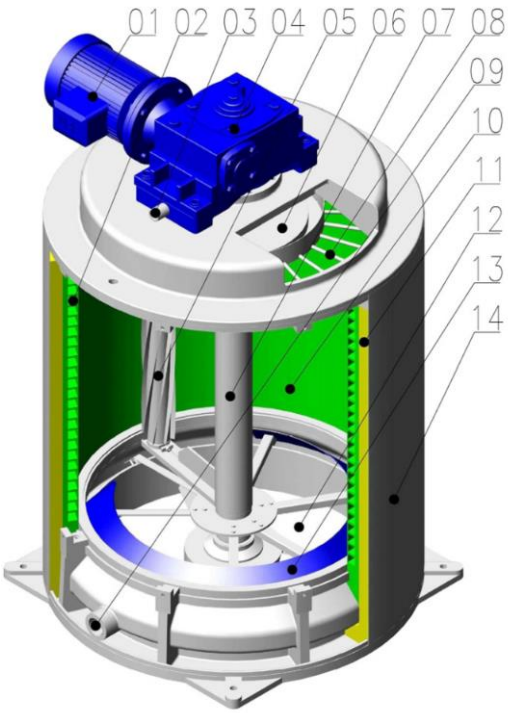

Figure 7. Schematic diagram of a flake ice drum with rotating scrapers. 01-motor, 02-spiral evaporation pipelines, 03-water supply inlet, 04-reducer, 05-ice blade, 06-water distribution pan, 07-main shaft, 08-water distribution tubes, 09-exit of water collection dish, 10-inner wall of evaporator, 11-insulation material, 12-ice storage bin, 13-ice drop opening, 14-outer shell.

The refrigerant temperature and the degree of subcooling, as well as the speed of rotation, are variables that may be changed during operation (Graham et al., 1993). They will affect the capacity of the machine and the thickness of the ice produced. The feed water temperature in the water supply pipes also affects the efficiency of the plant. These factors must be evaluated in combination to determine the optimal operating conditions.

The flake ice machine requires a refrigeration system, with a normal refrigerant temperature between -20 and -30 °C (Cao et al., 2015, Graham et al., 1993). These temperatures are lower compared to other types of machines, and are needed to ensure high production rates. This will keep the machine small and compact, but extra power is necessary to run the machine at such low temperatures. However, this extra power requirement is somewhat compensated for because the method does not require hot gas defrosting. Because the flake ice machine uses a mechanical method to remove the ice instead of a defrost procedure, there is no need for an additional heat source (Cao et al., 2015). Such machines also tend to exhibit a greater heat transfer coefficient than other ice production methods, and they are relatively simple to operate. Flake ice machines are widely used in industry for controlling chemical reactions, cooling concrete and producing ice from seawater to cool and store fish.

Pressure drop calculations for a flake ice system have been performed by Cao et al. (2015), who studied freeze water desalination on a FID by utilizing a hydrocarbon mixture as refrigerant. A cycle consisting of a FID with spiral evaporator pipelines and rotating scrapers, a heat exchanger and a circulation pump was approached theoretically. The pressure drop and lifting height for the flake ice machine and the pump were found to be 0.50 bar and 0.30 bar respectively.

3.2 Production of plate ice

Plate ice is formed by spraying water on a refrigerated vertical plate (Graham et al., 1993). The ice plates are released by running water on the other side of the plate to defrost them. Other types form ice on both surfaces by using an internal defrost process, illustrated in Figure 8 (Graham et al., 1993). The plate ice machine consists of multiple plate units arranged together, and the production rate of the machine can be adjusted by adding or removing one or more of the plates. An ice crusher is required to break the ice into suitable size for storage and use. The machine is operated as an automatically timed cycle, and the ice is transported to a storage area. Alternatively, if the machine is located directly above the storage area, gravity flow can be used to collect the ice.

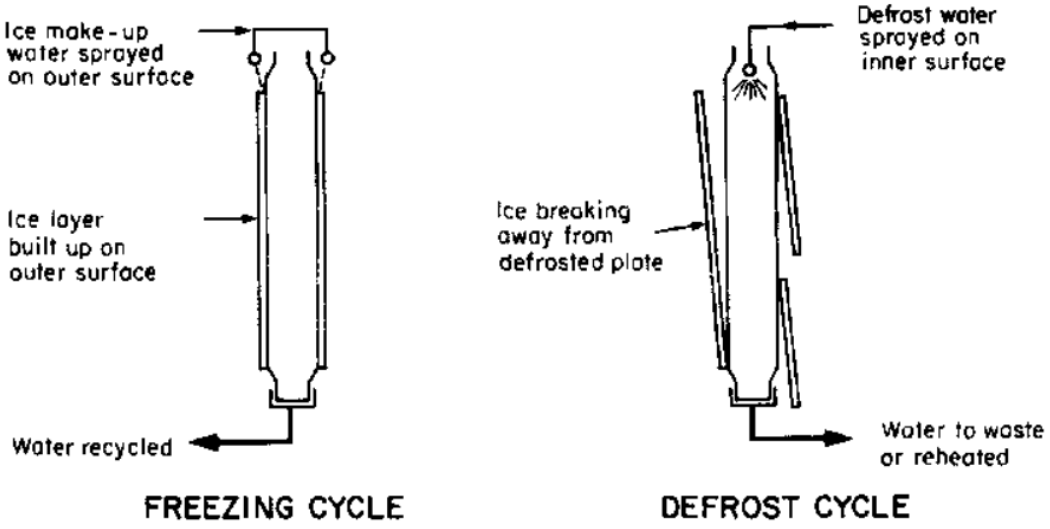

Figure 8. Schematic diagram of the working principle of a plate ice machine

The production capacity is highly dependent on feed water temperature and evaporation temperature of the machine. To improve the efficiency, the evaporation temperature should be as high as possible; and adapted to a level where the ice will have an acceptable core temperature and not feel wet. Typically, an evaporation temperature of -15 °C is desirable (Dieseth, 2016). The optimal thickness of the ice produced in plate ice machines is usually 10-12 mm, considerably thicker than the flake ice (Graham et al., 1993). This is due to the demand of defrosting, as extra power is needed to run the machine to ensure a sufficiently high defrost temperature of the feed water; thereby increasing the energy consumption of the plant compared to flake ice systems. The high energy consumption compared to the ice production rate makes it economically unprofitable to produce thinner ice.

3.3 Production of ice slurry

Ice slurry is a homogenous mixture of small ice particles and a liquid; containing up to 30 % water by weight (Graham et al., 1993, Kauffeld et al., 2010). The liquid can be either pure water or a binary solution consisting of water and a freezing point depressant (Kauffeld et al., 2010). Ice slurry has both high energy storage density and a fast cooling rate compared to other types of produced ice. These features make it beneficial for use in snow production (Bellas and Tassou, 2005).

3.3.1 Scraped surface ice slurry generator

The scraped surface ice slurry generator is currently the most technologically developed and widely accepted ice slurry generation technique over the last 20 years (Stamatiou et al., 2005). It typically consists of a circular shell-and-tube heat exchanger, which is cooled on the outer shell side by an evaporating refrigerant. It is mechanically scraped on its inner side by loaded rotating blades, orbital rods or brushes to prevent any ice crystals from forming a layer on the cooled surface. A schematic is shown in Figure 9 (Stamatiou et al., 2005). To prevent freeze-up on the walls, solutes are added to depress the freezing point of the solution. The rotating scraper blades assembled in the centre of the heat exchanger mechanically induce turbulence into the ice slurry flow; thereby increasing the heat transfer rates and maintaining a homogenous ice slurry mixture.

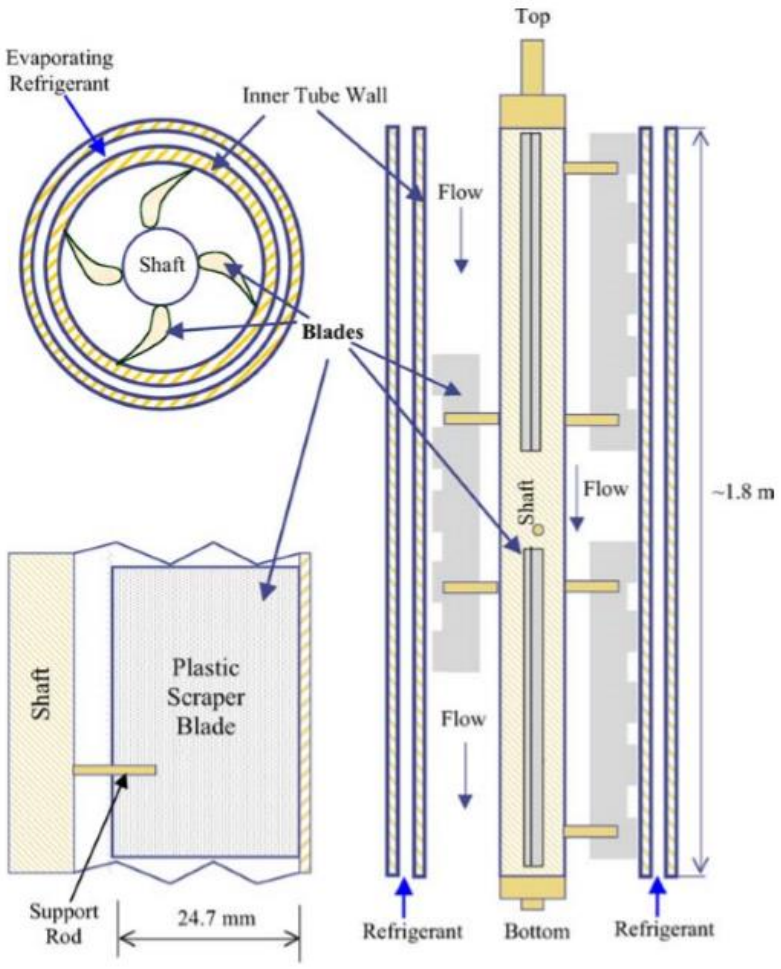

Figure 9. Schematic of a scraped surface ice slurry generator

The machine produces ice in the brine solution at various temperatures, depending on the solution concentration. The large surface area provides high production rates (Bédécarrats et al., 2010, Martínez et al., 2014). The small ice crystals formed on the tube surface are scraped off and mixed with unfrozen water. This mixture is further treated by removing most of the water to obtain a dry form of ice, applicable for snow production (Graham et al., 1993). Scraped surface generators are quite expensive and have high maintenance costs (Bédécarrats et al., 2010).

3.3.2 Vacuum ice maker

A typical vacuum ice system consists of an evaporator, a vacuum pump, a compressor and a condenser (Asaoka et al., 2009). The vacuum ice cycle is similar to an ordinary refrigeration cycle, except that the evaporator operates at triple-point[1] conditions (Moran et al., 2012d, Van Orshoven et al., 1993). The principle of this type of machine is to bring water to the triple-point, such that a small part of the water will evaporate, while the remaining water freezes and forms a water-snow mixture. The vacuum vessel can be regarded as approximately adiabatic, and the removal of latent heat during evaporation causes the remaining water to freeze. The produced ice is in form of a pumpable slurry, which is continuously removed from the evaporator and collected in a snow separator that separates the water from the snow crystals. As air is introduced with the water entering the system, the vacuum pump is required to remove bubbles from the ice maker to maintain the triple-point pressure. A schematic diagram of a vacuum ice machine is shown in Figure 10 (Van Orshoven et al., 1993).

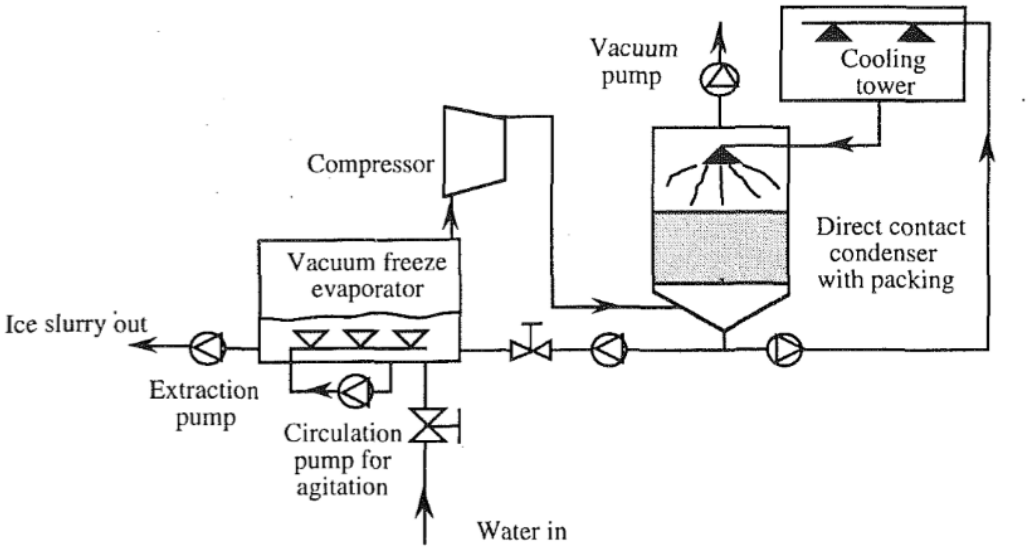

Figure 10. Schematic diagram of a vacuum ice maker with water as refrigerant and direct contact condensation

The low operating pressure of the vacuum ice cycle results in a large specific volume of the gas (Van Orshoven et al., 1993). This means that the compressor needs to handle large volumetric flows, thus posing stringent demands on the compressor size and capacity. Since water is used in the cycle, higher pressure ratios and consequently higher compression work will be obtained compared to other refrigerants. This will make the utilization of standard compressors very expensive, and special designed vacuum compressors should be used to keep the costs within acceptable limits.

[1] The triple point is characterized by the temperature and pressure at which the three phases of water (gas, liquid, solid) can coexist in thermodynamic equilibrium. This accounts for a vapour pressure of 611 Pa, which is less than 1 % of the atmospheric pressure, and a temperature of 0.01 °C.

4 Indoor snowmaking systems

4.1 Conventional indoor snow production

During the last 20 years, indoor skiing halls have become increasingly popular (Paul, 2003). The concept of producing snow in a cold controlled indoor environment provides decreased melting losses. It might be an alternative to TIS technology when outdoor TDS is not applicable. Indoor skiing halls have been installed several places in Europe and Asia. They offer shorter tracks, but can provide snow throughout the year, even in the summer. Different concepts for snowmaking have evolved; both with basis in TIS and TDS technology. In the following section, emphasis will be on TDS as source of snow.

In an indoor snow hall the cooling system is interrelated with the snowmaking system (Clulow, 2006). To avoid melting of the produced snow, both the room air and the floor have to be cooled. The main components of the total system are a refrigeration plant for floor freezing, a refrigeration plant for air cooling and the snow machine (Paul, 2003). A schematic is shown in Figure 11 (Paul, 2003). Alternatively, the two refrigeration plants can be combined into one (Clulow, 1993). The air is cooled to temperatures of about -5 °C, and extensive pipe work is installed in the floor with a circulating brine, usually glycol, at cold temperatures; to ensure that the floor is frozen (Paul, 2003). The floor arrangement is heavily insulated both on the top layer where the floor freezing pipes are accommodated, and in the bottom layer; to prevent ground freezing. Different refrigerants can be used, but there is an increasing focus on applying natural refrigerants such as ammonia or CO_2, instead of HCFCs (eurammon, 2008).

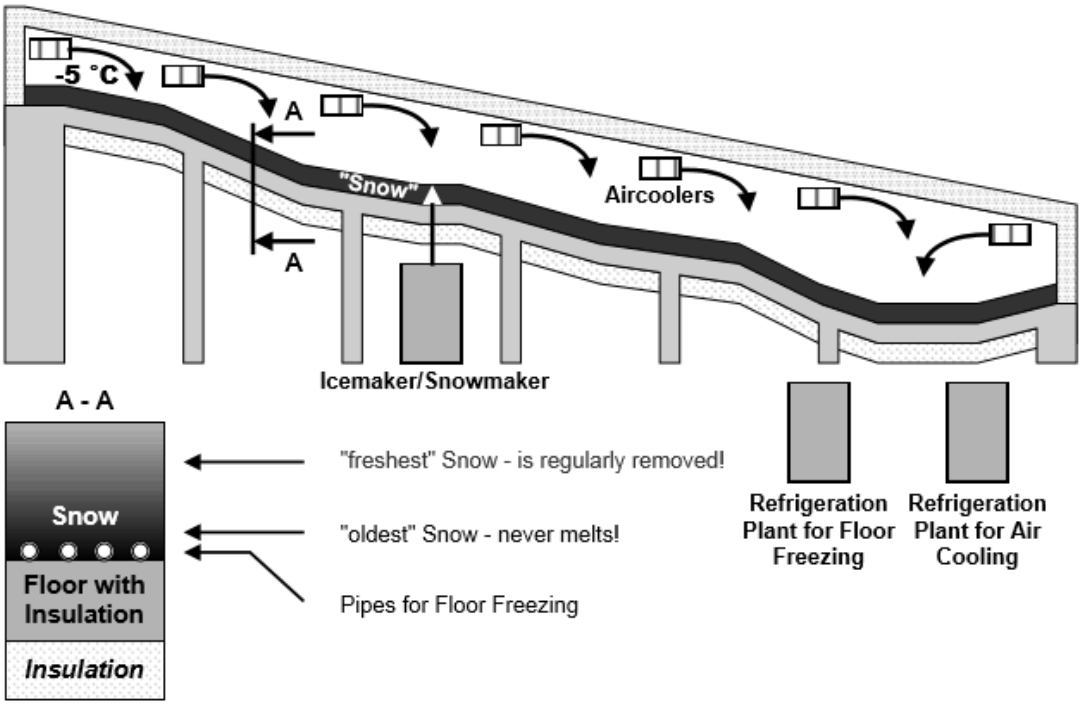

Figure 11. General concept of a conventional skiing hall and the main installations

The skiing hall is cooled during the night; to a temperature that is low enough to allow water, provided through a spray arrangement, to freeze and form ice particles (Paul, 2003). At daytime, when the hall is open to public, the temperature is increased to -1.5 °C (Clulow, 2006). Different outlet nozzles and ratios of water and compressed air can be used to provide various snow densities from the TDS equipment. The indoor snowmaker uses a mixture of compressed air and pressurized water, together with a water-jacketed mixing chamber. The thermodynamic process follows the same basic principles as described in Chapter 2.2. However, conventional outdoor snow guns are not suitable for indoor snowmaking; since the snow is too wet for indoor use. Indoor production requires adaption of the technology to obtain optimal results. Since no wind exists indoors, smaller droplet sizes can be produced.

The total refrigeration load associated with an indoor skiing hall can be divided into the following categories, where the snowmaking load constitutes the major part of the total load (Eikevik, 2015):

- **Transmission load**
  Heat transfer through walls, ceilings and floors.
- **Internal load**
  Heat from people, snow machine, lightning, electrical equipment etc.
- **Infiltration load**
  Heat by air leakage/infiltration through the building envelope, doors and openings, and through the ventilation system.
- **Equipment load**
  Heat from the refrigeration equipment; defrosting of evaporators and load from air cooler fans.
- **Product load**
  Heat removal from the snowmaking process.

The conditions of the air surrounding the snow machine are important for the production process and efficiency. As energy produced by the snow machines is transferred by phase change of water droplets into the air, temperature and dew point conditions of the surrounding air plume are critical. This air is entrained into the snowmaker plume to absorb the latent heat of fusion from the water droplets, and to transfer it to the cold surfaces in recirculation air coolers located in the ceiling (Clulow, 2006). Due to the large amount of water droplets sprayed into the air, the RH inside the hall will be high. The higher the RH, less energy can be dissipated for lowering the water temperature; thereby decreasing the evaporative cooling effect. Air coolers are an important part of this process. They are used to dehumidify the air to acceptable humidity ratios, and to preserve stable temperature conditions. Air coolers are usually installed in large scales, with a capacity dimensioned to cover the total refrigeration load of the hall. To improve the efficiency, they are applied with fins of wide spacing. This produces leaving air conditions that are not as close to air saturation as conventional types.

A challenge with indoor snowmaking is the defrost procedure of the air coolers. With a high RH in the refrigerated space, there will be frost formation on the surface of the evaporators. This causes an additional resistance to heat transfer and decreases the flow rate through the air

cooler. The frost layer should be removed regularly, and this introduces an extra energy demand to the system (Eikevik, 2015). As the refrigeration system cannot be run simultaneously as the defrost procedure, there will be a halt in the production process (Machielsen and Kerschbaumer, 1989). Air coolers should normally be defrosted up to two times during a 24 hours' period.

Pressure, fluid flow, temperature and RH sensors in the building, as well as valves and other control devices, are provided to a monitor that controls each parameter to ensure satisfactory operation and maintenance of the equipment (Clulow, 1993). The refrigeration gains of the indoor skiing hall are characterized by being non-continuous. This makes thermal storage an attractive choice in reducing the energy consumption (Clulow, 2006). By choosing walls, ceiling and furniture of materials with thermal inertia, rapid temperature fluctuations may be avoided. This reduces both the size of the refrigeration plant and the investment costs. Activated alumina is the most commonly media used for thermal storage.

4.2 Air refrigeration system

In the context of increased awareness of the fluorocarbon refrigerants' impact on global warming and ozone depletion (Chapter 7.2), the refrigeration system "Pascal Air" was developed (Boone and Machida, 2011). This system uses air as refrigerant; with basis in a Brayton refrigeration cycle (Chapter 7.4). It differs from the general Brayton power cycle in the reversion of heat dissipation and absorption. The refrigeration plant is composed of three main parts: an integrated turbo compressor and expander, a primary cooler and a cold heat recovery exchanger. The system directly circulates low-temperature air and is classified as being semi-open; in which the evaporator is eliminated from the cycle. A schematic of the system configuration is presented in Figure 12 (Mayekawa, 2010), while Figure 13 shows the corresponding temperature-entropy (T-s) diagram.

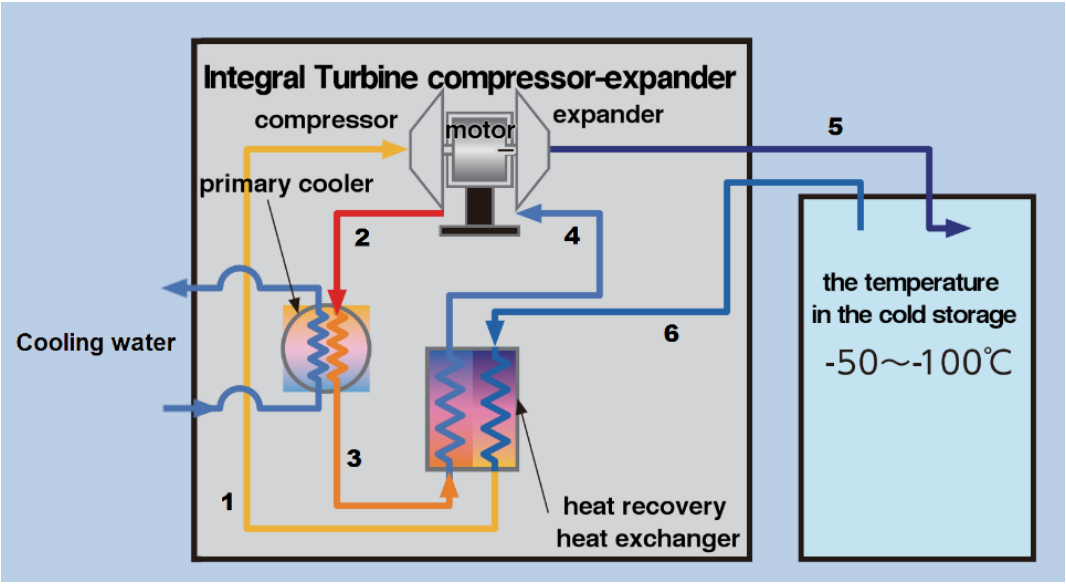

Figure 12. "Pascal Air" flow diagram

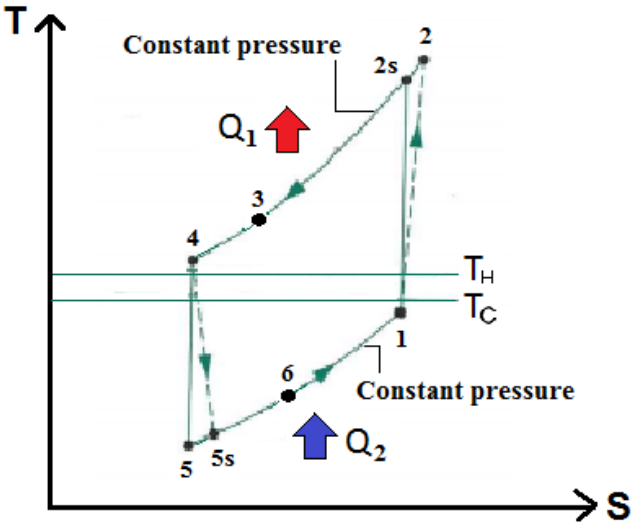

Figure 13. T-s diagram of the "Pascal Air" system

The system is mainly used for ultra-low temperature applications; with a warehouse temperature in the range between -50 and -120 °C (Andou and Okuda, 2004). There is no need for high-pressure equipment as the pressure is kept at low levels; with a maximum limit of 0.2 MPa at the outlet of the compressor (Hattori, 2017). This offers user safety and reduction of the investment costs. The combined turbo compressor and expander has a coaxial structure with a built-in motor in the centre. The work generated by the expander is used as auxiliary power input to the compressor; thereby reducing the compressor power and making operation highly efficient (Boone and Machida, 2011). Because there is no need for refrigerant refilling and recovery, or large-scale construction, the maintenance costs are reduced.

Compared to conventional refrigeration systems, the "Pascal Air" system eliminates the use of evaporators, air coolers and fans in the freezer area (Mayekawa, 2010). Frost from moisture in the air can be treated directly in the cooling system, and there is no need for installing air coolers in the ceiling. This means that the defrost procedure is avoided. Only air ducts for blown-out and intake are needed for the installations. Pipe dimensions are drastically reduced compared to conventional systems; since no secondary refrigerant is required. Due to widening differences between the outlet and inlet, it is possible to decrease the amount of refrigerant air. The air circulation can be one tenth of that in conventional systems, in which large-scale air flows are required to avoid operational problems. Figure 14 and Figure 15 (Andou and Okuda, 2004) gives a comparison of the schematic of a refrigeration system using ammonia and air respectively. The "Pascal Air" concept offers improved safety by avoiding use of traditional refrigerants such as ammonia, which is moderately flammable and highly toxic. Since air is highly available, it adds to a system with low costs (Mayekawa, 2010).

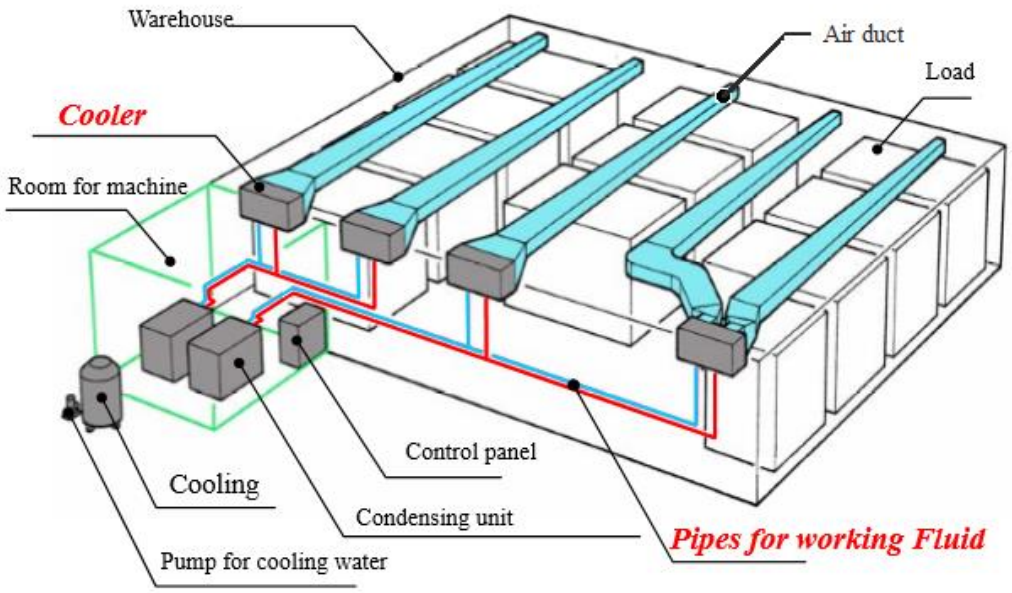

Figure 14. Schematic of a warehouse using ammonia as refrigerant

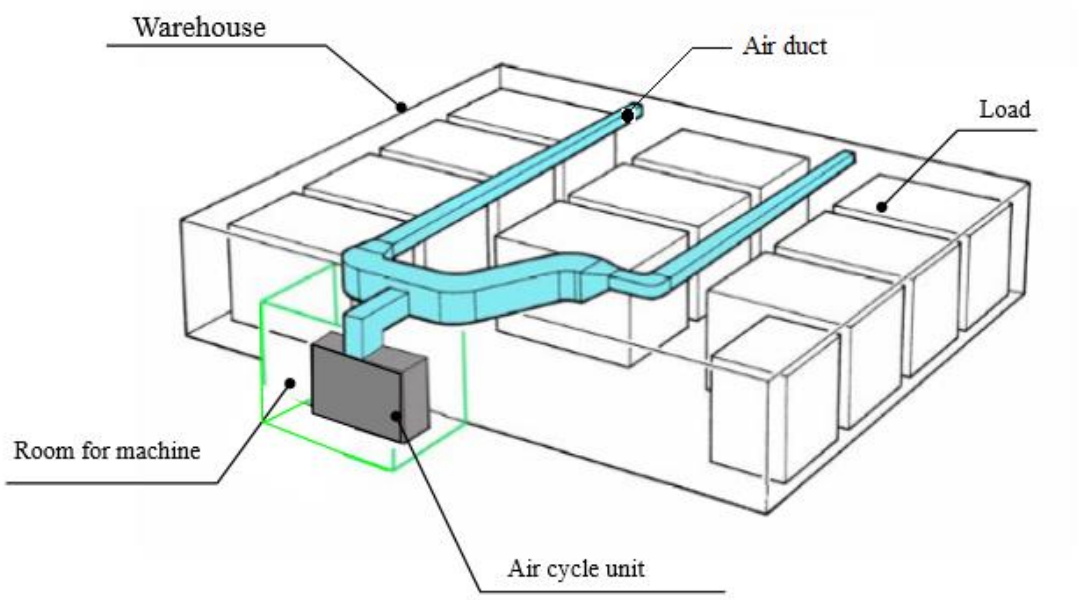

Figure 15. Schematic of a warehouse using air as refrigerant

Air refrigeration systems have generally been recognized by a low COP compared to conventional cycles (Andou and Okuda, 2004). However, at sufficiently low temperatures the air cycle allows equal, or even better, energy performance when the total efficiency of plant (OEEP) is considered. This includes power input both of the compressor and evaporator fans, and from defrosting. Andou and Okuda (2004) showed that an OEEP of 0.9 for an air refrigeration cycle equalled the efficiency of a traditional ammonia refrigeration cycle; with a refrigeration temperature of -30 °C and a load of 55 kW. Lowering the temperature to -60 °C, yielded a corresponding efficiency of 1.2. This is seen to be higher than for a conventional system (Boone and Machida, 2011).

Typical application areas are rapid freezing and ultra-low temperature storage of fish and meat, vacuum freeze dry applications and cooling of pharmaceuticals or semi-conductors (Mayekawa, 2016). No documentation is found on the applicability of using the "Pascal Air" concept in snow producing facilities. The air temperature of such a system would be significantly higher than in low-temperature commercial installations; when the required refrigeration temperature approaches 0 °C. Fleming et al. (1998) reported test data for an open air cycle at elevated temperatures; with the COP ranging from 0.25 to 0.4 in a refrigerated space, in an interval of -10 and 0 °C (Park et al., 2012). Other refrigerants, such as ammonia, usually offer a better COP in this interval; which is amplified by increasing air temperature. However, in a snow producing space the humidity of the air may impact strongly on the thermodynamic performance. A high RH is a drawback of conventional systems; due to the need of defrosting, which increases with the moisture content in the air (Chapter 4.1). This emphasizes the need of evaluating the OEEP, since the temperature and humidity may influence on the performance in different directions. Adaption to higher temperatures could consequently be an interesting field to explore; in order to see if such a cycle can be competitive with conventional refrigeration systems (Eikevik, 2017, Hattori, 2017).

5 System configurations and product data

5.1 Manufacturers of temperature independent snowmakers

The first TIS was manufactured in 1993, and the development of this type of technology has been growing since the early 2000s (Gjerland and Olsen, 2014, SnowMagic Inc., 2015a). Today there are several TIS machines in use, and practice have so far yielded good results. TIS technology has been used in both national and international skiing competitions of great importance, and it can be regarded as a promising future technology in the perspective of being able to provide good skiing conditions in warmer climates. In the following section is an overview of some manufacturers of such technology. Information about working principle, energy consumption and production capacity are provided, and the performances are compared. The energy consumption comprises both power input from the snow producing equipment, the control system and the required refrigeration system. Energy use from the supporting cooling system, necessary to ensure a sufficiently low feed water temperature, is not included.

5.1.1 TechnoAlpin AG

TechnoAlpin AG is an Italian company that provides both TDS and TIS. In 2014 they released their first TIS model applicable for ambient temperatures above 0 °C (TechnoAlpin, 2015b, TechnoAlpin, 2016). This model is not intended as a substitute for TDS equipment, but rather as a supplement to conventional snow guns. A wide range of models and sizes can be produced; depending on the application area and location of the system. They can be both mobile and stationary. The system is delivered in a container and does not require extensive building work or fittings (TechnoAlpin, 2015b). It is based on flake ice production and needs to be connected to a water and power supply. The system is composed of a refrigeration system, a flake ice machine, an ice distribution system and an ice breaking device (TechnoAlpin, 2015a). The snow can be distributed either by using a conveyor belt or an air fan, and the size of the ice particles is adapted to the refrigeration circuit utilized. The ice is produced without use of chemical additives. A schematic of the model SF220 is shown in Figure 16 (TechnoAlpin, 2015b). Technical data is provided in Table 1 (Dieseth, 2016, TechnoAlpin, 2016). Energy consumption is calculated based on an ambient temperature of 15 °C and a feed water temperature of 5 °C. The density of the snow is assumed to be 450 kg/m^3.

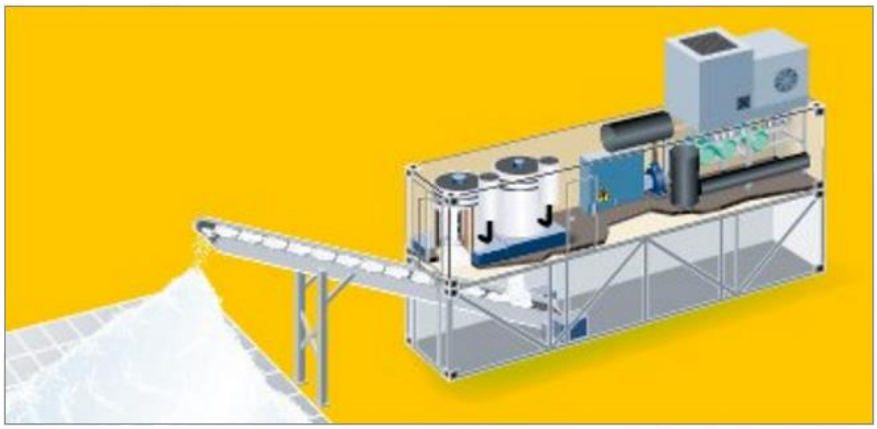

Figure 16. Schematic of the model SF220 from TechnoAlpin AG

Table 1. Technical data for the snow machines from TechnoAlpin AG

	SF100	**SF220**
Principle	Flake ice	Flake ice
Type	Mobile	Stationary
Refrigerant	R404a	R717
Production Capacity	45 tons/day	100 tons/day
	100 m^3/day	220 m^3/day
Cooling capacity	206 kW	640 kW
Power consumption	130 kW	230 kW
Water consumption	0.8 l/s	1.5 l/s
EVR	31.2 kWh/m^3	25.1 kWh/m^3
Operating air temperatures	-5 °C to +25 °C	-5 °C to +25 °C
Customers	Geilo, Norway	Sjusjøen, Norway
	Idre Fjäll, Sweden	
Size	1 x 40’ container	2 x 40’ container

5.1.2 SnowMagic Inc.

SnowMagic Inc. is a company originating from USA. It was the first manufacturer to provide snow producing equipment above 0 °C; in 1993 (SnowMagic Inc., 2015a). It uses a patented technology, Infinite Crystals Snowmaking (ICS), to produce plate ice (Snowmagic Inc., 2015b). The ICS system does not require any chemical additives, and the snow may be recycled and reused after melting. Different models are developed based on variable production capacity. Technical data for four models are presented in Table 2 (Dieseth, 2016, SnowMagic Inc., 2015c, Snowmagic Inc., 2015b, SnowMagic Inc., 2015d). The snow density at the outlet of the machines are about 490 kg/m^3, and the ice particles have a mean size of 0.1 to 0.3 mm in diameter. Energy consumption is calculated based on an ambient temperature of 22 °C.

Table 2. Technical data for the snowmaking machines from SnowMagic Inc.

	UMF-50T/D	UMF-100T/D	UMF-150T/D	UMF-200T/D
Principle	Plate ice	Plate ice	Plate ice	Plate ice
Type	Mobile	Mobile	Stationary	Stationary
Refrigerant	-	-	-	-
Production Capacity	50 tons/day	100 tons/day	150 tons/day	200 tons/day
	102 m^3/day	204 m^3/day	300 m^3/day	408 m^3/day
Cooling capacity	-	-	-	-
Power consumption	151 kW	248 kW	362 kW	545 kW
Water consumption	0.70 l/s	1.39 l/s	2.08 l/s	2.77 l/s
EVR	36.2 kWh/m^3	29.8 kWh/m^3	29.0 kWh/m^3	32.7 kWh/m^3
Operating air temperatures	-6 °C to +30 °C	-	-	-
Customers	Kanagawa, Japan	Prince, Myoko, Hakkejim; Japan	Ibukiyama, Gokase; Japan	Various ski resorts, Japan
Size	40’ container	40’ container	40’ container	40’ container

5.1.3 SnowTek

SnowTek is a manufacturer from Finland that offers two different snow systems (Pesonen, 2016). The first launched machine, SnowGen SI, was used during the Winter Olympics in Sochi in 2014, and it utilizes a scraped surface ice generator to produce ice slurry. The ice slurry system is mobile and uses a brine; consisting of water and a small amount of salt, to produce the snow. It is composed of a trailer and a snow separator; where the trailer includes a refrigeration system and a liquid snow generator, illustrated in Figure 17 (Pesonen, 2016). No harmful chemicals are used in the production process, and the machine can produce snow at temperatures up to 30 °C. The other system, SnowGen FI, is based on flake ice production. Both models have an adaptable production capacity and operating condition; thereby being scalable and easy to maintain. The models can be adjusted to work with practically any refrigerant. Technical data are provided in Table 3 (Pesonen, 2016). Energy consumption is calculated based on an ambient temperature of 10 °C and a feed water temperature of 8 °C. The density of the fresh produced snow from the flake ice and ice slurry machines is about 450 kg/m^3 and 550 kg/m^3 respectively.

Table 3. Technical data for the snowmaking machine from SnowTek

	SnowGen 100SI	SnowGen 100FI
Principle	Ice slurry, scraped surface	Flake ice
Type	Mobile or stationary	Stationary (mobile also possible)
Refrigerant	R404a, R507, R717	R404a, R507, R717
Production Capacity	100 tons/day 181 m^3/day	100 tons/day 222 m^3/day
Cooling capacity	Ca. 500 kW	-
Power consumption	280 kW	230 kW
Water consumption	1.39 l/s	0.97 l/s
EVR	Ca. 44 kWh/m^3	Ca. 45 kWh/m^3
Operating air temperatures	-10 °C to +30 °C	-10 °C to +30 °C
Customers	Sochi, Italy	Have yet not been supplied to ski resorts.
Size	40’ container + snow separator (20’ container)	40’ container

Figure 17. Illustration of SnowGen SI

5.1.4 IDE Technologies

IDE Technologies is a company from Israel that have developed a system using ice slurry, provided by a vacuum ice maker (VIM), to produce artificial snow (IDE Technologies, 2016b). The first TIS machine was released in 2005. Three models with different capacities are commercialized: VIM100, VIM400 and VIM850. Technical data for the models are provided in Table 4 (Hoch, 2016, IDE Technologies, 2014, IDE Technologies, 2016a). Energy consumption is calculated based on an ambient temperature of 20 °C and a feed water temperature of 4-6 °C.

Table 4. Technical data for the snow machines from IDE Technologies

	VIM100	VIM400	VIM850
Principle	Ice slurry, VIM	Ice slurry, VIM	Ice slurry, VIM
Type	Mobile	Stationary	Stationary
Refrigerant	Water	Water	Water
Production Capacity	112 tons/day 200 m^3/day	560 tons/day 860 m^3/day	1120 tons/day 1720 m^3/day
Cooling capacity	350 kW	1750 kW	3500 kW
Power consumption	<250 kW	235 kW	397 kW
Water consumption	1.3 l/s	6.5 l/s	12.9 l/s
EVR	20.4 kWh/m^3	6.6 kWh/m^3	5.5 kWh/m^3
Operating air temperatures	-40 °C to +35 °C	-40 °C to +35 °C	-40 °C to +35 °C
Customers	Have yet not been supplied to ski resorts	Pitztal, Austria Zermatt, Switzerland	Have yet not been supplied to ski resorts
Size	40’ container + 20’ container + snow separator	-	-

The VIM consists of a freezer and a compressor, illustrated in Figure 18 (IDE Technologies, 2016b). The models use different strategies to maintain vacuum in the freezer (IDE Technologies, 2010, IDE Technologies, 2014). In VIM100, water vapour is deposited on cold plates inside the freezer vessel, and the plates are frequently defrosted to keep continuous heat rejection in the freezer. In VIM400 and VIM850, water vapour is constantly sucked from the freezer, compressed in a centrifugal compressor and then fed into a condenser; in order to evacuate the vapour.

The average snow density at the outlet of the machine is dependent on the model. VIM100 has an average density of 560 kg/m^3, while the other models have a density of 650 kg/m^3. After the snow has been drained from excess water, it has a density of about 550 kg/m^3; which is used as basis when calculating the production capacity.

The power consumptions provided in Table 4 refer to the VIM unit only. It does not include the supporting cooling system; consisting of a chiller, cooling tower and circulation pump, which are necessary to operate the system. The total energy consumption of these machines will consequently be higher.

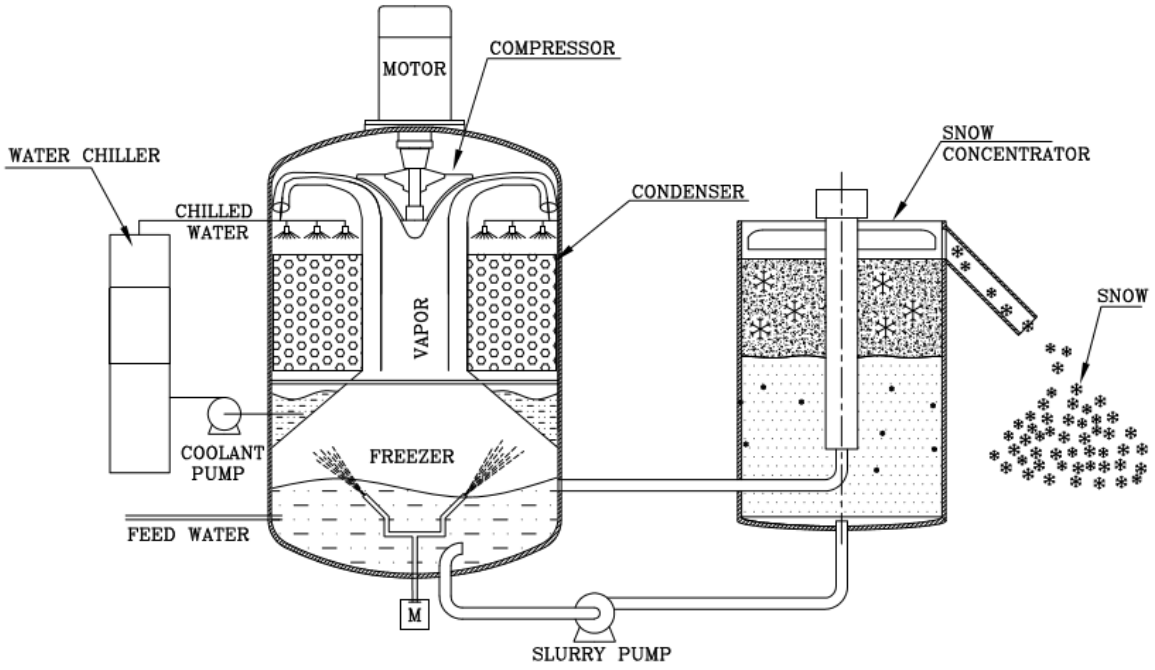

Figure 18. Schematic of a VIM provided by IDE Technologies

5.1.5 Comparison between the manufacturers

Since the scope of this thesis is to study snowmaking systems with a production of 100 tons/day, a comparison of the models with this capacity is presented in Table 5. The calculations are based on 24 hours of production each day. The technical data does not take into consideration the energy required for water supply, and the total energy consumption when integrating such systems will thereby be higher. A price estimation is omitted in the analysis due to the lack of data provided by the manufacturers. The price data is sensitive information which normally is provided with quotation and with signed NDA; dependent on the demands in a project (Pesonen, 2016). However, the TIS unit installed at Sjusjøen cost approximately 6 MNOK. It may serve as a first indication of the market price for such technology (Dieseth, 2016).

Table 5. Comparison between the manufacturer models with snow production of 100 tons/day

	SF220	UMF 100T/D	SnowGen 100SI	SnowGen 100FI	VIM100
Manufacturer	TechnoAlpin	SnowMagic Inc.	SnowTek	SnowTek	IDE Technologies
Principle	Flake ice	Plate ice	Ice slurry, scraped surface	Flake ice	Ice slurry, VIM
Capacity	220 m^3/day	204 m^3/day	181 m^3/day	222 m^3/day	200 m^3/day
Power consumption	230 kW	248 kW	280 kW	230 kW	250 kW
Water consumption	1.5 l/s	1.39 l/s	1.39 l/s	0.97 l/s	1.3 l/s
Refrigerant	R717	-	Any	Any	Water
EVR	25.1 kWh/m^3	29.8 kWh/m^3	Ca. 44 kWh/m^3	Ca. 45 kWh/m^3	20.4 kWh/m^3
Snow density	450 kg/m^3	490 kg/m^3	550 kg/m^3	450 kg/m^3	560 kg/m^3
Equivalent capacity	152 m^3/day	154 m^3/day	153 m^3/day	154 m^3/day	172 m^3/day
Equivalent EVR	36.2 kWh/m^3	38.7 kWh/m^3	43.9 kWh/m^3	35.9 kWh/m^3	34.8 kWh/m^3

The complexity of the snow production systems might make a good and objective comparison difficult. Different configurations and production technologies are developed, and the amount of available data varies among the models. The manufacturers use different dimensioning ambient and feed water temperatures when calculating the energy demand of their systems. These features are important to consider when studying the tables. Energy consumption depends on the environment, like ambient temperature, which affects the condensing temperature of the refrigeration system. Lowering the ambient temperature, lowers the condensing temperature; thereby increasing the COP of the refrigeration system. In addition, the evaporation temperature will vary with the technology used. This causes differences in efficiency refrigeration wise. The lower the feed water temperature, the less energy is needed to cool the water to the freezing point, and each 1 °C change of inlet water temperature will reduce the refrigeration power by 1 % (Pesonen, 2016).

Density considerations will also impact on the performance of the system, which should be taken into account when a comparison is made. Typically, the density at the outlet of the snow machine is used as basis for calculating the efficiency of the system. However, as the snow from the machines is processed further, which is common before it is placed on the ski track, the density will change. Typically, the equivalent snow density on a ready ski track is about 650 kg/m^3 (Pesonen, 2016). Calculations regarding energy consumption and production capacity will depend on which density measure is used. Using the equivalent density as basis makes the comparison most even-handed; since the production and energy use must be elevated at higher outlet densities to ensure the same volume after compaction. The equivalent capacity and equivalent EVR are included in Table 5, which can be seen to differ considerably from the given data provided by the manufactures.

It is seen that the machines using flake ice technology have the lowest power consumption. Both flake ice machines can use environmental friendly refrigerants. This contributes to obtaining a green solution; within the scope of the project “Snow for the future”. The energy

consumption and production capacity of the different models vary less when the equivalent density is used as a reference.

5.2 Indoor snow production systems

The following section describes different system configurations for indoor snow production. Information about capacity, dimensions of the hall and working principle are provided.

5.2.1 "Ski Dubai"

An indoor snow park in Dubai offers five skiing slopes, and consists of an area of 22,500 m^2 covered with more than 6000 tons of snow (eurammon, 2008). Energy efficient cooling is provided by an indirect ammonia refrigeration plant with a capacity of 2600 kW, which cools both the room air and the floor. Glycol is used as a secondary refrigerant to cool the snow in a floor piping system of 100 km in length, as well as feeding 29 air coolers in the ceiling of the hall. During production, the air temperature is kept at -8 °C, and with 30-40 tons of old snow being replaced each day. The walls are heavily insulated, and the refrigeration system is driven by three screw compressors and a number of PHEs. To increase the total efficiency of the system, the old snow being replaced each day is recycled to water into a melting pit. This cold water is used to provide cooling in an air conditioning system of a nearby shopping centre, as well as irrigation of surrounding gardens.

5.2.2 "DKB Ski Sport HALL"

A skiing hall in Oberhof, Germany, consists of a floor area of 10,000 m^2 covered with 1100 m^2 of snow produced by four snow machines (DKB Skisport-HALLE, 2013). Insulated panels are fixed to the walls, and a cooling technology of cogeneration is used. The air temperature during production is kept between -3 and -4 °C, with a relative humidity of 80-100 %. The refrigeration system has a capacity of 620 kW and is driven by two rotary screw compressors. The floor is cooled by a secondary circuit using Tyfocox as medium, and 10 air coolers are located in the ceiling to cool the air. To ensure a sufficient retention time in the air to allow for complete freezing of the water droplets under the prevailing conditions, the snowmakers are located in the ceiling; which is 6-8 m high.

5.3 "Pascal Air" system data

The "Pascal Air" system can be designed for different capacities and dimensions. Table 6 (Hattori, 2017, Mayekawa, 2016) provides data and standard specifications for a commercial model. Table 7 (Hattori, 2017) gives a comparison of the percentage energy use between this model and a typical conventional system with the same refrigeration capacity. It is seen that the "Pascal Air" system can save more than 25 % of energy compared to a conventional system; since it does not require defrosting of the evaporators.

Table 6. Specifications for the “Pascal Air” model PAS30-R

	“Pascal Air” PAS30-R
Refrigerant	Air
Refrigeration capacity	30 kW
Input power (compressor motor)	60 kW
MAWP	0.2 MPa
Warehouse temperature (inlet/outlet)	-80/-60 °C
RH inside warehouse	~100 %
Mass flow rate	1.48 kg/s
Integrated compressor and expander	Turbo
Primary heat exchanger	Plate type of aluminium
Cold recovery heat exchanger	SUS[2] with aluminium fins
Dimensions (length, width, height)	(5000, 2300, 2800) [mm]
Weight	5900 kg

Table 7. Comparison of systems

	Conventional system	PAS30-R
Heat entering through walls	30 %	30 %
Heat loss through opening refrigerator doors	5 %	5 %
Product cooling	25 %	25 %
Illumination	10 %	10 %
Heat generated by fan motor	20 %	-
Defrost procedure	5 %	-
Total	100 %	75 %

[2] Plate heat exchanger of stainless steel type

6 Snow quality

When developing future snow production technology, it is important to keep in mind that the different production techniques will provide different densities and sphere diameters of the snow particles. This may influence on the snow quality, which is an important aspect to consider when determining which technology to use. An overview of snow densities and sphere diameters for the technologies described in Chapter 2-4 are presented in Table 8 (Clulow, 2006, Hattori, 2017, Haugse et al., 2016). As a reference, pure ice and fresh natural snow have a density of 917 kg/m^3 and 100-300 kg/m^3 respectively.

Table 8. Comparison of snow densities and sphere diameters

	Density[3] [kg/m^3]	Sphere diameter [μm]
FID (SF220), TechnoAlpin	450	-
Outdoor snow production (TDS)	550	100-250
Indoor snow production (TDS)	100-500 [4]	10-50
Natural snow	100-300	10-100

Based on a study performed by Haugse et al. (2016), results show that hardness, compact conditions and durable snow characteristics are the most important features for the Norwegian ski sports. To obtain such conditions, the density of the compacted snow should be as high as possible, and with as many bindings between the snow particles as possible. When the outdoor temperature is increased, the microstructure of the snow will be of even greater importance, and the main challenge is to increase the binding area in the snow. This can be achieved by ensuring a well-graded variation in the size of the particles. Snow of smaller particles will obtain higher densities when compacted. By adding snow particles of smaller sizes to more coarse-grained structures, either in form of fresh natural snow or artificial snow (TDS), the air gaps and pores in the snow base can be sealed; hence increasing the number of bindings.

The snow particles obtained from flake ice production are larger and more coarse-grained than the particles obtained by other production technologies. This snow is favourable to use as a sole; in order to ensure a hard, durable and compact bottom layer of the track. It can then be supplemented with other snow technologies to cover the top layer. Flake ice may also serve as a stand-alone snow source; by using an ice crushing machine to divide the flake ice into smaller particles of varying size, small enough to not require supplementation from other snowmaking devices. Alternatively, flake ice can be used together with artificial or pure natural snow to create a durable snow mixture.

The snow produced in an indoor controlled environment, has a considerably smaller particle size than flake ice. This makes it applicable for use as a stand-alone snow source; as it offers maximized number of bindings compared to the other snow sources, with correspondingly higher densities when compacted. A snow nozzle that can provide variation in the particle size will be advantageous, in order to obtain optimal durability of the ski track. If indoor snow

[3] Density at the outlet of the snow machine, i.e. before preparation of snow on the ski track.
[4] Highly dependent on the nozzle arrangement and the water/air ratio.

production is combined with other snow technologies, it will contribute to increase the durability and hardness when the snow is compacted.

Due to the differences in the thermodynamic properties, the snow production technologies will offer variations in optimal application area. The optimal technology for a given production site will depend on both temperature and local climatic conditions, as well as different production periods of the season. Also, velocity and design of the snow groomer will influence on the density of the snow on the track after compaction (Gjerland and Olsen, 2014). Development of ice crushing devices and snow nozzles with varying outlet particle size is crucial for the future snow industry (Haugse et al., 2016). These features are important to consider; in order to obtain the desirable hardness and density of 650 kg/m^3 of the snow on the track after compaction (Chapter 5.1.5).

7 Theory

7.1 Basic principles of the refrigeration cycle

A refrigeration system that works as a standard subcritical vapour compression cycle consists of four main components: an evaporator, a compressor, a condenser and an expansion valve (Eikevik, 2015). A principle sketch of the refrigeration system is shown in Figure 19.

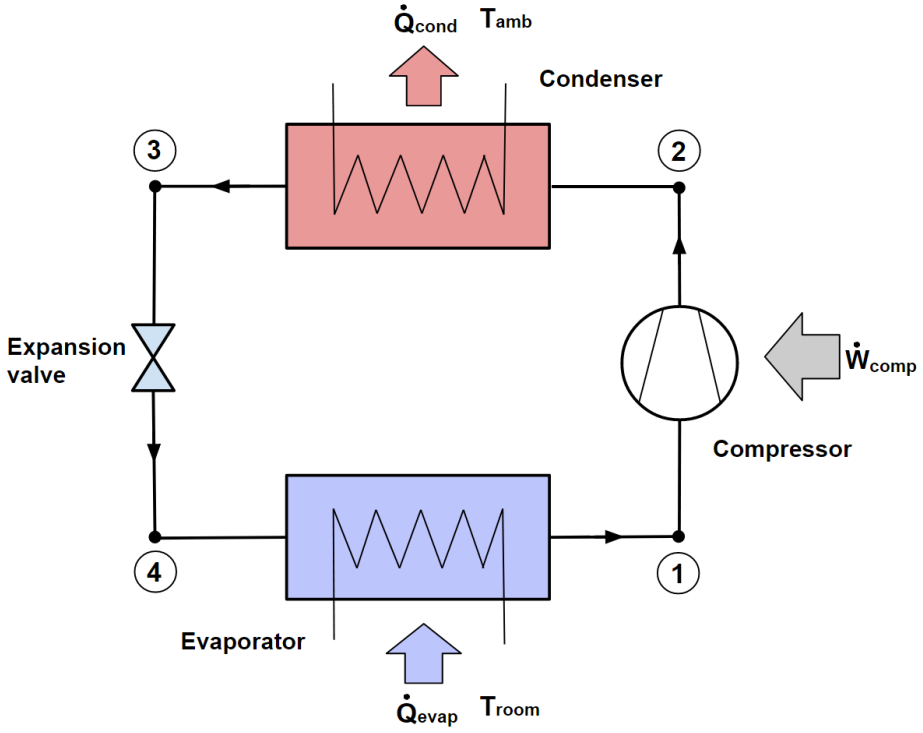

Figure 19. Principle sketch of a refrigeration system

The system removes heat from a heat source, which has low temperature and pressure (evaporator), into an area of higher temperature and pressure (condenser); equal to the refrigeration capacity ($\dot{Q}_{evap}$). This is done by use of a refrigerant or working fluid. In the evaporator, the working fluid has lower temperature than the heat source, and the working fluid will absorb the heat and evaporate. The amount of the heat transferred from the room is thus accumulated as heat of evaporation (latent heat) in the refrigerant vapour. The low pressure in the evaporator is maintained by the compressor, which removes the evaporated vapour continuously. The compressor will increase the pressure sufficiently such that the discharge[5] temperature out of the compressor is higher than the ambient temperature. To achieve this compression, high quality energy in form of mechanical work ($\dot{W}_{comp}$) is added. When the working fluid enters the condenser, heat in the working fluid ($\dot{Q}_{cond}$) is released to the ambient by condensation. The high-pressure fluid will return to the evaporator through a valve where the condensed working fluid is expanded, such that the pressure and temperature is decreased and the cycle can be repeated.

[5] The term “discharge” refers to the outlet state of the compressor.

The heat rejected in the condenser equals the sum of the heat absorbed in the evaporator (latent heat) and the work supplied by the compressor (sensible heat), as shown in Equation (7.1).

$$\dot{Q}_{cond} = \dot{Q}_{evap} + \dot{W}_{comp} \tag{7.1}$$

The COP is a measure of how energy efficient the system is. It is defined as the ratio of cooling or heating provided to the amount of work supplied; depending on whether the aim is the refrigeration effect or the available heat from the condenser. The term $\dot{W}_{tot}$ mainly accounts for the compressor work, but it may also include electric power supplies from other components; such as pumps or fans, if present in the system.

$$COP_{cooling} = \frac{\dot{Q}_{evap}}{\dot{W}_{tot}} \tag{7.2}$$

$$COP_{heating} = \frac{\dot{Q}_{cond}}{\dot{W}_{tot}} \tag{7.3}$$

The COP of a refrigeration cycle should in principle be given by the temperature differences between the evaporator and condenser if it is an ideal thermodynamically process. This will however not be the case in reality, since the use of working fluids present in the system will introduce losses regarding compression, superheat and expansion. There are two types of efficiencies which are important for the design of a refrigeration system: the isentropic efficiency and the volumetric efficiency, illustrated by Equations (7.4) and (7.5). The term "isentropic" refers to a process at constant entropy, and the isentropic efficiency accounts for energy loss due to compression. It is not possible to achieve adiabatic compression without any heat exchange with the surroundings, thus resulting in a higher power demand than the theoretical. The volumetric efficiency reflects the reduction of volumetric flow through the compressor, due to internal leakages between compression chambers, heat and flow related losses, and expansion of internal gas in the compressor cylinder. The suction volume is the required volume that needs to be removed from the evaporator to achieve the desired refrigeration capacity, while the stroke volume is the actual required volume. Due to volumetric losses, the stroke volume will be higher than the suction volume.

$$\eta_{is} = \frac{\dot{W}_{comp,is}}{\dot{W}_{comp}} \rightarrow \dot{W}_{comp} = \frac{\dot{W}_{comp,is}}{\eta_{is}} = \frac{\dot{m}_R(h_{2s} - h_1)}{\eta_{is}} \tag{7.4}$$

$$\lambda = \frac{\dot{V}_{suction}}{\dot{V}_{stroke}} \rightarrow \dot{V}_{stroke} = \frac{\dot{V}_{suction}}{\lambda} = \frac{\dot{m}_R}{\rho_1 \lambda} \tag{7.5}$$

7.2 Refrigerants

Different working fluids have different thermodynamic and physical properties, which will influence on the cycle losses. This results in a strong dependency between the choice of refrigerant and the size of losses, and it will lead to differences in COP. Therefore, it is important to select a working fluid with suitable properties for the system to be considered. However, there are many factors that will be of importance and should be taken into account. Some are practical aspects, while other are related to the thermodynamic process itself. All working fluids will have both favourable and less favourable properties. Depending on what

the aim is, there will be a certain trade-off between the different properties, in order to find the best suitable working fluid for a given application. Among the most important criteria to consider are (Eikevik, 2015, Maina and Huan, 2015):

- Safety (flammability and toxicity)
- Reliability
  - Chemical and thermal stability
  - Compatibility with materials and lubricants (oil, water)
- Suitable thermodynamic and physical properties
- Environmental impact
- Price and availability

Since the 1980s there has been an increased focus on choosing working fluids with low environmental impact (Eikevik, 2015). Stratospheric ozone depletion and impact on the atmospheric greenhouse effect, due to refrigeration emissions and leakages from the systems, have led to drastic changes in the refrigeration technology (BITZER Kühlmaschinenbau GmbH, 2014). After the CFC's were banned from the market in 1987, the chlorine-free HFC refrigerants, with an ODP of zero, have become widely established for many years; both in commercial refrigeration, air-conditioning and heat pump systems. However, the HFC's have been shown to have a high GWP value. Today, the focus is on developing refrigeration systems implemented with working fluids that have both ODP and GWP values close to zero. Applicable legal regulations to limit the amount of Fluorinated greenhouse gases (F-gases) are already in force; such as the EU Regulation on F-gases. The use of HFC's in refrigeration systems are not future viable solutions (Eikevik and Hafner, 2016).

In order to achieve the legal objectives, an increased use of natural refrigerants[6] will become necessary (BITZER Kühlmaschinenbau GmbH, 2014, The Linde Group, 2016). This require comprehensive testing of the refrigerants, as well as adjusted systems. Ammonia (NH_3), carbon dioxide (CO_2), hydrocarbons and water are the most commonly used natural working fluids today. Among these, emphasis will be on CO_2; as it has proven to be technically and economically competitive in refrigeration systems with integrated heat recovery (Eikevik, 2015). In addition, the use of air as refrigerant will be briefly discussed.

7.3 CO_2 as refrigerant

CO_2 has a long tradition in the refrigeration technology, reaching back to the 19th century (BITZER Kühlmaschinenbau GmbH, 2014). The main focus for applications were industrial use, including marine refrigeration. With the introduction of the synthetic refrigerants, CO_2 was gradually replaced, and since the 1950's it has been practically out of use. The reason for the reintroduction of CO_2 into the market was primarily due to the awareness of the ozone depleting properties of the CFC's and HCFC's, as well as the greenhouse effect of the HFC's (Eikevik, 2015). There was an urgent need to find a refrigerant that was environmental friendly, and neither toxic (as ammonia) nor flammable (as hydrocarbons). Traditionally, CO_2 has been

[6] The term "natural refrigerant" refers to molecular compounds or structures already existing in the atmosphere, within the nature's bio-chemical processes.

known to be less efficient in conventional subcritical refrigeration systems. By adapting the operating conditions to suitable applications, high efficiencies can be obtained.

CO_2 is either toxic nor flammable, with an OPD of zero and a GWP of 1 (Maina and Huan, 2015). It is widely available; both as a constituent in the atmosphere and as combustion product in industrial processes. The price is low, and with no need for recovery and disposal (BITZER Kühlmaschinenbau GmbH, 2014). It is compatible with normal lubricants and does not affect construction materials in refrigeration systems (Eikevik, 2015). The critical point[7] is characterized by simultaneous high pressure (73.8 bar) and low temperature (31.1 °C). The high critical pressure results in a high energy density and a high volumetric refrigeration capacity. This means that CO_2 systems can be designed for small compressor volumes. The dimensions of pipes and valves will consequently be smaller, but it is necessary to install equipment that can handle high pressures, which might be costly. In addition, CO_2 has very low viscosity. This means that most flows are naturally turbulent, with a corresponding high heat transfer rate (Maina and Huan, 2015). Operation close to the critical point will add to the high heat transfer; making it possible to reduce the size of heat exchangers drastically for the same amount of heat transfer to occur.

Due to the high absolute pressure level, CO_2 is less sensitive to pressure losses (Stene, 2016). Favourable thermodynamic properties; such as low viscosity, low volumetric efficiency and a low $\Delta T/\Delta p$ ratio, make it possible to reduce the pipeline dimensions, and to keep the pressure drop at an acceptable level (Eikevik, 2017). Usually, the pressure drop in pipelines is sufficiently low to be neglected by good approximation.

CO_2 can be used in conventional subcritical refrigeration systems, provided that a condensation temperature below 28-30 °C is possible. It is typically applied as secondary fluid in cascade systems in industrial and larger refrigeration plants. These configurations have shown to perform well. However, at high discharge pressures the temperature of the gas will be too high for condensation, and the discharge gas will be supercritical. The refrigeration cycle can still be carried out, but it must then operate in transcritical mode; where heat rejection occurs at supercritical pressure, while heat absorption occurs at subcritical pressure[8]. This will lead to significant changes in fluid properties. In the supercritical region, pressure and temperature are uncoupled, independent properties. Evaporation will still proceed at constant temperature, but heat rejection is characterized by proceeding an isobar where the gas is cooled at gliding temperature (BITZER Kühlmaschinenbau GmbH, 2014). The condenser must therefore be replaced by a gas cooler. The difference between the two operating modes is illustrated in a logarithmic pressure-enthalpy (log P-h) diagram, Figure 20 (Eikevik, 2015).

[7] The critical point is defined by the maximum temperature and pressure in which the liquid and vapour phases can coexist in equilibrium. In this point, temperature and pressure are referred to as "critical".

[8] The terms "subcritical" and "supercritical" refers to a pressure level below and above the critical pressure respectively. Conventional refrigeration cycles are usually subcritical; in that both heat rejection and heat absorption occurs at pressure levels below the critical point.

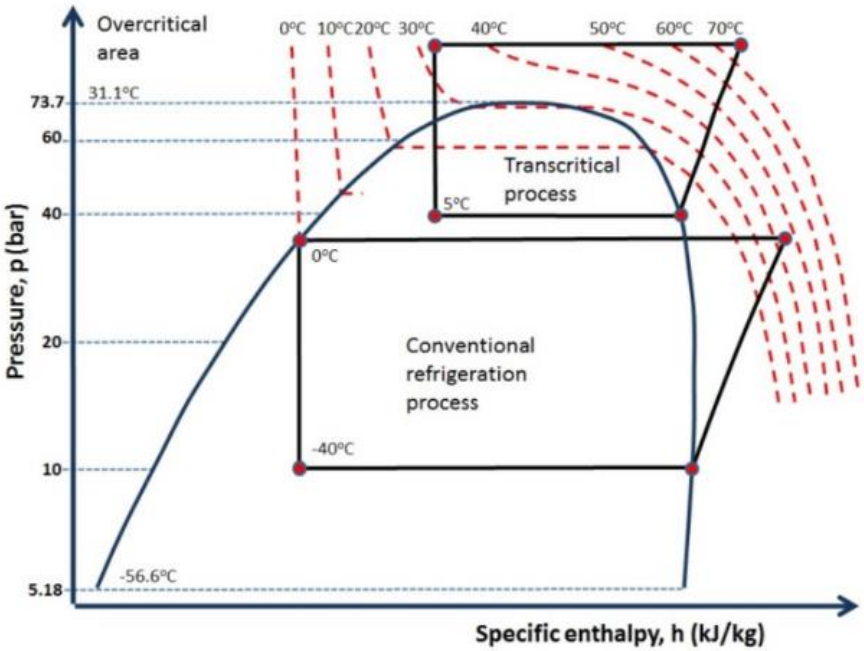

Figure 20. Subcritical and transcritical CO_2 cycle in a log P-h diagram

CO_2 is especially well suited for transcritical system configurations (Eikevik, 2015). The cycle enables good temperature match when heat rejection on the high temperature side causes a significant temperature rise in the heat receiving fluid, while heat absorption from the fluid to be cooled in the evaporator takes place at constant temperature. These features make it advantageous for heating of hot tap water, with a typical temperature rise of 50-60 °C. The best possible situation exists when heat rejection occurs with maximized temperature glide that is thermodynamically advantageous, at the same time as the fluid can be cooled to a low temperature in the gas cooler. The transcritical CO_2 cycle is especially efficient in applications where cooling can be combined with heat recovery.

Despite of several favourable properties, the CO_2 cycle is still affected by many losses (Maina and Huan, 2015). At high discharge pressures the transcritical cycle is affected by higher throttling losses compared to the conventional subcritical cycles. This may increase the required compressor power, and the losses should be reduced as much as possible to achieve the best overall performance. Some commonly used methods to improve the cycle efficiency are (a) use of internal heat transfer; in terms of a suction gas heat exchanger (SGHX) or a subcooler, (b) use of two-stage compression or expansion, and (c) recovery of expansion work by use of an ejector or expander (Stene, 2016). Figure 21 (Eikevik, 2015) shows the main components of a transcritical CO_2 cycle; in which a SGHX has been applied. Return system and auxiliary equipment, such as safety valves and filters, are not included in the figure (Stene, 2016).

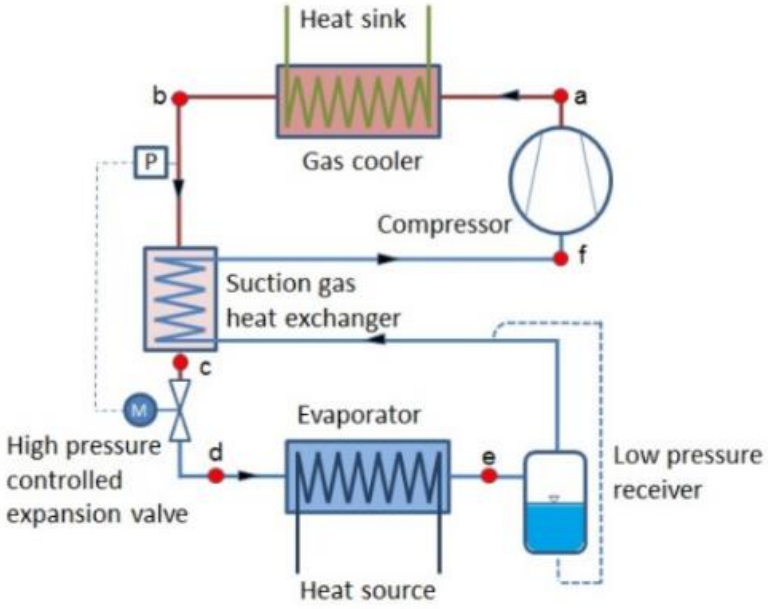

Figure 21. Example configuration of a transcritical CO_2 system

The SGHX is favourable in that it both subcools the liquid at the outlet of the gas cooler, at the same time as it provides superheat of the CO_2 gas at the inlet to the compressor. The combined superheat is a major advantage, as it offers compressor safety. The elevated temperature prevents the oil in the compressor from cooling excessively, which is beneficial to the compressor´s lubrication. Also, liquid slugging is avoided. This is desirable as compression of two-phase flow may lead to wear and tear of the construction components; which over time may harm the compressor and lead to failure.

7.3.1 Heat recovery in CO_2 systems

A snow production system will, similarly to conventional refrigeration systems in supermarkets and industry, produce a lot of excess heat. With the snow technology in use today, this excess heat is released directly to the ambient air. However, by applying a heat recovery system, it might be possible to utilize the heat from the system in suitable applications. Heat recovery from a refrigeration system has in fact been shown to be one of the most efficient ways of increasing the total efficiency; if there is need for simultaneous heating and cooling (Eikevik and Hafner, 2016). There are several configurations available to recover the waste heat; each depending on system design and refrigerant choice.

De-superheater/gas cooler

This configuration offers heat recovery in a de-superheater; which is installed before an air cooled condenser, as illustrated in Figure 22 (Sawalha, 2012). The system is suitable when the discharge temperature is high. It can provide heat at moderate to high temperatures; suitable for HVAC systems or floor heating. The regulating valve after the gas cooler will adjust the discharge pressure and the de-superheater capacity (Eikevik and Hafner, 2016). Alternatively, all the heat can be recovered in a gas cooler, which operates transcritically.

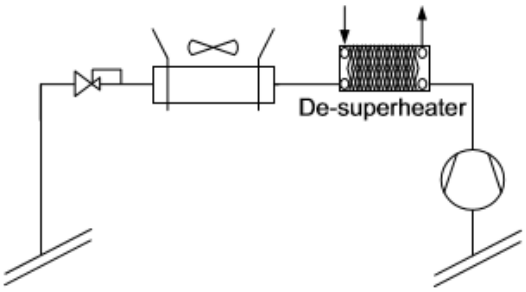

Figure 22. Heat recovery by using a de-superheater

Heat pump cascade

Two different cascade configurations are illustrated in Figure 23 (Sawalha, 2012). In the left configuration, heat is recovered from a condenser at low temperatures, and delivered to a heat pump as low-grade heat. The heat pump can transfer the heat to systems at higher temperature levels, for example to a HVAC system. With this operation, the refrigeration system is not required to run with high discharge pressures. In the right configuration, heat is recovered in a subcooler after a condenser/gas cooler. This will increase the efficiency of the refrigeration system; due to decreased outlet temperature of the exchanger. The system will provide heat at low to moderate temperatures; applicable in devices that can utilize heat at low temperatures, such as snow melting equipment or preheating of water or air.

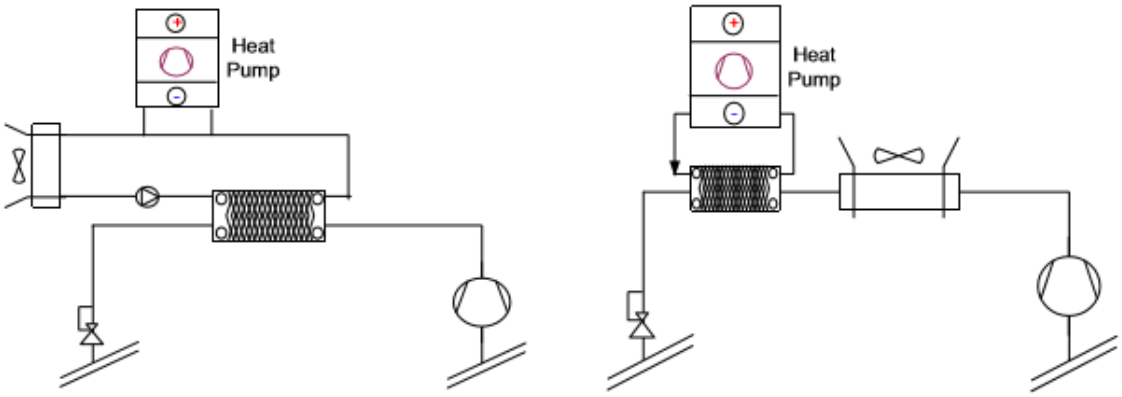

Figure 23. Heat recovery by using a heat pump cascade. To the left; heat is recovered in a condenser, and to the right; heat is recovered in a sub-cooler.

Fixed-head pressure heat recovery

Heat recovery in refrigeration systems in supermarkets have typically been done by fixing the head pressure. The condensing pressure is elevated to a level where it has the required temperature for the heating system, illustrated in Figure 24 (Sawalha, 2012). The heat is often released to a HVAC system, where a secondary fluid transfers the heat from the condenser to the HVAC unit. The configuration is mostly applied in conventional systems running with HFC's. Since the system will operate at moderate condenser temperatures, the CO_2 cycle must operate transcritically. This gives a relatively low COP compared to use of conventional working fluids.

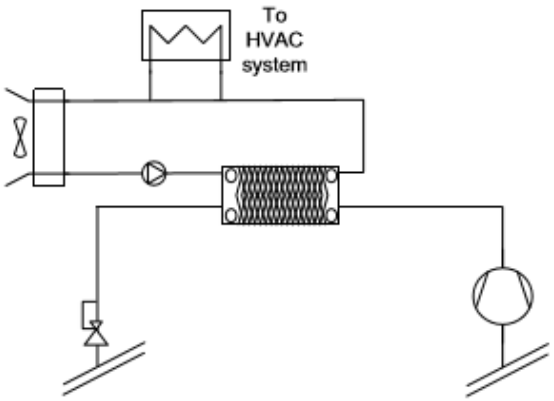

Figure 24. Heat recovery by using the fixed-head pressure method

Combined mode

It is possible to combine the different configurations described above. If there is a heating demand at different temperature levels, for example a combination of space heating and DHW heating, the transcritical cycle may provide good temperature match for both demands. This is illustrated in the temperature-enthalpy (T-h) diagram in Figure 25 (Eikevik, 2015, Stene, 2016). Three gas coolers can be connected in series in such a configuration. Tap water can be preheated in a subcooler, while CO_2 obtains maximum cool-down. A second heat exchanger can cover most of the duty; heating water for floor heating, while cooling the supercritical CO_2 gas. A de-superheater provides the final heating of tap water. Higher COPs can be obtained when operated in combined mode; due to a better temperature fit at a moderate pressure level (Stene, 2016).

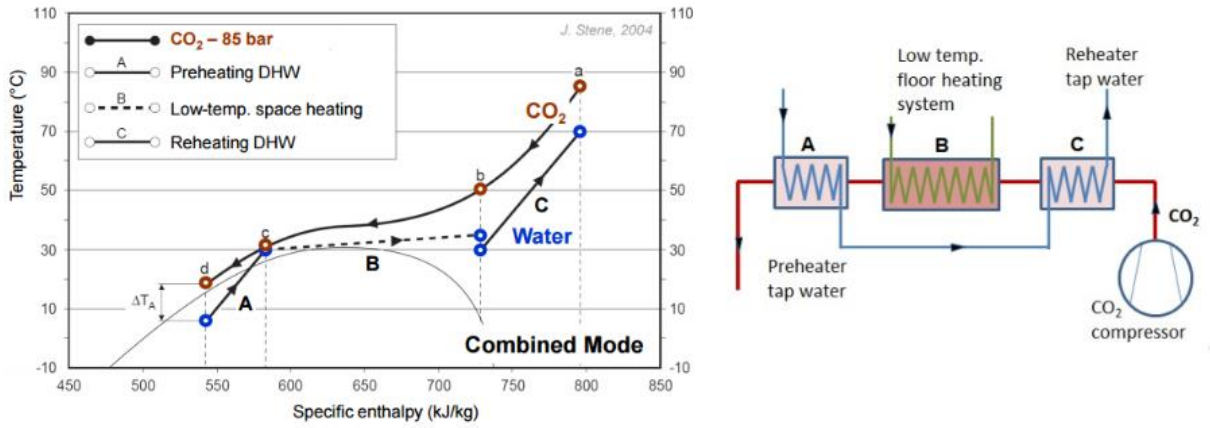

Figure 25. To the right; a gas cooler arrangement for combined DHW and space heating. To the left; an example of the corresponding cycle shown in a T-h diagram.

7.3.2 Gas cooler

Design of the gas cooler is important for the performance of the transcritical CO_2 cycle for two reasons (Yin et al., 2001). Firstly, is the effect on system capacity, COP, which is maximized by achieving maximum cool-down of the CO_2 gas before throttling; to reduce the throttling losses. An internal heat exchanger will also help reducing the temperature of CO_2 before throttling, but at the expense of increasing the compressor work caused by suction gas heating.

Maximum COP is thus obtained by maximizing the amount of heat rejected in the gas cooler. Secondly, correct design of the gas cooler is very important because it reduces the operating pressure; consequently reducing the compressor work.

Knowledge of the optimal pressure that yields the best system efficiency is an important factor in the design of a transcritical CO_2 cycle. At supercritical pressures, there will be significant variations in the specific heat capacity of the CO_2 gas (Stene, 2016). This leads to a non-monotonical increase of the COP; due to the fact that the heat rejection temperature is independent of the heat rejection pressure in the supercritical region (Liao et al., 2000). It is seen that the required compression work increases nearly linearly with increasing heat rejection pressure, while the gas cooler capacity varies non-linearly. This is illustrated in Figure 26 (Stene, 2016). The optimal pressure is to a great extent determined as a function of gas cooler outlet temperature; where there is a trade-off between the highest possible enthalpy difference in the gas cooler and simultaneous minimum compressor work. Accordingly, in a combined heating and refrigeration system, the amount of heat recovery needs to be evaluated continuously against the work input to determine the pressure which maximizes the COP.

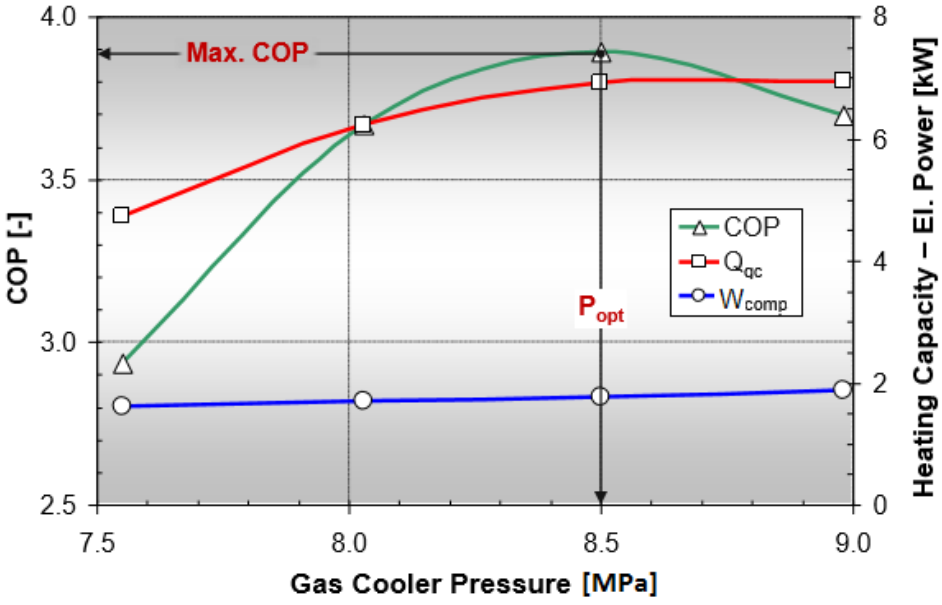

Figure 26. Influence of gas cooler pressure on heating capacity, compression work and COP

The point in the gas cooler with the lowest temperature difference between CO_2 and water is called the pinch point. To obtain maximum system efficiency, it is important that the pinch point is located at the outlet of the gas cooler. If the pinch point is located inside the gas cooler, it will act as a limiting factor; hampering the heat transfer, as illustrated in Figure 27.

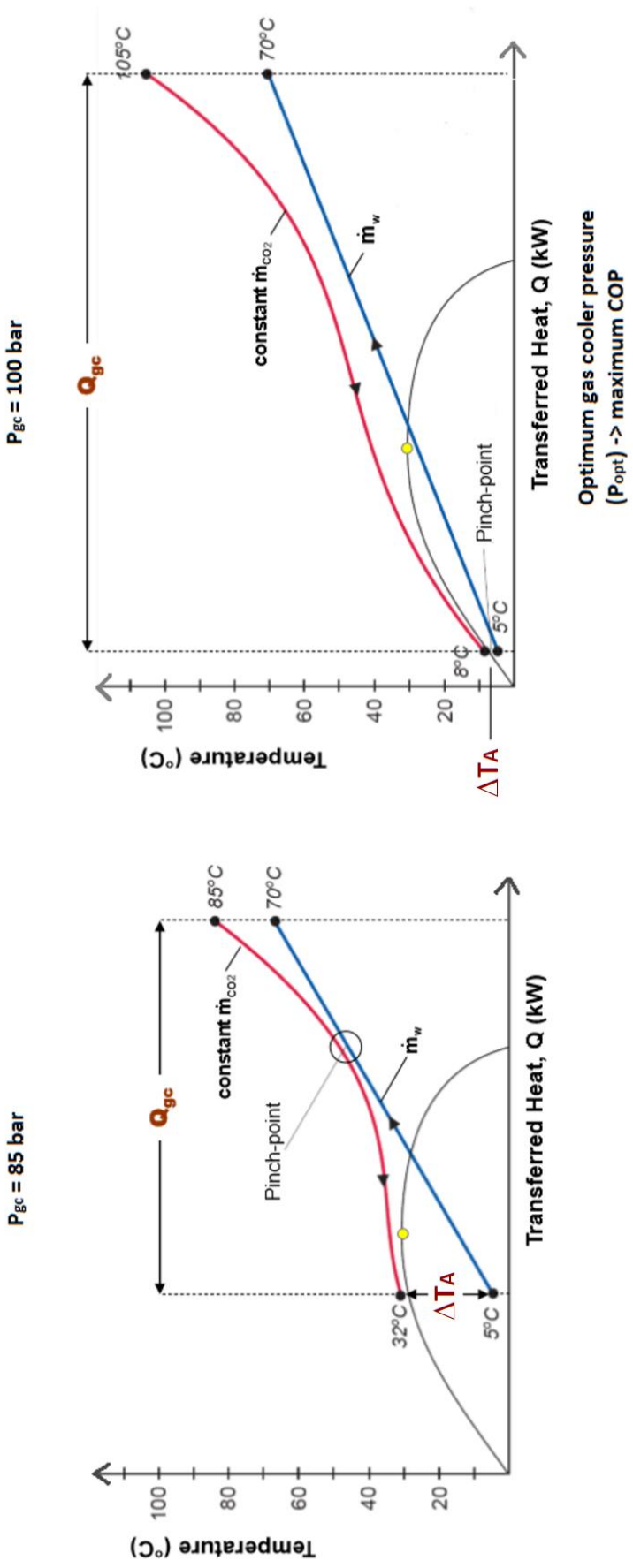

Figure 27. Dependency of gas cooler performance on the heat rejection pressure and the location of pinch point; when assuming fixed inlet and outlet water temperatures.

In order to optimize the gas cooler pressure in the heat recovery cycle of the flake ice system, different heat exchangers were investigated. Below follows a brief presentation of the heat exchanger types evaluated.

Plate heat exchangers

A plate heat exchanger (PHE) consists of thin, corrugated sheet metal plates that are pressed together and assembled in a frame with gaskets of rubber between each plate (Wang et al., 2007). The plates can either be welded or brazed together. The gaskets provide the flow channel space between the adjacent plates and ensure that the hot and cold fluid flow in alternate channels. The hot and cold fluid enter at the top and bottom of the heat exchanger respectively; distributed through inlet and outlet port connections. A schematic is shown in Figure 28 (Wang et al., 2007).

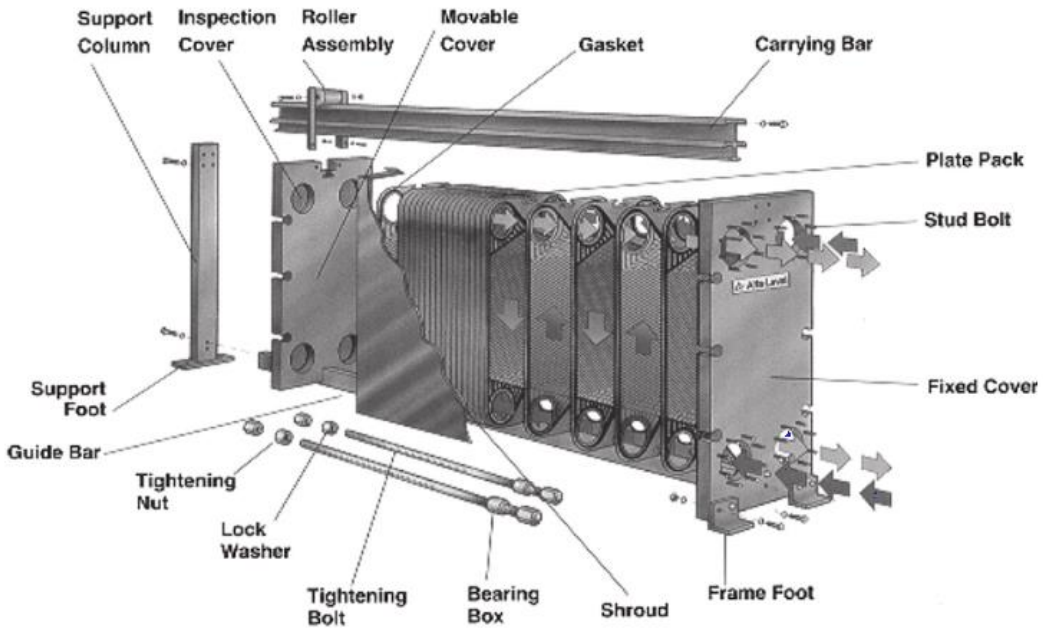

Figure 28. Schematic of a plate heat exchanger

The plates are produced with different patterns. Chevron pattern is the most usual. These induce high turbulence flow; with a following reduction of fouling, and an improvement of the heat transfer performance (Kaori Heat Treatment Co. Ltd., 2017). The plates are packed together with opposite angular pattern; causing contact points between the plates. This is illustrated in Figure 29 (Huang et al., 2012), where the chevron angle (β) is defined as the angle with the vertical axis. The plate surface is divided into a core heat transfer section and a flow distribution region at the top and bottom. Both regions constitute the active heat transfer surface (Wang et al., 2007). The distribution regions are designed to evenly distribute the incoming fluid from the inlet to the outlet port through the core region. Due to high heat transfer coefficients and counter-flow arrangement, PHEs may operate with very close temperature approach conditions ($\Delta t_A \sim 1$ °C). They usually have a much smaller thermal and physical size than conventional shell-and-tube heat exchangers.

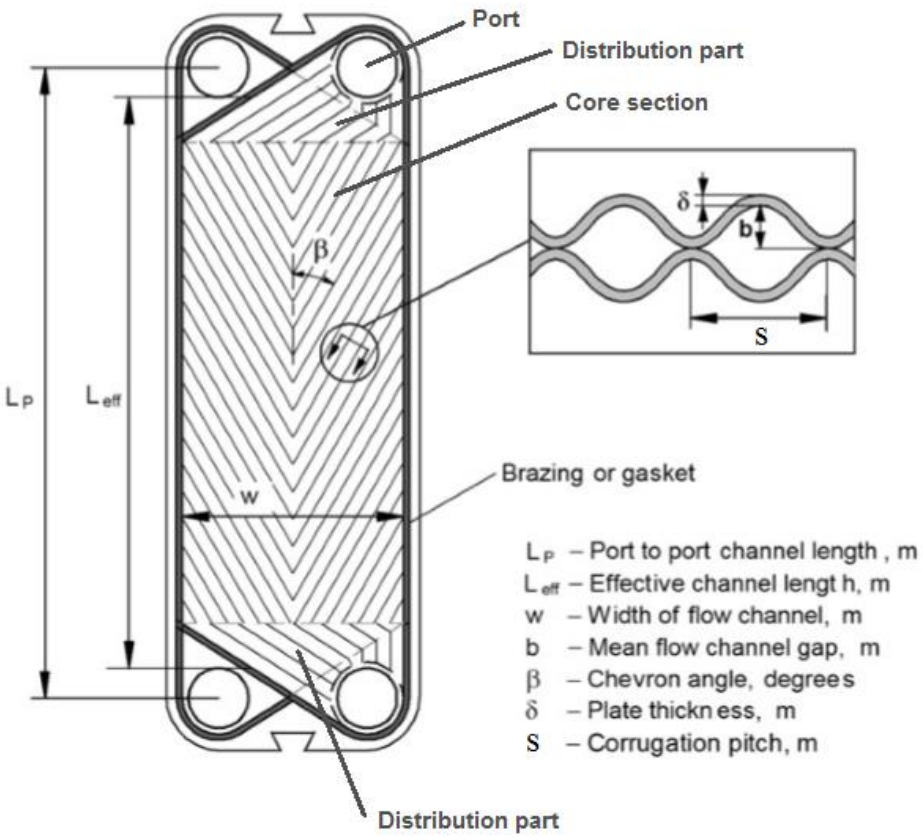

Figure 29. Schematic of chevron plate-corrugation pattern

The flow pattern of the fluids can be arranged as single-pass, two-pass or multi-pass. This is illustrated in Figure 30 (Kaori Heat Treatment Co. Ltd., 2017). In a standard single-pass arrangement, the working fluid flows in the same direction through the unit. In a multi-pass arrangement, the fluid can change its flow path direction. The heat exchanger can be designed with different number of passes, both on the hot and cold side. An increased number of passes through the exchanger leads to a lower cross-sectional area for heat transfer per pass; which causes a higher mass flux.

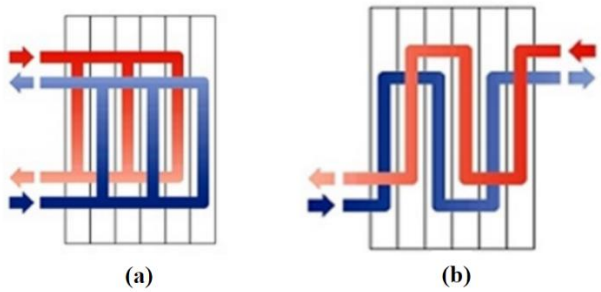

Figure 30. Schematic of the flow arrangement in a plate heat exchanger: (a) Single-single pass arrangement, (b) Multi-pass arrangement (three-three pass).

Coaxial heat exchanger

A coaxial heat exchanger consists of an outer shell with a number of smaller tubes inside, coiled together in a spiral formed and compact construction. The hot fluid flows through the inner tubes, while the cold fluid flows in between the inner tubes; usually in a counter-flow arrangement. The design is flexible, and the performance can be adapted by varying the number of inner tubes, length and internal dimensions. A schematic is shown in Figure 31 (Frigomec S.p.A., 2017, Pampanin, 2017).

Figure 31. Schematic of a coaxial heat exchanger. The cross-section is shown to the right.

The compact design of the heat exchanger prevents thermal fatigue. It increases the efficiency and reduces the overall size. The centrifugal forces, caused by fluid flow through the coil, give rise to a secondary current in the form of a double vortex. These improve the heat transfer significantly, but at the expense of increased pressure drop (VDI, 1993). The heat exchanger is ideal for high-temperature, high-pressure and low to moderate flow applications.

7.3.3 Economic aspects

The energy saving of using a heat pump, when compared to an alternative heating system with efficiency η, is defined by Equation (7.6). The efficiency of electric heaters is about 1 and of fuel-fired boilers between 0.5-0.95 (Maina and Huan, 2015). Utilizing a heat pump for production of hot water with CO_2 as refrigerant, and assuming an average COP of 3, can reduce the energy consumption by 67 % compared to electric heating. The saving is even larger compared to heating by fuel-fired boilers. Thus, there is a large economic potential for saving money if the refrigeration cycle is designed with heat recovery in the gas cooler.

$$\Delta E = Q_{gc}\left(\frac{1}{\eta} - \frac{1}{COP_{heating}}\right) \tag{7.6}$$

7.4 Air as refrigerant

Air is considered a natural working fluid, with GWP and ODP of zero (Andou and Okuda, 2004). It is a non-toxic, non-flammable fluid. When applied as working fluid to refrigeration systems, it offers design of a plant with low pressure levels; hence featuring user safety. Air is mainly used as refrigerant in air conditioning systems. It is implemented on many airplanes; in a configuration commonly known as “the Brayton refrigeration cycle”. Since air is widely available, the price is low. There is no need for disposal or refill during operation. Air cycle plants feature much higher fluid flow rates than conventional refrigeration systems; with a

sensible heat storage capability being one order of magnitude smaller than the latent heat storage, and with moderate/high expansion and compression ratios (Giannetti and Milazzo, 2014). It differs from a vapour compression system in that the working fluid always is in the gas phase, instead of having the working fluid alternately vaporized and condensed. While practical vapour compression systems normally dissipate work in a throttling valve to avoid two-phase expansion, the air cycle features expansion work recovery. The work developed by the turbine of a Brayton refrigeration cycle is significant compared to the compressor work input. A schematic is shown in Figure 32 (Moran et al., 2012b), together with the corresponding T-s diagram. This standard configuration is often adapted by integrating a regenerative heat exchanger or additionally coolers, dependent on the required refrigeration temperature.

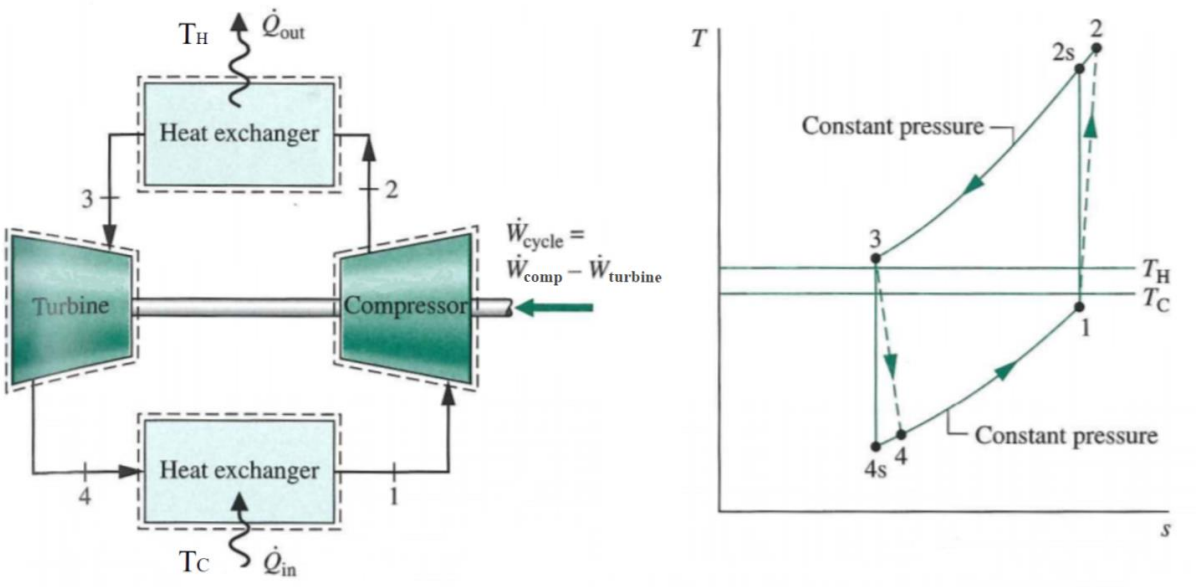

Figure 32. Schematic of a standard Brayton refrigeration cycle

The isentropic turbine efficiency and total power input of the air refrigeration cycle are defined by Equation (7.7) and (7.8). The compressor work was defined by Equation (7.4).

$$\eta_{is} = \frac{(\dot{W}/\dot{m})}{(\dot{W}/\dot{m})_{is}} = \frac{h_3 - h_4}{h_3 - h_{4s}} \tag{7.7}$$

$$\dot{W}_{tot} = \dot{W}_{comp} - \dot{W}_{turbine} \tag{7.8}$$

As air has a considerably lower specific heat capacity than other refrigerants, the COP of an air cycle will be lower than that of a vapour compression cycle. This is amplified by the fact that the vapour compression cycle features larger enthalpy differences; due to the latent heat released during evaporation. The Brayton cycle only operates with release and absorption of sensible heat, which usually is seen to be many times lower than the latent heat release. Commercially available air refrigeration systems are consequently rare. Nevertheless, it has been shown that the thermodynamic drawbacks of the air cycle narrow down progressively when the cold space temperature is lowered; making air competitive as a working fluid at ultra-low temperatures (Hattori, 2017).

Using an open air cycle configuration in which the evaporator is removed, means that some of the atmospheric natural humidity will condense when the dew point temperature is reached (Giannetti and Milazzo, 2014). Water may condense in or directly after the expander; hence releasing latent heat and decreasing the temperature drop through the turbine. For a given refrigeration temperature, this means that the compression ratio must be increased compared to the dry air case; leading to an increased compressor work and reduced COP. Moist air in the cycle may also lead to operational problems, as the condensed water can be troublesome if the turbine outlet temperature falls below 0 °C and icing occurs. In such cases, a de-humidification process can be performed on the process flow before entering the turbine; where the moisture in the air is reduced by collecting the condensed water from the mixture.

7.4.1 Psychrometric principles

In a moist air sample, the dry air and water vapour can each be treated as it was a pure component. The overall mixture and each mixture component will behave as ideal gases at the states under present consideration (Moran et al., 2012c). Each mixture component (i) is considered to act as it existed alone in the total volume (V) at the mixture temperature (T), exerting a part of the pressure (P_i), while obeying the ideal gas equation of state, Equation (7.9). The mixture pressure is the sum of the partial pressures of the dry air and the water vapour, Equation (7.10).

$$P_i = \frac{m_i(\bar{R}/M_i)T}{V} \tag{7.9}$$

$$P_{tot} = P_a + P_v \tag{7.10}$$

Moist air is commonly described by the RH and the absolute humidity (ω). The RH was defined in Chapter 2.2, and is given by Equation (7.11), where y_v and $y_{v,sat}$ denotes the mole fraction of water vapour in a moist air and a saturated moist air sample, at the same mixture temperature and pressure. The absolute humidity is defined as the ratio of the mass of water vapour to the mass of dry air, Equation (7.12).

$$RH = \frac{y_v}{y_{v,sat}}\Big]_{T,P} = \frac{P_v}{P_g}\Big]_{T,P} \tag{7.11}$$

$$\omega = \frac{m_v}{m_a} \tag{7.12}$$

When the partial pressure of the water vapour corresponds to the saturation pressure of water at the mixture temperature, the mixture is said to be saturated. In this point, partial condensation of water vapour will occur if the temperature is reduced. The saturation temperature corresponding to the partial vapour pressure is called the *dew point* temperature. A schematic is illustrated in Figure 33 (Moran et al., 2012c), where initial cooling at constant pressure and vapour fraction occurs from state 1 to d, while further cooling yields condensation of some of the water vapour initially present. At the final state, the gas phase of dry air is in equilibrium with saturated water, and the partial pressure of the water vapour will be lower than at the initial

state. If no condensation occurs during the cooling process, the partial vapour pressure, and hence the absolute humidity, will remain constant.

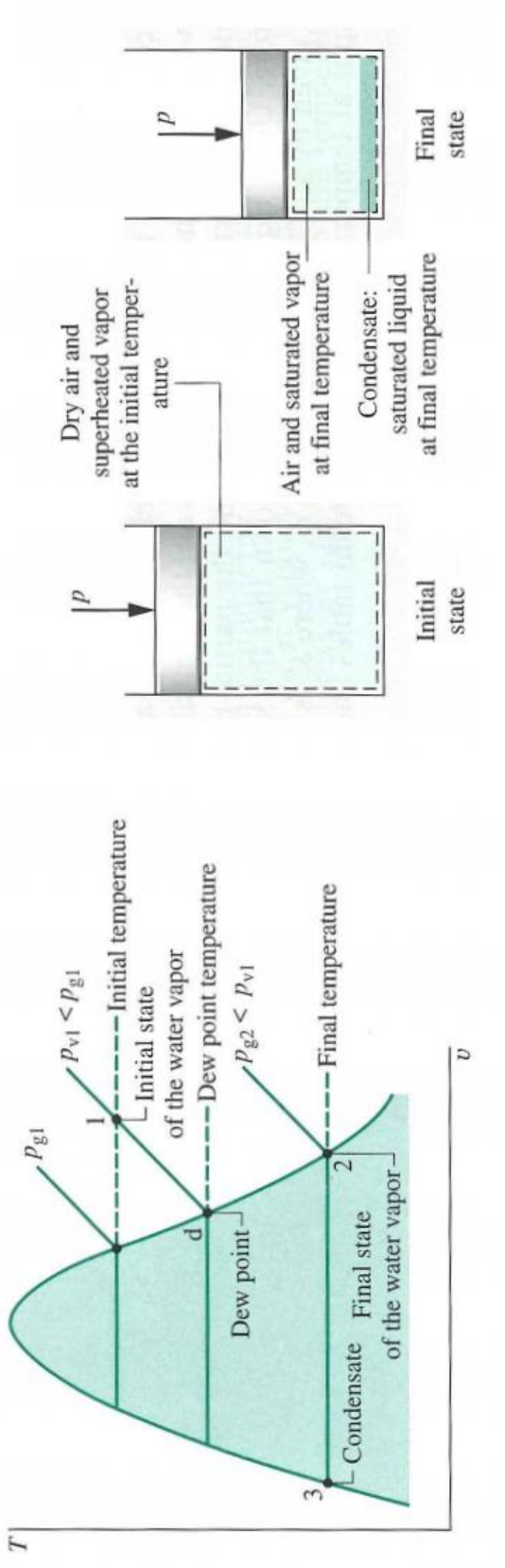

Figure 33. Cooling of moist air; illustrated in a T-v diagram for the water vapour in the air-water mixture

The basic equations presented in Chapter 7.1 apply also for an air refrigeration cycle. However, while simple vapour compression systems require only two independent intensive properties to specify a thermodynamic state point, three intensive properties must be known to fix the states in an air refrigeration system with moist air. This introduces additional computational effort.

In a cooling and dehumidification process the air is cooled sensibly, at the same time as some of the moisture is removed (Moran et al., 2012a). This is obtained when a moist air stream flows across a cooling coil at constant mixture pressure, and is cooled to at temperature below its dew point temperature. Figure 34 (Moran et al., 2012a) shows a schematic of a dehumidifier using this principle. Some of the water vapour initially present, will form dew on the surface of the coil. It will further condense, and a saturated moist air mixture exists the dehumidifier section. The condensate is extracted at the bottom of the schematic, while the saturated moist air stream is passed through a following heating section; where the temperature is increased and the RH reduced. The cooling and heating demands depend on the application area, and on the required water removal from the mixture, which is given by the conditions of the inlet stream.

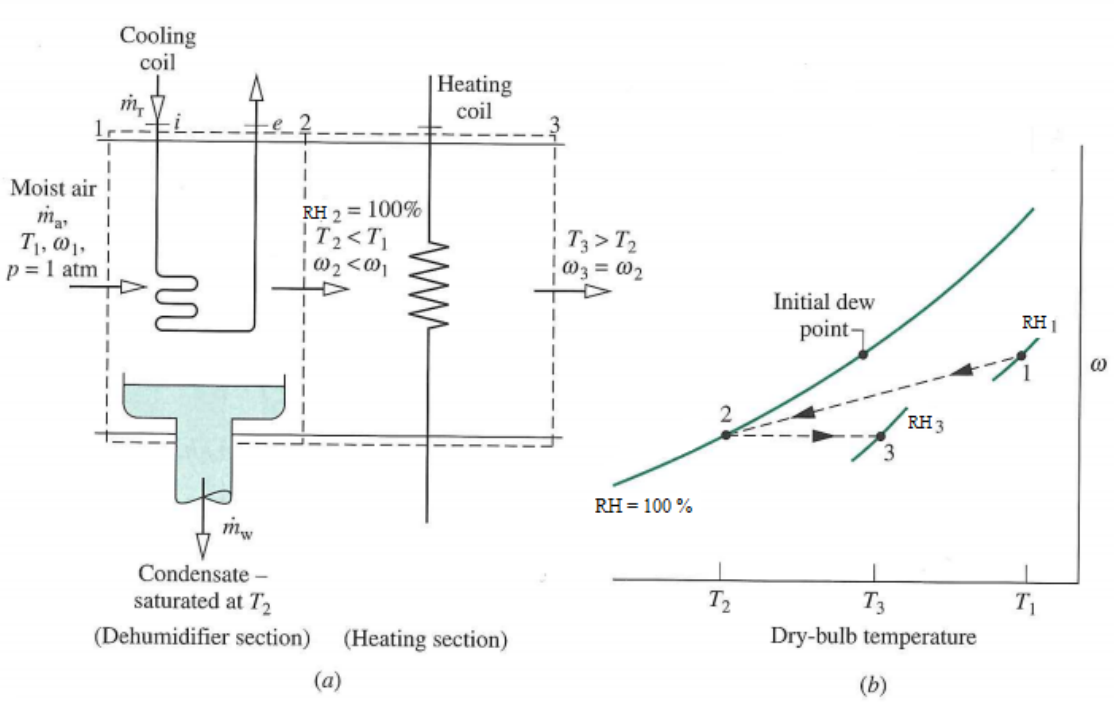

Figure 34. Dehumidification. (a) Schematic of the configuration, (b) representation in a psychrometric chart.

7.5 Flake ice drum

7.5.1 Materials

In order to maximize heat transfer in the FID, the selection of drum wall materials is important. The material should exhibit high thermal conductivity, and at the same time being able to withstand internal stresses induced by fluid flow in the construction. Table 9 (AZoM, 2012, Dieseth, 2016) shows the thermal conductivity, ultimate tensile strength (UTS) and costs of some commonly used metals. The properties are evaluated in EES at an evaporation temperature of -30 °C. The UTS denotes the maximum stress that the material can withstand while being stretched and pulled before breaking (Rao, 2017).

Table 9. Material properties of drum wall metals

	Thermal conductivity [W/mK]	UTS [MPa]	Price [NOK/kg]
Carbon steel (AISI1035)	71.6	585	4.081
Stainless steel (AISI302)	15.0	515	26.378
Aluminium	233.5	45	15.235

7.5.2 Heat transfer mechanisms

The heat transfer in the flake ice machine is governed by convection and conduction. Convection occurs both when heat is transferred from the incoming water to the ice layer, and by fluid flow through the refrigerant pipes in the drum wall. Conduction takes place by heat transfer through the growing ice layer and through the drum wall (Incropera et al., 2013e). A schematic of the freezing process is shown in Figure 35 (Cao et al., 2015).

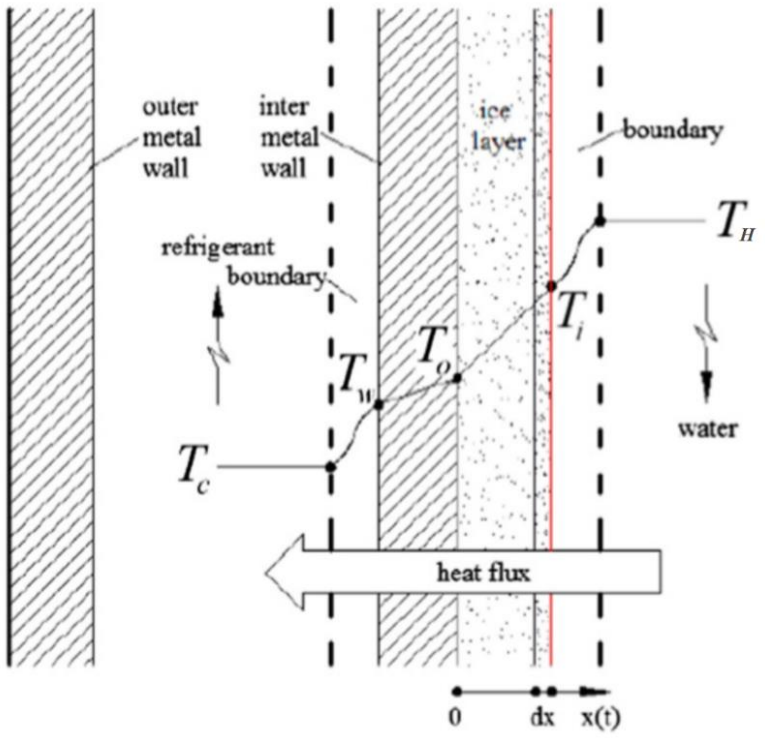

Figure 35. Schematic of the dynamic ice layer growth process in the FID

The freezing process of water is characterized by phase change, and it can be regarded as one-dimensional (Cao et al., 2015). In this simplified heat transfer model, there is a migrating interface between the solid and liquid phase during the dynamic process; where the latent heat of fusion is released at this interface. The position of the ice layer is a time dependent property. The phase change process begins at position x=0, and migrates along the x-axis when the layer grows. This is illustrated in Figure 35. As the thickness of the ice layer increases, the heat transfer coefficient gradually decreases; due to increased thermal resistance of the ice layer.

By applying heat and mass conservation, governing equations can be derived. There are two boundary conditions: energy conservation (Equation (7.13)) and temperature continuity at the inner drum wall boundary between the solid and the liquid refrigerant phase (Equation (7.14)). The final equations for the overall heat transfer coefficient of the structure and the ice growth rate are defined by Equation (7.15) and (7.16) respectively, where the subscript i accounts for the different materials used in the drum wall (Cao et al., 2015, Incropera et al., 2013b).

$$q_{ice} - q_w = (\rho u h)_{ice} - (\rho u h)_w = 0 \tag{7.13}$$

$$T_b = T_W \tag{7.14}$$

$$U = \frac{1}{\frac{1}{\alpha_{CO2}} + \sum_i \frac{\delta_i}{k_{W,i}} + \frac{x}{k_{ice}} + \frac{1}{\alpha_w}} \tag{7.15}$$

$$\frac{dx}{dt} = \frac{\frac{T_{ice} - T_{ref}}{\frac{1}{\alpha_{CO2}} + \sum_i \frac{\delta_i}{k_{W,i}} + \frac{x}{k_{ice}} + \frac{1}{\alpha_w}} - \alpha_w (T_W - T_{ice})}{\rho_w h_{fusion,w}} \tag{7.16}$$

8 Simulation model of flake ice system

The model of the flake ice system is developed in Engineering Equation Solver (EES), which is a simulation program that numerically can solve coupled non-linear algebraic and differential equations. EES provides many built-in mathematical and thermophysical property functions useful for engineering applications. It includes a thermodynamic property database of high accuracy that can be used together with the equation solving capability. This makes the program especially suitable for simulation of the snowmaking system, since it depends on an extensive use of thermophysical relations. The EES code for the flake ice system is given in Appendix D.

The model is an improvement of an adapted system proposed in the pre-study, which EES model was first developed by Dieseth (2016). The original model was implemented with a snow production of 50 tons/day and designed with a subcritical CO_2 heat recovery process. This model was in the pre-study modified to operate in transcritical mode, and with a snow production of 100 tons/day. The gas cooler was designed for heat recovery by DHW heating, in terms of a removable container configuration, and a case was performed to study how this system could be realized based on costs, market interest and thermodynamic performance.

In this thesis, the model from the pre-study is used directly as basis for further development. Thermodynamic correlations for the gas cooler are included, and an optimization process of the gas cooler pressure is carried out. Different commercial heat exchanger models are evaluated in order to find the best thermodynamic performance. Due to problems with complete integration of the different functionalities required by the calculations in EES, optimization is done in Excel. The results from Excel is imported to EES by developing simplified heat transfer characteristics, and the separate EES files from the pre-study are combined into one. Also, better suited correlations for the FID are included, and the dynamic ice growth process is studied more in detail. The main objective of the simulations is to investigate how the performance of the combined cycle changes (a) when the gas cooler pressure is optimized, and (b) when the production rate is doubled; without a simultaneous drop in the efficiency of the snow production. The simulation model only takes into account the stationary part of the combined refrigeration and heating system. The removable container configuration from the DHW case remains unchanged from the pre-study.

8.1 System design and adaption

The model is based on fundamental thermodynamics (Dieseth, 2016). This includes energy and mass balances, as well as empirical heat transfer correlations. The system is considered an indirect CO_2 system; where heat recovery from the refrigeration system is featured by a heat pump cascade (Chapter 7.3.1). The main components are: two compressors, an intercooler between the compressor stages, a gas cooler, a SGHX, an expansion valve, an evaporator/condenser (cascade heat exchanger), a liquid separator, a centrifugal pump and the FID. The cascade heat exchanger connects the refrigeration system from the snow machine with the heat recovery cycle. A schematic is shown in Figure 36. In the following discussion, the snow machine and the interrelated refrigeration system; containing the FID, liquid separator, centrifugal pump and the hot side of the cascade heat exchanger, is denoted the “bottom cycle”.

The upper part of the heat cascade is denoted the “heat recovery cycle”. The reader should note that the main focus of the analysis is on the thermodynamic performance of the components in the combined heating and refrigeration system; studied in combination with the efficiency of the dynamic water-to-snow conversion at the inner drum wall. Energy consumptions of equipment related directly to the snowmaking process, such as the rotating scraper and other electrical regulating and pumping devices, are not included in the thermodynamic analysis. This aspect will be elaborated in Chapter 11.5.

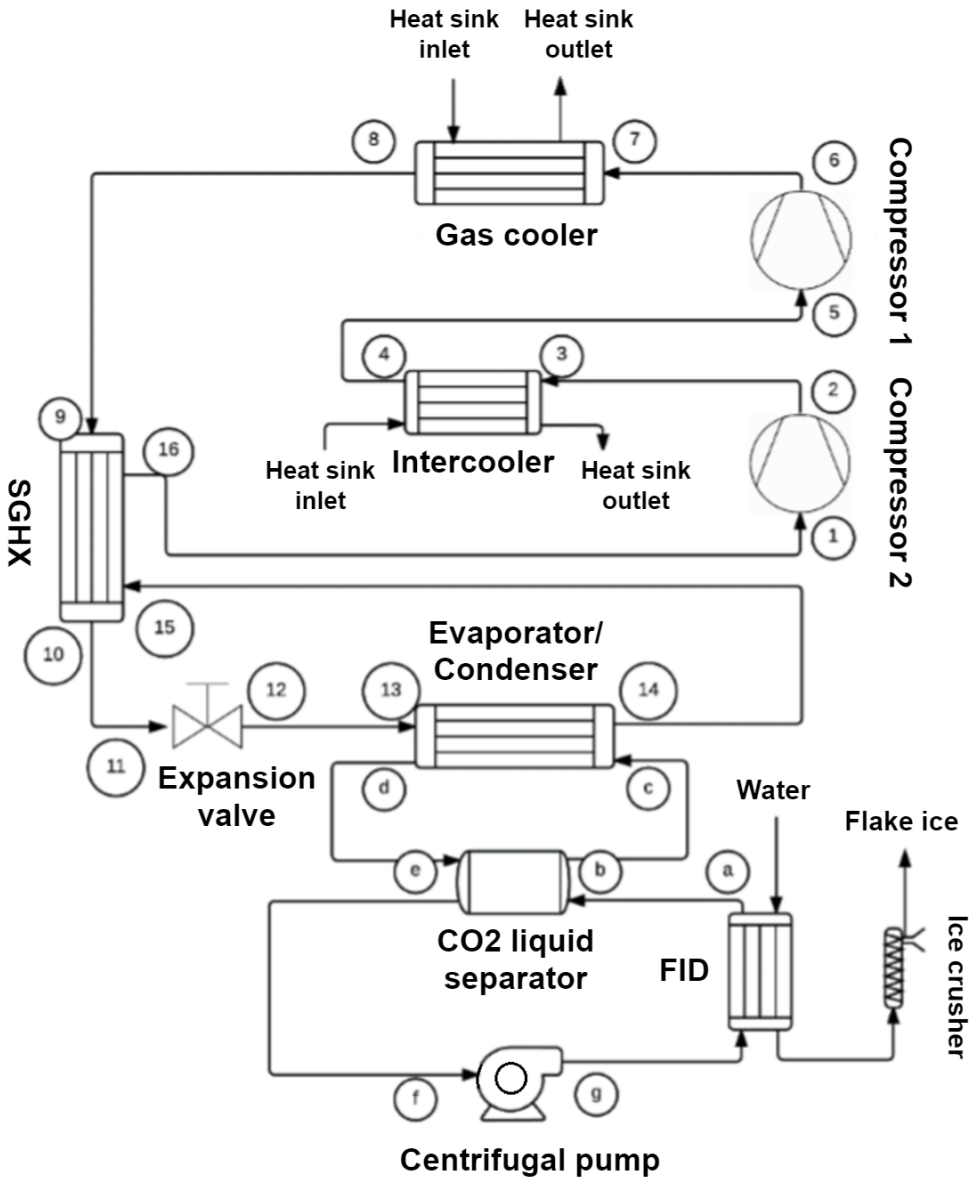

Figure 36. A schematic of the flake ice system

The state points 1-16 shown in Figure 36 are presented in Appendix B, with the corresponding log P-h diagram presented in Appendix A. The following simplifications and assumptions for the thermodynamic model have been made:

- Negligible heat loss to the ambient.
- The enthalpy through pipelines are constant.

- All inlet water to the FID is turned into snow.
- Energy use of the separate water cooling system is not included.
- Negligible pressure drops in pipeline 12-13 because the expansion valve is placed very close to the evaporator (short pipe length).

The choice of components in the system is based on the component choice of the original model. Changes are only made if the design is no longer suitable or within operational range of the components. All heat exchangers, except for the gas cooler, are modelled as counter-flow PHEs; based on commercially available models by Alfa Laval. An overview of the models is presented in Table 10 (Alfa Laval, 2016a, Alfa Laval, 2016b, Dieseth, 2016). Gas cooler design will be discussed further in Chapter 8.3.

Table 10. Heat exchanger models and relevant data

	Model	Width [mm]	Height [mm]	Number of plates	Q [kW]	U-value [W/m^{2}K]	ΔT_{LM} [K]	Area [m^2]
Evaporator/ condenser	AC1000DQ	356	615	154	442	2638	5.00	33.54
Intercooler	AXP52	160	466	48	79	790	27.41	3.67
SGHX[9]	AXP27	160	250	17	21	-	-	-

The models of both the intercooler and the SGHX are changed from those in the pre-study. The water flow rate through the intercooler was first adjusted to observe whether the original model could obtain the given heat duty without extending the maximum number of plates given by the manufacturer. This yielded too low cool-down, and a heat exchanger with larger thermal length was chosen to ensure an acceptable discharge temperature. The final water flow rate was set to 2 kg/s. The cascade heat exchanger and SGHX had fixed flow rates by the system configuration; with less degrees of freedom. The heat transfer area had to be changed respectively, in order to meet the required duty from the snowmaking load, as well as ensuring sufficient preheat and subcooling. Design of the compressor stages and selection of commercial models are not included in the simulation model.

The inlet water temperature from the grid is set to 8 °C. The grid temperature is assumed to be equal to the temperature of the ground water at the site; estimated by the sum of the annual average air temperature in Trondheim and 1°C (Eikevik, 2017).

The mass flow rate of CO_2 in the bottom cycle must be set manually in the script, and it is determined based on the following three criteria:

1. The mass flow must ensure the wanted snow conversion
2. Pressure drop in the bottom cycle must be within acceptable limits; (a) the total pressure drop through the refrigerant pipes in the FID should not exceed 1-2 bar, and (b) The maximum pressure drop of pipe sections and in heat exchangers is 1 bar (Hafner, 2017, Pesonen, 2016).

[9] Area consideration for the SGHX is not included as it follows a different calculation procedure than the other models (Chapter 8.2.1).

3. The refrigerant CO_2 gas should only be partwise evaporated through the FID, in order to enhance heat transfer. The outlet gas quality should be about 0.5 (Chapter 9.1).

The mass flow rate was found from a procedure with basis in complete evaporation. Firstly, the theoretical flow rate was calculated; assuming a gas quality of 0 and 1 at the inlet and outlet of the FID respectively. This represents the lowest possible flow rate to provide the given production rate. The theoretical mass flow was secondly adjusted by trial-and-error; by evaluating the changes in pressure drop, outlet enthalpy and gas quality of the FID. A final mass flow of 3 kg/s was chosen for the improved system, which satisfies the criteria above.

The height and diameter of the drum wall are based on the size of commercially available flake ice makers (GEA, 2016). The FID is modelled with straight refrigerant pipes in the wall construction (Figure 41). The dimensions are set equal to that of the original model, but new pressure drop correlations are introduced. In order to keep the pressure drop within acceptable limits, the number of refrigerant pipes are doubled to 600. The dimensions of the centrifugal pump in the bottom cycle are adjusted accordingly; to account for the increase in required lifting height. The pressure lift above the pump should equal the total pressure drop in the bottom cycle. The required work of the centrifugal pump is neglected in the COP calculations; as it is very small compared to the compressor work. This also makes it easier to compare the system performance with the previous simulation models, which use the same procedure. Dimensions of the other components in the bottom cycle will not be discussed further; and the EES script can be used as a reference (Appendix D).

The dynamic ice growth process on the inner drum wall of the flake ice machine is modelled by the procedure flakeicedrum; studied in combination with the performance of the transcritical CO_2 cycle. The drum wall is composed of a core that is made of aluminium, surrounded by an outer layer on both sides (Figure 41). Use of different materials in the outer layers are explored and compared in EES; to find which material provides the best thermal efficiency for the snowmaking.

The model is designed by fixing the CO_2 outlet temperature of the intercooler at 24 °C. This value is found by trial-and-error; with basis in two main operational aspects. Firstly, as the aim is to find the point where heat recovery from the system is maximized at simultaneous minimum compressor work, it is desirable to have a high discharge temperature out of the 2^{nd} compressor stage. Secondly, this temperature must not exceed 130 °C (which is regarded as the operational limit for commercial piston compressors) (Chapter 8.2.4). Therefore, it is recommended to fix the temperature to a level where the discharge temperature approaches, but does not exceed, the maximum limit. By the given design, a discharge temperature of 129.7 °C is obtained; equal to that in the pre-study, which eases the comparison. This temperature can easily be adjusted by changing the flow characteristics and dimensions of the intercooler, if more care should be taken regarding the compressor.

The cool-down temperature on the hot side of the SGHX is set to 3.95 °C, equal to that in the pre-study. This yields a relatively constant mass flow rate of CO_2 in the heat recovery cycle; easing the comparison of system performance.

The separate EES files from the pre-study have been included in the main program. This highly simplifies the solution procedure. Instead of solving the system manually by iteration, the system of equations and variables are solved automatically by the program. This reduces the error of calculation, and it provides more accurate results. The EES procedures of the intercooler and cascade heat exchanger are integrated directly into the main program. The performance of the SGHX is included by simultaneously running separate simulations around the dimensioning point; and thereby integrating suitable temperature and pressure characteristics in the main program. Pipe dimensions and U-values of the heat exchangers are adjusted during integration; in order for the program to converge. As EES had problems implementing a variable pressure drop in some of the pipe sections in the heat recovery cycle, these are modelled by manually fixing the pressure drop.

The flake ice machine will supply a ski track in Granåsen at the start-up of the season. The track will have the same dimensions as the original model; and 6000 m^3 of snow is required to produce a 2.5 km long ski track that is 6 m wide and 0.4 m deep. An increase in production capacity of 50 tons/day will halve the operational time of the snow machine; which accordingly must operate 30 days each season, based on a 24-hours production each day. The skiing season is assumed to begin at November the 1st. This requires the production to occur mainly during September and October. The simulation model does not take into consideration melting rate of snow on the track or in the pile of snow during production; which is a drawback of the model. This topic will be extended in Chapter 11.

The removable part of the heat recovery cycle was studied separately from the EES model in the pre-stud. It consists of a 40' standard container; with a series of hot water tanks placed on the inside, and with necessary piping, temperature sensors and mounting devices. The container is filled with cold water from the grid at the customer site. It is transported to Granåsen where it is connected to the stationary heat recovery system, and where the cold water will exchange heat with hot CO_2 gas in the gas cooler. The target temperature of the DHW is 80 °C, and a circulation pump is needed to push the water through the system. The removable part will not influence on the performance of the stationary part, except that the required pump work on the water side should be included in the optimization process of the gas cooler.

8.2 Correlations used in the EES model

8.2.1 Heat transfer

Overall heat transfer coefficient

In order to evaluate the performance of a heat exchanger, it is essential to determine the overall heat transfer coefficient (U-value) (Incropera et al., 2013f). It is defined in terms of the total thermal resistance to heat transfer on the warm fluid side, the plate wall and the cold fluid side, given by Equation (8.1). If the heat transfer coefficient on the cold side is sufficiently small, the plate thermal resistance can be neglected as it contributes little to the overall U-value.

$$U = \frac{1}{R_H + R_W + R_C} = \frac{1}{\frac{1}{\alpha_H} + \frac{\delta}{k_W} + \frac{1}{\alpha_C}} \tag{8.1}$$

One-phase flow in the intercooler

The intercooler is characterized by one-phase flow on each side of the heat exchanger. The Martin correlation for one-phase flow is used, Equation (8.2) (García-Cascales et al., 2007).

$$Nu = 0.122 Pr^{\frac{1}{3}} \left(\frac{\mu_f}{\mu_W}\right)^{\frac{1}{6}} (f Re^2 \sin(2\beta))^{0.374} \quad (8.2)$$

The friction factor (f) is defined by Equation (8.3), with empirical constants f_0 and f_1 given by the Reynolds number of the fluid flow, Equation (8.3) and (8.4). β is set to 45° in the EES model.

$$\frac{1}{\sqrt{f}} = \frac{\cos(\beta)}{\left(0.18\tan\beta + 0.36\sin\beta + \frac{f_0}{\cos\beta}\right)^{1/2}} + \frac{1-cos\beta}{\sqrt{3.8 f_1}} \quad (8.3)$$

$$f_0 = \begin{cases} \frac{64}{Re}, & Re < 2000 \\ (1.8\, log_{10}(Re) - 1.5)^{-2}, & Re \geq 2000 \end{cases} \quad (8.4)$$

$$f_1 = \begin{cases} \frac{597}{Re} + 3.85, & Re < 2000 \\ \frac{39}{Re^{0.289}}, & Re \geq 2000 \end{cases} \quad (8.5)$$

The heat transfer coefficient is found from the definition of the Nusselt number, where d_e is the equivalent diameter of the plate heat exchanger. This diameter is used as length scale for calculating the Reynolds number, Nusselt number and friction factor in PHEs.

$$Nu = \frac{\alpha_f d_e}{k_f} \quad \rightarrow \quad \alpha_f = \frac{Nu k_f}{d_e} \quad (8.6)$$

$$d_e = \frac{4 w H_i}{2(w + H_i)} \approx 2 H_i \quad (8.7)$$

Evaporation of CO_2

Evaporation of CO_2 occurs both in the refrigerant pipes of the FID and on the cold side of the evaporator/condenser. The heat transfer coefficient was developed by Choi et al. (2007) under the condition of forced flow. It can be regarded as a two-phase heat transfer correlation, where the first part accounts for heat transfer by nucleate boiling, while the second part describes heat transfer in terms of forced convective evaporation. The relation is given in Equation (8.8).

$$\alpha_{evap,\, CO_2} = S\alpha_{nb} + F\alpha_{evap} \quad (8.8)$$

The factors S and F are empirical terms, defined by Equation (8.9) and (8.10). S is the nucleate boiling suppression factor, and F is a factor developed to account for the increased convective turbulence; due to the presence of the vapour phase.

$$F = 0.05({\varphi_f}^2) + 0.95 \quad (8.9)$$

$$S = 7.269({\varphi_f}^2)^{0.0094} Bo^{0.2814} \quad (8.10)$$

The term ${\varphi_f}^2$, defined by Equation (8.11), is a two-phase frictional multiplier. It is a function of the Lockhart Martinelli parameter (X_{tt}), Equation (8.12). The boiling number (Bo) is a dimensionless number that represents the amount of vapour formation in the evaporator, Equation (8.13).

$$ {\varphi_f}^2 = 1 + \frac{C}{X_{tt}} + \frac{1}{{X_{tt}}^2} \tag{8.11} $$

$$ X_{tt} = \left(\frac{\mu_l}{\mu_g}\right)^{1/8} + \left(\frac{1-z}{z}\right)^{7/8} + \left(\frac{\rho_g}{\rho_l}\right)^{1/2} \tag{8.12} $$

$$ Bo = \frac{\frac{\dot{V}}{A}}{G h_{fg}} \tag{8.13} $$

The Chisholm parameter (C) is defined according to the flow characteristics. Since both heat exchangers are characterized by liquid-vapour flow conditions, with both the water and the CO_2 flow being turbulent, the value of C is set to 20 (Choi et al., 2007). In the correlations above, A represents the total heat transfer area with respect to the fluid flow.

The liquid heat transfer coefficient (α_{evap}) in terms of forced convective evaporation, is defined by the Dittus-Boelter correlation, Equation (8.14) and (8.6). For the FID with circular pipes, the equivalent diameter is replaced by the hydraulic diameter (d_h), Equation (8.36).

$$ Nu = 0.023 \left(\frac{G(1-z)d_e}{\mu_f}\right)^{0.8} {Pr_f}^{0.4} \tag{8.14} $$

The heat transfer coefficient for nucleate boiling is given by Equation (8.15) and (8.6), where the reduced pressure is given by the ratio of the saturation pressure in the evaporator and the critical pressure of CO_2, Equation (8.16).

$$ \alpha_{nb} = 55 {P_r}^{0,12} (-0.434 \ln(P_r))^{-0.55} M^{-0.5} q^{0.67} \tag{8.15} $$

$$ P_r = \frac{P_{sat}(T_{evap})}{P_{crit}} \tag{8.16} $$

Condensation of CO_2 in the evaporator/condenser

The condensation heat transfer coefficient is calculated using a correlation defined by Equation (8.17) (Park and Hrnjak, 2009).

$$ \alpha_{cond,CO_2} = \frac{{k_f}^{2/3} {C_{p,f}}^{1/3}}{{\mu_f}^{7/15}} \left[\frac{1-z}{z}\left(\frac{\rho_l}{\rho_g}\right)^{\frac{1}{2}} + 1\right] \tag{8.17} $$

Water heat transfer coefficient in the FID

The water flows on the inner cylindrical and subcooled surface of the drum wall, where the physical properties can be regarded as constant (Dieseth, 2016). The heat transfer coefficient is defined by Equation (8.18) and (8.19), where the empirical constant (B) is determined by the value of the critical Reynolds number; $Re_{crit} = 5 \cdot 10^5$ (Incropera et al., 2013d).

$$\alpha_w = 0.037\left(\frac{k_w}{H_{FID}}\right)\left[\left(\frac{u_w H_{FID}}{\nu_w}\right)^{\frac{4}{5}} - B\right] Pr_w^{\frac{1}{3}} \tag{8.18}$$

$$B = 0.037 Re_{crit}^{\frac{4}{5}} - 0.644 Re_{crit}^{\frac{1}{2}} \tag{8.19}$$

Modelling the SGHX

The SGHX is modelled as a counter-flow plate heat exchanger, with supercritical CO_2 on the hot side and subcritical CO_2 at the cold side. A schematic of the flow configuration is shown in Figure 37. To obtain a numerical solution, state equations must be derived and integrated numerically through the heat exchanger, Equation (8.20) and (8.21) (Nellis and Klein, 2009). These equations are obtained from differential energy balances of the hot and cold stream.

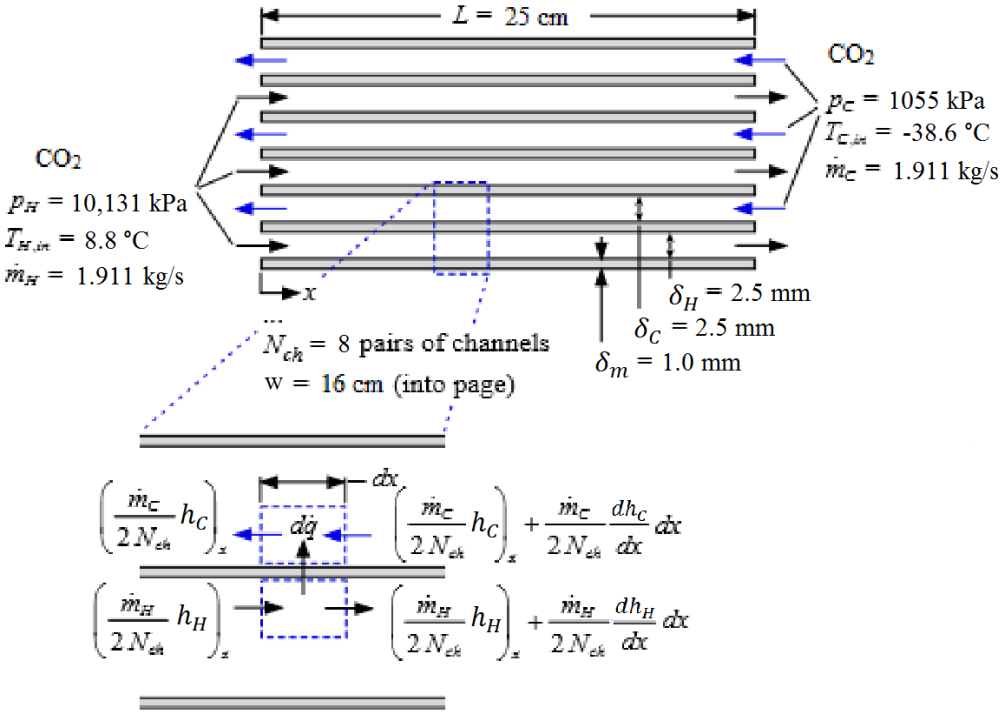

Figure 37. Plate heat exchanger in a counter-flow configuration

$$\frac{dT_H}{dx} = -\frac{2N_{ch}(T_H - T_C)}{\dot{m}_H C_{p,H}\left(\frac{1}{\alpha_H w} + \frac{\delta_W}{k_W w} + \frac{1}{\alpha_C w}\right)} \tag{8.20}$$

$$\frac{dT_C}{dx} = -\frac{2N_{ch}(T_H - T_C)}{\dot{m}_C C_{p,C}\left(\frac{1}{\alpha_H w} + \frac{\delta_W}{k_W w} + \frac{1}{\alpha_C w}\right)} \tag{8.21}$$

The state equations must be integrated from x=0 to x=L. This is done by using the Integral command in EES and a shooting technique, to find the outlet temperatures of the hot and cold stream. The iteration required by the shooting technique is accomplished by using the optimization algorithm in EES. The local heat transfer coefficients on the hot (α_H) and cold (α_C) side of the heat exchanger are obtained using the built-in procedure DuctFlow_local, which returns the local heat transfer coefficient for counter-current flow through a rectangular duct.

Further description of the corresponding equations can be found in the EES script, Appendix D.

Modelling the gas cooler

The theoretical approach for modelling a PHE and a coaxial heat exchanger differs considerably. Correlations must be well defined for both types.

- **Plate heat exchanger**

The plate heat exchanger is characterized by one-phase flow on both sides. The Martin correlation can be used, Equation (8.2) - (8.4), with f_1 defined by Equation (8.22). It takes into account the effect of the surface enhancement factor (φ), which describes how the chevron angle affects the size of the effective heat transfer surface. For the gas cooler, φ is set equal to 1.1 and β to 52.5° (Berntsen, 2013).

$$f_1 = \begin{cases} \frac{(1280/\varphi^2)}{Re} + \frac{5.63}{\varphi}, & Re < 2000 \\ \frac{(39/\varphi^{1.289})}{Re^{0.289}}, & Re \geq 2000 \end{cases} \tag{8.22}$$

- **Coaxial heat exchanger – hot fluid side (CO_2)**

The heat transfer coefficient is approximated by a correlation for flow through coils, which was developed by Schmidt and Gnielinski (VDI, 1993). In case of laminar flow (Re $\leq Re_{crit}$), the Nusselt number is defined by Equation (8.23), where the mean fluid temperature is used as reference for the physical properties.

$$Nu_{laminar} = \left(3.66 + 0.08\left[1 + 0.8\left(\frac{d}{D}\right)^{0.9}\right] Re^m Pr^{\frac{1}{3}}\right)\left(\frac{Pr}{Pr_W}\right)^{0.14} \tag{8.23}$$

The empirical constant (m), the average diameter of the tube (d), and the average diameter of curvature of the coil (D), is defined by Equation (8.24) – (8.28). The average diameter of the spiral (d_{spiral}) is given as a function of the number of turns (n), the pitch (H_{pitch}) and the pipe length (L), while $d_{winding}$ denotes the projected diameter of the winding.

$$m = 0.5 + 0.2903\left(\frac{d}{D}\right)^{0.914} \tag{8.24}$$

$$d_{spiral} = \frac{L}{n\pi} \tag{8.25}$$

$$d_{winding} = \sqrt{d_{spiral}^2 - \left(\frac{H_{pitch}}{\pi}\right)^2} \tag{8.26}$$

$$D = d_{winding}\left[1 + \left(\frac{H_{pitch}}{\pi D_{winding}}\right)^2\right] \tag{8.27}$$

$$Re_{crit} = 2300\left[1 + 8.6\left(\frac{d}{D}\right)^{0.45}\right] \tag{8.28}$$

When the flow through the coil is characterized by being turbulent (Re $> 2.2 \cdot 10^{-4}$), the Nusselt number is defined by Equation (8.29) and (8.30).

$$Nu_{turbulent} = \frac{\left(\frac{\xi}{8}\right) Re\, Pr}{1+12.7\sqrt{\xi/_8}\left(Pr^{\frac{2}{3}}-1\right)}\left(\frac{Pr}{Pr_W}\right)^{0.14} \quad (8.29)$$

$$\xi = \frac{0.3164}{Re^{0.25}} + 0.03\left(\frac{d}{D}\right)^{0.5} \quad (8.30)$$

In the transition zone ($Re < Re_{crit} < 2.2 \cdot 10^{-4}$) Gnielinski has shown that the Nusselt number can be found by linear interpolation of the laminar and turbulent Nusselt numbers, Equation (8.31) and (8.32). The heat transfer coefficient is found from the definition of the Nusselt number, Equation (8.6).

$$Nu = \gamma Nu_{laminar}(Re_{crit}) + (1-\gamma)Nu_{turbulent}(Re = 2.2 \cdot 10^{-4}) \quad (8.31)$$

$$\gamma = \frac{2.2 \cdot 10^{-4} - Re}{2.2 \cdot 10^{-4} - Re_{crit}} \quad (8.32)$$

- **Coaxial heat exchanger – cold fluid side (water)**

Since there exists little theory applicable for modelling heat transfer of laminar water flow (Re < 2300) through a coaxial heat exchanger, approximations have been made. A graphical approach was used to find the Nusselt number for fully developed laminar flow to a bank of circular tubes with constant heat rate per unit of tube length. Figure 38 (Kays and Crawford, 1980) was used as basis, and the Nusselt number was found by curve fitting in Excel, Equation (8.33). Here, *s* and r_0 is the horizontal centre-to-centre distance and the radius of the inner CO_2 tubes of the exchanger.

$$Nu = \begin{cases} -12.608\left(\frac{s}{r_0}\right)^2 + 50.408\left(\frac{s}{r_0}\right) - 36.097, & \left(\frac{s}{r_0}\right) < 2 \\ 6.4949\left(\frac{s}{r_0}\right)^{1.1941}, & \left(\frac{s}{r_0}\right) \geq 2 \end{cases} \quad (8.33)$$

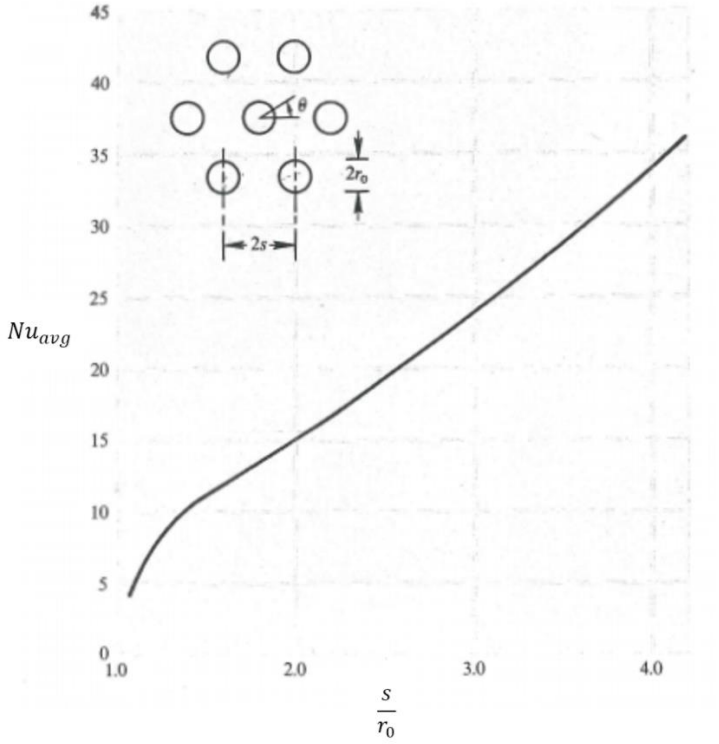

Figure 38. Nusselt numbers for fully developed laminar flow to a bank of circular tubes with constant heat rate per unit of tube length

In the case of turbulent or transitional flow, correlations developed by Gnielinski was used to calculate the heat transfer coefficient (VDI, 2010). The entrance effects are assumed to be negligible, and a correction factor of 1000 for the Reynolds number is introduced in the transitional zone (Næss, 2017).

$$Nu = \begin{cases} \dfrac{\left(\xi/_8\right) Re\ Pr}{1+12.7\sqrt{\xi/_8}\left(Pr^{\frac{2}{3}}-1\right)}, & Re > 10\,000 \\ \dfrac{\left(\xi/_8\right)(Re-1000)Pr}{1+12.7\sqrt{\xi/_8}\left(Pr^{\frac{2}{3}}-1\right)}, & 2300 < Re < 10\,000 \end{cases} \tag{8.34}$$

$$\xi = (1.8\ log_{10}(Re) - 1.5)^{-2} \tag{8.35}$$

The heat transfer coefficient is found from Equation (8.6), with the length scale defined by the hydraulic diameter instead of the equivalent diameter. The hydraulic diameter is defined by Equation (8.36) – (8.38), where A_c is the cross-sectional water flow area, p is the wetted perimeter and d_{shell} the diameter with respect to the outer shell. The variables d_{pipe} and δ_{pipe} denote the diameter and the thickness of the internal CO_2-pipes inside the shell respectively.

$$d_h = \frac{4A_c}{p} \tag{8.36}$$

$$A_c = \frac{\pi {d_{shell}}^2}{4} - n_{pipes}\frac{\pi\left(d_{pipe}+2\delta_{pipe}\right)^2}{4} \tag{8.37}$$

$$p = \pi d_{shell} + n_{pipes}\pi(d_{pipe} + 2\delta_{pipe}) \tag{8.38}$$

8.2.2 Area

The area (A) of the intercooler and the cascade heat exchanger is calculated for water-cooled counter-current plate heat exchangers. It is calculated based on the know values of the heat duty (Q), the logarithmic mean temperature difference (ΔT_{LM}) and U-values. The area calculations follow an iterative procedure. An initial U-value is guessed, and the number of plates is determined. The number of plates is based on the size of commercially available plate heat exchangers from Alfa Laval. A new U-value is then calculated based on this number, and the guessed U-value is updated. This process continues until the guessed value equals the calculated value. The correlations are presented in Equation (8.39) and (8.40) (Incropera et al., 2013c).

$$Q = UA\Delta T_{LM} \leftrightarrow A = \frac{Q}{U\Delta T_{LM}} \tag{8.39}$$

$$\Delta T_{LM} = \frac{(T_{H,in} - T_{c,in}) - (T_{H,out} - T_{c,out})}{\ln\left(\frac{T_{H,in} - T_{c,in}}{T_{H,out} - T_{c,out}}\right)} \tag{8.40}$$

The analysis of the gas cooler and the SGHX follows a different procedure. The effective heat transfer area of these models are determined from dimensions provided by the manufacturers.

8.2.3 Pressure drop

Pressure drop in plate heat exchanger

The pressure drop (ΔP) in a heat exchanger is the sum of smaller pressure drops; in terms of friction, gravitation, acceleration and manifold loss (Shah and Sekulić, 2007). The total pressure loss on the cold (evaporation) and hot (condensation) side will differ, and it is defined by Equation (8.41) and (8.42) respectively.

$$\Delta P_{\substack{tot,cold \\ /evap}} = \Delta P_{fric} + \Delta P_{man} + \Delta P_{acc} + \Delta P_{gr} \tag{8.41}$$

$$\Delta P_{\substack{tot,hot \\ /cond}} = \Delta P_{fric} + \Delta P_{man} - \Delta P_{acc} - \Delta P_{gr} \tag{8.42}$$

The frictional pressure drop is due to roughness of the channel walls in the plate heat exchanger and the colliding molecules. It is given by Equation (8.43). The mean density (ρ_m) is defined by Equation (8.44) and (8.45), for two-phase and single-phase flow respectively.

$$\Delta P_{fric} = \frac{2fG^2 H_{plate}}{d_e \rho} \tag{8.43}$$

$$\rho_{\substack{m,two- \\ phase}} = \frac{1}{\frac{z}{\rho_g} + \frac{1-z}{\rho_l}} \tag{8.44}$$

$$\rho_{\substack{m,single- \\ phase}} = \frac{\rho_{in} + \rho_{out}}{2} \tag{8.45}$$

The friction factor is defined according to whether the flow through the heat exchanger is characterized as one-phase or two-phase. In case of one-phase flow, it is calculated by Equation (8.46).

$$f = 0.8Re^{-1/4} \tag{8.46}$$

In the case of two-phase flow, the friction factor must be defined separately on each side of the heat exchanger. The frictional pressure drop on the evaporation side is calculated by the two-phase Fanning friction factor, given by the empirical correlations presented in Equation (8.47) and (8.48) (Amalfi et al., 2016). β_{max} is set to 70° in the EES script.

$$f = C\ 15.698\left(\frac{G^2 d_e}{\rho_m \sigma}\right)^{-0.475}\left(\frac{(\rho_l-\rho_g)g{d_e}^2}{\sigma}\right)^{0.255}\left(\frac{\rho_l}{\rho_g}\right)^{-0.571} \tag{8.47}$$

$$C = 2.125\left(\frac{\beta}{\beta_{max}}\right)^{9.993} + 0.955 \tag{8.48}$$

The frictional pressure drop on the condensing side is evaluated according to Equation (8.49) (Longo, 2010). This correlation is originally developed for hydrocarbons, but is assumed to provide a fairly good estimate also for CO_2.

$$\Delta P_{fric,cond} = \frac{1.9G^2}{2\rho_m} \tag{8.49}$$

The pressure drop due to gravitational forces is defined by Equation (8.50). This term is subtracted from the total loss on the condensing side since the hot fluid enters the condenser at the top of the heat exchanger. In the evaporator, the cold fluid, which is to be heated, enters at the bottom of the exchanger, and the term is added.

$$\Delta P_{gr} = \rho_m g H_{plate} \tag{8.50}$$

The acceleration loss is defined by Equation (8.51) and (8.52), for two-phase and one-phase flow respectively. It is the loss or gain in pressure, depending on whether the fluid accelerates or decelerates through the heat exchanger. The hot fluid will experience a smaller pressure loss because of deceleration, while the cold fluid will have an increase in pressure loss due to acceleration.

$$\Delta P_{\substack{acc,\ phase \\ change}} = G^2 \Delta z\left(\frac{1}{\rho_g} - \frac{1}{\rho_l}\right) \tag{8.51}$$

$$\Delta P_{\substack{acc,\ heating \\ or\ cooling}} = G^2\left(\frac{1}{\rho_{out}} - \frac{1}{\rho_{in}}\right) \tag{8.52}$$

The manifold loss, Equation (8.53), accounts for the loss due to fluid entrance at the inlet and outlet ports, and at the manifolds. It will constitute the major losses in most PHEs, and should be kept as low as possible (Dieseth, 2016).

$$\Delta P_{man} = 0.75\frac{G_p^2 N_{ch}}{\rho_m} \tag{8.53}$$

$$G_p = \frac{\dot{m}_{CO2}}{\left(\frac{\pi}{4}\right)d_p^2} \tag{8.54}$$

Pressure drop in coaxial heat exchanger

Since the geometry of the hot and cold fluid side of the coaxial heat exchanger differs considerably, pressure drop correlations must be defined separately for each side of the exchanger. Pressure drops due to gravitation and acceleration are small compared to the frictional pressure drop, and can thereby be neglected by good approximation. The total pressure drop will thus be a function of friction only.

- **Coaxial heat exchanger – hot fluid side (CO_2)**

The hot fluid side is characterized by internal flow through pipes with circular, constant cross-section. The pressure drop is defined by Equation (8.55) (Cengel and Cimbala, 2010a). The mean fluid temperature is used as reference for the physical properties.

$$\Delta P = \left(f\frac{L}{d_h}\frac{\rho u^2}{2}\right)n_{pipes} \tag{8.55}$$

The friction factor is composed of two parts; one referring to a straight duct, and the other to a bended duct (Cengel and Cimbala, 2010c, Hewitt, 2008). The equations are

$$\frac{f_{curvature}}{f_{straight}} = 1 + 0.033(logDe)^4, \qquad Re < Re_{crit} \tag{8.56}$$

$$\frac{f_{curvature}}{f_{straight}} = 1 + 0.075\left[Re\left(\frac{R}{r}\right)^2\right]^{0.25}, \qquad Re \geq Re_{crit} \tag{8.57}$$

$$De = Re\sqrt{\frac{R}{r}} \tag{8.58}$$

$$f_{straight} = \begin{cases} \frac{64}{Re}, & Re < Re_{crit} \\ \left(-1.8log_{10}\left[\frac{6.9}{Re} + \left(\frac{\varepsilon/d_h}{3.7}\right)^{1.1}\right]\right)^{-2}, & Re \geq Re_{crit} \end{cases} \tag{8.59}$$

$$f = f_{curvature} \tag{8.60}$$

where R is the radius of the cross-section of the pipes, r is the radius of curvature of the centreline of the bend, and ε is the surface roughness of the pipe material.

- **Coaxial heat exchanger – cold fluid side (water)**

The pressure drop on the cold fluid side is given by Equation (8.55), but with a friction factor defined by Equation (8.61). This expression is found by curve fitting in Excel, with basis in Figure 39 (Kays and Crawford, 1980).

$$f = 1.7695Re^{-0.407} \tag{8.61}$$

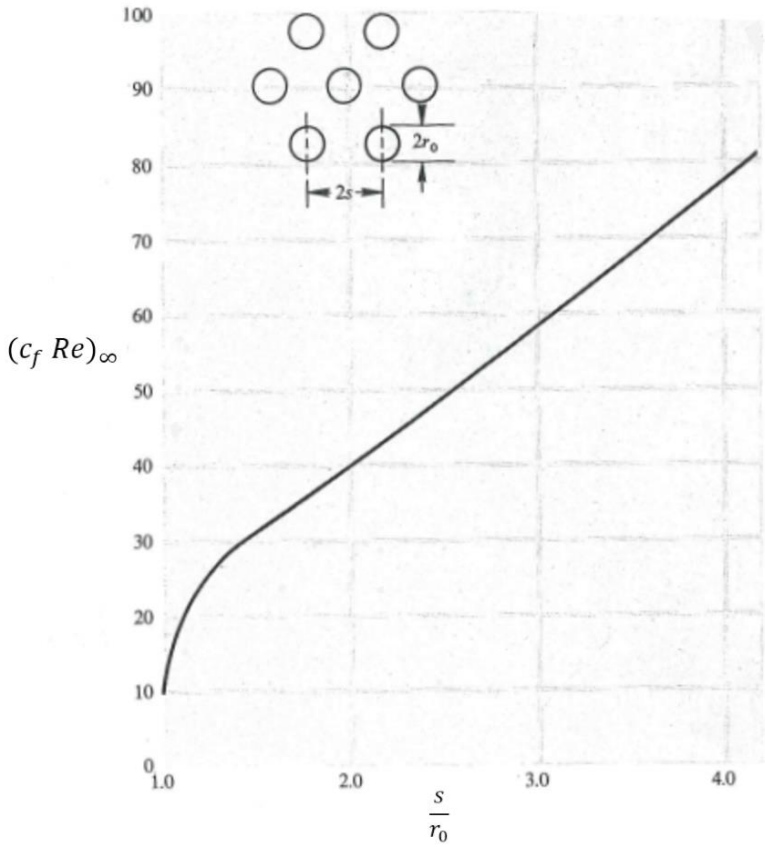

Figure 39. Friction coefficients for flow parallel to a bank of circular tubes

Pressure drops in pipelines

The pressure drops in pipelines are given by the Darcy-Weisbach equation (Equation (8.55)), and are calculated by using the built-in procedure PipeFlow in EES. The working fluid, temperature, pressure, mass flow, pipe diameter, length of the tube and relative roughness need to be known and given as input to the procedure. The procedure returns the lower and upper bounds of the average heat transfer coefficient and the pressure drop. Simultaneous hydrodynamic and thermally developing flow is assumed, and properties are evaluated at the bulk temperature and pressure.

Pressure drop in the flake ice drum

The pressure drop in the circular CO_2 pipes of the FID is the sum of pressure loss from friction, gravitation and acceleration; derived by the Energy equation and defined by Equation (8.62) (Cengel and Cimbala, 2010b).

$$\Delta P_{FID} = \Delta P_{fric} + \Delta P_{gr} + \Delta P_{acc} \tag{8.62}$$

The frictional pressure drop is given by Equation (8.55), with a friction factor approximated by S. E. Haaland, Equation (8.63). The pressure drops by acceleration and gravitation are defined by Equation (8.64) and (8.65) respectively.

$$\frac{1}{\sqrt{f}} = -1.8 \log\left[\frac{6.9}{Re} + \left(\frac{\varepsilon/d}{3.7}\right)^{1.11}\right] \tag{8.63}$$

$$\Delta P_{acc} = \rho \frac{(u_{out}^2 - u_{in}^2)}{2} \quad (8.64)$$

$$\Delta P_{gr} = \rho g H_{FID} \quad (8.65)$$

8.2.4 Compressor

The compression work is done in two stages, and piston compressors are assumed since this is the most commonly used compressor type for CO_2 (Stene, 2016). The heat loss factor is assumed to be 10 % for both stages, yielding an adiabatic efficiency of 0.90. The isentropic efficiency is calculated by a correlation developed by Eikevik (2015), Equation (8.66).

$$\eta_{is} = -0.00000461PR^6 + 0.00027131PR^5 - 0.00628605PR^4 + 0.0737025PR^3 - 0.46054399PR^2 + 1.406653347PR - 0.87811477 \quad (8.66)$$

The discharge temperature of the compressor should not exceed 130 °C, as this may lead to operational failure in the system (Eikevik, 2017). Due to the low evaporation temperature of the FID, two-stage compression with intermediate cooling between the stages is necessary in order to keep the compressor outlet temperature within the limit.

8.3 Optimization procedure of the gas cooler

To obtain an applicable optimization procedure, a literature study on gas cooler pressure was conducted. Different correlations were evaluated in order to find an appropriate empirical and simplified formula (Cecchinato et al., 2010, Chen and Gu, 2005, Kauf, 1999, Sarkar et al., 2004). However, as the pressure level is strongly dependent on the system design, none of the empirical formulas considered were suitable. Thus, the optimization algorithm had to be defined by scratch. The final procedure is described in the following; similar to that used by Berntsen (2013).

In order to find an optimal operating condition for the gas cooler and to assess the performance at different gas cooler pressures and water flow rates, a heat balance is established where the heat absorbed by the tap water/heat released from the CO_2 ($\dot{Q}_{co2}$) is set equal to the heat released in the gas cooler ($\dot{Q}_{trans}$). The gas cooler is divided into 15 sections of equal heat transfer area. The temperature of the fluid, pinch point, heat transfer and U-values are calculated for each part. Two different gas cooler models are assessed: a plate heat exchanger with chevron angles (model C202HP3 by Kaori Heat Treatment Co., Ltd.) and a coaxial heat exchanger (model WVCI serie 22 by Frigomec S.p.A.). Figure 40 illustrates the partitioning of the gas cooler, where the point "out" of the 1st part is the same point as "in" for the 2nd part, "out" for the 2nd part is the same point as "in" for the 3rd part, etc.

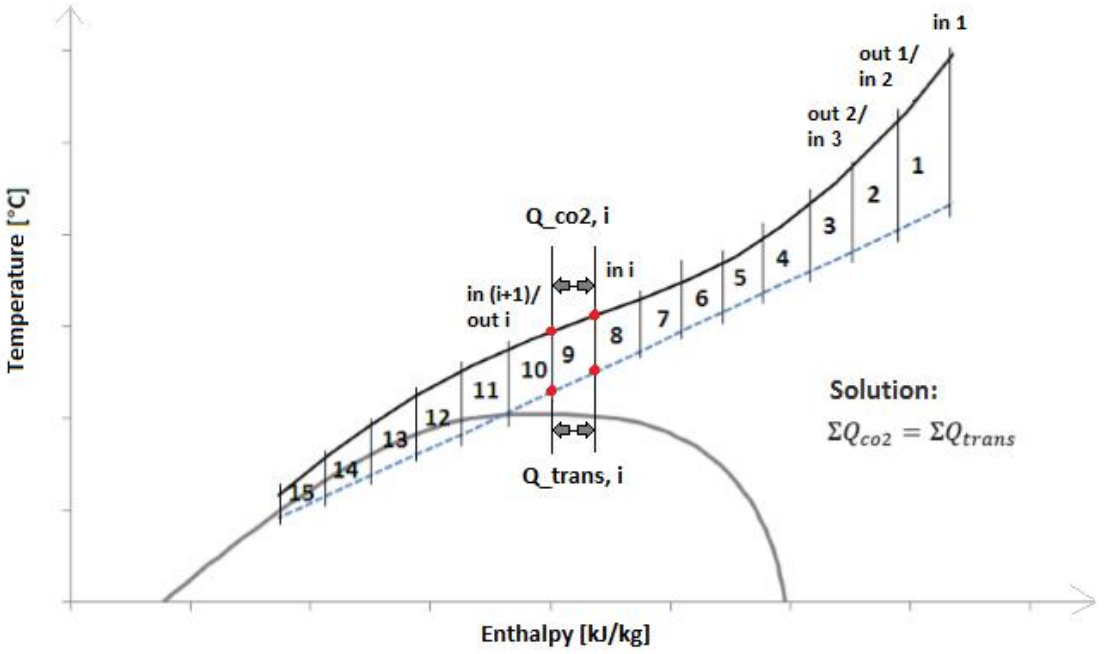

Figure 40. Determination of the gas cooler performance by heat balance

The heat released from the CO_2 is calculated using the parameters presented in Figure 41. The inlet CO_2 temperature to the gas cooler is estimated by using a routine library for working fluids in Excel (RnLib) and the following input parameters from the model in EES: (a) isentropic efficiency of the compressor, (b) suction gas pressure and temperature for the 2nd compressor stage, and (c) isentropic enthalpy at the inlet of the gas cooler. These parameters must be updated constantly with varying gas cooler pressure during optimization.

CO_2				H_2O				
T_{in}	T_{out}	h_{in}	h_{out}	T_{in}	T_{out}	h_{in}	h_{out}	Q_{CO2}
°C	*°C*	*J/kg*	*J/kg*	*°C*	*°C*	*J/kg*	*J/kg*	*W*

Figure 41. Parameters used to calculate the heat released from CO_2 in the gas cooler

The outlet CO_2 temperature at each section of the gas cooler is the variable that balances the heat balance. Enthalpy in and out of each section of the gas cooler is calculated by RnLib and the parameters temperature and pressure. The enthalpy difference and the mass flow are used to estimate the amount of heat transferred;

$$\dot{Q}_{co2} = \dot{m}_{co2}\,(h_{in,co2} - h_{out,co2}) \tag{8.67}$$

The incoming water temperature is set to 8 °C and will remain constant, and it is assumed to be saturated. The enthalpy at the inlet state is calculated by RnLib at the given saturation temperature. The outlet enthalpy of water for each section is calculated by Equation (8.68). The water temperatures at the inlet and outlet of each section are then given by the calculated enthalpy and RnLib.

$$h_{out,w} = h_{in,w} + \frac{\dot{Q}_{co2}}{\dot{m}_w} \tag{8.68}$$

The heat transfer between the two fluids is calculated by Equation (8.69), where the heat transfer coefficients are found from correlations described in Chapter 8.1.

$$\dot{Q}_{trans} = U_{tot} A \Delta T \tag{8.69}$$

The total U-value of the heat transfer process is approximated by Equation (8.70). Only the heat transfer coefficients of the fluids are considered, as the plate thermal resistance in Equation (8.1) is small and thus neglected[10]. The heat released in the gas cooler is calculated by the parameters provided in Figure 42. By using an iterative procedure and solving the system of equations by the problem solver algorithm in Excel, the heat transfer is balanced when setting the sum ($\dot{Q}_{diff}$) equal to zero by changing the outlet CO_2 temperature at each section of the gas cooler.

$$U_{tot} = \frac{1}{\frac{1}{\alpha_{CO2}} + \frac{1}{\alpha_w}} \tag{8.70}$$

Transmission						Difference
T_w	U_w	U_{CO2}	A	ΔT	Q_{trans}	$Q_{diff}=(Q_{CO2}-Q_{trans})^2$
°C	W/m^2K	W/m^2K	m^2	°C	W	W

Figure 42. Parameters for calculating heat transmission in the gas cooler

The area which is used in the calculations is the effective heat transfer area of the gas cooler model, divided by the number of sections. Because the problem solver in Excel had difficulties working with the logarithmic mean temperature difference, this is approximated by the arithmetic mean.

To find the optimal pressure for the heat exchanger models evaluated, the gas cooler pressure is varied between 85 and 115 bar. A simultaneous pinch point analysis is conducted at the different pressure levels, in order to maximize COP by locating the pinch point at the gas cooler outlet. The target temperature of the hot tap water is set to 80 °C at the outlet of the gas cooler, and the mass flow rate of water is adapted accordingly. The mass flow rate of CO_2 is given by the fixed features from the thermodynamic cycle, and it is kept constant during the optimization.

The dimensions of the heat exchanger models are provided by manufacturers and given as input data to the Excel sheet. These can be found in Appendix F (Chang, 2017, Pampanin, 2017). Model data and simulation results from EES were collected, and these are used as basis for developing a theoretical model in Excel; by use of appropriate correlations from literature and adapted thermodynamic input parameters from EES. The calculations in Excel are adapted to fit the performance from the simulation data provided by the manufacturers. In order to recover all the heat available from the system, two heat exchangers are needed. Both serial and parallel coupling have been investigated, but parallel coupling is selected as the pressure drop by this solution is the smallest. In addition, the results from Excel fitted best with the experimental results when parallel coupling was chosen.

[10] The error of approximation is below 5 %. Also, neglection of conduction through the wall gave best results with gas cooler data provided by manufacturers.

Running the simulations in Excel tended to be a time-consuming process, as the program contained several cross-references. The computational effort by using the problem solver algorithm was considerable. A lot of time has been spent on changing the input parameters and adapting the results. To ease the computational effort, the empirical correlations were tried implemented in Visual Basic; a programming language of Excel where the user can automate tasks by writing macros and define functions. Nevertheless, this measure did not give significant reduction in computational time.

The thermodynamic performance is used as the main criterion when determining the best suitable heat exchanger model for the system. This includes heat duty, temperature approach, outlet CO_2 temperature, pressure level and pressure drop, and required mass flow rate of water. In addition, the required work is crucial in order to determine the COP when the gas cooler is integrated. Other features, such as area and costs, are only discussed briefly.

8.4 Results and discussion

8.4.1 Selection of gas cooler model

The results from the optimization process can be found in Appendix E. Considering only the heat recovery cycle (Figure A-6), the coaxial heat exchanger is found to have the best thermodynamic performance. It obtains the highest COP and the largest heat duty regardless of the pressure level. The average heat transfer coefficient for the exchanger is considerably higher than for the plate model, and with a closer temperature approach and a lower temperature of the CO_2 gas at the outlet.

The required mass flow rate of water is in the same range for both exchangers, but the pressure drops in the coaxial model are significantly higher than those in the PHE. This will not have a very critical impact on the performance of the heat recovery cycle on the refrigerant side. However, the large pressure drop of water will demand a higher lifting height, and thus elevated energy consumption, of the required circulation pump (Chapter 8.1). This extra amount of work should be accounted for. This is achieved by evaluating the system COP, which includes the total amount of work; given as the sum of work input by the compressor and the water pump. The pump work is evaluated using the product finder at the web page of Grundfos; by entering the dimensioning water flow rates and lifting heights at the gas cooler pressures evaluated (Grundfos, 2017). The comparison is shown in Figure A-5, and the procedure provides a more objective evaluation basis. While the COP of the PHE barely is influenced by the additional pump work, it will differ significantly from the system COP when integrating the coaxial model. The difference in thermodynamic performance is seen to be lowered when the pump work is included. The COP of the coaxial model is highest if operated with a pressure below 102.5 bar, while the PHE obtains slightly higher efficiencies for pressures above this level.

The analyses show that both heat exchanger types achieve good thermodynamic performance at the optimal points, illustrated in Table 11. Using the system COP as decision basis, makes the difference in performance less distinct; and the efficiency can be regarded as equally good in an interval between 100 and 105 bar. Thus, both models could be chosen with satisfactory performance. The coaxial heat exchanger is however integrated in EES; due to the slightly

better heat transfer characteristics. As the PHE needs to be operated at a higher optimal pressure to obtain satisfactory temperature characteristics, the required compressor work is slightly elevated compared to that of the coaxial model. The available heat from the gas cooler is still the lowest for the PHE, despite of the heat exchanger being operated at higher pressure. This is a drawback concerning this model. A temperature-enthalpy diagram for the coaxial heat exchanger at optimal pressure is provided in Figure A-7.

Table 11. Gas cooler performance at optimal pressure

	PHE: C202HP3 (Kaori)	Coaxial heat exchanger: WVCI SERIE 22 (Frigomec)
Gas cooler pressure [bar]	105	102.5
Heat duty [kW]	622.4	629.4
Compressor work [kW]	267.6	266.1
Pump work [kW]	0.015	2.5
Total work [kW]	267.6	268.6
COP [-]	2.326	2.365
COP_system [-]	2.326	2.343
Average α [W/m^{2}K]	4272	8655
CO_2 outlet temperature [°C]	10.5	8.8
Approach temperature at pinch [°C]	2.5	0.8
Pressure drop, CO_2 [kPa]	12.6	97
Pressure drop, water [kPa]	25.1	583

Costs and dimensions are provided in Table A-4 in Appendix E. It may stand as an additional decision basis if the flake ice system is to be realized. However, both models are relatively small and compact compared to conventional shell-and-tube heat exchangers. Since the system is to be stationed outdoors without any stringent area restrictions, the difference in volume will not be crucial for the selection. The same accounts for the investment costs; which are seen to be in the same range. This suggests and confirms that the main focus of the selection process should be on the thermodynamic performance.

The flexibility to changes in production rate should also be considered. The flake ice system is designed for constant operating conditions; by means of (1) constant snow production rate, and (2) on/off regulation. In a future perspective; it is recommended to choose a gas cooler that can handle off-design operation without a drastic reduction in performance when the production time of the snow machine is adjusted to non-constant operation. Such conditions would typically be handled by adjusting the gas cooler pressure; in terms of lowering the pressure to achieve better performance at partial load. Since the coaxial heat exchanger has the closest temperature approach and the highest duty regardless of the pressure level, it would be favourable in this respect. The performance of the plate heat exchanger is seen to have a more drastic reduction when operated off-design; where the CO_2 cool-down temperature and approach temperature at pinch increase considerably when the pressure is lowered (Table A-3). This will hamper the heat transfer. The coaxial heat exchanger has the highest COP at pressures below the optimal range, and this model will provide superior flexibility when operated off-design.

8.4.2 Refrigeration and heat recovery system

The results from the optimization process have been imported to EES by use of curve fitting functionality in Excel. Simplified heat exchanger characteristics for the duty and pressure drop were developed with basis in the parametric sweep of the gas cooler pressure. The main results from the simulation are presented in Table 12, together with data from the original subcritical and transcritical models.

Table 12. Results from simulation in EES

	Subcritical cycle by Dieseth (2016)	Transcritical cycle from the pre-study	Transcritical cycle (adapted)
$COP_{heating}$ [-]	2.05	2.35	2.37
$COP_{cooling}$ [-]	2.65	1.70	1.66
$Q_{gc}/Q_{cond+sh}$ [kW]	276.3	611.8	629.4
Q_{evap} [kW]	213.9	442.4	442.4
W_{comp} [kW]	104.2	260.2	266.1
$W_{centrifugal\ pump}$ [kW]	0.13	0.12	1.5
$Q_{intercooler}$ [kW]	16	91.8	79
Q_{SGHX} [kW]	15.6	39.9	21
$\dot{m}_{co_2}$ [kg/s]	0.943	1.908	1.911

The duty of the gas cooler is seen to be extensive. The available surplus, when integrated with DHW heating, is 42.3 % larger than the required refrigeration load from snowmaking. Integration of heat recovery raises the required energy consumption of the refrigeration system; as the lifting height of the compressor must be elevated to a level suitable for heating of hot tap water. However, the overall energy efficiency of such a system is improved when heat can be utilized both on the hot and cold side; with the accessible gain from the system more than doubled. As the snow machine is seen to be highly energy-intensive, this suggest an operation where heat recovery should be implemented. Utilization of the surplus heat offers both increased energy efficiency and reduced net costs of the required energy use from refrigeration; thereby making implementation more reasonable, as the operating costs are reduced.

The efficiencies of the adapted transcritical cycle is only slightly changed compared to the model in the pre-study. The increase of the gas cooler duty is larger than the elevated compressor work when optimizing the gas cooler pressure. This improves the heat recovery performance slightly, which confirms that the pressure should be optimized. The increase in COP_heating is seen to be at the expense of the COP_cooling; due to the constant product load from the snow machine and simultaneous increase in compressor work. This means that more energy is needed to provide the same refrigeration effect. Maximizing the heat recovery potential from the combined system will however not hamper the efficiency of the snowmaking, which is desirable (Chapter 11.3). The dimensioning point is preserved for the snow machine, while heat recovery is designed accordingly. Due to the indirect coupling provided by the heat cascade configuration, refrigeration and heat recovery are interrelated without influencing the thermodynamics of the flake ice machine. This means that efficiency of the water-to-snow conversion in the FID will be unaffected by the reduction of the COP_cooling.

The performance in terms of heat recovery is best for the adapted transcritical cycle. The available surplus from the system is about 2.3 times higher than for the subcritical model; suggesting that the CO_2 cycle is most efficient when operated in trancritical mode. Also, the available surplus is increased by 422.4 kWh/day from the pre-study. The model yields an energy saving of 452,168 kWh/year (Chapter 7.3.3). The corresponding economic saving potential, which is increased by 6760 NOK, is approximately 240,000 NOK/year at an energy price of 0.80 NOK/kWh when compared to electric heating. This means that the excess heat from the snow machine would be available at a much lower price than from other conventional heating solutions.

An advantage of the adapted transcritical cycle is that the duty of both the intercooler and SGHX are reduced. As CO_2-systems are affected by relatively large throttling losses, it is essential to obtain low outlet temperatures and good temperature approach in the gas cooler. This is the main objective by introducing the SGHX to the cycle; as the superheating losses is not that critical for the cycle performance. Choosing a gas cooler model that can obtain larger cool-down of the CO_2 gas than the system from the pre-study is optimal because it reduces the demand of subcooling; with a corresponding reduction in suction gas heating. It is however still favourable with a little superheat out of the evaporator to avoid harming the 1st compressor stage; which is sensitive to two-phase flow at the inlet (Chapter 7.3). Too much superheat will on the other hand increase the required cooling demand of the intercooler between the compressor stages, and the amount of superheat, intercooling and subcooling must be balanced. Integration of the coaxial gas cooler reduces the cool-down from 13 to 8.8 °C; with a corresponding reduction in subcooling and superheat of 4.4 and 10.3 °C. The required cooling from the intercooler is reduced by 6.3 °C, which is closer to that of the subcritical cycle. The duty of the intercooler is still large, and the potential for heat recovery on the site may be explored if the system is implemented. Possible alternatives are low temperature space heating, or integrated preheating of tap water for the removable DHW system.

The reduced duty of the intercooler requires a smaller water flow rate. The flow rate has been adjusted from 3.5 to 2 kg/s. This yields a lower pressure drop on the water side of the PHE, and smaller dimensions of the heat exchanger; as a more compact model can be chosen.

The pipeline pressure drops in the heat recovery cycle are small and far below operational limits; in good agreement with theory. They could thereby be neglected in the analysis, but are included to give a complete picture of the real cycle performance. Compared to the pre-study, the pressure drops are in the same range; both in the pipe sections and through the heat exchangers. This is however not the case for the bottom cycle; where the modified correlations for the FID influence the thermodynamic state points in lower part of the heat cascade. The pressure drop of the drum is increased from 9 to 105 kPa; to a level somewhat larger that results from literature (Chapter 3.1). It is however still within the acceptable limits, outlined in Chapter 8.1, and yields a more correct estimate of the actual pressure drop. The required lifting height and the power input of the centrifugal pump are raised accordingly. Including this pump work in the COP calculations would hamper the objectivity of the comparison, as the previous simulations models are modelled with significantly lower pressure drops in the bottom cycle; which validates the exclusion. The dimensions of the pipe sections are adapted to fit the new

thermodynamic conditions, with slightly increased pressure drops. Nevertheless, the increase of the pressure drops is not considered critical regarding the performance; which easily may be adapted by adjusting the pipe dimensions and materials. The calculations only stand as a conceptual first design solution. The pipe sections should be studied more in depth in an optimization process if the solution is to be realized; to ensure optimal performance when integrating the components of the combined system.

8.4.3 Snow machine

The results from simulation of the dynamic ice growth process is shown in Appendix C. It is found that the increased production rate requires a higher overall heat transfer coefficient of the drum; as more heat must be removed from the water to provide sufficient cooling. The heat transfer coefficient of water is increased by 98 %, while the CO_2 heat transfer coefficient is lowered slightly. The U-value, which is calculated by Equation (7.11), will consequently be higher; regardless of which material is used in the drum wall, or at which time interval the comparison is made. The ice growth rate and the U-value are highest when aluminium is used in the drum wall. This means that the time needed to produce an ice layer of 3 mm, which is the desirable thickness before the inner drum wall is scraped (Chapter 3.1.1), is the shortest. The U-value will decrease most rapidly in the beginning of the ice layer formation and change less as the thickness increases; the trend being similar to the model by Dieseth (2016).

The efficiency of the flake ice machine is seen to be highly dependent on the production rate and design of the drum wall. The ice growth rate drops rapidly at a production of 100 tons/day when compared to a rate of 50 tons/day. This can be seen from Equation (7.12), and is to a great extent a result of the drastic increase of the water heat transfer coefficient. The increase in production time of the ice layer is substantial, regardless of which material is used in the construction; illustrated in Table 13. The ice thickness as a function of time will be lower at elevated production rates, thus providing poorer efficiency of the drum since the rotating period of the scraper is decreased. This emphasizes the importance of adapted design of the FID to obtain an acceptable efficiency at the prevailing operating conditions; pointing to the need of an optimization process and a prototype model. As the increase in production time is seen to be non-linear, attention should be directed to find the optimal thickness and material choice of the drum wall which maximizes the water-to-snow conversion at the given production rate. It should be explored in combination with simultaneous investments, UTS and displacements, which will be discussed in Chapter 9.

Table 13. Comparison of the required time needed to produce an ice layer of 3 mm for different construction materials of the flake ice drum, when considering different ice production rates.

	Construction material		
Ice production rate	Carbon steel	Stainless steel	Aluminium
50 tons/day	33 s	44 s	31 s
100 tons/day	58 s	90 s	53 s
Percentage increase	76 %	101 %	71 %

8.4.4 Final considerations

Comparison with commercial models

The power consumption of the simulation model is 16.3 % higher than that of commercially available flake ice machines with the same production capacity (Chapter 5). The adapted model is however simplified regarding losses. As the simulation model only comprises energy use of the required refrigeration system of the FID, the real power consumption is likely to be greater when considering additional contributions from the rotating scraper, ice crusher, control system and circulation pump. However, while the surplus heat from the commercial machines is released to the surroundings and thus wasted, the EES model is adapted to operations where all excess heat can be recovered. The total energy performance can therefore be equally good, or even better, considering the benefits of both refrigeration and heating from the system.

The difference in cooling capacity for SF220 and the EES model is about 200 kW (Table 1), thus considerable. While SF220 is based on real-simulated performance, the required refrigeration load from the snow production is based on a theoretical approach; where the load only includes heat removal from the water-to-snow conversion. Use of different refrigerants, dimensioning temperature and pressures, and efficiencies of the components will add to this difference. Also, the exclusion of snow melting and climatic impact is a drawback of the EES model, which is regarded the major reason for the difference. The required cooling capacity of the simulation model will consequently approach that of SF220 if such practical aspects are taken into account.

The water consumption of the FID in the simulated model is low; which makes the system efficient compared to commercial machines. The required water flow rate is 1.16 l/s for the drum modelled in EES, with corresponding flow rates of 1.5 and 0.97 l/s for SF220 and SnowGen 100FI respectively. The manufacturers report that the models can be implemented to work with natural working fluids, such as ammonia, which would make them equally good in terms of obtaining an environmental friendly profile. This would however require adaption of the design and the refrigeration components. None of the machines presented in Chapter 5 are reported to be implemented with CO_2 or heat recovery strategies. This analysis shows that use of CO_2 as refrigerant in a transcritical cycle contributes to obtain a system that is both energy efficient, in terms of heating and cooling, and environmentally friendly and viable for the future; hence a double effect.

Ammonia is regarded less suitable with respect to combined refrigeration and heating at the prevailing conditions. Since it is sensitive to high discharge temperatures, special care should be taken when designing for combined heat recovery, as the evaporation temperature is very low. Also, mandatory safety equipment is required; due to the toxicity of ammonia. This will increase the investment costs. Due to a high critical temperature, ammonia will be less suitable than CO_2 with respect to DHW heating; as the constant condensing temperature gives a lower temperature fit. If the commercial models should be implemented with combined heat recovery, alternatives should be explored: (a) look for other low-temperature heat recovery strategies, or (b) use ammonia as a low-temperature refrigerant in a heat pump cascade; implemented with a secondary refrigerant (such as CO_2) to raise the pressure to a level suitable for DHW heating.

By alternative (b), it might then be possible to carry out with the same strategy for heat recovery, without exceeding the maximum limit of 130 °C at the discharge.

Measures to improve the performance

Measures to make the heat recovery system more flexible should be explored if adapted to handle variable design conditions. A solution is to have an intermediate tank between the two compressor stages to handle flash/separation; where saturated liquid will flow to the evaporator before throttling to evaporation pressure, while a given amount of gas flows directly to the 2nd stage compressor through a by-pass line. This will increase the flexibility of the system and provide better performance when operated off-design in warmer climates. Such design will be favourable if the water from the containers has an incoming temperature above 8 °C. If the inlet water temperature approaches 20 °C, which may occur if the containers are exposed to the sun during spring/autumn or left at the production site at elevated outdoor temperatures, the gas cooler must operate with higher CO_2 outlet temperatures. This yields rather large throttling losses if no measure is implemented. An intermediate tank will keep the throttling losses to a minimum; by ensuring saturated liquid at the inlet to the 2nd throttling valve.

In order to improve the performance of the CO_2 refrigeration cycle, a configuration with an ejector could be explored (Figure A-16). The ejector features expansion work recovery in vapour compression systems. About 30 % of the expansion work available can be used to pump excess liquid through the evaporator; such that it is overfed with liquid and heat transfer in the drum walls are maximized (Elbel and Lawrence, 2016, Hafner, 2017). This will eliminate evaporator dry-out; resulting in improved evaporator performance (Chapter 9.1). It can also give some costs benefits, as the circulation pump, expansion valve and the cascade heat exchanger can be removed from the cycle. However, removing the cascade heat exchanger might make the efficiency of the snowmaking in the FID more sensitive to variations in the refrigeration system, as the indirect coupling is eliminated. Possible challenges, such as non-evenly distribution of the liquid to the 600 refrigerant pipes in the drum wall, or mixing of oil from the compressor that attaches as a film on the evaporator pipes, should be studied (Eikevik, 2017). These problems are avoided in the original configuration; by the pump and liquid separator. It might be easier to use a circulation pump instead of an ejector to ensure (a) evenly distribution to the evaporator pipes, and (b) optimal regulation. Which configuration is favourable, will be a question of design and adaption to the production criteria.

An alternative to the heat recovery configuration from the pre-study, is to fill and refill the containers with water at the production site; received from a local connection point in the water grid. This will reduce the operational costs and energy demand during transportation, as the container can be transported empty and with atmospheric pressure after use. With a pressure of 10 bar for the water grid, the natural driving forces by the pressure difference are sufficient to push the water through the gas cooler and into the container; consequently eliminating pump work during filling (Hafner, 2017). Instead, a small air compressor must be used to empty the container at the customer site. This configuration eliminates mixing of hot and cold water at the customer site, which was considered a drawback of the proposed solution. However, the system COP should be updated by including additional power consumption from the air compressor. It should be evaluated together with costs and infrastructure; in order to maximize the energy

efficiency of the removable system. The performance of the stationary part outlined in this chapter remain the same, regardless of the design of the removable configuration and connection strategy. These features should instead be included when evaluating the total feasibility of such a system, relevant if the case is to be realized.

9 Calculations of the flake ice drum using COMSOL

9.1 Model

COMSOL Multiphysics is a general-purpose software platform for physics-based modelling and simulation. It is based on advanced numerical methods, and enables the user to account for coupled or multiphysics phenomena. Integration and interaction of several physical phenomena can be studied together, which is advantageous when handling advanced and complex problems. This makes the program especially suitable for studying the design of the flake ice drum; which physics is governed by both heat transfer, phase change, turbulent flow and structural mechanics. COMSOL is used to analyse heat transfer, temperature distribution, displacements and stresses. The results are not implemented into the EES model, but are rather used to evaluate the plausibility of the calculations and assumptions used in EES.

The model is an improvement of the COMSOL model developed by Dieseth (2016), which was designed to describe the subcritical flake ice system. The geometry and design of the model is the same as the original, but input parameters and physics are improved to make it suitable for simulating the adapted EES model. The model drawn in COMSOL uses input parameters that are collected from EES. The following physics have been included:

- Heat transfer in solids
- Phase change material
- Turbulent flow, k-ε
- Solid mechanics

The multiphysics nodes "temperature coupling", "flow coupling" and "fluid-structure interaction" have been used to couple the liquid (CO_2) and solid (construction) domains of the model. The original model used average properties of CO_2 liquid and gas, evaluated at a mean gas quality to simplify the problem. Only one-phase flow was encountered. The adapted model takes into consideration the evaporation process in the refrigerant pipes; hence a variable heat transfer coefficient. The heat transfer model is extended to include two-phase, turbulent flow of CO_2; with a gas quality of about 0.5 at the outlet of the FID. While the original models used a constant velocity, changes in velocity is included in the "turbulent flow" physics. Since there exists no built-in property database for CO_2 in COMSOL, it had to be made. Properties for saturated liquid and saturated gas were calculated in Excel at the dimensioning temperature and pressure, before implementing them as global parameters in COMSOL. The CO_2 properties were assigned to the appropriate domains under the physics "phase change" and "turbulent flow", and at the respective interfaces. The following assumptions for the model have been made:

- The outer drum wall is modelled as an adiabatic surface; meaning there is no applied heat flux to the ambient wall ($\partial T/\partial x = 0$).
- Phase change of water and the dynamic model of the ice growth process on the freezing surface of the drum are not included. Instead, a constant heat flux from the water is assumed; corresponding to the required heat removal from water.

- CO_2 is entering the FID as saturated liquid.

The physics "phase change material" is used to model the evaporation process of liquid CO_2 in the refrigerant pipes. This functionality solves the heat equation by assuming that the transformation from liquid to gas occurs in a temperature interval where the material phase is modelled by a smoothed function (θ); representing the fraction of phase before transition. This temperature difference must be given as input to COMSOL. It is calculated in Excel by use of Equations (9.1)-(9.3) (Næss, 2012), where $r_{crit,max}$ and r_{crit} denote the opening and the critical radius of the bubbles respectively. The temperature difference, commonly known as the *excess temperature*, is estimated to 1 °C (Incropera et al., 2013a).

$$T_w - T_{sat,l} = \frac{2\sigma T_{sat,l}}{\rho_g h_{fg} r_{crit}} \tag{9.1}$$

$$r_{crit} = \min\left[r_{crit,max}, \sqrt{\frac{2\sigma T_{sat} k_l}{q h_{fg} \rho_g}}\right] \tag{9.2}$$

$$q = \frac{Q_w}{n\pi d_{pipe} H_{FID}} \tag{9.3}$$

The equations solved by the physics "turbulent flow, k-ε" are the Reynolds-averaged Navier-Stokes (RANS) equations for conservation of momentum, and the continuity equation for conservation of mass. Turbulence effects are modelled using the standard two-equation k-ε model with practical constraints. The flow near the wall is modelled using wall functions. The physics "solid mechanics" is intended for general structural analysis of the three-dimensional construction. The interface is based on solving the equations of motion together with a constitutive model for the solid materials assigned to the model. It is used in order to study the effect of displacements, stresses and strains. The stresses within the structure are calculated according to the von Mises yield criterion. They are compared to the metal's ultimate tensile strength by converting the complex stress state down into a single scalar number (Rao, 2017). This way, it is possible to check whether the drum design will withstand the given load condition at different operating conditions.

Only a section of the original drum wall is studied in COMSOL, based on symmetry assessments. The geometry is shown in Figure 43, where the drum wall area between two adjacent pipes is included. It is a sandwich construction composed of two steel layers, and with an inner aluminium profile with refrigerant pipes. The height of the flake ice drum in the EES model is 2.6 m, while the construction is simulated with a constant height of 0.1 m in COMSOL. This accounts for only 3.85 % of the actual height; which value was set to equal the height in the original model. These simplifications are implemented in order to ease the computational effort, as the simulation time was too high when studying the total height. Since the construction is modelled with symmetry in the z-plane, these simplifications will not have any stringent significance on the temperature distribution and stresses when the water heat flux is approximated as constant. The results from simulation of this section are assumed to be representative for the rest of the structure.

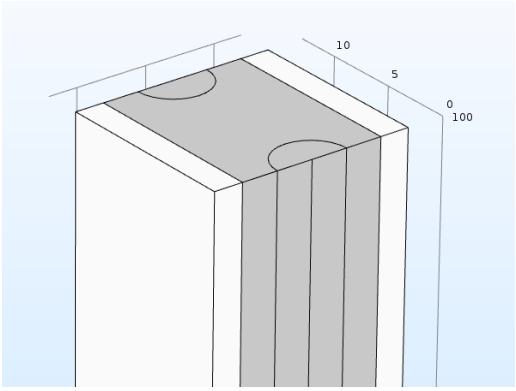

Figure 43. Geometry of the drum wall

In order to enhance heat transfer in the CO_2-pipes, the gas quality (z) at the outlet of the FID should not exceed 0.5. As the gas quality approaches 1, there is a drastic drop in the heat transfer coefficient, as illustrated in Figure 44 (Choi et al., 2007). The magnitude of the heat transfer coefficient is significantly higher before this drop, than after. Exactly at which quality the drop occurs, depends on many factors; such as geometry of the pipes (diameter), mass flux of CO_2, heat flux from water, evaporation temperature and pressure. An exact determination of the point which maximizes the heat transfer coefficient of CO_2 is beyond the scope of this thesis; as it requires extensive calculations and use of empirical cross-related formulas. However, the drop is assumed to occur somewhere in the interval of 0.5-0.7 (Eikevik, 2017). It is desirable that the refrigerant is only partwise evaporated to ensure an outlet gas quality below this interval, such that dry-patch is avoided. Further evaporation in the drum will hamper the heat transfer, as an increased amount of gas leads to poorer contact with the boiling surface; hence a lower heat transfer coefficient. An acceptable outlet gas quality of 0.45 was obtained from simulation in COMSOL; by adjusting the heat flux from water. This yields a circulation rate (γ) of 2.2 (Equation (9.4)), which is within acceptable limits of $\gamma \in (1.7, 3)$.

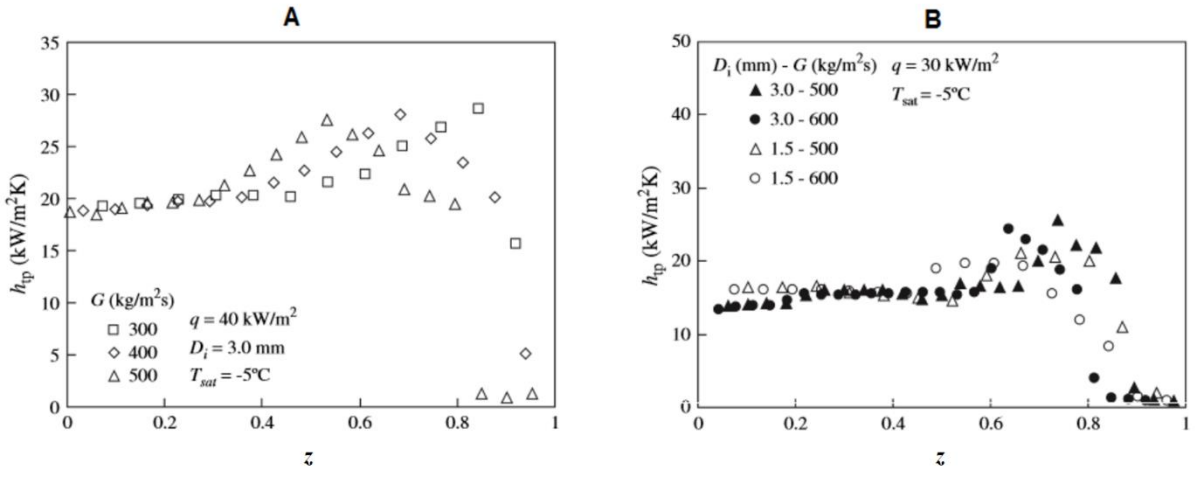

Figure 44. Heat transfer coefficient at varying gas qualities, for two different configurations; A and B.

$$\gamma = \frac{1}{z} \tag{9.4}$$

The model in COMSOL is not exact, but it will provide an estimation of the temperature distribution between the pipes and the freezing surface. Input values to the system are provided in Appendix G, together with input data from the original model.

9.2 Procedure

In order to study interaction of the physics, by using the multiphysics functionality provided by COMSOL, the solution procedure was adapted step-by-step. Simplifications have been introduced in order for the program to converge. These will be described in the following, together with a description of the final approach.

As a starting point, the different physics were solved separately, without using the coupling functionality. This was done in order to evaluate the validity of the input parameters, and to confirm that each physics worked properly. The main challenge occurred within "turbulent flow"; when coupled and solved simultaneously with the other physics. Using the same mesh size as in the original model of Dieseth (2016) introduced too many disturbances to the temperature profile to give an acceptable solution, and the mesh had to be adapted. Due to the trade-off between the accuracy of the mesh and the computational effort, normal element size was used where possible. The model was extended to finer mesh around the interfaces and edges of the refrigerant pipes, and boundary effects were included. A coarser mesh was chosen for the rest of the model; where the demand for high accuracy was less prudent. This adaption gave satisfactory simulation results, but at the expense of a drastic increase in computational time.

The fluid properties of the liquid and gas phase of CO_2 differ considerably. This leads to significant changes in the velocity field from inlet to outlet. As COMSOL had difficulties working with very rash changes in dynamic fluid properties, a correction term ($para$) was introduced to physics "turbulent flow"; to ease the computation (Nistad, 2017). This parameter is introduced in the expressions for viscosity and density, Equation (9.5) and (9.6), and it is implemented as a parametric sweep between 0 and 1. It will provide a smoother transition of the flow variables during phase change; such that a more linear approximation is obtained. The terms θ_1 and θ_2 denotes the fraction of the liquid and gas phase respectively.

$$\rho = \big(\theta_1 + \theta_2(1 - para)\big)\rho_l + \theta_2(para)\rho_g \tag{9.5}$$

$$\mu = \big(\theta_1 + \theta_2(1 - para)\big)\mu_l + \theta_2(para)\mu_g \tag{9.6}$$

Only stationary analyses have been encountered. The stationary solver was used as a starting point, but as the computations were so time-demanding, exploration of the time dependent solver was omitted. In addition, transient analysis increases the computational effort; which would have increased the computational time even more. Since the snow machine is operated with a constant production rate, transient analysis is not considered crucial; since it will only be of matter when the machine is turned on/off.

Temperature and displacement were studied separately, in order to ease the computational effort. Firstly, the physics "heat transfer" and "turbulent flow" were studied at the interfaces in order to find the temperature distribution in the construction; by simultaneously including all the multiphysics nodes. Secondly, "turbulent flow" and "solid mechanics" were investigated at the respective interfaces to study the load from the fluid on the structure, with similar multifunctionality. The final solution procedure for these features were different. While the variables and initial values from the displacement study were automatically controlled by the interface of the physics, the temperature study had to be implemented with user controlled initial values. Separate uncoupled physics were solved before combining the functionality, with the previous solution being used as initial value for the next simulation. The final procedure is defined below:

0) Improve the mesh
1) Solve just for heat transfer
2) Solve just for turbulent flow (CFD)
3) Solve for coupled physics

The width of the model, which is determined from the number of refrigerant pipes, is kept constant during the main simulation. The number of pipes was determined in EES in order to keep the pressure drop within limits. Simulation is used in order to verify that the corresponding temperature profile and stresses in the structure are reasonable, when the model is implemented with constant width and a corresponding pressure drop. Also, parametric sweep of the width requires change of input data (ΔP, u_{in}, dT), which introduces additional computational effort. It was not enough time to study this effect in detail. The main focus was to vary the depth of the model from 5 to 20 mm, in order to find an acceptable temperature profile, while simultaneously keeping the stresses and displacements within the UTS of the drum materials. The depth of the model corresponds to the thickness of the aluminium layer of the construction, while the steel layers at each side of the inner aluminium profile is set to 20 % of the depth.

Additional simulations were performed. The ratio of the metal thickness in the drum wall has been varied. Also, the effect of using 300 refrigerant pipes was briefly investigated in COMSOL.

9.3 Results

Temperature distribution

Figure 45 shows the temperature distribution between the refrigerant pipes and the freezing surface at different depths. The simulations reveal that increased thickness of the drum wall yields a greater temperature span of the construction. The evaporation temperature of the two-phase refrigerant in the pipes will remain constant, while the temperature on the freezing surface increases with the thickness. The temperature span is 2.34 °C, 3.61 °C, 4.97 °C and 6.27 °C for 5, 10, 15 and 20 mm respectively. The difference is about 1.3 °C for each 5 mm increase, and no stabilization of the temperature range is seen. This means that increased wall thickness will provide a poorer potential for water-to-snow conversion; due to an elevated freezing temperature.

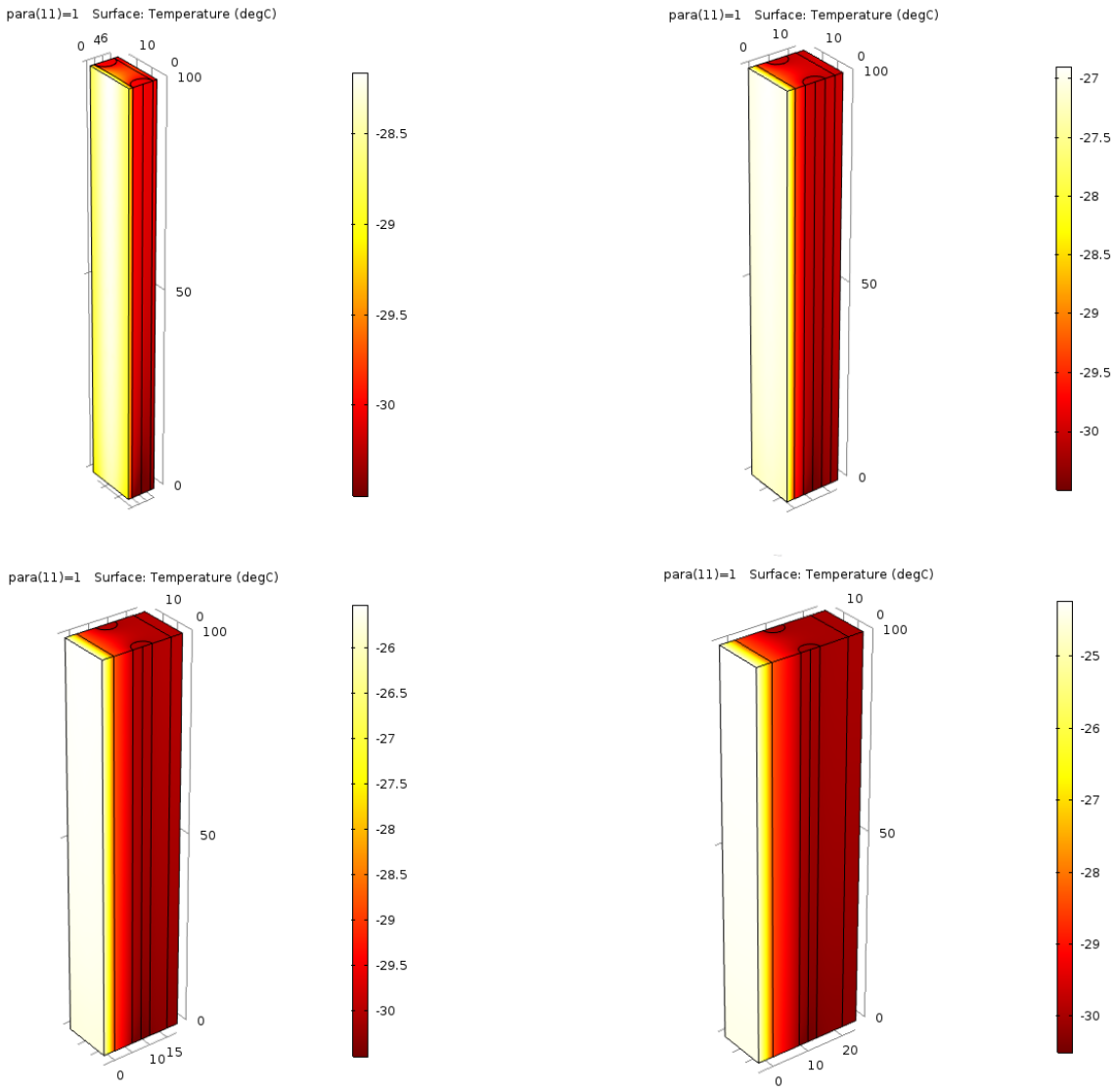

Figure 45. Temperature distribution at varying depth of model

The temperature level at the freezing surface will vary considerably when the thickness is increased, but with a fairly even temperature distribution at each depth, as indicated in Figure 45. The temperature difference at the freezing surface of water is only 0.96 °C, 0.40 °C, 0.25 °C and 0.20 °C, at corresponding depths of 5, 10, 15 and 20 mm. This temperature span is not that significant as the span for the whole construction. The trend is a lower temperature difference at increased wall thickness. A low temperature variation at the freezing surface is desirable in order to avoid an uneven ice layer, which may influence on the production capacity.

Displacement and structural integrity

The maximum displacement of the construction at varying drum thickness is shown in Figure 46. Corresponding displacement profiles are provided in Appendix H, Figure A-8. As the outer drum wall is modelled as an adiabatic surface, thus representing a fixed constraint in COMSOL, this will not displace. The greatest displacement is in direction of the freezing surface and around the refrigerant pipes, and it will increase with decreasing wall thickness. Simulations reveal that the maximum displacement of 0.00039 mm in the construction at depth 5 mm, is about three times higher than at depth 10 mm; hence a significant drop in this interval. The minimum displacement is found at depth of about 11.5 mm, and the displacement increases slightly above this drum wall thickness. However, the displacement is rather small for all depths considered. This is desirable, as displacements may lead to an uneven inner surface of the drum wall; which may cause damage to the rotating scraping device when the ice is removed and collected.

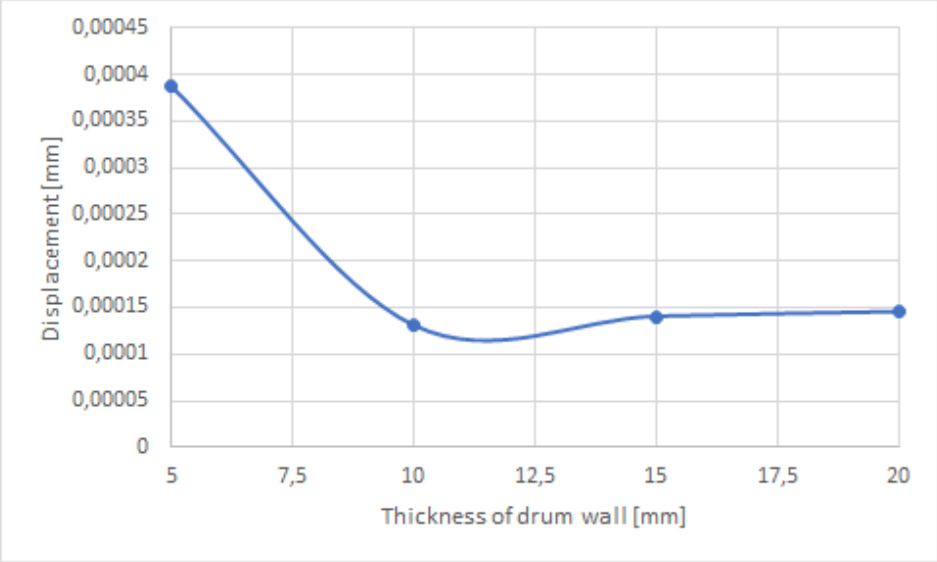

Figure 46. Maximum displacement at different depths

The distribution of the stresses follows the same trend as the displacement; with the largest stresses centred around the pipes in direction of the inner drum wall. This is indicated in Figure A-9, Appendix H. The stresses are induced by the fluid flow in the refrigerant pipes, and they should be kept at an acceptable level, as high stresses in the structure may lead to failure in the operation. Figure 47 shows the maximum von Mises stresses within the construction at varying depths. The maximum stress occurs at thickness 5 mm, with a value of 5.7 MPa. Increasing the thickness of the drum wall will reduce the von Mises stresses in the structure; both the maximum value and the span of stresses within the structure. The lowest stresses occur at the same depth as for the minimum displacement; thereby suggesting and confirming the strong dependency of internal stresses on displacement. If the stresses within the structure are more dominant, so are the displacement.

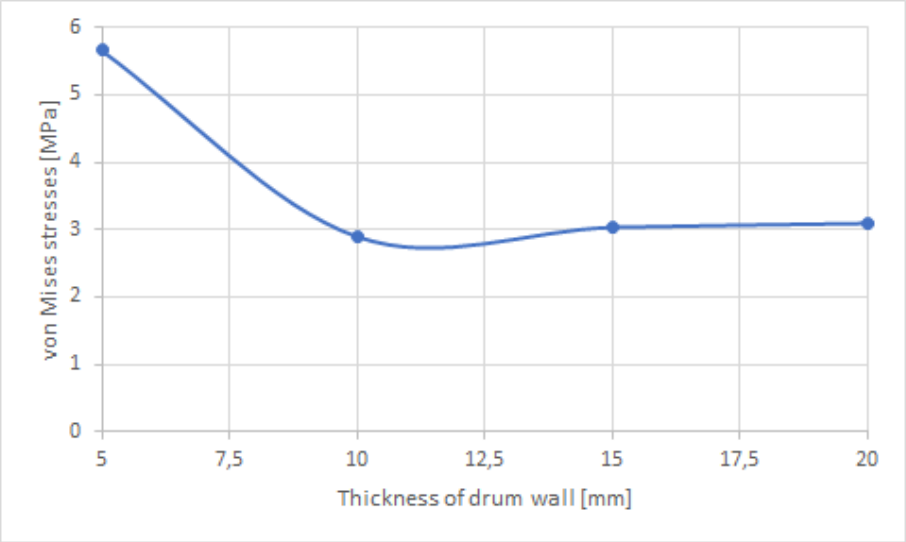

Figure 47. Maximum stresses within the structure at different depths

9.4 Discussion

The results reveal that there is a trade-off between increased surface temperature and simultaneous even temperature at the freezing surface. As the thickness of the drum wall is increased, the temperature span of the whole construction increases, while the span on the freezing surface decreases. As both temperature ranges will influence on the production capacity, both should be kept within practical limits. Since the surface temperature of the inner drum wall is well below the freezing point of water at all depths, the thickness is not very critical in this perspective. In this interval, all depths are considered to provide performance within acceptable limits. It is more a question of efficiency, as a lower temperature at the freezing surface temperature provides a faster water-to-snow conversion, with possibilities of increased water flow rate. The analyses suggest that the temperature variation at the freezing surface should be the focus of attention; since the production capacity is more sensitive to variations at the surface than within the construction. This difference is seen to stabilize at depths above 10 mm; thereby suggesting a desirable depth larger than 5 mm, to have an even temperature distribution.

The freezing surface may become rough and bumpy, due to displacements within the construction. This can lead to wear or failure of the ice scraper during ice harvesting, as well as harming the inner drum wall itself. It is important to keep the displacement to a minimum to avoid operational problems. The displacement in this case is rather small for all depths evaluated, and operation is likely not to be affected. The same accounts for the von Mises stresses. When using 600 refrigerant pipes in the construction, the pressure drop of the fluid flow in the pipes, as well as the induced stresses in the construction, are within practical limits at all depths. The von Mises stresses in the structure are considered small and well below the UTS of the materials presented in Chapter 7.7.1. The structure will therefore withstand the given load. However, the stress and displacement distributions seem to stabilize at a minimum level, at depths larger than or equal to 10 mm. This corresponds to the same optimal depth range suggested by the temperature analysis.

Based on the evaluation of the results from the COMSOL model, the assumed dimensions and calculations of the EES model seem plausible. The temperature profile of the freezing surface yields satisfactory performance, and the displacement and strength are within limits of the metals. The optimal depth of the drum wall is assumed to lie somewhere between 10 and 20 mm, but a final conclusion will not be drawn here. In addition to evaluating temperature, stresses and displacement of the structure, features such as material costs, efficiency and production methods should be included in the overall evaluation; together with a proper optimization process to determine the desirable thickness.

9.5 Final considerations

The COMSOL model uses the same material ratio of the thickness of the sandwich construction that was used in the original model developed by Dieseth (2016). The steel layer composes 40 % of the total depth, and is implemented to strengthen the structure so it will degrade less when the ice layer is scraped off the inner surface. Additional simulations were performed; investigating both decrease and increase of the steel layer and aluminium thickness, Appendix H. These reveal that more aluminium in the structure yields a lower temperature on the freezing surface; due to the greater thermal conductivity, but at the expense of increased stresses within the structure. This increase is however very small, and it is not considered critical regarding the UTS of the materials. In this respect, it is more a question of efficiency and costs. Since the price of aluminium is lower than that of steel (Table 9), there will be a trade-off between thermodynamic performance, minor costs and acceptable tensile strength. This offers the possibility of reducing the required drum wall thickness; by choosing materials of improved thermal efficiency.

The COMSOL model uses a different stainless steel type (AISI4340) than that used in EES. This is because the simulation programs provide different built-in materials. The thermal properties will hence be slightly different, but within a magnitude that is considered acceptable regarding the correspondence of the results from the two simulation programs. It is the trend that is important, not the definite temperatures.

It is seen that the simulation problem is highly dependent on the pressure drop of the fluid flow, which is directly interrelated with the number of refrigerant pipes. Additional simulations show a significant influence on the temperature characteristics when adjusting this drop. Implementing the adapted model with negligible pressure drop through the 600 pipes, gives a considerably lower freezing temperature at the inner drum wall. Lowering the number of refrigerant pipes to 300, results in a correspondingly elevated drop of 184.4 kPa. It is seen that the average temperature at the freezing surface is increased by 0.97 °C. The larger width also leads to a more uneven temperature distribution, Figure A-13. These features confirm the validity of the assumed width and pressure drop correlations implemented in EES. The number of refrigerant pipes should not be lower than 600, as it will provide poorer performance refrigeration wise.

The results from the adapted model differ with simulations of the simplified model of Dieseth (2016), when comparing the performance by using the same amount in refrigerant pipes. The temperature span, both within the structure and at the freezing surface, is larger for model in this thesis. The temperature at the freezing surface is about 4 °C warmer. Also, the adhering displacements and stresses are a little higher, consequently adding to the poorer performance. An even-handed comparison of the performance is however difficult; due to the introduction of new better-suited pressure drop correlations, doubled production rate and adjusted input data. It will be difficult to evaluate the exact influence related to the extended two-phase flow on the structure, since the model is adjusted on many fronts. Although the improved model is not exact, it will provide the most realistic, non-ideal result of the physical interaction.

A drawback with the model, is that it does not take into account the phase changing process of water; which physics is studied separately in EES. This should be included in the COMSOL model when performing a proper optimization of the geometry, as it will influence on both the temperature distribution and the heat transfer characteristics. While the ice layer at the inner freezing surface grows, the total thermal resistance of the structure will increase. This leads to a lower U-value, which hampers the heat transfer. In addition, reduced depth of the model gives a lower temperature at the freezing surface and a simultaneous drop in the U-value; which by Equation (7.12) influences the ice growth rate in different directions. This makes it difficult to predict the outcome without including the coupled physics. The same accounts for variations in choice and ratio of the materials used in the construction. The design parameters should be studied simultaneously, with increased focus on interaction of the variables, before drawing a final conclusion on the optimal depth and the other design parameters. Adaption of the diameter of the refrigerant pipes in the drum wall should also be encountered in a final analysis. It would be relevant to make a prototype model that can be stationed in Granåsen.

10 Air cycle refrigeration system for indoor snow production

In this chapter, indoor snowmaking is investigated in Excel by use of an air cycle refrigeration system. The concept is that the snow is produced in an indoor, controlled environment for extraction to the outdoor ski tracks. The idea behind this model is that the melting losses could be reduced compared to outdoor production methods; thus reducing the required operational time, and offering possibilities of increased production rate. The production hall uses the "Pascal Air" concept to obtain the required refrigeration capacity. The commercial model PAS30-R from Mayekawa (Chapter 5.3) is used as a design reference. Possibilities of heat recovery from the system are explored, and the performance is compared with a conventional refrigeration system using CO_2 as refrigerant.

10.1 Dimensioning of the production hall

The indoor production hall will be placed at the ski arena in Granåsen, close to the outdoor ski tracks. The dimensions are based on the following criteria:

- The hall must be large enough to store the snow produced in a 30 days' period, assuming operation at full load. This accounts for a volume that is large enough to cover the proposed track of 2.5 km (Chapter 8.1).
- The snow machine must have a sufficient height above the snow/floor at any time; to ensure that the water droplets have sufficient time in the air to freeze.
- The production hall should be as small and compact as possible, given the two previous criteria.

The snow machine is dimensioned for a production of 100 tons/day, and an outlet density of 450 kg/m^3. This yields a corresponding snow volume of 6667 m^3, Equation (10.1). As basis for a first estimation, the snow is assumed to constitute one third of the total volume, while the air makes up the remaining two thirds (Eikevik, 2017). This requires the production hall to have a total volume of 20,000 m^3. The minimum height at the outlet of the TDS machine is based on both (a) data from commercial models, and (b) dimensions of existing indoor snow halls (Chapter 2.2). It is set to 6 m (Demaklenko, 2017, Sufag, 2017). A quadratic building shape is chosen in order to minimize the external exposure to the outside; which minimizes the respective heat loss from the building. The dimensions of the building are presented in Table 14. The reader should note that these refer to the internal dimensions of the hall.

$$V_{snow} = \frac{100\,\frac{tons}{day} * 30\ days * 10^3 \frac{kg}{tons}}{450 \frac{kg}{m^3}} = 6667\ m^3 \qquad (10.1)$$

Table 14. Dimensions of the indoor production hall

Length [m]	45
Width [m]	45
Height [m]	10
Total volume [m^3]	20,250
Volume snow [m^3]	6667
Volume air [m^3]	13,583

Among the TDS technologies described in Chapter 2.1, a lance is chosen as the source of snow. A solution with fan guns was also evaluated, but considered less suitable; due to a long throw length, a higher energy consumption, risk of snow to attach on walls, and with higher technical demands for the required control system. As product data from commercial lance models shows that the production capacity is large enough to cover the required rate of 100 tons/day, only one lance is chosen in this first estimated configuration. This will keep the investment to a minimum. More lances can easily be added to the hall, if the production capacity should be extended.

The lance will be mounted on rails in the ceiling, and it is assumed that the snow is evenly distributed on the floor. This is achieved by a configuration where the lance head both can rotate and translate in the volume. The lance is designed with a rotating coupling, both on the air and water side, which is attached to rails, such that it can move in the ceiling. It is supplied with an automatic monitoring system with sensors that can register the differences in snow layer thickness on the floor, and thereby regulate the position of the lance head accordingly. The configuration can alternatively be combined with additional functionalities, such as an automatic rake system, to increase the reliability. The advantage with this configuration is that occupation of vehicles or staff in the hall is avoided during operation. The production process will be fully automated, which reduces the internal heat load. Vehicles are only needed at the end of the production period, when the snow is extracted to the outdoor ski track.

To ensure good snowmaking conditions, the design of the indoor temperature and humidity are important. As a large amount of water droplets are sprayed into the air through the nozzle arrangement during production, the air will contain a substantial amount of water. The RH is set to 90 % (Eikevik, 2017). The dimensioning indoor air temperature (dry-bulb) is set to -7 °C; which value is determined from Figure 6. Since the temperature inside the hall is kept relatively constant, the shape, structure and properties of the snow particles will not change significantly when the snow is accumulated as a layer on the floor without processing. Storage for 30 days without relocation is assumed to have negligible significance on the snow quality (Eikevik, 2017).

By the proposed dimensions of the hall, the height of the snow layer at the end of the 30 days' production period will be 3.29 m. The height above the snow layer at the outlet of the nozzle is then 6.71 m. This gives an extra margin of 0.71 m, in order to ensure sufficient retention time in the air for nucleation.

10.2 Refrigeration load

In the refrigerated space the total refrigeration load have to be balanced with the refrigeration system capacity, in order to keep a constant temperature of the hall. The refrigeration load accounts for the heat generated inside, and the heat transmission into the refrigerated space; due to temperature differences with the ambient. The air cycle plant is dimensioned to cover the load from both air and floor cooling. The different categories of this load (Chapter 4.1) should be calculated in order to determine the dimensioning refrigeration capacity.

The transmission load (Q_{trans}) is calculated for the walls, ceiling and floor, by Equation (10.2). The area used in these calculations is the effective surface area of the hall for each section. The walls, ceiling and floor are heavily insulated to reduce the heat loss to the ambient. The U-values are based on typical commercial and industrial panels used in larger refrigerators or freezers, as well as requirements from TEK15. They are set to 0.12, 0.10 and 0.13 W/m^{2}K for walls, ceiling and floor respectively (HUURRE, 2017, Lavenergiprogrammet, 2016). Since there are no people present during production, windows are not required by TEK15. They are therefore excluded in the building envelope, as they otherwise would have increased the heat loss. The ambient temperature is set to 7°C, and is assumed to equal the average ambient temperature in Trondheim during September and October; at the start-up of the production season (Eikevik, 2017, Meteorologisk institutt, 2017). Variations in temperature and heat load are not taken into account.

$$Q_{trans} = UA(T_{amb} - T_{room}) \tag{10.2}$$

The internal loads include heat losses from illumination and the snow machine. The heat loss from the lance is assumed to be 5 % of the total power input. The power input is based on performance of commercial models, and is set to 2 kW (Sufag, 2017). LED is used as illumination in the hall in order to reduce the heat emission, which is assumed to be 0.80 W/m^2 (Eikevik, 2015). Heat loss from people or vehicles can be neglected, as they are not present during production. Additional losses from other electrical equipment, such as the monitoring system and the sensors, are assumed to be sufficiently small to be neglected in the analysis by good approximation.

The infiltration load is calculated with EES software, provided by CoolPack. It uses a recommended air change factor of 0.5. This number is based on dimensions, temperature and RH conditions of the hall, and it gives a volumetric air flow rate of 421.9 m^3/h. The ambient outdoor air is assumed to have an average RH of 80 % (Meteorologisk institutt, 2017). The air change factor takes into consideration natural infiltration only. This means that heat losses from ventilation, and from opening and closing of doors are excluded in the analysis. Since there are no pollution or emissions from the snow machine, people or other technical equipment, the hall is designed without a controlled air change system (Eikevik, 2017).

Since the "Pascal Air" system excludes the use of evaporators, air coolers and fans in the refrigerated space, heat losses from defrosting or load of air cooler fans are eliminated. The equipment load of this configuration will consequently be zero. This is seen in contrast to the product load, which constitutes the main load of the system. The heat released from the

snowmaking process is calculated in EES by Equation (10.3). This load is equal to the required heat removal in the flake ice system; when assuming no precooling of the grid water before the droplets are sprayed into the air.

$$Q_{prod} = \dot{m}_w(c_{p,w,l}T_{w,in} + h_{fusion,w} + c_{p,ice}\Delta T_{sc}) \qquad (10.3)$$

The estimated refrigeration load of the hall, which is given by the sum of the different heat categories discussed in the previous, is presented in Table 15.

Table 15. Total refrigeration load of the indoor snow production hall

Transmission load [kW]	9.454
Internal load [kW]	1.720
Infiltration load [kW]	3.358
Equipment load [kW]	~0
Product load [kW]	442.4
SUM [kW]	457.023
Estimated value [kW]	460

10.3 System configuration

The model is based on fundamental thermodynamics and theory presented in Chapter 7. It uses a routine library for humid air in Excel (hxLib) to calculate the thermodynamic state points in the cycle. The system can be considered semi-open on the cold side, as the evaporator is eliminated. The main components are an integrated turbo compressor and expander, a primary cooler for heat recovery and an internal heat exchanger. A schematic is shown in Figure 48, together with thermodynamic state points 1-6 from the final analysis. Extended information of is presented in Appendix I, together with state points for PAS30-R. The following simplifications and assumptions for the thermodynamic model have been made:

- Air is treated as an ideal gas with constant specific heat (c_p varies within 0.5 % for $250 < T < 350\ K$).
- Compression and expansion are adiabatic.
- The internal regenerative heat exchanger is adiabatic.
- Negligible pressure drops in pipelines.
- The heat exchangers are implemented with a pressure drop of 2 bar on the air side, similarly to that of the reference model. Simplified state point calculations are used in the model, and empirical correlations for heat transfer in the heat exchangers are not included.
- There is no air leakage from the system.

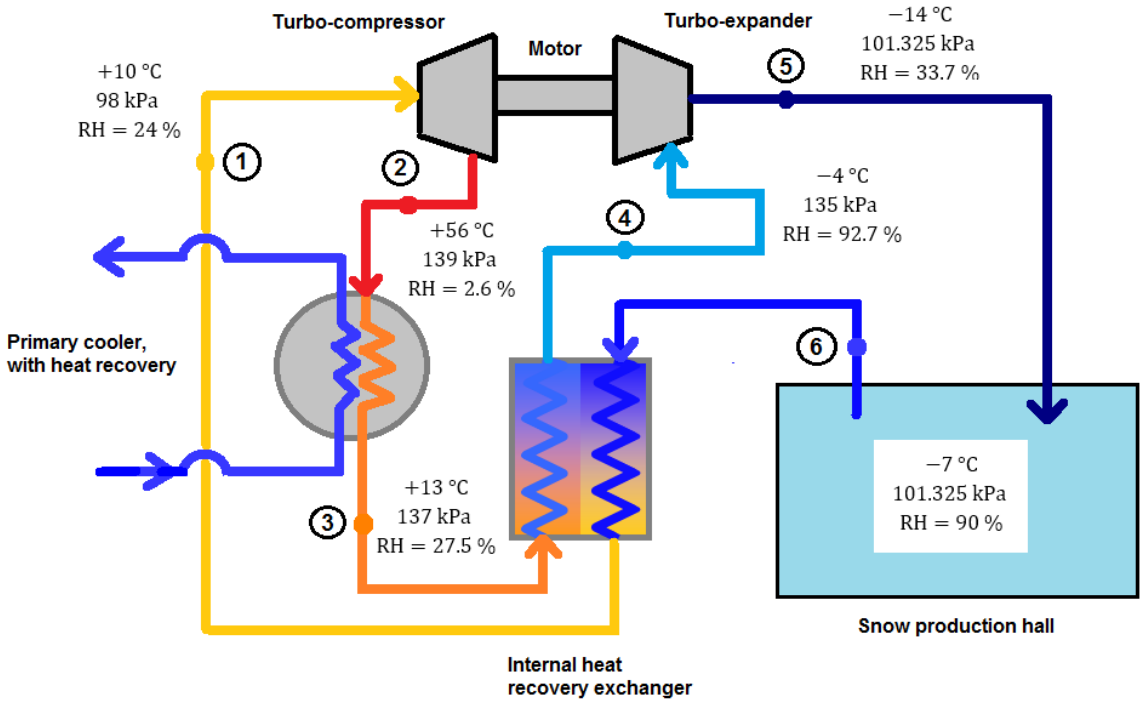

Figure 48. Schematic of the air refrigeration cycle for indoor snow production

The reference model PAS30-R has been used as basis when selecting the design and appropriate pressure levels for the model. As the temperature and humidity conditions inside the hall differ considerably from the reference, adaption of temperatures and pressures in the cycle is required in order for the system to work properly. The system is simulated using efficiencies that are within typical values for low-temperature air compressors and expanders. The isentropic efficiencies are set to 0.65 and 0.55 respectively (Eikevik, 2017, Hafner, 2017). The reader should note that these efficiencies may decrease when the refrigeration temperature is elevated to -7 °C. This is however not explored further, as the analysis is conceptual. The cycle is supposed to stand as a simplified first estimate; in order to highlight the significance of having such an air-cooled system.

10.4 Procedure and design criteria

The snowmaking process is the dimensioning point in the system, which efficiency should be unaffected by the design of the refrigeration system. This poses restrictions on the corresponding thermodynamic conditions (temperature, pressure and RH) inside the hall. In order to find an applicable solution of the air refrigeration cycle, a procedure was conducted, based on trial-and-error. Adaption of the compression ratio and the fixed temperature states were explored simultaneously; by using a parametric sweep. The final solution was based on the following criteria:

- States 1 and 3 are determined by choosing appropriate temperature levels. Firstly, the temperature in state 3 must be chosen such that the approach temperature in the primary cooler is large enough. This approach is restricted by heat recovery when using grid water with an inlet temperature of 8 °C on the cold side. The minimum limit is set to 3 °C, as a lower value would lead to a drastic increase in both the area and the cost of

the heat exchanger (Eikevik, 2017). Secondly, the temperature in point 1 is important because it poses a restriction for cool-down on the hot side of the internal recovery heat exchanger. Since state 4 is fixed by the enthalpy difference on the cold side, it is important that the temperature in point 1 provides temperature and humidity conditions at the inlet of the hall that are within acceptable limits.

- The discharge temperature and pressure must be suitable for heat recovery.
- The discharge pressure should not exceed the MAWP of 0.2 MPa (Chapter 5.3).
- The system must be designed such that icing is avoided.
- The volumetric air flow rate must be within capacity of commercial system components. The compressor, heat exchangers and pipe sections must consequently be designed to handle large flow rates.
- The temperature into the hall (state 5) must be low enough to provide sufficient cooling effect. If this temperature is too high, operational problems will occur, and the refrigeration hall will hamper the efficiency of the water-to-snow conversion.
- Given the previous criteria, the discharge pressure should be designed as low as possible; in order to minimize the compressor work and maximize the COP.

10.5 Results and discussion

The main results from the simulation in Excel are provided in Table 16. This table presents the closest to optimal performance, according to the design criteria. It is seen that the COP of the refrigeration system fits well with test data reported by Fleming et al. (1998) (Chapter 4.2). Nevertheless, the efficiency is lower than that of PAS30-R and typical conventional systems, which configurations have a lower refrigeration temperature. This is illustrated in Figure A-10, Appendix I (Hattori, 2017). Although 30 % of the compressor work is recovered in the expander, which significantly reduces the total power input, the amount of work is increased relative to the evaporator duty compared to other systems. This indicates that the air cycle is not the best system efficiency wise for use in an indoor snow production facility.

Table 16. Results from simulation in Excel

	Air refrigeration cycle
$COP_{cooling}$	0.332
$COP_{heating}$	1.332
Q_{evap}	460 kW
$Q_{primary\ coooler}$	1845 kW
$Q_{internal\ heat\ exchanger}$	734 kW
W_{comp}	1974 kW
$W_{expander}$	590 kW
$\dot{m}_{air}$	115 544 m^3/h
	41.13 kg/s
Formation of ice/condensate in the expander	229.5 kg/h
	0.0637 kg/s

The duties of the heat exchangers and the work demand of the compressor are considerable. They are significantly larger than for the reference model. This is to a great extent a direct consequence of the elevated volumetric air flow rate, which is increased drastically from 1.48 to 41.13 kg/s; due to the very high product load from the snowmaking process, as well as lower enthalpy difference between the inlet and outlet of the production hall (Hattori, 2017). The refrigeration capacity is increased above tenfold. The temperature difference is reduced from 20 to 7 °C compared to PAS30-R, which directly influences the enthalpy difference. By the required thermodynamic conditions of the indoor space, it was not possible to obtain the same temperature difference without exceeding any of the design criteria. As much as 80 % of the water vapour must be extracted from the air flow, in terms of condensate/ice, in order to achieve an acceptable cool-down. This cool-down was the lowest possible to be obtained, when designing for simultaneous heat recovery in the primary cooler, as well as keeping extraction of vapour to a minimum.

The large duties of the turbomachinery and the heat exchangers are not considered an operational problem, as such high duties are used extensively in related industries, especially in gas power cycles (Moran et al., 2012b, Park et al., 2012). However, special care should be taken regarding the high volumetric flow rate; to ensure that the components can handle such large air flows at the given pressure ratio and temperature range, without a significant drop in the efficiency (Bakken, 2017). It is clear that the dimensions in the reference models are too small and no longer applicable for the adapted design. Larger heat transfer surfaces are required, and with stricter demands on the axial compressor and expander design. In particular, since the COP depends significantly on the efficiency of the compressor and turbine, it is evident that the competitiveness of the air cycle depends strongly upon achieving high component performance. Due to rapid technological development, dynamic compressors and expanders can easily deal with high flow rates. Commercial manufactures report data of turbo compressors that can provide flow rates of 50,000 to 1,300,000 m^3/h at the given compression ratio, and with high efficiencies (Giannetti and Milazzo, 2014, MAN Diesel & Turbo, 2017, Siemens AG, 2008). Thus, design for the flow rate is more a question of ensuring a reliable and flexible system; that is compatible with the snow production.

The analyses show that a significant amount of ice will be generated in the expander. This is critical for the performance. The expander is sensitive to saturation, and the substantial amount of generated ice will lead to operational problems, and in worst case failure. By the given conditions of the indoor hall, it was difficult to find an acceptable performance that simultaneously satisfied each design criterion. The combination of high RH and elevated refrigeration temperature, leads to a substantial increase in the absolute humidity compared to the reference. With a higher indoor temperature, the air may contain significantly more water vapour (Chapter 2.2), which increases the potential for condensation or icing; if the dew point temperature is below 0 °C. The high mass flow rate will amplify the influence on differences in absolute humidity throughout the cycle, which determines the amount of saturated vapour. Also, a large flow rate would increase turbulence of the air, and hence the risk of directly circulating moisture from the snowmaking apparatus through the refrigeration cycle.

Since icing in the expander will lead to operational problems, separation of liquid before this unit is crucial in order for the system to work properly. In order to solve this problem, possibilities of integrating a dehumidifier in the cycle was investigated. The position of a dehumidifier was evaluated at various points in the cycle. Integration at state point 3 or 4 resulted in a cool-down temperature above 0 °C, when adjusting the dew point temperature at the inlet of the dehumidifier to a level slightly above 0 °C to avoid icing. Regardless of the compression ratio chosen, no valid solution was obtained; since the temperature at the inlet to the hall cannot be higher than that inside. Integration at state point 2 was also considered, but considered inappropriate; due an unrealistic high and dominating duty of the dehumidifier, large temperature differences within the unit, high outlet temperature and insufficient cool-down. At all cases evaluated, the dehumidifier would require compression above the MAWP, and with corresponding lower cool-down into the hall. This adds to a poorer refrigeration performance and an increased mass flow rate.

Valid solutions for the expander were only obtained with a dew point temperature of the dehumidifier below the freezing point. This resulted in a similar or slightly increase in the COP compared to the proposed solution. However, such design conditions would not ease the operational problems of the thermodynamic cycle. As long as the dew point is below 0 °C, icing will occur instead of condensation. This leads to operational problems in the dehumidifier; as collection of ice can be critical and difficult during extraction. Also, the heat transfer performance would decline drastically with frosting. Thus, the frost problem would not be solved, but rather moved from the expander to the heat exchanger. A defrost procedure similar to that of air coolers in conventional refrigeration systems would be required in such a case; to melt the dynamically growing ice layer and remove condensate. This would consequently eliminate the advantage of removing the evaporator from the open air cycle (Chapter 4.2).

Hattori (2017) has reported test data of frost formation in the reference model. Frost is seen to be accumulated in the internal heat recovery exchanger or in the air ducts between the warehouse and the heat exchanger. Regardless, as the amount of saturated liquid is quite low, it takes long time for an ice layer to attach on the surfaces. Experience shows that the frost that accumulates falls into the warehouse, but that most of it sublimates once it enters the warehouse. Since the frost formation is sufficiently small at ultra-low temperatures inside the warehouse, this phenomenon will not cause any operational problems. This is seen in contrast to the simulated performance for indoor snow production. The different nature of the application areas for the two models, both with respect to the size of the product load, which directly is a result of the large snow production rate, and the moisture content from the snowmaking, can explain this difference. Regardless of the design chosen, it is seen to be impossible to thermodynamically avoid ice formation of any kind; by the given dimensional point from snowmaking, and the assumed component efficiencies.

Adaption of the mass flow rate will not remove the frost problem, as the state points are unaffected by the flow rate. It might however improve the scope of it. It will be a question of the design and capacity of the expander, or alternatively the dehumidifier, on how much frost formation is allowed, if any, to ensure problem free operation without a required production halt. The amount of ice formation is too high to be tolerated by the proposed configuration

(Eikevik, 2017, Hattori, 2017). Possible measures to reduce the flow rate could alternatively be explored, such as (a) precooling of water to the lances, or (b) reduction of the snow production rate. Precooling from 8 to 2 °C would reduce the product load by 29.1 kW, but at the expense of increased power input to the cooling device. Since most of the product load is associated with the latent heat of water however, precooling is seen not to have the largest influence on the air flow rate. For alternative (b), the influence on decreased air flow rate is seen to be more efficient, depending on the reduction in snow production rate. However, this reduction must be rather large, in order to obtain a valid solution. Applying the same air flow rate as used in PAS30-R to the indoor hall, gives a frost formation of 0.0023 kg/s in the expander. The icing is thereby reduced by 96 %, with a corresponding refrigeration duty of 17 kW. Hence, a less distinct problem regarding icing at lower refrigeration demands, but at the expense of a drastic reduction of the snowmaking efficiency and substantial increase of the required production time. This makes alternative (b) unacceptable for the case in Granåsen.

Heat recovery

The duty of the primary cooler is 1845 kW. This is four times the refrigeration effect, and it represents a large potential for heat recovery. Due to the extensive amount of energy used for providing an indoor refrigerated space cold enough for storage and production, the total efficiency would be improved if heat from the primary cooler could be utilized. The compression ratio of the air cycle is not increased in terms of heat recovery; due to the amplified frost problematics in the expander with increasing discharge pressure. Utilization of the excess heat from the system will therefore not be at the expense of the refrigeration effect, and it may contribute to defend the investment costs of such a facility.

The inlet and outlet temperature of the primary cooler is 56 and 13 °C, and these will determine the suitability of possible heat recovery strategies. By the proposed design criteria, the approach temperature should not be lower than 3 °C on both sides of the heat exchanger. This means that the heat receiving fluid can be heated from maximum 10 to 53 °C. Also, as the snowmaking is operated constantly at full load during production, this will determine the utilization time of the excess heat. Heat recovery will only be available during snow production, which in this thesis is intended to be in the autumn; with possibilities of extension to include the winter months. Table 17 provides an overview of some relevant strategies at the site, together with corresponding temperature ranges for each application. The reader should note that these temperatures are reference values at design conditions. They are thereby not definite, and may be adapted to fit a specific application.

Table 17. Heat recovery strategies for the indoor air refrigeration cycle

Strategy	Forward and return temperatures at design conditions
Floor heating	40 °C / 30 °C
Low temperature radiators	55 °C / 45 °C
Snow melting	35 °C /20 °C
Ventilation system[11]	60 °C / 30 °C
Heating of hot tap water[12]	80 °C / 8 °C

An exact description of a heat recovery configuration is not included; as the frost problematics must be solved before heat recovery can be implemented. Possible solutions will only be briefly outlined. Since the maximum outlet temperature is limited to 53 °C, low-temperature solutions will be the most relevant. Strategies with a utilization time that follows the snow production closely will be favourable. In this respect, snow melting at parking lots and entrances to buildings at the ski arena wold be a good solution; as the demand is only present during the winter/autumn. The heating demand of the buildings surrounding the ski arena is highest during winter, and the excess heat can also be used to cover the peak loads of this demand. The temperature range is applicable both for floor heating, radiators and ventilation devices respectively. Alternatively, the excess heat can be used for preheating of hot tap water, where the rest of the DHW demand is covered elsewhere. The available heat may not necessarily cover the total demand for a given application. Instead, the surplus can be used in a mode where different strategies are combined (Chapter 7.3.1). An example of a possible configuration is shown in Figure 49. This may improve the performance; due to a better temperature fit between the heat receiving and heat rejecting fluid. It might be necessary with such a configuration if the demand for a single strategy is not large enough to cover the total surplus.

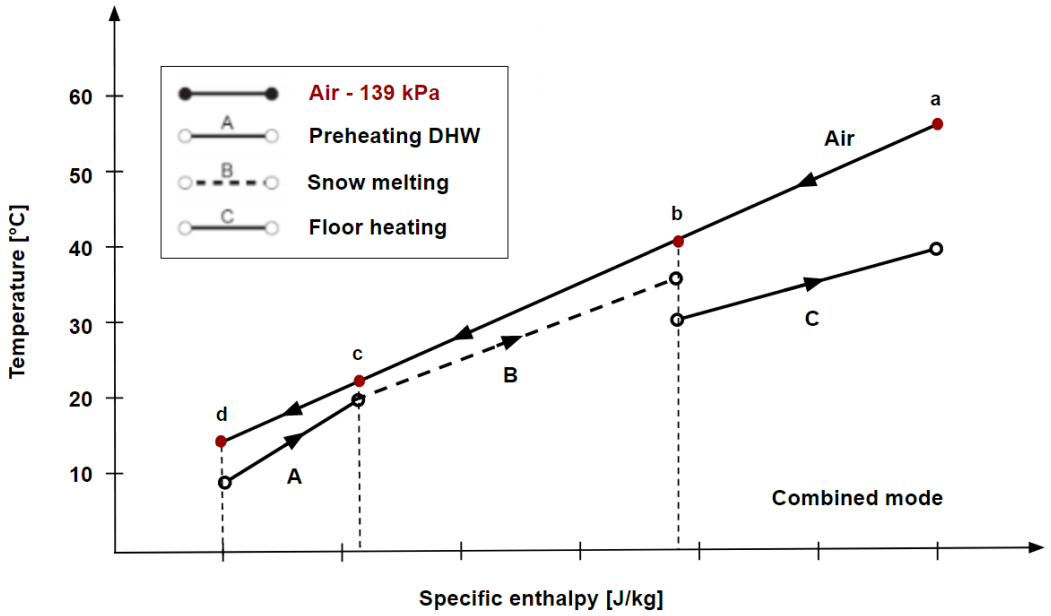

Figure 49. Heat recovery in combined mode

[11] The temperature levels depend on many factors; such as the building code standard, type of ventilation system, requirements for the indoor air quality, climate and ambient conditions.
[12] Assuming a similar principle to that of the DHW case for the flake ice system (Chapter 8).

PAS30-R and the proposed system by Andou and Okuda (2004) use a cooling tower and air-to-air heat exchanger to dump the excess heat from the system respectively. When these systems are implemented with low air flow rates and refrigeration loads, the heat recovery potential is too low for implementation to be economically profitable (Hattori, 2017). This is seen in contrast to the proposed model, Figure 48. Since the snowmaking process poses a high demand on the refrigeration load, heat recovery is crucial in order to obtain a system with an environmental friendly profile; within the scope of "Snow for the future".

10.6 Comparison with traditional refrigeration system

In order to compare the performance of the air refrigeration cycle with a traditional refrigeration system for indoor snow production, a simplified model was developed. This system uses CO_2 as working fluid in a trancritical cycle. It is designed for the same product load and indoor thermodynamic conditions as the air cycle. A schematic is shown in Figure 50. The model is developed in Excel and uses RnLib to calculate the thermodynamic state points of the cycle. These are provided in Figure A-11, Appendix J. The calculations are based on fundamental thermodynamics, and simplified state point calculations are used to estimate the cycle performance. The system is implemented with heat recovery in the gas cooler; with a pressure of 85 bar[13] and an outlet temperature of 13 °C. An approach temperature of 6 °C is used for the evaporator, and with 5 °C superheat provided by the SGHX. The compressor is simulated with a heat loss factor of 10 % and an isentropic efficiency calculated by Equation (8.70). Pressure losses through the heat exchangers and the pipelines are neglected.

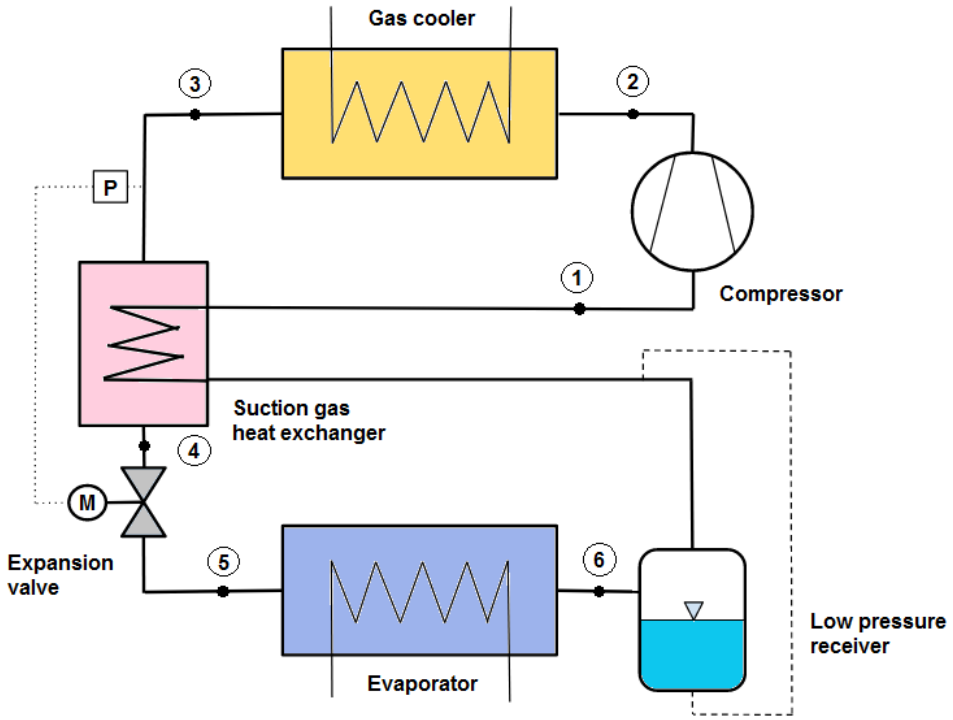

Figure 50. Schematic of the CO_2-refrigeration cycle

[13] The gas cooler pressure is not optimized in terms of maximized heat recovery, and the location of the pinch point is not evaluated. The state points are fixed, similarly to the procedure in the pre-study.

The excess heat in the gas cooler is used for DHW heating; with heating from 8 to 80 °C. The strategy is similar to that described in the pre-study. The level of heat recovery can easily be adapted by changing the gas cooler pressure, but at the expense of increased power input to the compressor. 85 bar is chosen in this first design solution, and changes will not be explored (Eikevik, 2017).

10.6.1 Extension of the refrigeration load

The estimated refrigeration load from Chapter 10.2 must be extended to include heat loss from evaporator fans and defrosting of air coolers when applied in a traditional refrigeration system for indoor snow production (Chapter 4.1). This equipment load is calculated with basis in a commercial air cooler model by Goedhart/GEA: LLK.s-481 m^2 (Comron International BV, 2016). This model is applicable with CO_2 as refrigerant, and it is applied with electrical defrost in a drip tray, shut-off hoods at defrosting, and wide fin spacing. One unit covers a refrigeration capacity of 140 kW, and it is supplied with four fans, each of 4 kW. Based on recommendations by ASHRAE, the heat loss from the fans and defrost procedure are estimated to be 20 % of the total load (ASHRAE, 2010). As four air coolers are required to deliver the specific refrigeration capacity, the estimated equipment load is found to be 12.8 kW. This gives a total load of 470 kW for the production hall.

10.6.2 Results and comparison

The main results from the simulations are provided in Table A-8, Appendix J. As can be seen, the mass flow rate is reduced drastically and to a more reasonable range, compared to the air refrigeration cycle. The mass flow rate of CO_2 is only 5.3 % of the required air flow rate, which gives a correspondingly lower duty of the heat recovery unit, as well as significantly lower energy use for the compressor. This is seen as a direct result of the different thermodynamic properties of the air cycle and the vapour compression cycle, featured in Chapter 7.4. With an evaporator installed inside the hall, instead of an open cycle where the air is circulated directly, the enthalpy difference between the inlet and outlet state will be much higher. This gives a correspondingly lower mass flow rate to provide the required cooling effect. The CO_2 cycle will not be affected by operational problems, such as icing. Since the design of the refrigeration system is indirect[14], it will be easier to design a refrigeration cycle that provides sufficient cooling effect, without influencing on the efficiency of the snowmaking process. This is seen in contrast to the direct air circulation of the "Pascal Air" cycle; where the refrigeration system and the indoor conditions are highly interrelated. The air cycle provides the same refrigeration effect, but with larger difficulties regarding appropriate design of the state points and blown-in temperature to the hall, in order to avoid icing. The CO_2 cycle will thus be easier to regulate, if ambient or indoor conditions where to change.

The drawback with applying a conventional refrigeration system, is that the air coolers must be defrosted regularly to avoid operational problems and decreased heat transfer performance. This leads to an increase of the refrigeration load of 2.2 % compared to the air cycle. However, as

[14] "Indirect design" refers to a configuration where the air inside the hall is not in direct contact with the components in the refrigeration system. The separation takes place in terms of the evaporator in the system, which transfers heat from the air to the refrigerant.

the product load from the snowmaking constitutes 94 % of the total load, this extra load will be less distinct. Due to better efficiencies of the components in the vapour compression cycle, higher heat transfer coefficients of CO_2 compared to air, and a considerably smaller volumetric flow rate, the drawback from the defrost procedure will be negligible; as the efficiency of the CO_2 cycle is better. The COP for cooling and heating is about 3 and 10 times greater. This is despite of a higher pressure ratio and pressure levels, as well as no expansion work recovery in the CO_2 cycle. Also, eliminating the evaporators from the refrigeration system by using air both as refrigerant and as substitute in the snowmaking process, tends to be difficult if a simultaneous frost-free procedure and good cycle efficiency should be obtained. Frost formation in some way will occur regardless of the cycle chosen, but with considerably less operational problems and better performance for the CO_2 cycle at the dimensioning indoor conditions. Thus, the conventional system solution is preferred.

The duty of the gas cooler comprises only 33.4 % of the duty from the primary cooler in the air cycle. However, as the duties are large for both systems, the potential for heat recovery from the transcritical CO_2 cycle is considerable, although it is smaller than for the air cycle. The discharge temperature from the compressor is 97 and 56 °C for the CO_2 and air cycle respectively, and with a cool-down temperature of 13 °C for both systems. This indicates differences in optimal heat recovery strategies. The heat receiving fluid can be heated to higher temperatures when CO_2 is used as refrigerant. While the transcritical cycle is applicable for complete DHW heating to reach its target temperature of 80°C, additional heating is needed to cover the total DHW demand when the air cycle is applied. Other combined solutions might be more suitable for the air configuration. Also, if the air flow rate is adjusted to a more reasonable range, the duty of the recovery heat exchanger would decline drastically. This would lead to a following reduction in the heat recovery potential and a relative improvement of the gas cooler duty.

10.7 Final considerations

By the given nature of the snowmaking process, especially the high product load, the air refrigeration model proposed here will not be suitable for cooling the indoor production hall. The temperature and humidity range is by the analysis seen not to be compatible with the high refrigeration load; as a large amount of ice will be generated in the expander. Applying a dehumidifier to the cycle will not solve the operational problems; as the dew point temperature of the unit will be below 0 °C, regardless of the position. The operational problems are removed from the expander to this unit, and with a required defrost procedure of the dehumidifier, similar to that of conventional air coolers applied in indoor snow facilities.

As the heat load from the snowmaking constitutes the major part of the total load, the heat loss from evaporator fans, air coolers and defrosting will be negligible if a traditional refrigeration system is applied, such as the CO_2 cycle evaluated in this chapter. This means that the advantage of directly circulating air through an open configuration, in which the evaporator is removed, will narrow down. When the product load is this high, it will be irrespective of which refrigeration temperature is chosen. The performance compared to conventional systems will be worse when the refrigeration temperature is elevated, as the frost formation is amplified.

Also, the COP of the “Pascal Air” system narrows down respectively when the temperature approaches 0 °C, and the efficiency of a traditional refrigeration system is seen to be significantly higher. Thus, if the air refrigeration cycle is to be competitive with other solutions, the analyses point to an operating condition where the refrigeration load is lowered considerably, and with a simultaneous reduction in refrigeration temperature. These considerations confirm the results from literature (Chapter 4.2).

In order for the air refrigeration cycle to be competitive with other refrigeration systems, the temperature inside the production hall must be lowered. With a lower temperature, the ability of the air to contain moisture will decline, and less moisture would be circulated through the system. It would consequently be easier to design the system with lower cool-down temperature into the hall, without reaching saturation. Also, the volumetric flow rate would be reduced in such a case. However, adaption to lower temperatures inside the hall would increase the total refrigeration load; both from the snowmaking process, and from transmission and infiltration. As the product load from the snowmaking already is considerable, this would be unfortunate. The aim is to keep the indoor temperature to a level where the refrigeration load is reduced to a minimum, at the same time as it is beneficial and applicable for providing good snowmaking conditions. Lowering the temperature to avoid icing would then be at the expense of increased energy consumption. The dimensioning point would thereby be removed from the snowmaking process to the refrigeration system, which is undesirable. The performance of a traditional refrigeration system would be much better in this respect; as it can easily be designed to fit the optimal thermodynamic conditions of snowmaking, without operational problems or drop in efficiency. Also, since conventional systems can be applied with environmental friendly refrigerants, such as CO_2, this will not be a drawback in terms of obtaining a green solution.

11 Comparison of the snowmaking systems

11.1 Production capacity

The simulation models are designed with the same production capacity, in order to cover the total volume of the proposed ski track at the start-up of the season (Chapter 8.1). They are simulated with a production time of 30 days per season, based on a continuous 24 hours' production each day. The density from the FID is assumed to be 500 kg/m^3, equal to the average density of the flake ice models, SF220 and SnowGen 100FI, presented in Table 5. Since the density of the snow produced by the lance is set to be lower, the indoor facilities will be more effective productivity wise; as they can produce more snow during 30 days (Table 16). This is amplified by decreased melting losses during operation when the production is moved from outdoors to an indoor controlled environment (Chapter 11.4).

Although the above considerations have been used as basis for the simulation models, the operational time will most likely be extended. In a future perspective, it is reasonable to assume that the models not only should supply snow at the start of the season, but also throughout the season if needed. Also, the proposed ski track may be extended, such that the ski resort can provide more and longer tracks. These features imply that the results from this thesis only will serve as conservative estimates of the performances. Increasing the production time will raise both the power consumption and the excess heat, in which highlights the importance of heat recovery from such systems.

11.2 Thermodynamic performance

The main results from the thermodynamic analyses of the different simulation models developed in this thesis are tabulated in Table 18.

Table 18. Comparison of main results

	Flake ice system	Indoor air refrigeration cycle with TDS	Indoor transcritical CO_2 cycle with TDS
Q_{ref}	442 kW	460 kW	470 kW
W_{tot}	266 kW	1384 kW	147 kW
$COP_{cooling}$	1.66	0.33	3.20
$Q_{heat\ recovery}$	629 kW	1845 kW	617 kW
$COP_{heating}$	2.37	1.33	4.20
$\dot{m}_R$	1.91 kg/s	41.13 kg/s	2.17 kg/s

It is seen that the air refrigeration cycle has the worst performance efficiency wise; both regarding refrigeration and heating. Since operational problems cannot be avoided during production, the air cycle is concluded to be unsuitable for indoor snowmaking. It will be discarded from further discussion. Although the efficiencies of the integrated compressor and turbine were to be improved, it would not be sufficient for the air cycle to be competitive with traditional systems; due to the substantial gap in COP at the indoor design criteria.

The efficiencies of the indoor CO_2 cycle are seen to be considerably higher than those of the flake ice system. Less energy is needed to provide the required refrigeration effect for a production rate of 100 tons/day, although the refrigeration load is increased when production occurs in an indoor controlled environment. Also, the heat recovery potential from the gas cooler is in the same range as that in the flake ice system, but with a significantly lower compressor work to obtain the same duty. These features can be seen as a direct consequence of the different refrigeration temperatures required for the FID and the lance. While the FID needs a refrigeration temperature in a range below -20 °C to obtain efficient water-to-snow conversion, lances may cope with a considerably higher refrigeration temperature, closer to the freezing point of water. The refrigeration temperatures in the heat recovery configurations are -35 °C and -13 °C for the two systems respectively. While two-stage compression is needed for the flake ice system to obtain sufficiently high discharge temperatures, without exceeding the maximum capacity of the compressor, one-stage compression can be applied in an indoor system. Hence, the indoor transcritical CO_2 cycle will be favourable efficiency wise.

The simulation models are analysed using different assumptions and amount of simplifications. Firstly, while the flake ice model has been adapted from the pre-study and included with proper heat transfer and pressure drop correlations for the complete system, the indoor transcritical cycle uses simplified state point calculations; with no pressure drop through the cycle components. Hence, the performance in terms of the indoor cycle will be closer to an ideal case. The flake ice system gives a more accurate description of the actual performance. Secondly, as the gas cooler pressure is raised to an optimal level, which maximizes heat recovery from the FID at the given production rate, the COPs will decrease compared to the indoor system. Adapting the indoor CO_2 cycle to include proper empirical correlations and optimized gas cooler pressure, would make the comparison more even-handed. The difference in cycle efficiencies is expected to narrow down, by the above considerations. Regardless, indoor production with basis in TDS is still assumed to provide the best performance efficiency wise; due to the fundamental difference in refrigeration temperature.

11.3 Design criteria and operational aspects

In addition to evaluate the thermodynamic performance, the following design criteria should be fulfilled:

1. The refrigerant flow rate should be within reasonable limits.
2. Design of the system must be such that distinct operational problems are avoided during snow production.
3. The total system should have good overall performance; both regarding heating and refrigeration. Utilization of the surplus energy should not be at the expense of decreased efficiency of the snow production. The snowmaking should be the dimensioning point in the system, while heat recovery is designed accordingly.
4. The heat recovery system should be both flexible and reliable, and adaptable to changes in the production rate or the ambient environment.
5. There must exist a sufficient market and demand in the nearby area, to accommodate the strategies for utilizing the surplus heat from the system.

Both CO_2 cycles feature reasonable flow rates; within the same practical range. While the "Pascal Air" concept was affected by frost formation and icing, use of CO_2 as refrigerant, both in the outdoor and indoor models, yields problem free operation. This is crucial for the system to work properly. Both solutions are suitable in this respect.

Both systems satisfy criterion 3. The snowmaking load remains the dimensioning point, which is desirable, while the surplus is maximized at the fixed optimal conditions of the snowmaking process. The COP_cooling is seen to be lowered when adapting the gas cooler pressure to a level suitable for heat recovery. However, the fundamental properties of the snow producing process remain constant. This means that heat recovery is implemented without affecting the efficiency of the water-to-snow conversion. The efficiency of the snowmaking unit is on the other side seen to be highly dependent on the production rate, especially for the FID. Increasing the capacity of the snow producing equipment from 50 to 100 tons/day emphasizes the importance of optimized design; to ensure maximum efficiency. This should have increased focus in a further design process; since the snow producing equipment is more sensitive to changes in the production rate than in the heat recovery cycle.

The systems will also satisfy criterion 4 to a great extent. As both CO_2 systems are indirect, the thermodynamic conditions of the snowmaking will not be influenced by changes in the heat recovery cycle in the same manner as the "Pascal Air" model. The heat recovery systems are designed such that they can be adaptable to changes in the snowmaking process; which makes both systems flexible and reliable. Measures can be implemented to improve the performance if the operating conditions should change (Chapter 8.4.4).

Adjusting the refrigeration system to operate with supercritical heat release, offers good potential for heat recovery. DHW heating is implemented for both cycles. The DHW case from the pre-study was considered the preferred heat recovery solution among a selection of different strategies. High discharge temperatures are obtained for both CO_2 systems, and the outlet temperature of the gas cooler can easily be regulated to ensure sufficient cool-down. The flake ice system obtains somewhat lower outlet temperature, but it is reasonable to assume equally good performance if the indoor cycle is optimized. The surplus heat available at a production rate of 100 tons/day and such a configuration is seen to be extensive. In order for the systems to be realizable, it requires that criterion 5 is fulfilled. This topic was explored in the pre-study; where a simplified market analysis suggested that the DHW case was be feasible if (a) implementation was economically profitable, and (b) a sufficient number of customers were willing to accommodate the solution. The response was positive among a limited selection of customers, and the analysis showed that there is an increasing interest to accommodate green solutions. At this stage in the study, it is still too early to draw a final conclusion; as more extensive analyses are required to determine the exact market potential.

11.4 Snow melting and climatic impact on production rates

The systems evaluated in this thesis are simulated without taking into consideration the effect of snow melting and climatic impact on the production rates. With increased melting rate, the flake ice system will be less efficient compared to the indoor CO_2 cycle. This amplifies the thermodynamic preference for the indoor production methods. Removing the production from outdoors to an indoor controlled environment would reduce the melting rate during production. The flake ice system must increase the production time, in order for the system to obtain the same volume as in the indoor transcritical refrigeration system. The extent of the melting is however difficult to evaluate without a proper model. The climatic conditions may vary considerably from year to year; both with respect to temperature, wind and precipitation. The EES model should be combined with models for snow melting and climatic impact on production rates; in order to obtain a more realistic picture of the system efficiency.

In the further course of developing solutions, it will also be crucial to consider the melting rate on the ski track. It should be evaluated if temporary storage of the snow, or extended supply during the season, are necessary, and to which extent. The reader can expect the production rate to be elevated considerably compared to the rate outlined in this thesis; which only serves as a first conservative estimate. Increasing this theoretical production time will elevate the available surplus at the expense of increased power input. This emphasizes the importance of implementing such systems with heat recovery; in order to obtain an energy and cost-efficient system within the scope of "Snow for the future".

11.5 Additional considerations

As part of the process of finding the optimal system solution for Granåsen ski arena, a proper cost analysis is required. Both investment and operational costs must be included in the evaluation. Also, a feasibility study of the required infrastructure and space demand should be carried out. While the indoor system directly circulates the air in an open system configuration, the flake ice system uses a heat pump cascade to lift the low temperature and pressure to an acceptable level for heat recovery. This way, it is possible to reduce the piping and the number of heat exchangers in the indoor system. However, the indoor hall requires a larger floor area (and volume) than the proposed flake ice system; with outer dimensions that must be accurately planned to fit with the infrastructure surrounding the ski arena. This was outlined by Vagle (2016). A sufficient number of air coolers must be installed in the ceiling, as well as evaporator fans, heavily insulated walls and floor, and automatized rail and monitoring system with lances in the ceiling. The indoor configuration is thus expected to be both more space demanding and expensive than the flake ice model. However, a proper analysis should be carried out; as these factors are mutually dependent and highly interrelated with the other criteria.

The different production strategies may offer variations in optimal application area, as outlined in Chapter 6. Since the snow from the systems is intended for cross-country skiing, to be used on a proposed ski track, it should provide a compact, hard and even surface; that is durable and with good lubricating properties. By the analysis performed in this thesis it is difficult to evaluate such aspects, since the main focus have been on the design of a suitable refrigeration and heat recovery system, when fixing the thermodynamic snowmaking conditions.

Optimization with respect to snow quality from the production unit is not included, as well as climatic impact and properties of the snow on the ready ski track. It is hence difficult to say whether indoor TDS or outdoor TIS will provide the best suitable snow conditions for the site. Possible differences are not accounted for in the recommended system solution (Chapter 11.7). In the further course of developing solutions, the snow quality aspect should be included in an overall evaluation; studied in close association with the local climatic conditions.

It should also be emphasized that the thermodynamic performance evaluated in this thesis is directly related to the combined refrigeration and heating system. It is the compressor that mainly provides the required refrigeration effect, and only compressor work is included in the efficiency calculations of the refrigeration systems. Care should however be taken using these results as a stand-alone decision basis, since additional energy requirement is present due to the snowmaking devices. This should be included in an overall evaluation. For the flake ice system, additional electrical consumption from the scraping device, ice crusher, distribution system, circulation pumps and regulating devices should be considered. In an indoor production hall, additional energy demand to evaporator fans, the defrost procedure, lances and automatic monitoring and rail system in the ceiling are present. Extending the simulation models to include such factors will improve the validity of the analysis; and thereby provide a more accurate estimation of the overall system performance. If differences in the electrical power consumption related directly to the snow producing unit (FID/lance) are distinct, the error by evaluating only the efficiency of the required refrigeration system can be significant. This points to the need of a more extensive analysis.

11.6 Lines to the previous master assignments

Dieseth (2016) investigated outdoor snow production by comparing the performance of a VIM and a FID, when integrated with an appropriate refrigeration system. The performance of both systems was good in terms of achieving a high production rate and an efficient refrigeration system, in favour of the VIM. However, when implemented with heat recovery, the VIM system was found to be less appropriate; as it is sensitive to elevated discharge temperatures, which must be balanced to avoid operational problems for the compressor. Dieseth concluded that the snow produced by both technologies was expensive and with an extensive amount of surplus heat available, and that heat recovery should be implemented to make the machines more reasonable.

Vagle (2016) studied four separate cases, where different production methods and heat recovery strategies at the specific production site were investigated. Simplified estimates of investment costs and melting rates were obtained. They were reviewed together with thermodynamic models for combined refrigeration and heating; with the main focus on implemented heat recovery. Snow storage with basis in outdoor TDS was considered the cheapest solution, but it suffered from the lack of possibility to produce supplementary snow at marginal temperatures. An extra volume of snow must be stored as a precaution for the unpredictability of the weather, which decreased the effectiveness and reliability of this case. Furthermore, TIS with basis in flake ice production was adapted to a configuration where both direct and indirect heat recovery was considered. The surplus heat was designed to meet the heating and DHW demand of three

planned buildings at the ski arena in Granåsen. The direct solution used the heating demand as the dimensioning point; with snow production adjusted accordingly. Extending the FID to operate constantly throughout the whole year decreased both the flexibility and efficiency of the snow production; as there is an antagonism between the need of heat and the need of snow. The indirect solution with BTES solved this problem by storing the heat in the ground, to be drawn to the buildings when the demand was present. The dimensioning point was thereby preserved for the snow machine, but the solution suffered from high investments costs compared to the amount of recovered energy.

The fourth system was based on indoor production, using similar principles as the conventional CO_2 refrigeration system outlined in this thesis. Vagle (2016) concluded such a system to be favourable if a large heating demand was present; due to minimized melting losses and good flexibility and reliability – possibly in combination with BTES to ensure long term storage of heat. This solution suffered from extensive investment costs however. While the investment cost of the outdoor flake ice system was roughly estimated to 17.2 MNOK, it was 32 MNOK for the indoor facility. The operating costs were seen to be reduced when implementing the snow production equipment with heat recovery, but with a substantially lower EVR and a faster pay-back period for the FID technology.

While no proper model for snow melting and climatic impact has been included in this thesis, Vagle (2016) used the Degree-day method to get a rough first estimate of the melting rate associated with the uncovered snow pile during production. For the FID evaluated in combination with both direct and indirect heat recovery, the melting losses were estimated between 56 and 68 %. This emphasizes the distinct drawback of outdoor production systems, and it confirms the discussion from Chapter 11.4.

Vagle (2016) concluded snow storage to be the most suitable solution, since an accessible heating demand for a continuous operation of the snowmaking equipment was considered not to be present at the ski arena. However, the DHW strategy evaluated in the pre-study pointed to the feasibility of utilizing the surplus from snowmaking; provided that the market analysis was extended to include relevant customers in the nearby area, such as schools, swimming pools and hotels – and not only heating demand at the specific production site. This supports the favourability of a combined heating and refrigeration system, which operation was outlined by Dieseth (2016).

Reviewing the conclusions from the previous master assignments and the pre-study in combination with results from this thesis, indicates that both indoor TDS and outdoor FID solutions can be applicable; depending on the economic interest and available budget. Nevertheless, indoor snowmaking is outlined as the best suitable solution for the site within the scope and framework of these assignments. It is considered the most viable system in a future perspective; due to the benefits of superior thermodynamic efficiency, minor melting losses and good regulating options. This is provided that there are sufficient demands in the project. Although this solution is regarded as the most expensive configuration, in terms of the extensive investment costs, commercialization of such systems is increasingly common (Chapter 4.1). The impact of snow melting on outdoor production methods will not be efficient in a future

perspective, in the light of shorter and milder winters. The FID system will not be competitive with indoor production methods, unless some measure is implemented.

11.7 Final recommendation

Through this discussion, the following aspects have been highlighted:

- Indoor versus outdoor snow production
- TDS versus TIS
- Direct versus indirect refrigeration system
- Use of refrigerant: air versus CO_2
- Appropriate heat recovery strategies adapted to the refrigeration systems
- Utilization of the surplus heat to (a) cover the energy demand directly at the specific production site, or (b) extension to cover the demand in the nearby area
- Location of the dimensioning point: snowmaking versus heat recovery

As indicated through this chapter, the process of finding the optimal system solution for the ski arena is complex. It requires different criteria to be studied simultaneously. The thermodynamic results from this thesis should be combined with complete models for snow melting and climatic impact on production rates. This must further be seen in combination with simultaneous investment costs, infrastructure, market analyses, operational aspects and adaptivity to changes in production rate. Component performance, especially for the indoor CO_2 cycle, could be analysed more in depth. Possibilities for temporary storage of the snow during outdoor production and adaption of the FID to indoor production should be explored. As the production time is likely to be extended to supply with snow when there is a demand during the season, on/off operation becomes more important. A climatic analysis based on historical data should be carried out; to get an overview of when the snow machine can be expected to operate. Moving the FID indoors, would offer possibilities of elevating the evaporation temperature. Trade-off between the thermodynamic conditions, the production rate and the dimensions of the snow producing units (FID/lance) should be investigated more in depth in a proper optimization process. Extending the scope of this thesis to include such features should be the direction and focus of further study; in order to strengthen or rebut the theories and conclusions from this work.

By these considerations, it is clear that a more extensive analysis should be performed before drawing a final conclusion. However, based on the available results and efforts provided so far in the project, the recommendation is indoor production by TDS equipment. Since the surplus heat available from a production rate of 100 tons/day is extensive, implementation of heat recovery is preferred. This will make the snow producing equipment more reasonable as the operating costs are reduced. Use of CO_2 as refrigerant contributes to obtain a system that is both highly energy efficient, when used in transcritical mode, and environmental friendly. It is recommended that the snowmaking process is kept the dimensioning point in the system, while heat recovery is designed accordingly. This will give the best overall performance for both demands. Utilizing the surplus heat for DHW heating is considered the best suitable heat recovery strategy.

12 Sources of error

Limitations with regard to the validity of the results and the assumptions of the models should be emphasized. The systems are implemented with applicable correlations and efficiencies collected from literature and manufacturers. Plausible assumptions have been made in dialog with professors and other available competence in the research community. The simulation models will provide reasonable estimates of the general feasibility of such systems, and the error of the analysis is supposed to be within acceptable limits. In a further evaluation, the features discussed in Chapter 11 should be studied more in detail; in order reduce the error and improve the validity of the models.

The main limitation of the simulation models is the exclusion of snow melting and climatic impact on production rates. It was not enough time to study the influence of the ambient thermodynamic conditions on outdoor production rates for the FID, as well as melting of snow on the ski track. This is a drawback concerning the objectivity of the comparison between the different models.

Questions should be raised regarding the validity of the design of the snowmaking units and the close interrelation with the refrigeration system. As the main focus has been on the design of the combined heating and refrigeration system, it is essential to confirm that the snowmaking equipment is compatible with the proposed refrigeration system. Effort should be made to evaluate whether the snow equipment provides acceptable snow quality and efficiency, and that no distinct operational problems are seen by the proposed conditions of the refrigeration systems. Optimization and accurate design of the snowmaking devices becomes important in this respect. Comparison of the energy consumption should be extended to include all devices and components – and not only that in directly association with the refrigeration systems.

13 Conclusions and suggestions for further work

13.1 Conclusion

In order to counter the challenges of the climate changes and maintaining good skiing conditions in the winters to come, snow production equipment that can operate in ambient temperatures above 0 °C will be important for future applications. The analyses show that the snow produced by such technology is both expensive and energy-intensive, generating an excessive amount of surplus heat available. Integrating the snow producing equipment with a combined refrigeration and heat recovery system improves the overall energy efficiency; as heat can be utilized both on the hot and cold side of the system. Heat recovery makes this technology more reasonable as the operating costs are reduced. Use of CO_2 as refrigerant contributes to obtaining a thermodynamic cycle that is both highly energy efficient; when used in transcritical mode, as well as being environmental friendly.

The analysis points to indoor TDS combined with the transcritical CO_2 cycle and heat recovery by DHW heating as the best solution for the site. Compared to the outdoor flake ice system, this solution has superior thermodynamic efficiencies and minor melting losses. The air refrigeration system is unsuitable for indoor snow production; due to the poor efficiencies and the operational problems with ice generated in the expander. The theories, conclusions and models developed through my work will make it possible to approach a practical application for "energy efficient and environmental friendly snow production" – and thereby fulfill the ambitions within the scope of "Snow for the future". Some further analysis is however required before drawing a final conclusion, and the results should be seen in combination with total costs and models for snow melting and climatic impact on production rates.

13.2 Suggestions for further work

Based on the work carried out in this thesis, the following proposal for further work are suggested:

- Extend the COMSOL model to include phase change of water.
- Perform a proper optimization process of the flake ice drum, and investigate a FID with spiral tubing, instead of straight refrigerant pipes.
- Investigate use of an ejector in the bottom cycle of the flake ice system.
- Study the effect of snow melting and climatic impact on production rates, and look into possibilities of improving the efficiency of outdoor production methods.
- Extend the analysis to include investment costs, infrastructure, market demand, operational aspects and adaption to non-constant operation.
- Investigate the possibility of adapting the FID to indoor production.
- Study climate statistics based on historical data for the production site, and obtain an estimate of the expected production time and duration; when evaluating the demand of excess supply and temporary storage of snow during the season.
- Build a prototype of the flake ice system suitable for the lab.

14 References

ALFA LAVAL. 2016a. *AC* [Online]. Available: http://www.alfalaval.no/produkter/heat-transfer/plate-heat-exchangers/Brazed-plate-heat-exchangers/AC/ [Accessed December 4 2016].

ALFA LAVAL. 2016b. *AlfaNova* [Online]. Available: http://www.alfalaval.no/produkter/heat-transfer/plate-heat-exchangers/Fusion-bonded-plate-heat-exchangers/AlfaNova/ [Accessed December 4 2016].

AMALFI, R. L., VAKILI-FARAHANI, F. & THOME, J. R. 2016. Flow boiling and frictional pressure gradients in plate heat exchangers. Part 1: Review and experimental database. *International Journal of Refrigeration,* 61**,** 166-184.

ANDOU, K. & OKUDA, S. 2004. Development of air refrigerant system. *6th IIR Gustav Lorentzen Conf. Nat. Work. Fluids.*

ASAOKA, T., SAITO, A., OKAWA, S., KUMANO, H. & HOZUMI, T. 2009. Vacuum freezing type ice slurry production using ethanol solution 2nd report: Investigation on evaporation characteristics of ice slurry in ice production. *International Journal of Refrigeration,* 32**,** 394-401.

ASHRAE 2010. Refrigerated facility-loads. *2010 ASHRAE Handbook - Refrigeration.* SI Edition ed.: American Society of Heating, Refrigerating and Air-Conditioning Engineers, Inc., pp. 24.1-24.8.

AZOM. 2012. *AISI 1035 Carbon Steel (UNS G10350),* [Online]. Available: http://www.azom.com/article.aspx?ArticleID=6540 [Accessed April 24 2017].

BAKKEN, L. E. 2017. Discussion and meetings. NTNU.

BÉDÉCARRATS, J.-P., DAVID, T. & CASTAING-LASVIGNOTTES, J. 2010. Ice slurry production using supercooling phenomenon. *International Journal of Refrigeration,* 33**,** 196-204.

BELLAS, I. & TASSOU, S. A. 2005. Present and future applications of ice slurries. *International Journal of Refrigeration,* 28**,** 115-121.

BERGWITZ-LARSEN, K. 2016. *Energy Efficient and Environmental Friendly Snow Production Equipment at Ambient Temperature above 0 °C.* Project work, Department of Energy and Process Engineering. Norwegian University of Sciency and Technology.

BERNTSEN, M. R. 2013. *Optimalisering av CO2-varmepumpe for kjøling av isvann / oppvarming av tappevann til 85oC.* Master thesis, Department of Energy and Process Engineering. Norwegian University of Sciency and Technology.

BITZER KÜHLMASCHINENBAU GMBH. 2014. *Refrigerant report 18* [Online]. Germany: BITZER Kühlmaschinenbau GmbH,. Available: https://www.bitzer.de/no/en/news/media/downloads/ [Accessed October 30 2016].

BOONE, J. & MACHIDA, A. 2011. *Development of air refrigeration system "Pascal Air"* [Online]. Prague: Mayekawa. Available: http://www.mayekawa.eu/en/media/brochure-downloads [Accessed January 25 2017].

CAO, W., BEGGS, C. & MUJTABA, I. M. 2015. Theoretical approach of freeze seawater desalination on flake ice maker utilizing LNG cold energy. *Desalination,* 355**,** 22-32.

CECCHINATO, L., CORRADI, M. & MINETTO, S. 2010. A critical approach to the determination of optimal heat rejection pressure in transcritical systems. *Applied Thermal Engineering,* 30**,** 1812-1823.

CENGEL, Y. A. & CIMBALA, J. M. 2010a. Laminar flow in pipes. *Fluid Mechanics Fundamentals and Applications.* Second edition in SI units ed.: Mc Graw Hill Higher Education pp. 343-351.

CENGEL, Y. A. & CIMBALA, J. M. 2010b. Piping networks and pump selection. *Fluid Mechanics Fundamentals and Applications.* Second edition in SI units ed.: Mc Graw Hill Higher Education pp. 371-380.

CENGEL, Y. A. & CIMBALA, J. M. 2010c. Turbulent flow in pipes. *Fluid Mechanics Fundamentals and Applications.* Second edition in SI units ed.: Mc Graw Hill Higher Education pp.351-364.

CHANG, C. 2017. Mail correspondence. Kaori Heat Treatment Co., Ltd.

CHEN, Y. & GU, J. 2005. The optimum high pressure for CO 2 transcritical refrigeration systems with internal heat exchangers. *International Journal of Refrigeration,* 28**,** 1238-1249.

CHOI, K.-I., PAMITRAN, A. S. & OH, J.-T. 2007. Two-phase flow heat transfer of CO 2 vaporization in smooth horizontal minichannels. *International Journal of Refrigeration,* 30**,** 767-777.
CLULOW, M. G. 1993. *Snow making equipment. Patent number: US005230218A.* US patent application.
CLULOW, M. G. 2006. Indoor snowmaking. *ASHRAE Journal,* 48**,** 18-23.
COMRON INTERNATIONAL BV. 2016. *Evaporators, Coolers, Heatexchangers.* [Online]. Available: https://www.comronusedfreezers.com/EN/Products/ProductsList/view/list/cat/7/cu/evaporators_coolers_heatexchangers/merk/alles [Accessed May 9 2017].
DEMAKLENKO. 2016. *Snow with system* [Online]. Available: http://www.demaclenko.com/en/information/index/1-0.html [Accessed September 23 2016].
DEMAKLENKO. 2017. *Lances* [Online]. Available: http://www.demaclenko.com/en/lances/our-lances/42-0.html [Accessed March 19 2017].
DIESETH, J.-B. R. 2016. *Snow Production Equipment at Ambient Temperatures Above Zero Degrees Celcius.* Master thesis, Department of Energy and Process Engineering. Norwegian University of Science and Technology.
DKB SKISPORT-HALLE. 2013. *Facts and figures* [Online]. Available: http://www.oberhof-skisporthalle.de/en/skihalle/facts-and-figures/ [Accessed January 16 2017].
EIKEVIK, T. M. 2015. Compendium TEP4255. Trondheim: NTNU.
EIKEVIK, T. M. 2017. Mail correspondence and weekly meetings. NTNU.
EIKEVIK, T. M. & HAFNER, A. 2016. Compendium TEP09. Trondheim: NTNU.
ELBEL, S. & LAWRENCE, N. 2016. Review of recent developments in advanced ejector technology. *International Journal of Refrigeration,* 62**,** 1-18.
EURAMMON. 2008. *Winter sports fun all year round, thanks to natural refrigerants* [Online]. Available: http://v2.r744.com/knowledge/papersView/winter_sports_fun_all_year_round_thanks_to_natural_refrigerants [Accessed February 24 2017].
FAUVE, M. & RHYNER, H. U. 2004. Physical description of the snowmaking process using the jet technique and properties of the produced snow. *In:* BARTELT, P., ADAMS, E., CHRISTEN, M., SACK, R. & SATO, A. (eds.) *Snow Engineering V: Proceedings of the Fifth International Conference on Snow Engineering, 5-8 July 2004, Davos, Switzerland.* Hoboken: Taylor and Francis pp. 215-218.
FRIGOMEC S.P.A. 2017. *Coaxial heat exchangers up to max. 130 bar* [Online]. Available: http://www.frigomec.com/index.php/en/en-coaxial-heat-exchangers-up-to-max-130-bar [Accessed March 20 2017].
GARCÍA-CASCALES, J. R., VERA-GARCÍA, F., CORBERÁN-SALVADOR, J. M. & GONZÁLVEZ-MACIÁ, J. 2007. Assessment of boiling and condensation heat transfer correlations in the modelling of plate heat exchangers. *International Journal of Refrigeration,* 30**,** 1029-1041.
GEA. 2016. *Ice generators* [Online]. Available: http://www.gea.com/en/products/ice-generators.jsp [Accessed May 2 2017].
GIANNETTI, N. & MILAZZO, A. 2014. Thermodynamic analysis of regenerated air-cycle refrigeration in high and low pressure configuration. *International Journal of Refrigeration,* 40**,** 97-110.
GJERLAND, M. & OLSEN, G. Ø. 2014. *Snøproduksjon og snøpreparering* [Online]. regjeringen.no. Available: https://www.regjeringen.no/no/dokumenter/Veileder---Snoproduksjon-og-snopreparering-V-0965/id764367/ [Accessed September 16 2016].
GRAHAM, J., JOHNSTON, W. A. & NICHOLSON, F. J. 1993. Ice in fisheries. *Ice in fisheries*.
GRUNDFOS. 2017. *Find produkter, løsninger og dokumentation* [Online]. Available: http://product-selection.grundfos.com/front-page.html?custid=GDK&time=1491828123031&qcid=114325449 [Accessed April 5 2017].
HAFNER, A. 2017. Mail correspondence. NTNU.
HATTORI, K. 2017. Mail correspondence. Mayekawa.

HAUGSE, H., HENRIKSEN, D. G., SKARPEID, H., SVENDSEN, A., VIE, E. & WILLMANN, E. S. 2016. Snøkvalitet. NTNU, Trondheim.
HEWITT, G. F. 2008. Single-phase fluid flow. *In:* HEWITT, G. F., BARBOSA, J., CELATA, G. P., MUELLER-STEINHAGEN, H., POSKAS, P., CHUDNOVSKY, Y., KANDLIKAR, S., PALEN, J. & TABOREK, J. (eds.) *Heat exchanger design handbook 2008.* Connecticut: Begell House, Inc. pp. 16-17.
HOCH, E. 2016. Mail correspondence. IDE Technologies,.
HUANG, J., SHEER, T. J. & BAILEY-MCEWAN, M. 2012. Heat transfer and pressure drop in plate heat exchanger refrigerant evaporators. *International Journal of Refrigeration,* 35**,** 325.
HUURRE. 2017. *Industripaneler* [Online]. Available: http://www.huurre.no/kjol-og-fryserom/industripaneler/ [Accessed April 25 2017].
IDE TECHNOLOGIES. 2010. *All Weather Snowmaker* [Online]. Available: http://www.ide-snowmaker.com/downloads/ [Accessed September 16 2016].
IDE TECHNOLOGIES. 2014. *VIM100 All Weather Snowmaker* [Online]. Available: http://www.ide-snowmaker.com/downloads/ [Accessed September 16 2016].
IDE TECHNOLOGIES. 2016a. *All Weather Snow Making* [Online]. Available: http://www.ide-snowmaker.com/all-weather-snow-making/ [Accessed September 9 2016].
IDE TECHNOLOGIES. 2016b. *Vacuum Ice Maker (VIM)* [Online]. Available: http://www.ide-snowmaker.com/vacuum-ice-maker-vim/ [Accessed September 16 2016].
INCROPERA, F. P., DEWITT, D. P., BERGMAN, T. L. & LAVINE, A. S. 2013a. Boiling modes. *Principles of heat and mass transfer.* 7th ed.: John Wiley & Sons, Inc. pp. 655-660.
INCROPERA, F. P., DEWITT, D. P., BERGMAN, T. L. & LAVINE, A. S. 2013b. Boundary and Initial Conditions. *Principles of heat and mass transfer.* 7th ed.: John Wiley & Sons, Inc. pp. 90-93.
INCROPERA, F. P., DEWITT, D. P., BERGMAN, T. L. & LAVINE, A. S. 2013c. Heat Exchanger Analysis: Use of the Log Mean Temperature Difference. *Principles of heat and mass transfer.* 7th ed.: John Wiley & Sons, Inc. pp. 711-721.
INCROPERA, F. P., DEWITT, D. P., BERGMAN, T. L. & LAVINE, A. S. 2013d. Mixed Boundary Layer Conditions. *Principles of heat and mass transfer.* 7th ed.: John Wiley & Sons, Inc. pp. 444-445.
INCROPERA, F. P., DEWITT, D. P., BERGMAN, T. L. & LAVINE, A. S. 2013e. One-Dimensional, Steady-State Conduction. *Principles of heat and mass transfer.* 7th ed.: John Wiley & Sons, Inc. pp. 111-228.
INCROPERA, F. P., DEWITT, D. P., BERGMAN, T. L. & LAVINE, A. S. 2013f. The Overall Heat Transfer Coefficient. *Principles of heat and mass transfer.* 7th ed.: John Wiley & Sons, Inc. pp. 708-711.
KAORI HEAT TREATMENT CO. LTD. 2017. *How BPHEs Work* [Online]. Available: http://www.kaori-bphe.com/en/products/page/How_BPHEs_Work [Accessed March 2 2017].
KAUF, F. 1999. Determination of the optimum high pressure for transcritical CO 2-refrigeration cycles. *International Journal of Thermal Sciences,* 38**,** 325-330.
KAUFFELD, M., WANG, M. J., GOLDSTEIN, V. & KASZA, K. E. 2010. Ice slurry applications. *International Journal of Refrigeration,* 33**,** 1491-1505.
KAYS, W. M. & CRAWFORD, M. E. 1980. Laminar flow inside tubes. *In:* CERRA, F. J. & MAISEL, J. W. (eds.) *Convective heat and mass transfer.* 2nd ed.: McGraw-Hill pp. 103-105.
LAVENERGIPROGRAMMET. 2016. *Dette er de nye energikravene i byggteknisk forskrift* [Online]. Available: http://lavenergiprogrammet.no/aktuelt/nye-energikrav-i-byggteknisk-forskrift/ [Accessed April 19 2017].
LIAO, S., ZHAO, T. & JAKOBSEN, A. 2000. A correlation of optimal heat rejection pressures in transcritical carbon dioxide cycles. 20**,** 831-841.
LONGO, G. A. 2010. Heat transfer and pressure drop during hydrocarbon refrigerant condensation inside a brazed plate heat exchanger. *International Journal of Refrigeration,* 33**,** 944-953.
MACHIELSEN, C. H. M. & KERSCHBAUMER, H. G. 1989. Influence on frost formation and defrosting on the performance of air coolers: standards and dimensionless coefficients for the system designer. Delft University of Technology, The Netherlands.

MAINA, P. & HUAN, Z. 2015. A review of carbon dioxide as a refrigerant in refrigeration technology. *South African Journal of Science,* 111**,** 15.
MAN DIESEL & TURBO. 2017. *Axial compressors* [Online]. Available: http://turbomachinery.man.eu/products/compressors/axial [Accessed May 11 2017].
MARTÍNEZ, D. S., SOLANO, J. P., ILLÁN, F. & VIEDMA, A. 2014. Analysis of heat transfer phenomena during ice slurry production in scraped surface plate heat exchangers. *International Journal of Refrigeration,* 48**,** 221-232.
MAYEKAWA. 2010. *Pascal Air* [Online]. Available: http://www.mayekawa.com.au/products/pascal-air/ [Accessed January 18 2017].
MAYEKAWA. 2016. *Pascal air* [Online]. Available: http://www.mayekawausa.com/products/coolingsystems/pascalair.html [Accessed January 10 2017].
METEOROLOGISK INSTITUTT. 2017. *Datosøk Trondheim (Sør-Trøndelag)* [Online]. Available: https://www.yr.no/sted/Norge/S%C3%B8r-Tr%C3%B8ndelag/Trondheim/Trondheim/almanakk.html?dato=2016-09-15 [Accessed April 25 2017].
MORAN, M. J., SHAPIRO, H. N., BOETTNER, D. D. & BAILEY, M. B. 2012a. Dehumidification. *Principles of Engineering Thermodynamics.* John Wiley & Sons pp. 683-686.
MORAN, M. J., SHAPIRO, H. N., BOETTNER, D. D. & BAILEY, M. B. 2012b. Gas Refrigeration Systems. *Principles of Engineering Thermodynamics.* John Wiley & Sons pp. 552-559.
MORAN, M. J., SHAPIRO, H. N., BOETTNER, D. D. & BAILEY, M. B. 2012c. Introducing Psychrometric Principles. *Principles of Engineering Thermodynamics.* John Wiley & Sons pp. 664-675.
MORAN, M. J., SHAPIRO, H. N., BOETTNER, D. D. & BAILEY, M. B. 2012d. Temperature. *Principles of Engineering Thermodynamics.* John Wiley & Sons pp. 15-19.
NELLIS, G. & KLEIN, S. 2009. Numerical Model of Parallel- and Counter-Flow Heat Exchangers. *Heat transfer.* 1st ed. New York: Cambridge University Press pp. 888-903.
NISTAD, B. 2017. Mail corresponding and meetings. COMSOL.
NÆSS, E. 2012. Kompendium i TEP-07 Industriell varmeteknikk. Trondheim: NTNU.
NÆSS, E. 2017. Mail correspondance and meetings. NTNU.
PAMPANIN, R. 2017. Mail correspondence. Frigomec S.p.A.,.
PARK, C. Y. & HRNJAK, P. 2009. CO 2 flow condensation heat transfer and pressure drop in multi-port microchannels at low temperatures. *International Journal of Refrigeration,* 32**,** 1129-1139.
PARK, S. K., AHN, J. H. & KIM, T. S. 2012. Off-design characteristics of an open-cycle air refrigeration system. *Int. J. Refrig. 35, 2311-2320.*
PAUL, J. 2003. Concept of Operating Indoor Skiing Halls with "Binary Snow" as Snow Substitute *Proceedings of 21st International Congress of Refrigeration. International Institute of Refrigeration IIF/IIR, Paris/Washington.*
PESONEN, H. 2016. Mail correspondence. SnowTek.
RAO, J. S. 2017. *Simulation Based Engineering in Solid Mechanics*, Springer International Publishing.
RATNIK INDUSTRIES INC. 2015. *Low Energy Air/Water Systems* [Online]. Available: http://www.ratnik.com/ss2.html [Accessed September 20 2016].
ROUNDTOP MOUNTAIN RESORT. 2016. *Snowmaking* [Online]. Available: https://www.skiroundtop.com/how-snowmaking-works [Accessed September 19 2016].
SARKAR, J., BHATTACHARYYA, S. & GOPAL, M. R. 2004. Optimization of a transcritical CO2 heat pump cycle for simultaneous cooling and heating applications. *International Journal of Refrigeration,* 27**,** 830-838.
SAWALHA, S. 2012. Investigation of heat recovery in CO2 trans-critical solution for supermarket refrigeration. *International journal of refrigeration,* 36**,** 145-156.
SHAH, R. K. & SEKULIĆ, D. P. 2007. Heat Exchanger Pressure Drop Analysis. *Fundamentals of Heat Exchanger Design.* Hoboken, NJ, USA: John Wiley & Sons, Inc. pp. 397-399.

SIEMENS AG. 2008. *STC-SX Siemens Turbocompressor – Single Shaft, Axial Design.*, [Online]. Available: https://www.energy.siemens.com/br/pool/hq/compression/single-shaft-compressors/downloads/STC_SX_EN.pdf [Accessed May 11 2017].
SMI SNOWMAKERS. 2012. *Snowmaking Basics* [Online]. Available: http://www.snowmakers.com/snowmaking-basic.html [Accessed September 18 2016].
SNOWATHOME. 2016. *Snowmaking Weather Tools* [Online]. Available: http://www.snowathome.com/snowmaking_weather_tools.php [Accessed August 30 2016].
SNOWMAGIC INC. 2015a. *About Us* [Online]. Available: http://www.snowmagic.com/about-us/ [Accessed September 21 2016].
SNOWMAGIC INC. 2015b. *How It Works* [Online]. Available: http://www.snowmagic.com/how-it-works/ [Accessed September 9 2016].
SNOWMAGIC INC. 2015c. *Ski Resorts* [Online]. Available: http://www.snowmagic.com/ski-resorts/ [Accessed September 26 2016].
SNOWMAGIC INC. 2015d. Snowmagic ICS unit module 50T/D.
STAMATIOU, E., MEEWISSE, J. W. & KAWAJI, M. 2005. Ice slurry generation involving moving parts. *International Journal of Refrigeration,* 28**,** 60-72.
STENE, J. 2016. Carbon Dioxide (R744) as Working Fluid in Heat Pumps. Trondheim: NTNU.
SUFAG. 2017. *Tower guns comparator* [Online]. Available: http://www.sufag.com/en/gamme_products/gamme-perches-en/ [Accessed March 19 2017].
TECHNOALPIN. 2015a. *Snowfactory 365 days of snowmaking* [Online]. Available: http://www.technoalpin.com/en/downloads/brochures.html [Accessed September 9 2016].
TECHNOALPIN. 2015b. *Snowfactory - snow-making at above-zero temperatures* [Online]. Available: http://www.technoalpin.com/en/snow-guns/snowfactory.html [Accessed September 9 2016].
TECHNOALPIN 2016. Snowfactory in Northern Europe. *Snow experts magazine*. 01/2016 ed.
THE LINDE GROUP. 2016. *Natural Refrigerants* [Online]. Available: http://www.linde-gas.com/en/products_and_supply/refrigerants/natural_refrigerants/index.html [Accessed October 5 2016].
VAN ORSHOVEN, D., KLEIN, S. A. & BECKMAN, W. A. 1993. An investigation of water as a refrigerant. *Journal of Energy Resources Technology,* 115.
VDI 1993. Heat transfer in flow through coils. *In:* ASSOCIATION OF GERMAN ENGINEERS / VDI SOCIETY FOR CHEMICAL AND PROCESS ENGINEERING (ed.) *VDI Heat Atlas.* 1st. ed. Düsseldorf: VDI pp. Gc1-Gc2.
VDI 2010. Heat Transfer in Pipe Flow. *In:* STEPHAN, P., KABELAC, S., KIND, M., MARTIN, H., MEWES, D. & SCHABER, K. (eds.) *VDI Heat Atlas Second Edition.* 2nd ed. Berlin: Springer pp. 696.
WANG, L., SUNDÉN, B. & MANGLIK, R. M. 2007. Construction and operation. *Plate heat exchangers.* Boston: WIT Press pp. 11-25.
YIN, J. M., BULLARD, C. W. & HRNJAK, P. S. 2001. R-744 gas cooler model development and validation. *International Journal of Refrigeration,* 24**,** 692-701.

Appendix

A. Log P-h diagram

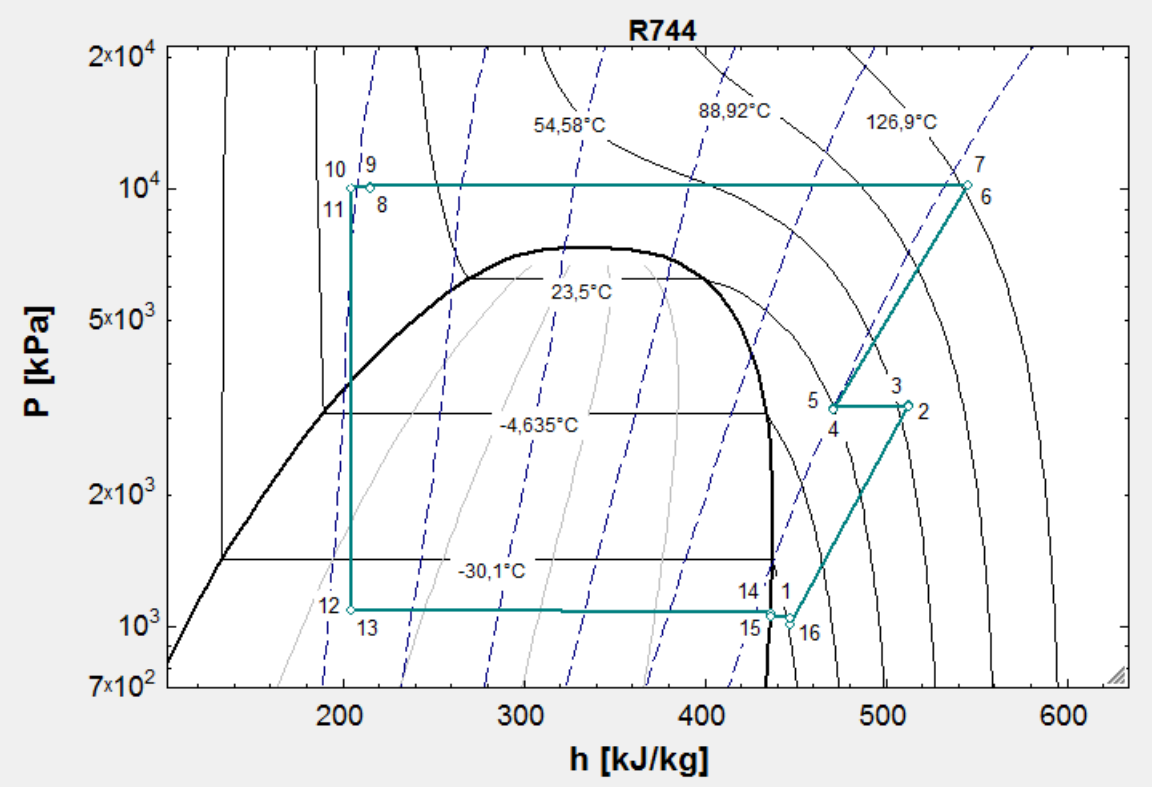

Figure A- 1. Log P-h diagram for the flake ice system

B. Thermodynamic state points of the flake ice system

Table A- 1. State points for the heat recovery cycle of the flake ice system

State point	Pressure [kPa]	Temperature [°C]	Enthalpy [kJ/kg]	Entropy [kJ/kgK]	Gas quality [-]
1	1016	-28.49	446.7	2.094	
2	3227	60.94	512.1	2.128	
3	3199	60.70	512.1	2.129	
4	3187	24.00	470.7	1.998	
5	3153	23.62	470.7	2.000	
6	10,250	129.80	544.6	2.031	
7	10,240	129.80	544.6	2.031	
8	10,143	8.809	215.2	1.029	
9	10,131	8.805	215.2	2.029	
10	10,127	3.955	204.2	0.9895	
11	10,116	3.952	204.2	0.9896	
12	1096	-37.60	204.2	1.053	0.2718
13	1096	-37.60	204.2	1.053	0.2718
14	1076	-38.11	435.7	2.039	1
15	1055	-38.56	435.7	2.042	
16	1047	-27.91	446.7	2.089	

C. Performance of the flake ice drum

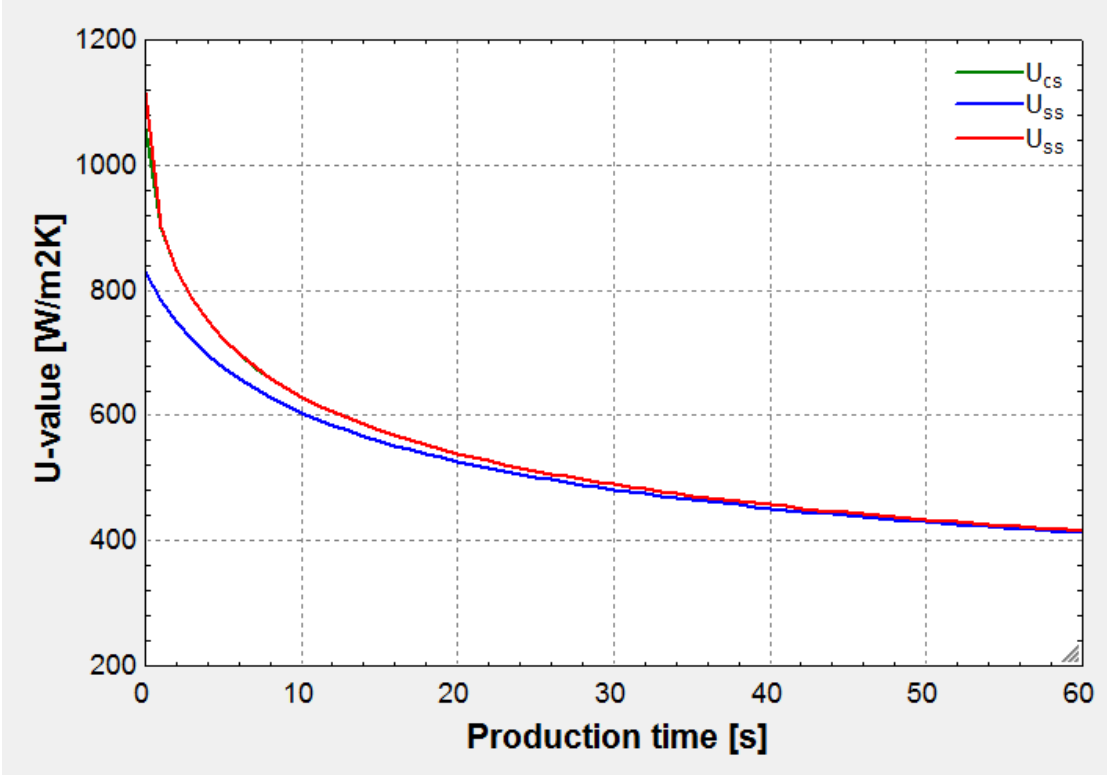

Figure A- 2. Change of U-value with production time

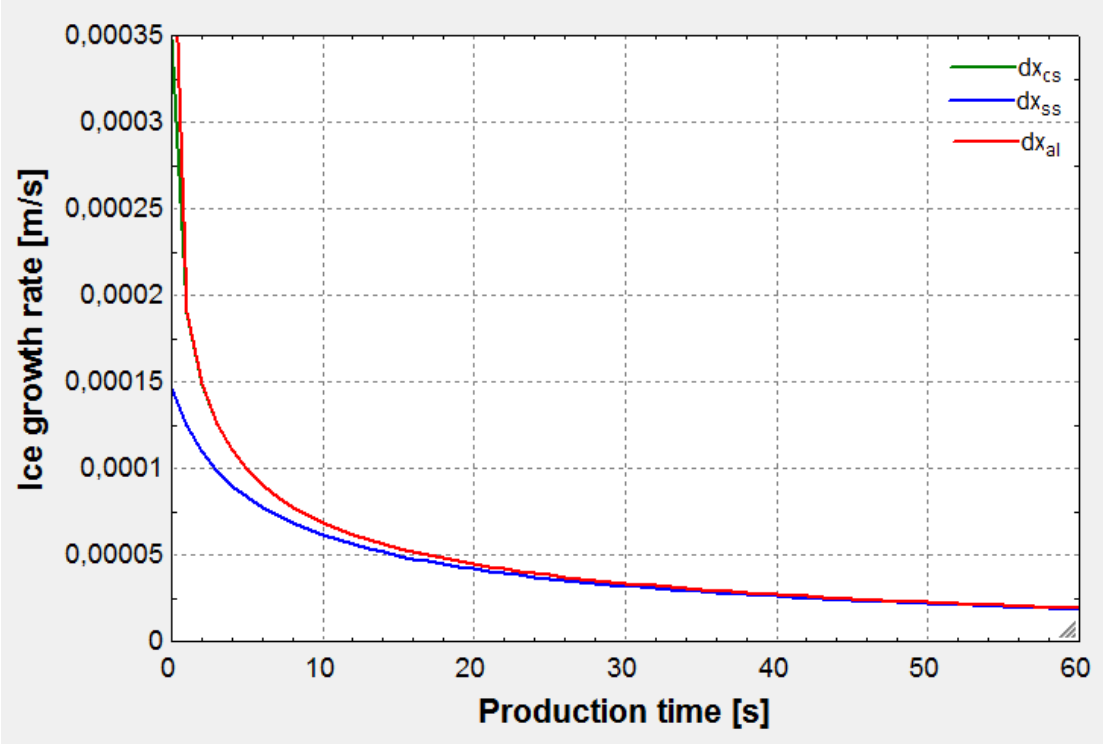

Figure A- 3. Change of ice growth rate with production time

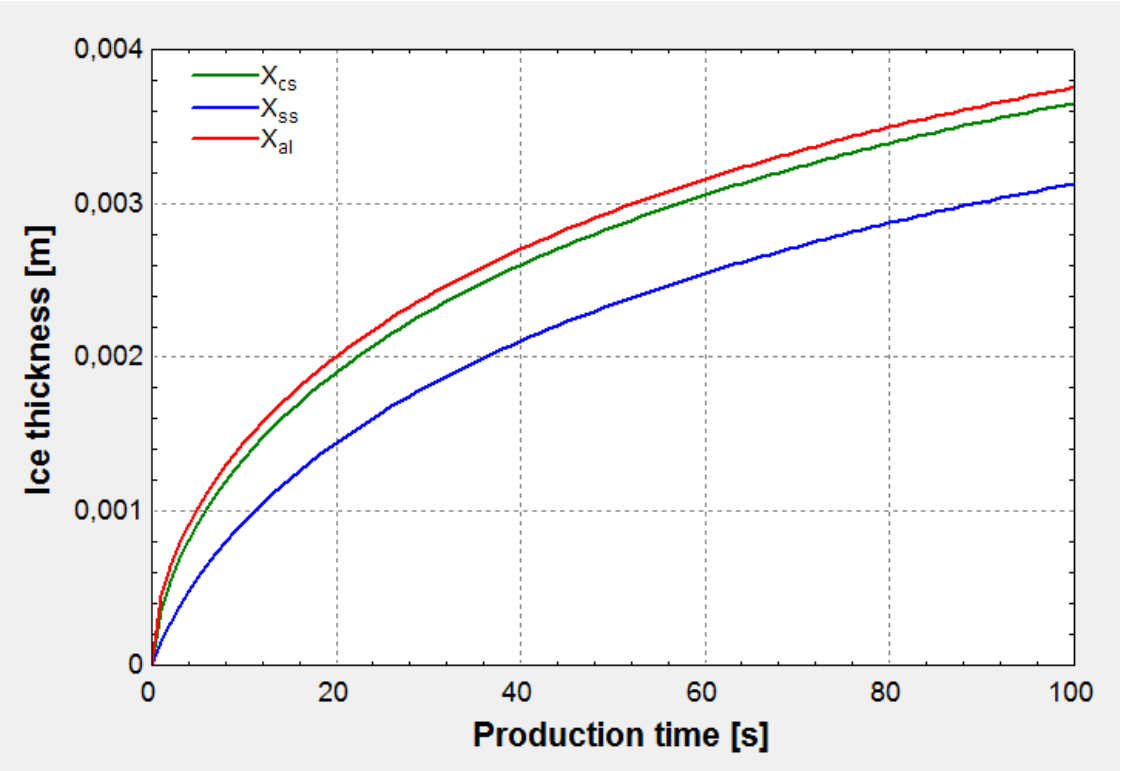

Figure A- 4. Change of ice thickness with production time

D. EES code

```
$UnitSystem SI MASS RAD PA K J

"------------------------------------------------------------------------
   Suction gas heat exchanger (SGHX).
------------------------------------------------------------------------"

"!Counter current plate heat exchanger"
{Calculates the heat transfer coefficients, pressure drop and heat transfer
for the hot and cold side}
{Model: Alfa Laval AXP27}

"Input values"
W=16 [cm]*convert(cm;m)                    "Width of heat exchanger"
L=25 [cm]*convert(cm;m)
   "Length of heat exchanger in flow direction"
N_ch=8 [-]                                 "Number of channel pairs"
th_H=2,5 [mm]*convert(mm;m)                "Channel width on hot side"
th_C=2,5 [mm]*convert(mm;m)                "Channel width on cold side"
th_m=1 [mm]*convert(mm;m)                  "Thickness of plate"

p_H=10131 [kPa]*convert(kPa;Pa)
   "Hot side pressure, outlet of gas cooler"
p_C=1055 [kPa]*convert(kPa;Pa)
   "Cold side pressure, outlet of evaporator"
m_dot_H=1,911 [kg/s]                       "Mass flow rate on hot side"
m_dot_C=m_dot_H                            "Mass flow rate on cold side"
H$='R744'                                  "Hot fluid"
C$='R744'                                  "Cold fluid"
T_H_in=281,95 [K] {8,8 C}                  "Inlet temperature of hot fluid"
T_C_in=234,59 [K] {-37,7 C}                "Inlet temperature of cold fluid"

c_H=cP(H$;p=p_H;T=T_H)                     "Specific heat capacity, hot
side"
c_C=cP(C$;p=p_C;T=T_C)                     "Specific heat capacity, cold
side"

call DuctFlow_local(H$;T_H;p_H;m_dot_H/N_ch;th_H;W;x;0:h_H; h_H_H ; dpdx_H)
   "Local heat transfer coefficient on hot side"
call DuctFlow_local(C$;T_C;p_C;m_dot_C/N_ch;th_C;W;x;0:h_C; h_H_C ; dpdx_C)
   "Local heat transfer coefficient on cold side"

k_m=k_('Aluminum'; (T_H+T_C)/2)
   "Metal conductivity at local average temperature"

dTHdx=-2*N_ch*(T_H-T_C)/(m_dot_H*c_H*(1/(h_H*W)+th_m/(k_m*W)+1/(h_C*W)))
   "State equation for T_H"
dTCdx=-2*N_ch*(T_H-T_C)/(m_dot_C*c_C*(1/(h_H*W)+th_m/(k_m*W)+1/(h_C*W)))
   "State equation for T_C"

{"Arbitrary state variables to establish evaluation of the state equations"
x=0,1 [m]                                  "Position in heat exchanger"
T_H=300 [K]                                "Hot-side temperature"
T_C=100 [K]                                "Cold-side temperature"}

{T_C_out=290 [K]}                          "Assumed value of the cold outlet
fluid"

N = 15 [-]                                 "Number of integration steps"
```

```
DELTAx=L/N                                    "Integration step size"
T_H=T_H_in+INTEGRAL(dTHdx;x;0;L;DELTAx)   "Integral state equation for T_H"
T_C=T_C_out+INTEGRAL(dTCdx;x;0;L;DELTAx)  "Integral state equation for T_C"

err=Abs(T_C-T_C_in)
   "Error between calculated and specified T_C_in"
$IntegralTable x:DELTAx;T_H;T_C;dpdx_H;dpdx_C
p_H_out=p_H+INTEGRAL(dpdx_H;x;0;L;DELTAx)
   "Integral state equation for T_H"
p_C_out=p_C+INTEGRAL(dpdx_C;x;0;L;DELTAx)
   "Integral state equation for T_C"

DELTAP_H=p_H-p_H_out                          "Pressure drop on hot side"
DELTAP_C=p_C-p_C_out                          "Pressure drop on cold side"

"!Heat transfer calculations"
h_h_in=enthalpy(H$;T=T_H_in;P=p_H)         "Inlet enthalpy, hot side"
h_h_out=enthalpy(H$;T=T_H;P=p_H_out)       "Outlet enthalpy, hot side"
q_dot_h=m_dot_H*(h_h_in-h_h_out)*convert(w;kW)
   "Heat transfer for hot side"

h_c_in=enthalpy(C$;T=T_C_in;p=P_C)         "Inlet enthalpy, cold side"
h_c_out=enthalpy(C$;T=T_C_out;P=p_C_out)   "Outlet enthalpy, cold side"
q_dot_c=m_dot_C*(h_c_out-h_c_in)*convert(w;kW)
   "Heat transfer for cold side"


"-------------------------------------------------------------------------
   Main script
-------------------------------------------------------------------------"

$UnitSystem SI C kPa kJ mass
$Reference R744 IIR

"-------------------------------------------------------------------------

To better understand the script, it is recommended to go directly to the
state point calculations.
The procedures are placed at the top of the script; due to syntax reasons.
They are solved chronologically from top to bottom.
This is not the case for the main body however, which is solved in an
interactive way. EES automatically identifies and groups equations
that must be solved simultaneously, and decides what to calculate first.
Thus, debugging the code might be quite tedious.
Using the state point calculations as a start point may ease the
understanding; as the set of equations and variables are
defined non-chronologically.

-------------------------------------------------------------------------"


"-------------------------------------------------------------------------
   PROCEDURES
-------------------------------------------------------------------"

PROCEDURE flakeicedrum(T_evap_flake;m_co2_fl_real;T_water_in;m_w;x_pipe;
Q_water:U1[1];U1_avg)
{Calculation of propagation of the ice layer and overall heat transfer
coefficient considering different vessel materials.
In addition it determines the required heat exchanger surface area}

$ARRAYS ON
```

```
"!Forced flow refrigerant side"
R$='R744'                                   "Refrigerant string, CO2"
h_flake=2,6 [m]                             "Height of flake ice drum"
d_flake=2,5 [m]                             "Diameter of flake ice drum"
u_w=1,0 [m/s]                               "Velocity of water along drum"

A_flake=pi*d_flake*h_flake                  "Surface area of flake ice drum"

P_ref=p_sat(R$;T=T_evap_flake)              "Pressure"
k_ref=conductivity(R$;T=T_evap_flake;P=P_ref+0,01)
   "Thermal conductivity"
sigma_ref=surfacetension(R$;T=T_evap_flake)
   "Surface tension CO2, input to COMSOL"

d=5 [mm]*convert(mm;m)                      "Diameter of pipe"
d_hyd=d                                     "Hydraulic diameter"

"Two-phase correlation: Evaporation of CO2 (Choi et al., 2007)"
mu_f=viscosity(R$;T=T_evap_flake;x=0)       "Dynamic viscosity liquid"
mu_g=viscosity(R$;T=T_evap_flake;x=1)       "Dynamic viscosity gas"
rho_f=density(CarbonDioxide;T=T_evap_flake;x=0)
   "Density liquid"
rho_g=density(CarbonDioxide;T=T_evap_flake;x=1)
   "Density gas"
h_fg=enthalpy_vaporization(R$;T=T_evap_flake)
   "Enthalpy of vaporization"
M=molarmass(R$)                             "Molar mass"
k_f=conductivity(R$;T=T_evap_flake;x=0)     "Thermal conductivity liquid"
k_g=conductivity(R$;T=T_evap_flake;x=1)     "Thermal conductivity gas"
cp_f=cp(R$;T=T_evap_flake;x=0)              "Specific heat capacity liquid"
cp_g=cp(R$;T=T_evap_flake;x=1)              "Specific heat capacity gas"
C=20
   "Turbulent-turbulent Chisholm factor"
PC=p_crit(R$)                               "Critical pressure, kPa"
P_r=P_ref/PC                                "Reduced pressure"
G=m_co2_fl_real/((x_pipe*pi*(d_hyd^2))/4)   "Mass flux through one CO2 pipe"
q=(Q_water*1000)/(pi*d_hyd*h_flake*x_pipe)
   "Heat flux, per m^2"
Bo=(Q_water/(pi*d_hyd*h_flake*x_pipe))/(G*h_fg)
   "Boiling number"
Pr_f=prandtl(R$;P=P_ref+0,01;x=0)           "Prandtl number, liquid CO2"

x[1]=0,1
dx=0,1
N=6

DUPLICATE i=2;N
x_ma[i-1]=(mu_f/mu_g)^(1/8)*((1-x[i-1])/x[i-1])^(7/8)*(rho_g/rho_f)^0,5
   "Lockhart Martinelli parameter"
phi_f[i-1]=1+(C/x_ma[i-1])+(1/(x_ma[i-1]^2))
   "Two-phase frictional multiplier"
F[i-1]=(0,05*phi_f[i-1])+0,95               "Correlation factor"
S[i-1]=7,2694*(phi_f[i-1]^0,0094)*(Bo^0,2814)
   "Nucleate boiling suppression factor"

h_nbc[i-1]=55*(P_r^0,12)*((-0,4343*ln(P_r))^(-0,55))*(M^(-0,5))*(q^0,67)
   "Nucleate boiling heat transfer coefficient"
h_lo[i-1]=0,023*(k_f/d)*(((G*(1-x[i-1])*d)/mu_f)^0,8)*(Pr_f^0,4)
   "Forced convective evaporation heat transfer coefficient, Dittus-Boelter
correlation"
```

```
alpha_ref[i-1]=S[i-1]*h_nbc[i-1]+F[i-1]*h_lo[i-1]
   "Heat transfer coefficient CO2"
x[i]=x[i-1]+dx

END

alpha_ref=1/(N-1)*sum(alpha_ref[i];i=1;(N-1))

"!Free flow on water side."
"Correlation for turbulent flow over flat plate (Incropera et al., 2013)"
W$='water'                                  "Water string"
P_w=101,325 [kPa]                           "Atmospheric pressure at inlet"
k_w=conductivity(W$;T=T_water_in;P=P_w+0,01[kPa])
   "Thermal conductivity water"
rho_w=density(W$;T=T_water_in;P=P_w+0,01) "Density water"
nu_w=kinematicviscosity(W$;T=T_water_in;P=P_w+0,01)
   "Kinematic viscosity"
c_p_w=specheat(W$;T=T_water_in;P=P_w+0,01)
   "Specific heat capacity"
Pr_w=prandtl(W$;T=T_water_in;P=P_w+0,01)  "Prandtl number"
Re_w=(u_w*h_flake)/nu_w                     "Reynolds number"
Re_x_c=5*10^5                               "Critical Reynolds number"
A=0,037*Re_x_c^(4/5)-0,664*Re_x_c^(1/2)   "Correlation factor"
alpha_w=(k_w/h_flake)*(0,037*Re_w^(4/5)-A)*(Pr_w^(1/3))
   "Heat transfer coefficient water"

"!Carbon steel drum"
delta_wall=0,5 [cm]*convert(cm;m)           "Thickness of drum wall"
delta_wall_2=0,5 [cm]*convert(cm;m)         "Thickness of second drum wall"
k_al=conductivity(Aluminum; T=-30)          "Conductivity aluminium"
S_u_al=ultimatestress(Aluminum; T=-30)      "UTS aluminium"
k_ice=conductivity(Ice;T=0;P=101,325)       "Thermal conductivity ice"
k_cs=conductivity(Carbon_steel; T=-30)      "Conductivity carbon steel"
S_u_ss=ultimatestress(Stainless_AISI302; T=-30)
   "UTS stainless steel"

T_i=0 [C]
DELTAh_fusion=enthalpy_fusion(W$)*convert(kJ/kg;J/kg)

X1[1]=0
dt=1
t[1]=0
Time=120

DUPLICATE i=2;time

"Overall heat transfer coefficient"
U1[i-1]=1/((1/alpha_ref)+(delta_wall_2/k_cs)+(delta_wall/k_al)+(x1[i-
1]/k_ice)+(1/alpha_w))

"Ice thickness as function of time"
dx1[i-1]=((((((T_i-
T_evap_flake)/((1/alpha_ref)+(delta_wall_2/k_cs)+(delta_wall/k_al)+(X1[i-
1]/k_ice)))-alpha_w*(T_water_in-T_i))))*dt)/(rho_w*DELTAh_fusion)

X1[i]=X1[i-1]+dx1[i-1]
t[i]=t[i-1]+dt
```

```
"Ice growth rate [m/s]"
ds\dt1[i-1]=((((T_i-
T_evap_flake)/((1/alpha_ref)+(delta_wall_2/k_cs)+(delta_wall/k_al)+(X1[i-
1]/k_ice)))-alpha_w*(T_water_in-T_i)))/(rho_w*DELTAh_fusion)

END

U1_avg=sum(U1[i];i=1;70-1)/70              "Average U-value, carbon steel"
Q_cs=U1_avg*h_flake*pi*d_flake*(T_water_in-T_evap_flake)
   "Heat transfer with drum wall of carbon steel"

"!Stainless steel drum"
k_ss=conductivity(Stainless_AISI302; T=-30)  "Conductivity stainless steel"
X2[1]=0

DUPLICATE i=2;time

"Overall heat transfer coefficient"
U2[i-1]=1/((1/alpha_ref)+(delta_wall_2/k_ss)+(delta_wall/k_al)+(X2[i-
1]/k_ice)+(1/alpha_w))

"Ice thickness as function of time"
dx2[i-1]=((((((T_i-
T_evap_flake)/((1/alpha_ref)+(delta_wall_2/k_ss)+(delta_wall/k_al)+(X2[i-
1]/k_ice)))-alpha_w*(T_water_in-T_i))))*dt)/(rho_w*DELTAh_fusion)

X2[i]=X2[i-1]+dx2[i-1]

"Ice growth rate [m/s]"
ds\dt2[i-1]=((((T_i-
T_evap_flake)/((1/alpha_ref)+(delta_wall_2/k_ss)+(delta_wall/k_al)+(X2[i-
1]/k_ice)))-alpha_w*(T_water_in-T_i)))/(rho_w*DELTAh_fusion)

END

U2_avg=sum(U2[i];i=1;70-1)/70
   "Average U-value, stainless steel"
Q_ss=U2_avg*h_flake*pi*d_flake*(T_water_in-T_evap_flake)
   "Heat transfer with drum wall of stainless steel"

"!Aluminum drum"
X3[1]=0

DUPLICATE i=2;time

"Overall heat transfer coefficient"
U3[i-1]=1/((1/alpha_ref)+(delta_wall_2/k_al)+(X3[i-
1]/k_ice)+(delta_wall/k_al)+(1/alpha_w))

"Ice thickness as function of time"
dx3[i-1]=((((((T_i-
T_evap_flake)/((1/alpha_ref)+(delta_wall_2/k_al)+(delta_wall/k_al)+(X3[i-
1]/k_ice)))-alpha_w*(T_water_in-T_i))))*dt)/(rho_w*DELTAh_fusion)

X3[i]=X3[i-1]+dx3[i-1]

"Ice growth rate [m/s]"
ds\dt3[i-1]=((((T_i-
T_evap_flake)/((1/alpha_ref)+(delta_wall_2/k_al)+(delta_wall/k_al)+(X3[i-
1]/k_ice)))-alpha_w*(T_water_in-T_i)))/(rho_w*DELTAh_fusion)
```

```
END

U3_avg=sum(U3[i];i=1;70-1)/70              "Average U-value, aluminium"
Q_al=U3_avg*h_flake*pi*d_flake*(T_water_in-T_evap_flake)
   "Heat transfer with drum wall of stainless steel"

END

"-------------------------------------------------------------------------"

PROCEDURE
heattransferic(m_dot_co2;m_dot_water_ic;T_water_in;P[3];T[3];P[4];
T[4];T_ref_avg_ic;T_w_avg_ic;w_plate_ic;x_plate_ic:U_ic)
"!Assuming forced and one-phase flow at both sides"
{Calculates the heat transfer coefficients and U-value for the intercooler}

$ARRAY ON
W$='Water'                                 "Water string"
R$='R744'                                  "Refrigerant string. CO2"
delta_wall_ic=1 [mm]*convert(mm;m)         "Thickness of heat exchanger
plates"
k_ss=conductivity(Stainless_AISI302; T=17)
   "Thermal conductivity stainless steel"
d_e_ic=7 [mm]*convert(mm;m)                "Equivalent diameter"

"!Cold side: water"
P_cold=101,325 [kPa]                       "Atmospheric pressure at water
inlet"
k_cold=conductivity(W$;T=T_water_in;P=P_cold)
   "Thermal conductivity"
mu_cold=viscosity(W$;T=T_water_in;P=P_cold)
   "Dynamic viscosity"
mu_wall_water=viscosity(W$;T=(T_ref_avg_ic+T_w_avg_ic)/2;P=P_cold+0,01)
   "Viscosity at wall interface"
A=(d_e_ic)*w_plate_ic*0,5*x_plate_ic       "Total flow area"
G=m_dot_water_ic/A                         "Mass flux"
Pr_cold=prandtl(W$;T=T_water_in;P=P_cold)  "Prandtl number"
Re_cold=(G*d_e_ic)/mu_cold                 "Reynolds number"

"Martin correlation for one-phase water flow"
beta_cold=45                               "Chevron angle"
f0_martin_cold = 64/Re_cold
   "Parameter for friction factor calculation"
f1_martin_cold= 597/Re_cold+3,85
   "Parameter for friction factor calculation"
f_martin_cold=(1 /
(cos(beta_cold)/sqrt(0,18*tan(beta_cold)+0,36*sin(beta_cold)+(f0_martin_col
d/cos(beta_cold))) + ((1-cos(beta_cold))/(sqrt(3,8*f1_martin_cold)))) )^2
   "Friction factor"
Nusselt_cold=0,122*(Pr_cold^(1/3))*((mu_cold/mu_wall_water)^(1/6))*(f_marti
n_cold*( (Re_cold^2)*sin(2*beta_cold)))^0,374
   "Nusselt number"
alpha_cold = (Nusselt_cold*k_cold)/d_e_ic "Heat transfer coefficient water"

"!Warm side: CO2"
k_warm_i=conductivity(R$;P=P[3];T=T[3])    "Thermal conductivity at inlet"
k_warm_o=conductivity(R$;P=P[4];T=T[4])    "Thermal conductivity at outlet"
k_avg=(k_warm_i+k_warm_o)/2                "Average thermal conductivity"
mu_warm_i=viscosity(R$;P=P[3];T=T[3])      "Dynamic viscosity at inlet"
mu_warm_o=viscosity(R$;P=P[4];T=T[4])      "Dynamic viscosity at outlet"
mu_avg=(mu_warm_i+mu_warm_o)/2             "Average dynamic viscosity"
```

```
mu_wall_ref=viscosity(R$;T=(T_ref_avg_ic+T_w_avg_ic)/2;P=P_cold+0,01)
   "Viscosity at wall interface"
G_warm=m_dot_co2/A                          "Mass flux"
Pr_warm=prandtl(R$;T=(T[3]+T[4])/2;P=P[3])
   "Prandtl number"
Re_warm=(G_warm*d_e_ic)/mu_avg              "Reynolds number"


"Martin correlation for one-phase CO2 flow"
beta_warm=45                                "Chevron angle"
f0_martin = (1,8*log10(Re_warm)-1,5)^(-2)
   "Parameter for friction factor calculation"
f1_martin= 39/(Re_warm^0,289)
   "Parameter for friction factor calculation"
f_martin=(1 /
(cos(beta_warm)/sqrt(0,18*tan(beta_warm)+0,36*sin(beta_warm)+(f0_martin/cos
(beta_warm))) + ((1-cos(beta_warm))/(sqrt(3,8*f1_martin)))) )^2
   "Friction factor"
Nusselt_w=0,122*(Pr_warm^(1/3))*((mu_avg/mu_wall_ref)^(1/6))*(f_martin*(
(Re_warm^2)*sin(2*beta_warm)))^0,374
   "Nusselt number"
alpha_warm= (Nusselt_w*k_avg)/d_e_ic        "Heat transfer coefficient CO2"
U_ic=1/((1/alpha_cold)+(delta_wall_ic/k_ss)+(1/alpha_warm))
   "U-value of intercooler"

END

"-------------------------------------------------------------------------"

PROCEDURE heattransfercondevap(m_dot_co2;m_co2_fl_real;T_evap;T_evap_flake;
x[13];w_plate_ec;h_plate_ec;x_plate_ec;b_plate_ec:U_cond_evap;G_2)
{Calculates the heat transfer coefficients and U-value for the
condenser/evaporator. Assuming forced flow on both sides.}

$ARRAY ON
R$='R744'                                   "Refrigerant string. CO2"
delta_wall_condevap=1 [mm]*convert(mm;m)    "Thickness of heat exchanger
plates"
k_ss=conductivity(Stainless_AISI302; T=17)
   "Thermal conductivity stainless steel"
d_e=7 [mm]*convert(mm;m)                    "Equivalent diameter"

"!Cold side: Evaporation of CO2. Formulas by Choi et al. (2007)"
P_cold=p_sat(R$;T=T_evap)                   "Pressure"
mu_f=viscosity(R$;T=T_evap;x=0)             "Dynamic viscosity liquid"
mu_g=viscosity(R$;T=T_evap;x=1)             "Dynamic viscosity gas"
rho_f=density(CarbonDioxide;T=T_evap;x=0)   "Density liquid"
rho_g=density(CarbonDioxide;T=T_evap;x=1)   "Density gas"
h_fg=enthalpy_vaporization(R$;T=T_evap)     "Enthalpy of vaporization"
M=molarmass(R$)                             "Molar mass of CO2"
k_f=conductivity(R$;T=T_evap;x=0)           "Thermal conductivity CO2"
cp_f=cp(R$;T=T_evap;x=0)                    "Specific heat capacity"
C=20                                        "Turbulent Chisholm factor"
PC_ec=p_crit(R$)                            "Critical pressure"
P_r_ec=P_cold/PC_ec                         "Reduced pressure"
A_ce=(d_e)*w_plate_ec*0,5*x_plate_ec        "Total flow area"
G_2=m_dot_co2/A_ce                          "Mass flux"
q=427,8*1000/(2*w_plate_ec*h_plate_ec*x_plate_ec)
   "Heat flux, per m^2"
Bo=(427,8/(2*w_plate_ec*h_plate_ec*x_plate_ec))/(G_2*h_fg)   "Boiling
number"
```

```
Pr_f=prandtl(R$;P=P_cold+0,01;x=0)          "Prandtl number"
g=9,81                                      "Gravitational constant"

x[1]=0,1
dx=0,1
N=10

DUPLICATE i=2;N
x_ma[i-1]=(mu_f/mu_g)^(1/8)*((1-x[i-1])/x[i-1])^(7/8)*(rho_g/rho_f)^0,5
   "Lockhart Martinelli factor"
phi_f[i-1]=(1+C/x_ma[i-1]+1/(x_ma[i-1]^2))
   "Two-phase frictional multiplier"
F[i-1]=0,05*(phi_f[i-1])+0,95               "Correlation factor"
S[i-1]=7,2694*(phi_f[i-1])^0,0094*Bo^0,2814
   "Nucleate boiling suppression factor"
h_nbc[i-1]=55*P_r_ec^0,12*(-0,4343*ln(P_r_ec))^(-0,55)*M^(-0,5)*q^0,67
   "Nucleate boiling heat transfer coefficient"
h_lo[i-1]=0,023*(k_f/(1,2*d_e))*((G_2*(1-x[i-
1])*(1,2*d_e))/mu_f)^0,8*((Pr_f)^0,4)
   "Forced convective evaporation heat transfer coefficient, Dittus-Boelter
correlation"
alpha_ref[i-1]=S[i-1]*h_nbc[i-1]+F[i-1]*h_lo[i-1]
   "Heat transfer coefficient evaporation"

x[i]=x[i-1]+dx

END

alpha_cold=1/9*sum(alpha_ref[i];i=1;9)      "Average heat transfer
coefficient cold side"

"!Warm side: Condensation of CO2. Formulas by Park and Hrnjak (2009)"
P_warm=p_sat(R$;T=T_evap_flake)             "Saturation pressure"
k_warm_o=conductivity(R$;P=P_warm+0,01;x=0)
   "Thermal conductivity"
mu_warm_o=kinematicviscosity(R$;P=P_warm+0,01;x=0) "Viscosity"
rho_warm_o=density(R$;P=P_warm+0,01;x=0)    "Density saturated liquid"
rho_warm_i=density(R$;P=P_warm+0,01;x=1)    "Density saturated gas"
Cp_l=cp(R$;P=P_warm+0,01;x=0)               "Specific heat capacity liquid"

DUPLICATE i=2;N
alpha_warm[i-1]=(k_warm_o^(2/3)*Cp_l^(1/3))/mu_warm_o^(7/15)*((x[i-1]/(1-
x[i-1]))*(rho_warm_o/rho_warm_i)^0,5+1)
   "Heat transfer coefficient condensation"
x[i]=x[i-1]+dx
END

alpha_warm=1/9*sum(alpha_warm[i];i=1;9)
   "Average heat transfer coefficient warm side"
U_cond_evap=1/((1/alpha_cold)+(delta_wall_condevap/k_ss)+(1/alpha_warm))
   "U-value for evaporator/condenser unit"

END

"-------------------------------------------------------------------------"
```

```
PROCEDURE deltap_coaxial(P_opt: DELTAP_gc)
"!Calculates the pressure drop of CO2 in the coaxial heat exchanger, 2
units in parallel"
"Formula found by curve fitting in Excel, pressure drop in kPa"
P=P_opt*convert(kPa;bar)                    "Convert pressure to bar"
DELTAP_gc=20233*(P^(-1,154))                "Pressure drop"

END

"-------------------------------------------------------------------------"

PROCEDURE deltap_plate(P_opt: DELTAP_gc)
"!Calculates the pressure drop of CO2 in the plate heat exchanger, 2 units
in parallel"
"Formula found by curve fitting in Excel, pressure drop in kPa"
"P_opt must be calcuted with [bar] as input unity"
P=P_opt*convert(kPa;bar)                    "Convert pressure to bar"
DELTAP_gc=0,0238*(P^2)-5,6089*P+338,99      "Pressure drop"

END

"-------------------------------------------------------------------------"

PROCEDURE gc_plate(P_opt: Q_gc)
"!Calculates the heat duty of the gas cooler - plate model (2 units)"
"Heat duty found by curve fitting in Excel, duty in kW"
P=P_opt*convert(kPa;bar)                    "Convert pressure to bar"
Q_gc=(-0,2161*(P^2))+(47,875*P)-2019,2      "Heat duty of gas cooler"

END

"-------------------------------------------------------------------------"

PROCEDURE gc_coaxial(P_opt: Q_gc)
"!Calculates the heat duty of the gas cooler - coaxial model (2 units)"
"Heat duty found by curve fitting in Excel, duty in kW"
P=P_opt*convert(kPa;bar)                    "Convert pressure to bar"
Q_gc1=(-0,073*(P^2))+(16,485*P)-296,9       "Heat duty of gas cooler by
formula"
err=(629,4-Q_gc1)/Q_gc1                     "Error of curve fitting"
Q_gc=Q_gc1*(1+err)                          "Heat duty of gas cooler -
updated"

END

"-------------------------------------------------------------------------"

PROCEDURE area_gc(HEX_type: A_gc)
"!Calulates the total heat transfer area of two parallel heat exchangers
with model as input"

A_plate=14,16 [m^2]     "Heat transfer area, model C202HP3 (Kaori)"
A_coaxial=9,613 [m^2]   "Heat transfer area, model WVCI serie22 (Frigomec)"

If (HEX_type = 1) Then
   A_gc=2*A_plate
Else
   A_gc=2*A_coaxial
Endif

END
```

```
"-------------------------------------------------------------------------"

"!Calling procedure to get arrays"
CALL flakeicedrum(T_evap_flake;m_co2_fl_real;T_water_in;m_w;x_pipe;Q_water:
U1[1];U1_avg)

"-------------------------------------------------------------------------
  General information
-------------------------------------------------------------------------"

R$='R744'                                   "Refrigerant string"
W$='water'                                  "Water string"

P_opt=10250
  "Pressure in gas cooler; value from optimization process in Excel"
HEX_type=2
  "Heat exchanger type: 1 = plate, 2 = coaxial"

"-------------------------------------------------------------------------
  Flake ice machine and bottom cycle. Solution by control volume
-------------------------------------------------------------------------"

{Control volume: Flake ice maker}

m_ice=100000 [kg]                           "Production capacity"
rho_ice=density(Ice;T=0;P=101,325)          "Density of ice"
V_ice=m_ice/rho_ice                         "Volume of produced ice [m^3]"
V_dot_ice=V_ice/(3600*24)
  "Volume flow rate of produced ice per day"
m_w=V_dot_ice*rho_ice                       "Water consumption, [kg/s]"
T_water_in= 8 [C]                           "Temperature of inlet water"
DELTAT_sc_w=7 [C]                           "Subcooling of ice"
c_P_w_lq=specheat(W$;T=T_water_in;x=0)
  "Specific heat capacity of liquid water"
h_fusion_w=enthalpy_fusion(W$)              "Enthalpy of fusion"
DELTAh_vap_co2=enthalpy_vaporization(R$;T=T_evap_flake)
  "Enthalpy of vapourization for CO2"
c_P_w_s=specheat(W$;T=-1;x=0)
  "Specific heat capacity of vapour water"

"!Heat transfered from water to CO2"
Q_water = m_w*(c_P_w_lq*(T_water_in) + h_fusion_w + c_P_w_s*(DELTAT_sc_w))
  "Heat removed from water"

"!Flake ice machine: refrigerant side (CO2)"
T_evap_flake=-30 [C]
  "Evaporation temperature of flake ice drum"
P_evap_flake=p_sat(R$;T=T_evap_flake)       "Evaporation pressure"
m_co2_fl_real=3,0 [kg/s]                    "Actual flow rate flake ice drum"
h_fl_co2_in=enthalpy(R$;P=P_evap_flake;x=0)
  "Inlet enthalpy"
h_fl_co2_out=h_fl_co2_in+Q_water/m_co2_fl_real
  "Outlet enthalpy"
h_out_th=enthalpy(R$;P=P_evap_flake;x=1)    "Theoretical outlet enthalpy"
m_co2_th=Q_water/(h_out_th-h_fl_co2_in)     "Theoretical mass flow assuming
saturated CO2 gas at outlet of flake ice drum"
Q_co2=m_co2_fl_real*(h_fl_co2_out-h_fl_co2_in)
  "Heat absorbed by CO2 in the bottom cycle"
x_fl_co2_out=quality(R$;P=P_evap_flake;h=h_fl_co2_out)
  "Gas quality at outlet of FID"
```

```
"!Pressure drop of flake ice drum"
d_flake=2,5 [m]
   "Diameter of flake ice drum, value from TechnoAlpin"
h_flake=2,6 [m]
   "Height of flake ice drum, value from TechnoAlpin"
mu_fl=viscosity(R$;T=T_evap_flake;h=h_fl_co2_in)
   "Dynamic viscosity at inlet of flake ice drum"
rho_fl=density(R$;T=T_evap_flake;h=h_fl_co2_in)
   "Density at inlet of flake ice drum"
d_pipe=5 [mm]*convert(mm;m)                "Refrigerant pipe diameter"
x_pipe=600                                 "Number of refrigerant pipes"
g=9,81 [m/s^2]                             "Gravitational constant"

sigma_fl_cold=surfacetension(R$;T=T_evap_flake)  "Surface tension"
rho_fl_f=density(R$;T=T_evap_flake;x=0)    "Density liquid CO2"
rho_fl_g=density(R$;T=T_evap_flake;x=1)    "Density vapour CO2"

mu_fl_f=viscosity(R$;T=T_evap_flake;x=0)   "Dynamic viscosity liquid CO2"
mu_fl_g=viscosity(R$;T=T_evap_flake;x=1)   "Dynamic viscosity vapour CO2"
x_m_fl=(x_fl_co2_out+0)/2                  "Average gas quality"
rho_fl_m=(x_m_fl/rho_fl_g+(1-x_m_fl)/rho_fl_f)^(-1)
   "Average density"

m_dot_pipe=m_co2_fl_real/x_pipe            "Mass flow through one pipe"
A_c_fl=(pi/4)*(d_pipe^2)
   "Cross-sectional area of CO2 pipe"
G_pipe_fl=m_dot_pipe/A_c_fl                "Mass flux through one pipe"
u_avg=m_dot_pipe/(((rho_fl_f+rho_fl_out)/2)*A_c_fl)
   "Average velocity through pipe"
mu_fl_out=(x_fl_co2_out/mu_fl_g+(1-x_fl_co2_out)/mu_fl_f)^(-1)
   "Average viscosity"
Re_fl=(((rho_fl_f+rho_fl_out)/2)*u_avg*d_pipe)/((mu_fl_f+mu_fl_out)/2)
   "Average Reynolds number"
rho_fl_out=density(R$;T=T_evap_flake;h=h_fl_co2_out)
   "Outlet density of drum"
u_in=(4*(m_co2_fl_real/x_pipe))/(rho_fl_f*pi*(d_pipe^2))
   "Inlet velocity to drum"
u_out=(4*(m_co2_fl_real/x_pipe))/(rho_fl_m*pi*(d_pipe^2))
   "Oulet velocity to drum"

"!Assume turbulent flow, friction factor by the Haaland equation (1983)"
eps=0,0015[mm]*convert(mm;m)
   "Surface roughness, stainless steel"
f_pipe=(-1,8*log10((6,9/Re_fl)*((eps/d_pipe)/3,7)^1,1))^(-2)
   "friction factor"

DELTAP_flake_friction=f_pipe*(h_flake/d_pipe)*((((rho_fl_f+rho_fl_out)/2)*(
u_avg^2))/2)*x_pipe*convert(Pa;kPa)
   "Pressure drop, friction - all CO2 pipes included"
DELTAP_flake_gravity=((rho_fl_f+rho_fl_out)/2)*g*h_flake*convert(Pa;kPa)
   "Effect of gravity on pressure drop"
DELTAP_flake_acceleration=((rho_fl_f+rho_fl_out)/2)*0,5*((u_out^2)-
(u_in^2))*convert(Pa;kPa)
   "Effect of acceleration on pressure drop"

DELTAP_flake=DELTAP_flake_friction+DELTAP_flake_gravity+DELTAP_flake_accele
ration  "Total pressure drop of FID on evaporation side"

P_a=P_evap_flake-DELTAP_flake
```

```
{Control volume: Pipe flake ice drum to Liquid drum}
"!Pipe Information"
e_ab=0,000015[m]                              {Roughness, Drawn Tubing}
D_ab=5,2[cm]*convert(cm;m)                    {Pipe Diameter}
RR_ab=e_ab/D_ab                               {Relative Roughness}
L_ab=1 [m]                                    {Length of pipe}

"!Pressure drop"
Call
pipeflow(R$;T_evap_flake;P_a+0,01;m_co2_fl_real;D_ab;L_ab;RR_ab:{h_T_ab};
{h_H_ab};DELTAP_ab;{Nusselt_T_ab};f_ab;Re_ab)

P_b_1=P_a-DELTAP_ab
T_b_1=temperature(R$;P=P_b_1;h=h_fl_co2_out)

{Control volume: Liquid drum}
"Assuming no pressure drop in the liquid tank"
m_dot_cond=x_fl_co2_out*m_co2_fl_real
   "Mass flow of vapour CO2 to condenser"
P_liq_drum=P_b_1                              "Pressure of liquid drum"
T_liq_drum=t_sat(R$;P=P_liq_drum)             "Temperature of liquid drum"
h_b=enthalpy(R$;P=P_liq_drum+0,01;x=1)        "Enthalpy at inlet of liquid
drum"

{Control volume: Pipe Liquid drum to condenser/evaporator}
"!Pipe Information"
e_bc=0,000015[m]                              {Roughness, Drawn Tubing}
D_bc=2,2[cm]*convert(cm;m)                    {Pipe Diameter}
RR_bc=e_bc/D_bc                               {Relative Roughness}
L_bc=1 [m]                                    {Length of pipe}

"!Pressure drop"
Callpipeflow(R$;T_liq_drum;P_liq_drum+0,01;m_dot_cond;D_bc;L_bc;RR_bc:{h_T_
bc};{h_H_bc};DELTAP_bc;{Nusselt_T_bc};f_bc;Re_bc)

P_c=P_liq_drum-DELTAP_bc
T_c=temperature(R$;P=P_c;h=h_fl_co2_out)

{Control volume: Evaporator/Condenser}
{Model: Alfa Laval AC1000DQ}
DELTAT_evap_cond=5 [K]
   "Approach temperature in evaporator/condenser"
T_evap = T_c-DELTAT_evap_cond                 "Evaporation temperature"
h_c=h_b                                       "Enthalpy"

UA_cond_evap=Q_water/DELTAT_evap_cond         "UA-value"
U_c_evap=2638 [W/m^2*K]                       "!U-value; trial-and-error(Ch.
8.2)"
w_plate=356 [mm]*convert(mm;m)                "Alfa Laval AC1000DQ plate width"
h_plate=615 [mm]*convert(mm;m)                "Alfa Laval AC1000DQ plate
height"
A_cond_evap=(UA_cond_evap*1000)/U_c_evap      "Surface area of heat exchanger"
x_plate=round(A_cond_evap/(2*h_plate*w_plate))
   "Number of plates in the plate heat exchanger on each side"
A_o_evap_cond=0,5*x_plate*w_plate*d_e         "Flow area"

"!Pressure drop on evaporation side, bottom cycle"
mu_cd=viscosity(R$;T=T_c;P=P_c+0,01)          "Dynamic viscosity"
rho_cd_i=density(R$;P=P_c+0,01;x=1)           "Density at inlet"
rho_cd_o=density(R$;P=P_c+0,01;x=0)           "Density at outlet"
rho_cd=(rho_cd_o+rho_cd_i)/2                  "Average density"
```

```
D_P_cd=22 [mm]*convert(mm;m)                    "Port inlet"
G_p_cd=(m_dot_cond)/((pi/4)*D_p_cd^2)           "Mass flux through the port"
G_cd=(m_dot_cond)/A_o_evap_cond                 "Mass flux through the core"
n_p_cd=1                                        "Number of passer on warm side"

DELTAP_cd_g = rho_cd*g*h_plate                  "Gravitational pressure drop"
DELTAP_cd_acc = (G_cd^2)*1*( (1/rho_cd_i) - (1/rho_cd_o))
  "Acceleration pressure drop, quality change is 1 (complete evaporation)"
DELTAP_cd_p = (0,75*(G_p_cd^2)*n_p_cd)/rho_cd  "Manifold pressure drop"
DELTAP_cd_fr = (1,9*G_cd^2)/(2*rho_cd)          "Frictional pressure drop"
DELTAP_cd = (DELTAP_cd_fr+DELTAP_cd_p - DELTAP_cd_acc -
DELTAP_cd_g)*convert(Pa;kPa)
  "Total pressure drop"

P_d=P_c-DELTAP_cd                               "Outlet pressure"
h_d=h_c-Q_water/m_dot_cond                      "Outlet enthalpy"
T_d=temperature(R$;P=P_d;h=h_d)                 "Outlet temperature"
Q_evap_warm=m_dot_cond*(h_c-h_d)
  "Heat released in evaporator/condenser, equals Q_water"

{Control volume: Pipe evaporator/condenser to liquid drum
"!Pipe Information"
e_de=0,000015[m]                                {Roughness, Drawn Tubing}
D_de=2,2[cm]*convert(cm;m)                      {Pipe Diameter}
RR_de=e_de/D_de                                 {Relative Roughness}
L_de=1 [m]                                      {Length of pipe}

"!Pressure drop"
Call pipeflow(R$;T_d;P_d+0,01;m_dot_cond;D_de;L_de;RR_de:{h_T_de};{h_H_de}
;DELTAP_de;{Nusselt_T_de};f_de;Re_de)

P_e=P_d-DELTAP_de
T_e=temperature(R$;P=P_e;h=h_d)

{Control volume: Pipe liquid drum to pump}
"!Pipe Information"
e_ef=0,000015[m]                                {Roughness, Drawn Tubing}
D_ef=3,2[cm]*convert(cm;m)                      {Pipe Diameter}
RR_ef=e_ef/D_ef                                 {Relative Roughness}
L_ef=1 [m]                                      {Length of pipe}

"!Pressure drop"
Call
pipeflow(R$;T_e;P_e+0,01;m_co2_fl_real;D_ef;L_ef;RR_ef:{h_T_ef;{h_H_ef}
;DELTAP_ef;{Nusselt_T_ef};f_ef;Re_ef)

P_f=P_e-DELTAP_ef
T_f=temperature(R$;P=P_f;h=h_d)

{Control volume: CO2-pump}
N_co2_pump=948[1/min]*convert(1/min;1/s)  "RPM pump"
D_co2_pump=0,30 [m]                             "Diameter of pump"
D_hub_co2=0,16[m]                               "Diameter of pump hub"
Call centrifugalpump1_cl( R$; 0; T_f; P_f+0,01;m_co2_fl_real; N_co2_pump;
D_co2_pump; D_hub_co2: P_g; T_g; W_co2_pump; eta_co2_pump)
DELTAP_pump=P_g-P_f                             "Pressure lift of pump"
```

```
{Control volume: Pipe pump to flake ice drum}
"!Pipe Information"
e_g=0,000015[m]                              {Roughness, Drawn Tubing}
D_g=3,2[cm]*convert(cm;m)                    {Pipe Diameter}
RR_g=e_g/D_g                                 {Relative Roughness}
L_g=1 [m]                                    {Length of pipe}

"!Pressure drop"
Call pipeflow(R$;T_g;P_g+0,01;m_co2_fl_real;D_g;L_g;RR_g:{h_T_g};{h_H_g};
DELTAP_g;{Nusselt_T_g};f_g;Re_g)

P_g_fl=P_g-DELTAP_g
T_g_fl=temperature(R$;P=P_g_fl;x=0)

DELTAP_cycle=DELTAP_flake+DELTAP_ab+DELTAP_bc+DELTAP_cd+DELTAP_de+DELTAP_ef
+DELTAP_g

"-------------------------------------------------------------------------
  Heat recovery cycle. Solution by control volume
-------------------------------------------------------------------------"

m_dot_co2=Q_water/(h[14]-h[13])
  "Mass flow in heat recovery cycle"

{State 1 to state 2}
{Control volume: 1st stage compressor}
"!State points 1: compressor inlet"
P[1]=P[16]-31{-DELTAP_161}                   "Pressure"
h[1]=h[16]                                   "Enthalpy"
T[1]=temperature(R$;P=P[1];h=h[1])           "Temperature"
s[1]=entropy(R$;h=h[1];P=P[1])               "Entropy"
V_dot_sg_1=(m_dot_co2/density(R$;P=P[1]+0,01;T=T[1]+0,01))*3600
  "Suction gas volume of first stage compressor"

eta_ad=0,90 [-]                              "Adiabatic efficiency"

"!State points 2: compressor outlet"
P[2]=sqrt(P[1]*P_opt)                        "Discharge pressure"
PR_12=P[2]/P[1]                              "Pressure ratio, 1st stage"
eta_IS_12=-0,00000461*PR_12^6+0,00027131*PR_12^5-
0,00628605*PR_12^4+0,07370258*PR_12^3-0,46054399*PR_12^2+1,40653347*PR_12-
0,87811477
  "Isentropic efficiency"
h_2_is=enthalpy(R$;P=P[2];s=s[1])            "Isentropic enthalpy"
h[2]=h[1]+((h_2_is-h[1])/eta_IS_12)*eta_ad
  "Real enthalpy, including losses"
T[2]=temperature(R$;h=h[2];P=P[2])           "Discharge gas temperature"
s[2]=entropy(R$;h=h[2];P=P[2])               "Entropy"

W_comp_1=m_dot_co2*(h[2]-h[1])               "Compressor work at 1st stage"


{State 2 to 3}
{Control volume: connecting pipe}
"!Pipe information"
e_23=0,000015 [m]                            {Roughness, drawn tubing}
D_23=3,2 [cm]*convert(cm;m)                  {Pipe diameter}
RR_23=e_23/D_23                              {Relative roughness}
L_23=1 [m]                                   {Length of pipe}
```

```
"!Pressure drop"
Call pipeflow(R$;T[2];P[2];m_dot_co2;D_23;L_23;RR_23:{h_T_23};{h_H_23};
DELTAP_23;{Nusselt_T_23};f_23;Re_23)

{State 3 to 4}
{Control volume: intercooler}
{Plate heat exchanger: Alfa Laval AXP52}
"!Inlet intercooler"
P[3]=P[2]-28,5{-DELTAP_23}                    "Pressure"
h[3]=h[2]                                     "Enthalpy"
T[3]=temperature(R$;h=h[3];P=P[3])            "Temperature"
s[3]=entropy(R$;h=h[3];P=P[3])                "Entropy"
mu[3]=viscosity(R$;P=P[3];h=h[3])             "Dynamic viscosity"
rho[3]=density(R$;P=P[3];h=h[3])              "Density"

"!Pressure drop and size of intercooler"
Call
heattransferic(m_dot_co2;m_dot_water_ic;T_water_in;P[3];T[3];P[4];T[4];
T_ref_avg_ic;T_w_avg_ic;w_plate_ic;x_plate_ic:U_ic)

m_dot_water_ic=2 [kg/s]                       "Mass flow rate of water, cold
side"
T_out_ic=T_water_in+Q_ic/(m_dot_water_ic*C_p_w)
   "Outlet water temperature"
T_w_avg_ic=(T_water_in+T_out_ic)/2
   "Average water temperature in intercooler"
Q_ic=(m_dot_co2)*(h[3]-h[4])                  "Heat duty of intercooler"
T_ref_avg_ic=(T[3]+T[4])/2
   "Average CO2 temperature in intercooler"
P_cold=101,325 [kPa]
   "Atmospheric pressure at water inlet, cold side"
C_p_w=specheat(W$;T=T_water_in;P=P_cold+0,01)
   "Specific heat capacity of water"

dt_1_ic=T[4]-T_water_in                       "Temperature difference cold
side"
dt_2_ic=T[3]-T_out_ic                         "Temperature difference hot side"
DELTAT_ic_lmtd=((dt_1_ic)-(dt_2_ic))/ln((dt_1_ic)/(dt_2_ic))
   "Logaritmic mean temperature difference"

UA_ic=Q_ic/DELTAT_ic_lmtd                     "UA-value"
U_ic_1=810,7 [W/m^2*K]                        "U-value; trial-and-error(Ch.
8.2)"
A_ic=(UA_ic*1000)/U_ic_1                      "Surface area of PHE"
w_plate_ic=160 [mm]*convert(mm;m)             "Width of heat exchanger"
h_plate_ic=466 [mm]*convert(mm;m)             "Height of heat exchanger"
x_plate_ic=round(A_ic/(2*w_plate_ic*h_plate_ic))
   "Number of plates in heat exchanger per side"
d_p=0,052 [m]                                 "Port diameter"
d_e=0,007 [m]                                 "Equivalent diameter of
intercooler"

"Pressure drop"
mu_ic=(mu[3]+mu[4])/2                         "Average dynamic viscosity"
rho_ic=(rho[3]+rho[4])/2                      "Average density"

G_p_ic=(m_dot_co2)/((pi/4)*d_p^2)             "Mass flux through the port"
A_o_ic=0,5*x_plate_ic*w_plate_ic*d_e          "Flow area"
G_ic=(m_dot_co2)/A_o_ic                       "Mass flux through the core"
Re_ic=(G_ic*d_e)/mu_ic                        "Reynolds number"
f_ic=0,8*Re_ic^(-0,25)                        "Friction factor"
```

```
n_p_ic=1                                    "Number of passes"

DELTAP_g_ic = rho_ic*g*h_plate_ic
  "Gravitational pressure drop"
DELTAP_man_ic = (0,75*(G_p_ic^2)*n_p_ic)/rho_ic
  "Manifold pressure drop"
DELTAP_fr_ic = 2*f_ic*(h_plate_ic*G_ic^2)/(d_e*rho_ic)
  "Frictional pressure drop"
DELTAP_acc_ic=(G_ic^2)*((1/rho[4])-(1/rho[3]))
  "Pressure drop from acceleration"
DELTAP_ic = (DELTAP_fr_ic+DELTAP_man_ic+DELTAP_acc_ic - DELTAP_g_ic)/1000
  "Total pressure drop of intercooler"

P[4]=P[3]-11,4{-DELTAP_ic}

"!Outlet intercooler"
T[4]=24
  "Temperature, fixed in order to keep T[6] below 130 C"
h[4]=enthalpy(R$;P=P[4];T=T[4])             "Enthalpy"
s[4]=entropy(R$;P=P[4];T=T[4])              "Entropy"
mu[4]=viscosity(R$;P=P[4];h=h[4])           "Dynamic viscosity"
rho[4]=density(R$;P=P[4];h=h[4])            "Density"

DELTAT_ic=T[3]-T[4]                         "Temperature change,
intercooling"

{State 4 to 5}
{Control volume: connecting pipe}
"!Pipe information"
e_45=0,000015 [m]                           {Roughness, drawn tubing}
D_45=3,2 [cm]*convert(cm;m)                 {Pipe diameter}
RR_45=e_45/D_45                             {Relative roughness}
L_45=1,5 [m]                                {Length of pipe}

"!Pressure drop"
Call pipeflow(R$;T[4];P[4];m_dot_co2;D_45;L_45;RR_45:{h_T_45};{h_H_45};
DELTAP_45;{Nusselt_T_45};f_45;Re_45)

{State 5 to 6}
{Control volume: 2nd stage compressor}
"!State points 5: compressor inlet"
P[5]=P[4]-34{-DELTAP_45}                    "Pressure"
h[5]=h[4]                                   "Enthalpy"
T[5]=temperature(R$;h=h[5];P=P[5])          "Temperature"
s[5]=entropy(R$;h=h[5];P=P[5])              "Entropy"
V_dot_sg_2=(m_dot_co2/density(R$;P=P[5];T=T[5]))*3600
  "Suction gas volume of second stage compressor"

"!State points 6: compressor outlet"
P[6]=P_opt                                  "Optimal gas cooler pressure"
PR_56=P[6]/P[5]
  "Pressure ratio for 2nd compressor stage"
eta_IS_56=-0,00000461*PR_56^6+0,00027131*PR_56^5-
0,00628605*PR_56^4+0,07370258*PR_56^3-0,46054399*PR_56^2+1,40653347*PR_56-
0,87811477
  "Isentropic efficiency"
h_6_is=enthalpy(R$;P=P[6];s=s[5])           "Isentropic enthalpy"
h[6]=h[5]+((h_6_is-h[5])/eta_IS_56)*eta_ad
  "Real enthalpy including losses"
T[6]=temperature(R$;P=P[6];h=h[6])          "Temperature"
s[6]=entropy(R$;P=P[6];h=h[6])              "Entropy"
```

```
W_comp_2=m_dot_co2*(h[6]-h[5])                "Compressor work at 2nd stage"

{State 6 to 7}
{Control volume: connecting pipe}
"!Pipe information"
e_67=0,000015 [m]                             {Roughness, drawn tubing}
D_67= 3,2 [cm]*convert(cm;m)                  {Pipe diameter}
RR_67=e_67/D_67                               {Relative roughness}
L_67=1 [m]                                    {Length of pipe}

"!Pressure drop"
Call pipeflow(R$;T[6];P[6];m_dot_co2;D_67;L_67;RR_67:{h_T_67};{h_H_67};
DELTAP_67;{Nusselt_T_67};f_67;Re_67)

{State 7 to 8}
{Control volume: gas cooler}
"!State points 7: gas cooler inlet"
P[7]=P[6]-DELTAP_67                           "Pressure"
h[7]=h[6]                                     "Enthalpy"
T[7]=temperature(R$;P=P[7];h=h[7])            "Temperature"
s[7]=entropy(R$;P=P[7];h=h[7])                "Entropy"
rho[7]=density(R$;P=P[7];h=h[7])              "Density"
mu[7]=viscosity(R$;P=P[7];T=T[7])             "Viscosity"

{Gas cooler performance - modelled in Excel}
Call gc_coaxial(P_opt: Q_gc)
Call deltap_coaxial(P_opt: DELTAP_gc)

"!State points 8: gas cooler outlet"
h[8]=h[7]-(Q_gc/m_dot_co2)                    "Enthalpy"
P[8]=P[7]-DELTAP_gc                           "Pressure"
T[8]=temperature(R$; P=P[8];h=h[8])           "Temperature"
s[8]=entropy(R$;T=T[8];P=P[8])                "Entropy"
rho[8]=density(R$;T=T[8];P=P[8])              "Density"
mu[8]=viscosity(R$;T=T[8];P=P[8])             "Viscosity"

T_water_in_gc=8[C]                            "Inlet temperature water"
T_water_out_gc=80[C]                          "Set-point temp. water, outlet"
h_w_in=enthalpy(W$;T=T_water_in_gc;P=1000)
  "Inlet enthalpy water"
h_w_out=enthalpy(W$;T=T_water_out_gc;P=1000)
  "Outlet enthalpy water"
m_dot_w_gc=Q_gc/(h_w_out-h_w_in)
  "Mass flow of water through gas cooler"

DELTAT_1_gc=T[7]-T_water_out_gc               "Temperature difference hot side"
DELTAT_2_gc=T[8]-T_water_in_gc                "Temperature difference cold
side"
LMTD_gc=(DELTAT_1_gc-DELTAT_2_gc)/ln(DELTAT_1_gc/DELTAT_2_gc)
  "Logaritmic mean temperature difference"
Call area_gc(HEX_type: A_gc)                  "Effective heat transfer area"
U_gc=(Q_gc*1000)/(A_gc*LMTD_gc)               "U-value of gas cooler"
DELTAT_a=DELTAT_2_gc                          "Approach temperature at outlet"

{State 8 to 9}
{Control volume: connecting pipe}
"!Pipe information"
e_89=0,000015 [m]                             {Roughness, drawn tubing}
D_89=2,2 [cm]*convert(cm;m)                   {Pipe diameter}
RR_89=e_89/D_89                               {Relative roughness}
```

```
L_89=1 [m]                                  {Length of pipe}

"!Pressure drop"
Call pipeflow(R$;T[8];P[8];m_dot_co2;D_89;L_89;RR_89:{h_T_89};{h_H_89};
DELTAP_89;{Nusselt_T_89};f_89;Re_89)

{State 9 to 10}
{Control volume: suction gas heat exchanger (SGHX), warm side}
"!State points 9: Inlet SGHX"
P[9]=P[8]-DELTAP_89                         "Pressure"
h[9]=h[8]                                   "Enthalpy"
T[9]=temperature(R$;P=P[9];h=h[9])          "Temperature"
s[9]=entropy(R$;P=P[9];h=h[9])              "Entropy"
Q_SGHX=21
   "Heat duty adapted to the dimensioning point"
DELTAP_SGHX_hot=4                           "Pressure drop hot side"

"!State points 10: Outlet SGHX"
{From procedure SGHX_counterflow}
h[10]=h[9]-(Q_SGHX/m_dot_co2)               "Enthalpy"
P[10]=P[9]-DELTAP_SGHX_hot                  "Pressure"
T[10]=temperature(R$;P=P[10];h=h[10])       "Temperature"
s[10]=entropy(R$;P=P[10];T=T[10])           "Entropy"

{State 10 to 11}
{Control volume: connecting pipe}
"!Pipe information"
e_1011=0,000015 [m]                         {Roughness, stainless steel}
D_1011=2,2 [cm]*convert(cm;m)               {Pipe diameter}
RR_1011=e_1011/D_1011                       {Relative roughness}
L_1011=1 [m]                                {Length of pipe}

"!Pressure drop"
Call pipeflow(R$;T[10];P[10];m_dot_co2;D_1011;L_1011;RR_1011:{h_T_1011};
{h_H_1011};DELTAP_1011;{Nusselt_T_1011};f_1011;Re_1011)

{State 11 to 12}
{Control volume: expansion valve}
"!State points 11: Inlet of expansion valve"
P[11]=P[10]-DELTAP_1011                     "Pressure"
h[11]=h[10]                                 "Enthalpy"
T[11]=temperature(R$;P=P[11];h=h[11])       "Temperature"
s[11]=entropy(R$;P=P[11];h=h[11])           "Entropy"

"!State points 12: Outlet of expansion valve"
h[12]=h[11]                                 "Enthalpy"
P[12]=p_sat(R$;T=T_evap)                    "Pressure"
T[12]=temperature(R$;P=P[12];h=h[12])       "Temperature"
x[12]=quality(R$;h=h[12];T=T[12])           "Gas quality"
s[12]=entropy(R$;T=T[12];x=x[12])           "Entropy"

{State 12 to 13}
{Control volume: connecting pipe}
"!Negligible pressure drop, exp. valve very close to evaporator"
P[13]=P[12]                                 "Constant pressure"

{State 13 to 14}
{Control volume: evaporator/condenser}
{Plate heat exchanger: Alfa Laval AC1000DQ}
"!State points 13: inlet of evaporator"
h[13]=h[12]                                 "Enthalpy"
```

```
T[13]=temperature(R$;P=P[13];h=h[13])      "Temperature"
x[13]=quality(R$;h=h[13];T=T[13])          "Gas quality"
s[13]=entropy(R$;T=T[13];x=x[13])          "Entropy"
mu[13]=viscosity(R$;P=P[13];x=0)           "!Dynamic viscosity calculated at
x=0, EES will not calculate for x[13] in the two-phase region"
rho[13]=density(R$;P=P[13];x=x[13])        "Density"

"!Pressure drop and size of evaporator/condenser"
Call
heattransfercondevap(m_dot_co2;m_co2_fl_real;T_evap;T_evap_flake;x[13];
w_plate_ec;h_plate_ec;x_plate_ec;b_plate_ec:U_cond_evap;G_2)

h_plate_ec=615 [mm]*convert(mm;m)          "Heigth of heat exchanger"
w_plate_ec=356 [mm]*convert(mm;m)          "Width of heat exchanger"
x_plate_ec=round(A_cond_evap/(2*h_plate_ec*w_plate_ec))
   "Number of plates in plate heat exchanger per side"
b_plate_ec=0,0035 [m]                      "Channel spacing"
n_p_ec=1                                   "Number of passes (single-pass)"

"Pressure drop on condensation (cold) side"
D_p_ec=0,052 [m]                           "Port diameter"
G_p_ec=(m_dot_co2)/((pi/4)*D_p_ec^2)       "Mass flux through the port"
sigma_cold=surfacetension(R$;T=T_evap)     "Surface tension"
rho_f=density(R$;T=T_evap;x=0)             "Density liquid"
rho_g=density(R$;T=T_evap;x=1)             "Density gas"
x_m=(x[13]+x[14])/2                        "Average gas quality"
rho_m=(x_m/rho_g+(1-x_m)/rho_f)^(-1)       "Average density"
We_m=(G_2^2*d_e)/(rho_m*sigma_cold)        "Weber number"
Bd_m=((rho_f-rho_g)*g*d_e^2)/sigma_cold    "Bond number"
rho_ast=(rho_f/rho_g)                      "Density ratio: Liquid/gas"
beta_ast=45/70                             "Ratio: beta/beta_max"
C_ec=2,125*beta_ast^9,993+0,955            "Correlation factor"
f_tp=C_ec*15,698*We_m^(-0,475)*Bd_m^0,255*rho_ast^(-0,571)
   "Two-phase friction factor"

DELTAP_evap_fr=2*f_tp*(h_plate_ec*G_2^2)/(d_e*rho_m)
   "Frictional pressure drop [Pa]"
DELTAP_evap_g=rho_m*g*h_plate_ec           "Gravitational pressure drop[Pa]"
DELTAP_evap_acc=(G_2^2)*(x[14]-x[13])*(1/rho_g-1/rho_f)
   "Acceleration pressure drop [Pa]"
DELTAP_evap_man=(0,75*(G_p_ec^2)*n_p_ec)/rho_m
   "Manifold pressure drop [Pa]"
DELTAP_evap_cond=(DELTAP_evap_man+DELTAP_evap_acc+DELTAP_evap_g+DELTAP_evap
_fr)*convert(Pa;kPa)
   "Total pressure drop"

"!State points 14: Outlet of evaporator"
{Pressure drop is calculated from procedure: Evaporator/condenser}
P[14]=P[13]-20{-DELTAP_evap_cond}           "Pressure"
x[14]=1                                    "Gas quality"
h[14]=enthalpy(R$;P=P[14]+0,01;x=x[14])    "Enthalpy"
T[14]=temperature(R$;P=P[14]+0,01;x=x[14])
   "Temperature"
s[14]=entropy(R$;P=P[14];h=h[14])          "Entropy"
mu[14]=viscosity(R$;P=P[14];x=x[14])       "Dynamic viscosity"
rho[14]=density(R$;P=P[14];x=x[14])        "Density"

{State 14 to 15}
{Control volume: connecting pipe}
"!Pipe information"
e_1415=0,000015 [m]                        {Roughness, stainless steel}
```

```
D_1415=4,2 [cm]*convert(cm;m)                {Pipe diameter}
RR_1415=e_1415/D_1415                        {Relative roughness}
L_1415=1,5 [m]                               {Length of pipe}

"!Pressure drop"
Call pipeflow(R$;T[14]+0,01;P[14]+0,01;m_dot_co2;D_1415;L_1415;RR_1415:
{h_T_1415};{h_H_1415};DELTAP_1415;{Nusselt_T_1415};f_1415;Re_1415)

{State 15 to 16}
{Control volume: suction gas heat exchanger, cold side}
"!State points 15: Inlet of SGHX"
P[15]=P[14]-21{-DELTAP_1415}                 "Pressure"
h[15]=h[14]                                  "Enthalpy"
T[15]=temperature(R$;P=P[15];h=h[15])        "Temperature"
s[15]=entropy(R$;T=T[15];h=h[15])            "Entropy"

"!State points 16: Outlet of SGHX"
{From procedure SGHX_counterflow}
h[16]=h[15]+(Q_SGHX/m_dot_co2)               "Enthalpy"
DELTAP_SGHX_cold=8                           "Pressure loss cold side"
P[16]=P[15]-DELTAP_SGHX_cold                 "Pressure"
T[16]=temperature(R$;P=P[16];h=h[16])        "Temperature"
s[16]=entropy(R$;T=T[16];h=h[16])            "Entropy"

{State 16 to 1}
{Control volume: connecting pipe}
"!Pipe information"
e_161=0,000015 [m]                           {Roughness, stainless steel}
D_161=3,2 [cm]*convert(cm;m)                 {Pipe diameter}
RR_161=e_161/D_161                           {Relative roughness}
L_161=0,5 [m]                                {Length of pipe}

"!Pressure drop"
Callpipeflow(R$;T[16];P[16];m_dot_co2;D_161;L_161;RR_161:{h_T_161};{h_H_161
}; DELTAP_161;{Nusselt_T_161};f_161;Re_161)

"-------------------------------------------------------------------------
  Cycle performance. Efficiency calculations
-------------------------------------------------------------------------"

W_tot=W_comp_1+W_comp_2                      "Total compressor work"
COP_cooling=Q_co2/W_tot                      "COP cooling"
COP_heating=Q_gc/W_tot                       "COP heating"

W_pump=2,5 [kW]
  "Additional work by circulation pump"
COP_system_heating=Q_gc/(W_tot+W_pump)
  "System COP (heat recovery)"
```

E. Results from optimization process of the gas cooler

Table A- 2. Performance of the gas cooler models when integrated in the EES model

Gas cooler pressure [bar]	115	110	105	100	95	90
Heat duty PHE [kW]	630.6	627.8	622.4	609.8	581	536.4
Compressor work PHE [kW]	277.4	272.9	267.6	263.8	259.2	254.5
Pump work PHE [kW]	0.015	0.015	0.015	0.015	0.015	0.015
Total work PHE [kW]	277.4	272.9	267.6	263.8	259.2	254.5
COP PHE [-]	2.273	2.300	2.326	2.312	2.242	2.108
COP_system PHE [-]	2.273	2.300	2.326	2.311	2.242	2.108
Heat duty coaxial [kW]	633.8	631.2	631.6	622.6	607.2	596.8
Compressor work coaxial [kW]	277.4	272.9	267.6	263.8	259.2	254.5
Pump work coaxial [kW]	3	2.5	2.5	2.5	2.5	2.5
Total work coaxial [kW]	280.4	275.4	270.1	266.3	261.7	257
COP coaxial [-]	2.285	2.313	2.360	2.360	2.343	2.345
COP_system coaxial [-]	2.260	2.292	2.338	2.338	2.320	2.322

Table A- 3. Pressure drop, temperature approach and U-values

Gas cooler pressure [bar]	115	110	105	100	95	90
ΔP_{co2} PHE [kPa]	8.8	10.2	12.6	16.0	21.2	27.0
ΔP_{water} PHE [kPa]	24.3	24.6	25.1	25.8	26.0	25.0
ΔP_{co2} coaxial [kPa]	83	88	97	105	101	112
ΔP_{water} coaxial [kPa]	639	628	607	587	599	569
ΔT_A at pinch, PHE [°C]	0.9	1.4	2.5	5.1	10.8	18.4
ΔT_A at pinch, coaxial [°C]	0.1	0.6	0.4	2.3	5.4	7.2
Outlet CO_2 temp. PHE [°C]	8.9	9.4	10.5	13.1	18.8	26.4
Outlet CO_2 temp. coaxial [°C]	8.1	8.6	8.4	10.3	13.4	15.2
U-value PHE [W/m^{2}K]	1871	1879	1879	1889	1866	1840
U-value coaxial [W/m^{2}K]	3623	3689	3650	3810	4101	4372

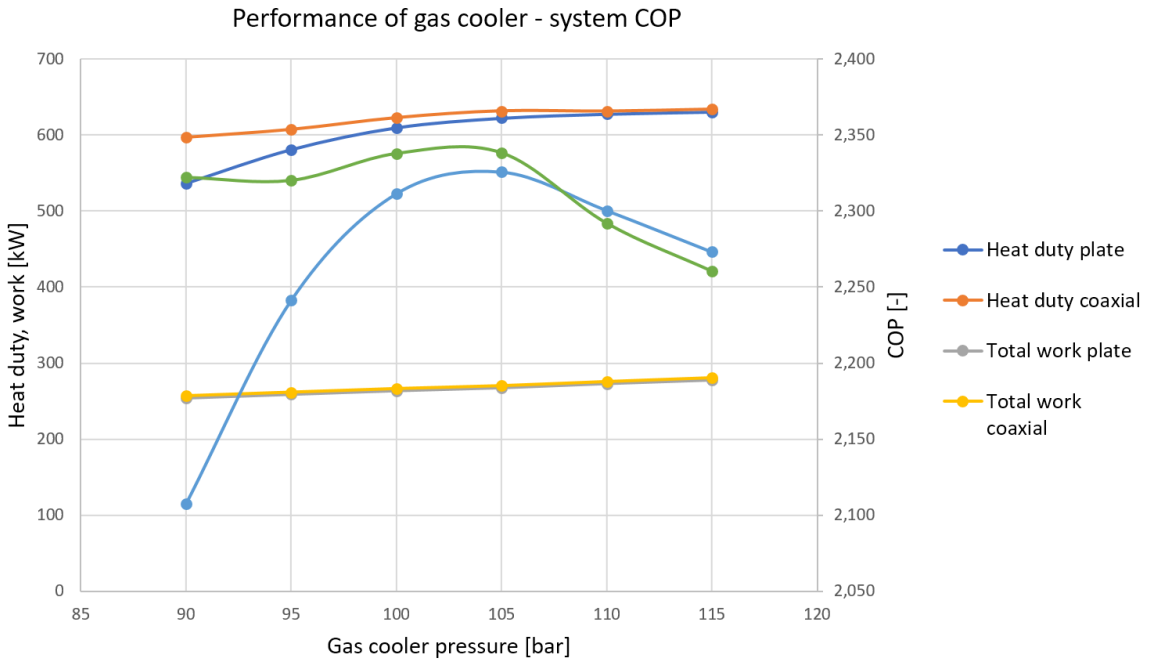

Figure A- 5. COP at different gas cooler pressures when work from both compressors stages and the pump is taken into consideration

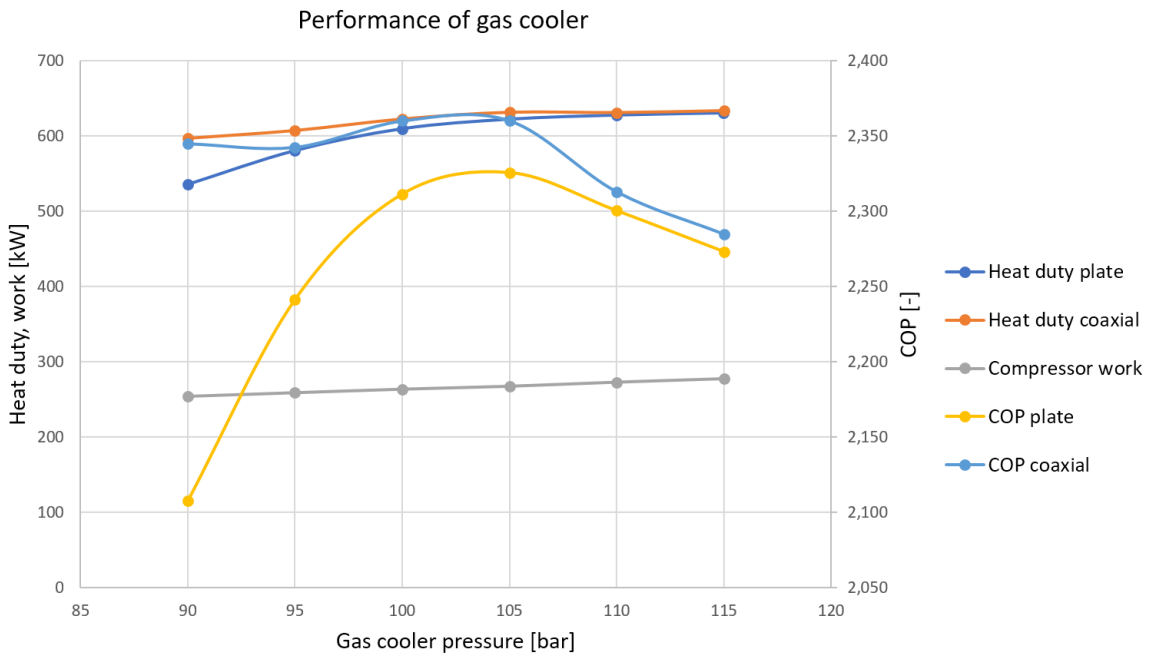

Figure A- 6. COP at different gas cooler pressures, when only compressor work is considered

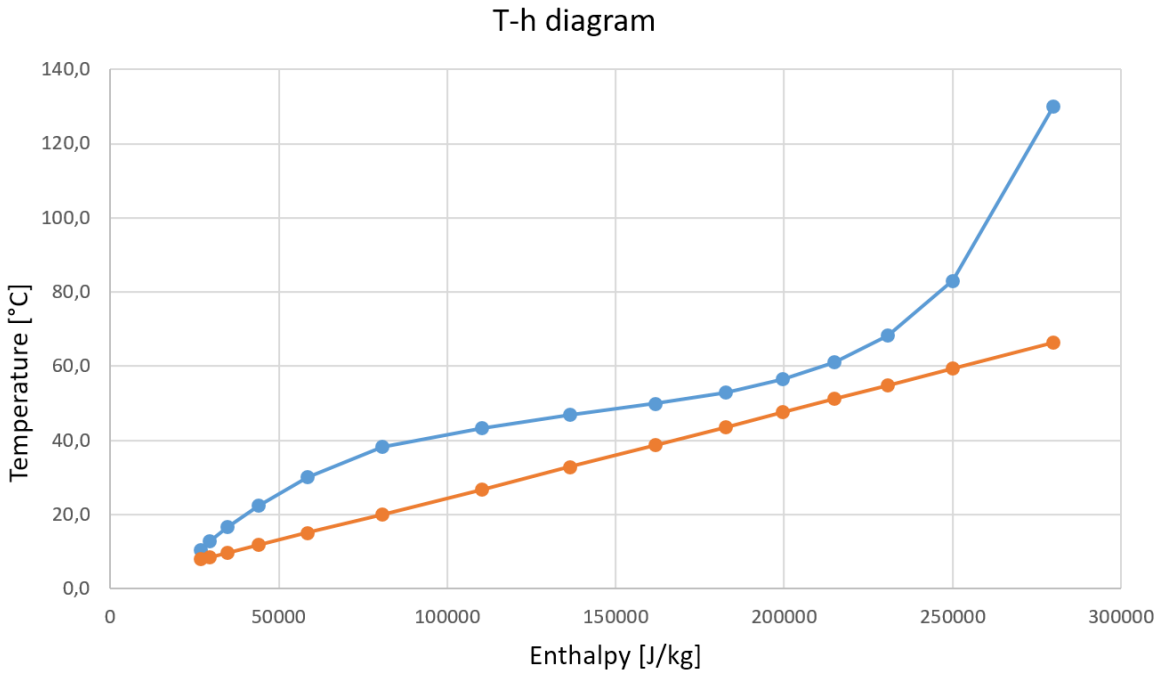

Figure A- 7. T-h diagram for the coaxial model operated at optimal pressure level

Table A- 4. Heat exchanger dimensions and investment costs

	PHE: C202HP3 (Kaori)	Coaxial: WVCI serie 22 (Frigomec)
Price (excl. transportation) [NOK]	17,083	21,673
Production site	Taiwan	Italy
Outer dimensions:		
Height [m]	0.616	0.462
Width [m]	0.189	0.502
Length/depth [m]	0.3365	0.502

F. Gas cooler data

Kaori Heat Treatment Co., Ltd. – model C202HP3

KAORI Heat Treatment Co.,Ltd.
No.5-2, Chi-Lin N.Road,Chung-Li Industrial District, Taoyuan City, TAIWAN 320
Tel: 886-3-4626958 Fax: 886-3-4628021
PLATE HEAT EXCHANGER DATA SHEET

Customer name : NTNU - Department of Energy and Process Engineering
Project name :
Date : 2017/2/20

Heat transfer device	: Cooler		PHE Code	: C202HP3*150	
No. of plates	: 150		Series * Parallel	: 1*2	
Length	: 613.0	mm	Height	: 336.5	mm
Width	: 186.0	mm	Weight	: 125.66	kg

	Side 1	Side 2	Unit
Fluid name	R744(100bar)	Water	
Mass Flow rate	1.897	2.029	kg/s
Inlet temp.	130.00	8.00	C
Exit temp.	13.00	80.00	C
Pressure drop	84.0	43.2	kPa
Allowable press. drop	100.0	50.0	kPa
Fouling Resistance	0	0	m^2,C / W
No. of channel	72	75	
Reference temp.	71.5	44.0	C
Density	377.1	989.2	kg/m^3
Specific heat capacity	2.747	4.174	kJ/kg,C
Thermal conductivity	0.031	0.635	W/m,C
Viscosity	0.036	0.606	cP
Channel velocity	0.29	0.11	m/s

Log mean temp. diff.	19.543	C
Heat transfer area	27.216	m^2
Heat load	610	kW
Margin	38.5	%

Plate material	316
Solder	Copper
Working Press.	140/30 bar (max.)
Testing Press.	200/43 bar (min.)
Flow arrangement	Countercurrent

	Inch	Connection Type		Inch	Connection Type
A1			B1		
A2			B2		
C1			D1		
C2			D2		

S02-702-03

C Series- CO_2 Super High Pressure Brazed Plate Heat Exchanger

KAORI patented solution with C series is specially designed for Gas cooler, condenser, evaporator and economizer in R744 (CO_2) heat pump and refrigeration system. Different designs with max. working pressure 140 bar, 100 bar and 70 bar are available for Supercritical, Transcritical and Subcritical CO_2 heating and cooling systems.

Compact size, outstanding heat transfer performance and low pressure drop are the three key features. The quality and the durability of C series is proven by thorough inspection, achieving the burst test pressure up to 650 bar and cycle test over 100,000 cycles.

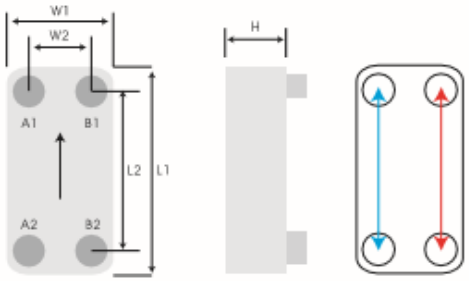

Brazing Material		Copper		
Model		C020,C040 C095,C200	C021,C041 C096,C201	C022,C042 C097,C202
		(A1,A2/B1,B2)		
Max. Working Pressure	(bar)	70/30*	100/30*	140/30*
Min. Test Pressure	(bar)	100/43*	143/43*	200/43*
Max. Working Temperature (°C)		200°C		

* For higher working pressure request on B1/B2, please contact KAORI representative.

Model	L1 (mm)	L2 (mm)	W1 (mm)	W2 (mm)	H Thickness (mm)	Weight*(kg) (Without Connection)	Heat Transfer Area/ plate (m^2)	Total Heat Transfer Area (m^2)	Volume/ Channel (liter)	Total Volume (liter)
C020	191	154	77	40	9.5+1.10*N	1.12+0.042*N	0.01109	(N-2)*0.01109	0.009	(N-1)*0.009
C040	314	275	76	40	13.0+2.00*N	1.74+0.145*N	0.0193	(N-2)*0.0193	0.030	(N-1)*0.030
C095	524	466	108	50	13.2+2.16*N	5.52+0.320*N	0.0475	(N-2)*0.0475	0.071	(N-1)*0.071
C200	616	519	189	92	14.0+2.15*N	12.39+0.603*N	0.0950	(N-2)*0.0950	0.156	(N-1)*0.156

Model	L1 (mm)	L2 (mm)	W1 (mm)	W2 (mm)	H Thickness (mm)	Weight*(kg) (Without Connection)	Heat Transfer Area/ plate (m^2)	Total Heat Transfer Area (m^2)	Volume/ Channel (liter)	Total Volume (liter)
C021	191	154	77	40	9.5+1.10*N	1.14+0.042*N	0.01109	(N-2)*0.01109	0.009	(N-1)*0.009
C041	314	275	76	40	13.0+2.00*N	1.83+0.145*N	0.0193	(N-2)*0.0193	0.030	(N-1)*0.030
C096	524	466	108	50	13.2+2.16*N	5.68+0.320*N	0.0475	(N-2)*0.0475	0.071	(N-1)*0.071
C201	616	519	189	92	14.0+2.15*N	12.56+0.631*N	0.0950	(N-2)*0.0950	0.156	(N-1)*0.156

Model	L1 (mm)	L2 (mm)	W1 (mm)	W2 (mm)	H Thickness (mm)	Weight*(kg) (Without Connection)	Heat Transfer Area/ plate (m^2)	Total Heat Transfer Area (m^2)	Volume/ Channel (liter)	Total Volume (liter)
C022	191	154	77	40	9.5+1.10*N	1.126+0.042*N	0.01109	(N-6)*0.01109	0.009	(N-5)*0.009
C042	314	275	76	40	13.0+2.00*N	1.75+0.152*N	0.0193	(N-2)*0.0193	0.030	(N-1)*0.030
C097	524	466	108	50	13.2+2.16*N	5.90+0.346*N	0.0475	(N-2)*0.0475	0.071	(N-1)*0.071
C202	616	519	189	92	14.0+2.15*N	12.41+0.755*N	0.0950	(N-2)*0.0950	0.156	(N-1)*0.156

N: number of plates

Standard Connections

Model	Thread Connections PT/ NPT/ GB											Height (mm)
	3/8"	1/2"	3/4"	1"	1 1/4"	1 1/2"	2"	2 1/2"	3"	3 1/2"	4"	
010	◎	●										15/20
015	◎	◎	●									15/20
020/021/022	◎	◎	●									15/20
025	◎	◎	●									15/20
030		◎	◎									15/20
035			○	○								27
040/041/042		◎	●									15/20
045		◎	●									15/20
050/051		◎	◎	◎	●							27
060		◎	●									27
070		◎	◎	◎	◎	●						27
085			○	○	○	○						27
095/096/097		◎	◎	◎	●							27
105		◎	◎	◎	◎	●						27
200/201/202				◎	◎	◎	●	●				27/54
205				◎	◎	◎	●					27/54
210				◎	◎	◎	◎	◎	●★			27/54
215				◎	◎	◎	◎	●				27/54
400/401						◎	◎★	◎★	◎★			27/54/81
415/416						◎	◎★	◎★	●★			27/54/81
600/601						◎	◎★	◎★	◎★	◎★	●★	27/54/81

◎ Male/Female Thread ○ Female Thread ● Male Thread ★ Flange

Model	Solder Connections														Height (mm)
inch	1/4"	3/8"	1/2"	5/8"	3/4"	7/8"	1"	1 1/8"	1 3/8"	1 5/8"	2 1/8"	2 1/2"	2 5/8"	3 1/8"	
mm	6.6	9.73	12.9	16.15	19.25	22.36	25.6	28.8	35.25	41.5	54.3	63.5	67	79.4	
010	▲	▲													15/20
015	▲	▲	▲	▲											15/20
020/021/022	▲	▲													15/20
025	▲	▲	▲	▲											15/20
030			▲	▲	▲	▲									15/20
040/041/042			▲	▲	▲										27
045			▲	▲	▲										27
050/051			▲	▲	▲	▲	▲	▲							15/20
060			▲	▲	▲										27
070			▲	▲	▲	▲	▲	▲	▲						27
095/096/097			▲	▲	▲	▲	▲	▲	▲						27
105			▲	▲	▲	▲	▲	▲	▲	▲					27
200/201/202			▲	▲	▲	▲	▲	▲	▲	▲	▲				27
205			▲	▲	▲	▲	▲	▲	▲	▲	▲				27/54
210						▲	▲	▲	▲	▲	▲	▲	▲	▲	27/54
215			▲	▲	▲	▲	▲	▲	▲	▲	▲	▲	▲		27/54
400/401						▲	▲	▲	▲	▲	▲	▲	▲	▲	27/54/81
415/416						▲	▲	▲	▲	▲	▲	▲	▲		27/54/81
600/601						▲	▲	▲	▲	▲	▲	▲	▲	▲	27/54/81

Frigomec S.p.A. – model WVCI serie 26

KLIMAL by FRIGOMEC S.p.A.

Plant 2 : Via del Commercio, 3 - 37049 - Italy - **VILLA BARTOLOMEA** (VR)
Tel. +39 - 0442 - 35637 / Fax +39 - 0442 - 35514 - info@frigomec.com
Register office : Via Massimo D'Antona, 5 - 37045 - Italy - **S.PIETRO di LEGNAGO** (VR)
R.E.A. N° 197728 - C.F. / P.IVA 0180631 023 9 - Cap. Soc. € 256.164,00 i.v.
REG. IMP. VR N° 0180631 023 9 - VAT NUMBER: IT 01806310239

Costruzione
Componenti
Refrigerazione
Condizionamento

To: **NTNU Department of Energy and Process Engineering**
No-7491 Trondheim
Mail: armin.hafner@ntnu.no
Telefax no.

O F F E R no.17428RA
Reference: L = 6 m
Date: 16-03-2017

K L I M A L - Coaxial exchanger
Cooler Type **WVCI serie 26**
Tube Material: Copper (K)
Shell Material: Steel (S)
Dimensions L/D/H/A: 1025/70 /285/650 mm
Connections - tube side:
- Inlet: Threaded connection 1 1/2"-NPT
- Outlet : Threaded connection 1 1/2"-NPT
Connections - shell side:
- DN 40 (G 1 1/2" (F))

Operating data:
Power: 498,83 kW

Shell-side			
Cooling medium:	Water		
-Density:	1,00000	kg/dm³	
-Specific heat:	4,186	kJ/kg K	
-Thermal conductivity:	0,636	w/m K	
-Viscosity:	0,605	mPa.s	0,60 mm²/s
-Inlet temperature:	8,0	°C	
-Outlet temperature:	80,0	°C	
-Flow rate:	5958,3	l/h	1,655 l/s
-Flow rate:	5958,3	kg/h	1,655 kg/s
-Pressure drop:	4,52	bar	452 kPa
-Velocity - average:	2,38	m/s	
-Fouling factor:	0,000043	m²K/w	
Connections flow velocity:	1,13	m/s	

Tube-side:			
Gas:	R744		
-Density:	0,24273	kg/dm³	
-Specific heat:	2,751	kJ/kg K	
-Thermal conductivity:	0,034	w/m K	
-Viscosity:	0,023	mPa.s	0,09 mm²/s
-Absolute Pressure:	100,00	bar-abs.	
-Inlet temperature:	130,0	°C	
-Outlet temperature:	13,0	°C	
-Flow rate:	22988,6	l/h	6,386 l/s
-Flow rate:	5580,0	kg/h	1,550 kg/s
-Pressure drop:	2,00	bar 200 kPa	
- Velocity:	5,98	m/s	
- Fouling factor:	0,000043	m²K/w	
Connections flow velocity:			
-Inlet	5,81	m/s	
-Autlet	1,03	m/s	

It is not permitted to use Velocities higher than the max advised value by increasing the fluid quantity in operation. For damages deriving from wrong installation or operation or maintenance or due to cavitation, erosion and corrosion or by natural wear, any guarantie is excluded.

Volume - Cooling liquid:	4,34	dm³
- Gas:	6,86	dm³
Weight/empty (ca.+/-15%):	114	kg

Shell Side: (SDP:301A)	-Allowable pressure	10 bar
	-Allowable temperature	-10/120°C
Tube Side: (SDP:2D02)	-Allowable pressure	-1/120 bar
	-Allowable Temperature	-10/150°C

Required quantity: 1 piece

Regards
R. Pampanin

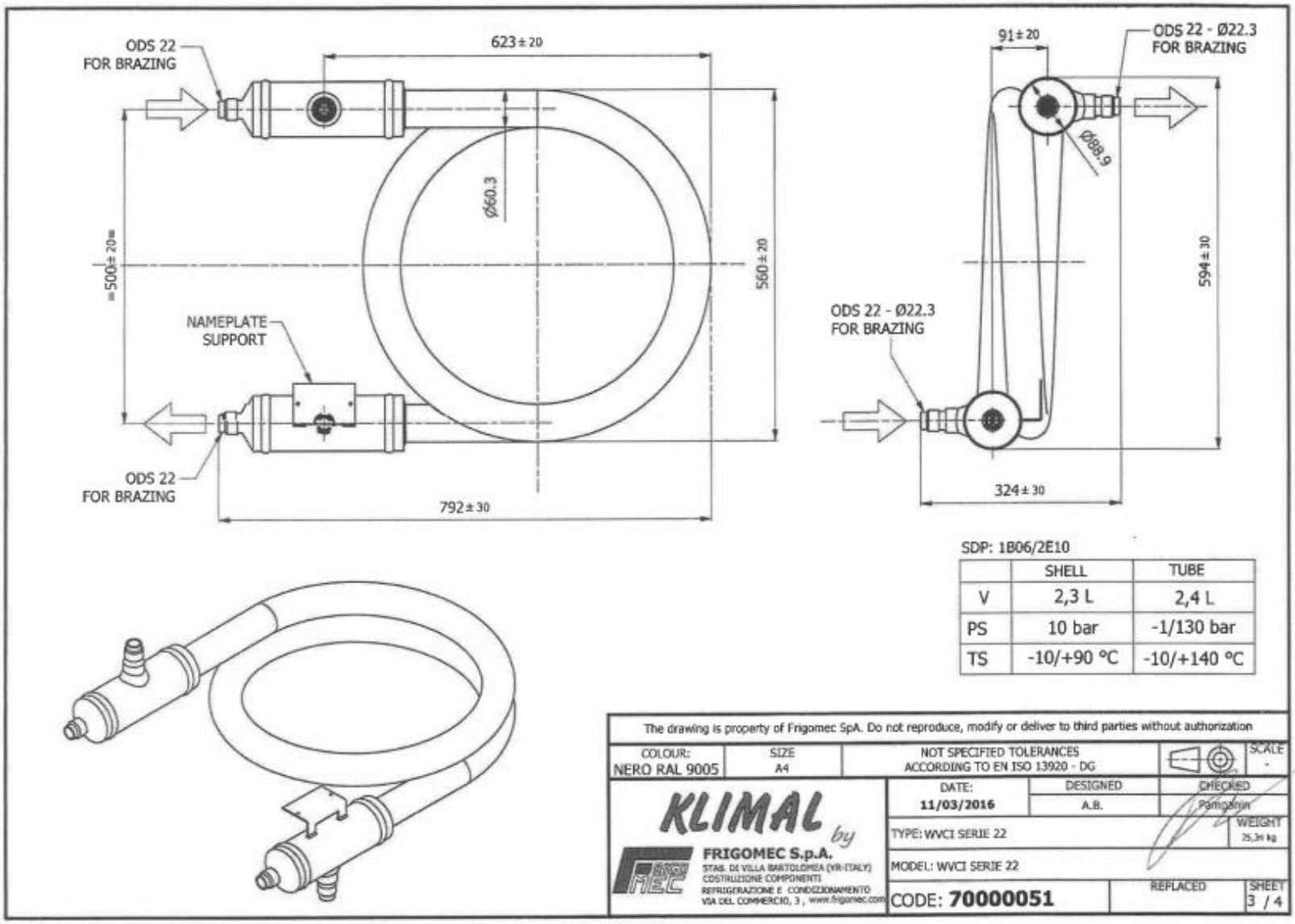

SDP: 1B06/2E10

	SHELL	TUBE
V	2,3 L	2,4 L
PS	10 bar	-1/130 bar
TS	-10/+90 °C	-10/+140 °C

COLOUR:	SIZE	NOT SPECIFIED TOLERANCES	SCALE
NERO RAL 9005	A4	ACCORDING TO EN ISO 13920 - DG	-

KLIMAL by

FRIGOMEC S.p.A.
STAB. DI VILLA BARTOLOMEA (VR-ITALY)
COSTRUZIONE COMPONENTI
REFRIGERAZIONE E CONDIZIONAMENTO
VIA DEL COMMERCIO, 3 , www.frigomec.com

DATE:	DESIGNED	CHECKED
11/03/2016	A.B.	Pomponin

TYPE: WVCI SERIE 22 — WEIGHT 25,3± kg

MODEL: WVCI SERIE 22

CODE: **70000051** — REPLACED — SHEET 3 / 4

N°55 TUBI Ø6X1

CRONOLOGIA REVISIONI				
REV	DESCRIZIONE	DATA	AUTORE	APPROVATO
2	AGGIUNTO PUNTO DI RIFERIMENTO	20/04/2016	L.P.	PAMPANIN
1	MODIFICATO Ø	29/03/2016	A.B.	PAMPANIN

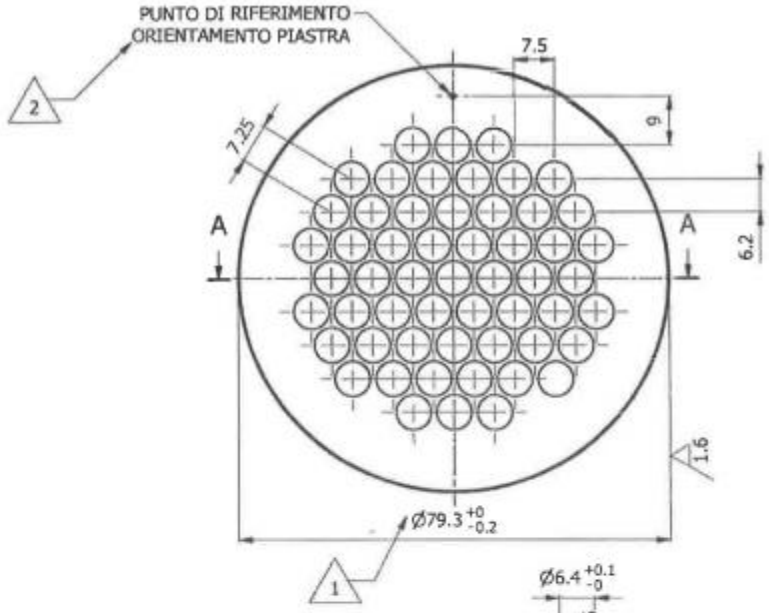

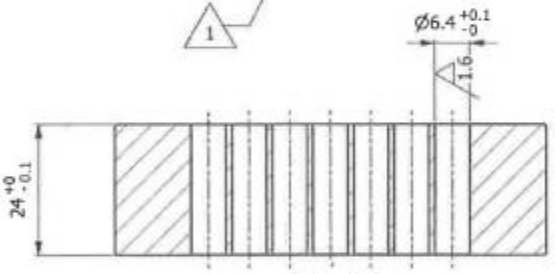

SEZ. A-A

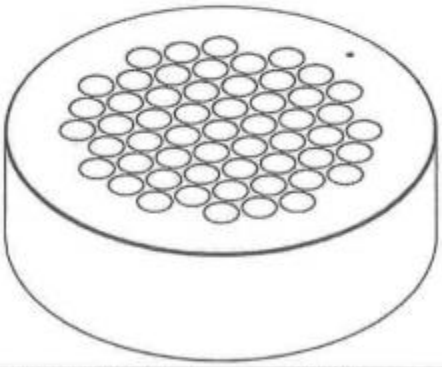

SBAVARE TUTTI GLI SPIGOLI

SMUSSI NON QUOTATI TUTTI 0.5x45°

3.2 (1.6)

"M" Middle class	NOT SPECIFIED TOLERANCES ACCORDING TO UNI EN 22768/1						MATERIAL		SCALE
	Da 0,5 a 3 ±0.1	Da 3 a 6 ±0.1	Da 6 a 30 ±0.2	Da 30 a 120 ±0.3	Da 120 a 400 ±0.5	Da 400 a 1000 ±0.8	S355J2+N - EN 10025-2		-

The drawing is property of Frigomec SpA. Do not reproduce, modify or deliver to third parties without authorization	SIZE	DATE:	DESIGNED	CHECKED
	A4	18/04/2014	A.B.	Pampanin

KLIMAL by FRIGOMEC S.p.A.
STABIL. DI VILLA BARTOLOMEA (VR-ITALY)
COSTRUZIONE COMPONENTI REFRIGERAZIONE E CONDIZIONAMENTO
VIA DEL COMMERCIO, 3 - www.frigomec.com

TYPE: PIASTRA TUBIERA D.79,3 N.55 FORI D.6,4	REPLACED
MODEL: PIASTRA TUBIERA D.79,3 N.55 FORI D.6,4	NOZZLE / SOCKET -
CODE: **3700195A**	WEIGHT / N/A — SHEET 1 / 1

serie	Internal shell pipe ID	Internal pipe ID	Pipe thickness	Number of pipes	Available pipe lenght						
	mm	mm	mm		mm	mm	mm	mm	mm	mm	liter
1	13.2	3	1	4	500	1000	1500	2000	3000	6000	0.01
2	16.7	3	1	7	500	1000	1500	2000	3000	6000	0.02
3	16.7	4	1	4	500	1000	1500	2000	3000	6000	0.03
4	21.7	3	1	12	500	1000	1500	2000	3000	6000	0.04
5	21.7	4	1	7	500	1000	1500	2000	3000	6000	0.04
6	24.8	3	1	14	500	1000	1500	2000	3000	6000	0.05
7	24.8	4	1	12	500	1000	1500	2000	3000	6000	0.08
8	27.9	3	1	19	500	1000	1500	2000	3000	6000	0.07
9	27.9	4	1	14	500	1000	1500	2000	3000	6000	0.09
10	32.2	3	1	26	500	1000	1500	2000	3000	6000	0.09
11	32.2	4	1	19	500	1000	1500	2000	3000	6000	0.12
12	38.1	3	1	35	500	1000	1500	2000	3000	6000	0.12
13	38.1	4	1	26	500	1000	1500	2000	3000	6000	0.16
14	41.9	3	1	44	500	1000	1500	2000	3000	6000	0.16
15	41.9	4	1	31	500	1000	1500	2000	3000	6000	0.19
16	44.6	3	1	52	500	1000	1500	2000	3000	6000	0.18
17	44.6	4	1	37	500	1000	1500	2000	3000	6000	0.23
18	53.9	3	1	61	500	1000	1500	2000	3000	6000	0.22
19	53.9	3	1	73	500	1000	1500	2000	3000	6000	0.26
20	53.9	4	1	48	500	1000	1500	2000	3000	6000	0.30
21	53.9	3	1	91	500	1000	1500	2000	3000	6000	
22	53.9	4	1	55	500	1000	1500	2000	3000	6000	
23	62.8	3	1	85	500	1000	1500	2000	3000	6000	
24	62.8	4	1	64	500	1000	1500	2000	3000	6000	
25	62.8	3	1	109	500	1000	1500	2000	3000	6000	
26	62.8	4	1	85	500	1000	1500	2000	3000	6000	

G. Input variables for the COMSOL model

Table A- 5. Input variables to COMSOL

Parameter	Value original model	Value adapted model	Unit	Description
μ_g	0.00001246	0.00001246	kg/ms	Dynamic viscosity of CO_2 gas
μ_l	0.0001642	0.0001642	kg/ms	Dynamic viscosity of liquid CO_2
ρ_g	37.1	37.1	kg/m^3	Gas density of CO_2
ρ_l	1076	1076	kg/m^3	Liquid density of CO_2
$c_{p,g}$	1141	1141	J/kgK	Specific heat capacity of CO_2 gas
$c_{p,l}$	2073	2073	J/kgK	Specific heat capacity of liquid CO_2
k_g	0.01342	0.01342	W/mK	Thermal conductivity of CO_2 gas
k_l	0.1463	0.1463	W/mK	Thermal conductivity of liquid CO_2
h_{water}	575	1411	W/m^2K	Water heat transfer coefficient
T_{ext}	278.15	281.45	K	External temperature (T_{water})
T_{co2}	234.15	234.15	K	Evaporation temperature
P_{co2}	1428	1428	kPa	Evaporation pressure
L_{co2}	303.5	303.5	kJ/kg	Enthalpy of evaporation
u_{in}	0.244	0.2367	m/s	Inlet velocity to CO_2 pipes
ΔP	30	105	kPa	Total pressure loss in refrigerant pipes
dT	-	1	K	Temperature difference during evaporation
Height	100	100	mm	Height of model
Width	13-78	13	mm	Width of model, from centre to centre of CO_2 pipes
Depth	5-20	5-20	mm	Thickness of aluminium layer
para	-	(0,0.1,1)	[-]	Correction term

H. Results from simulation in COMSOL

Results from main simulation

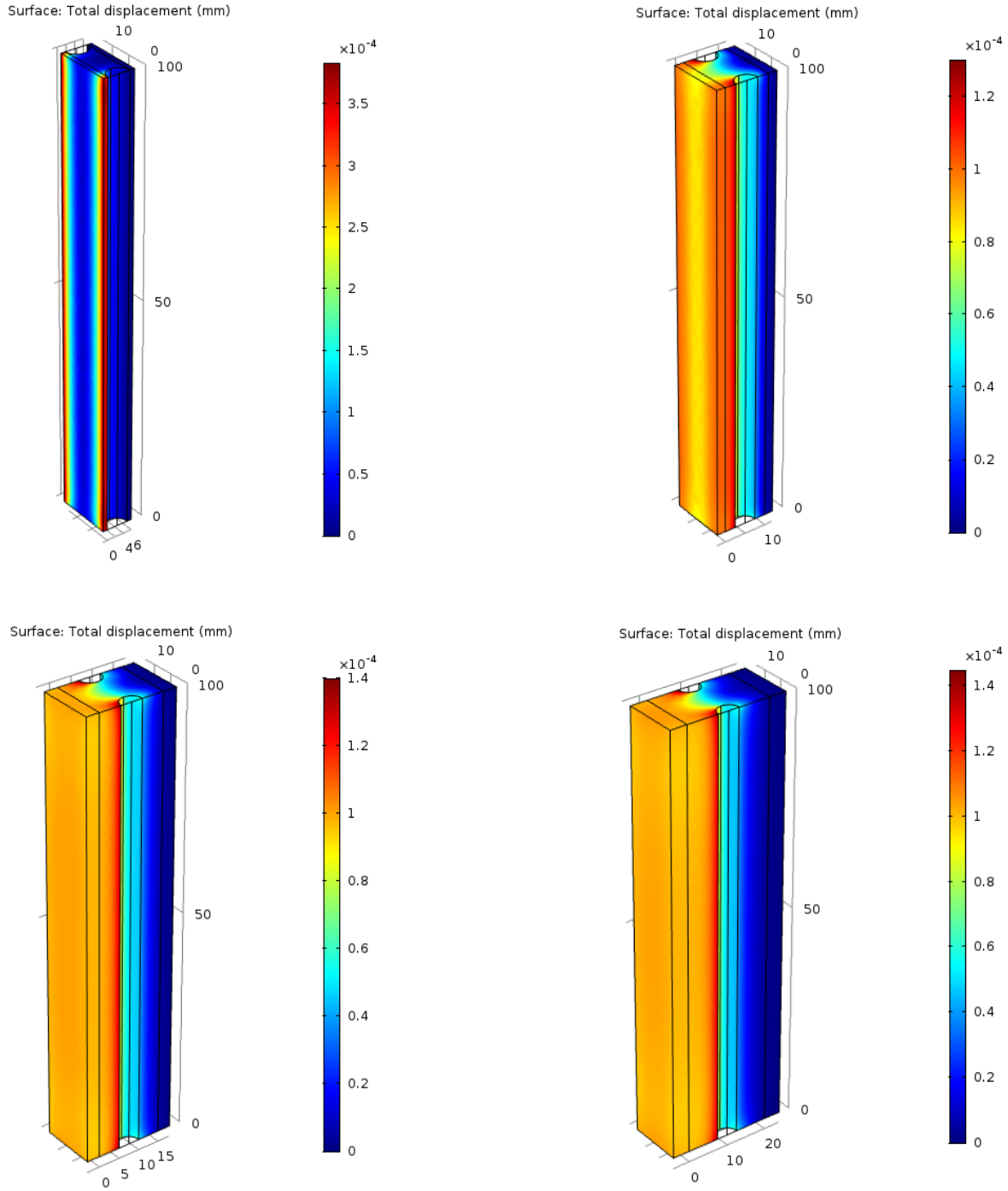

Figure A- 8. Total displacement at varying depth of model

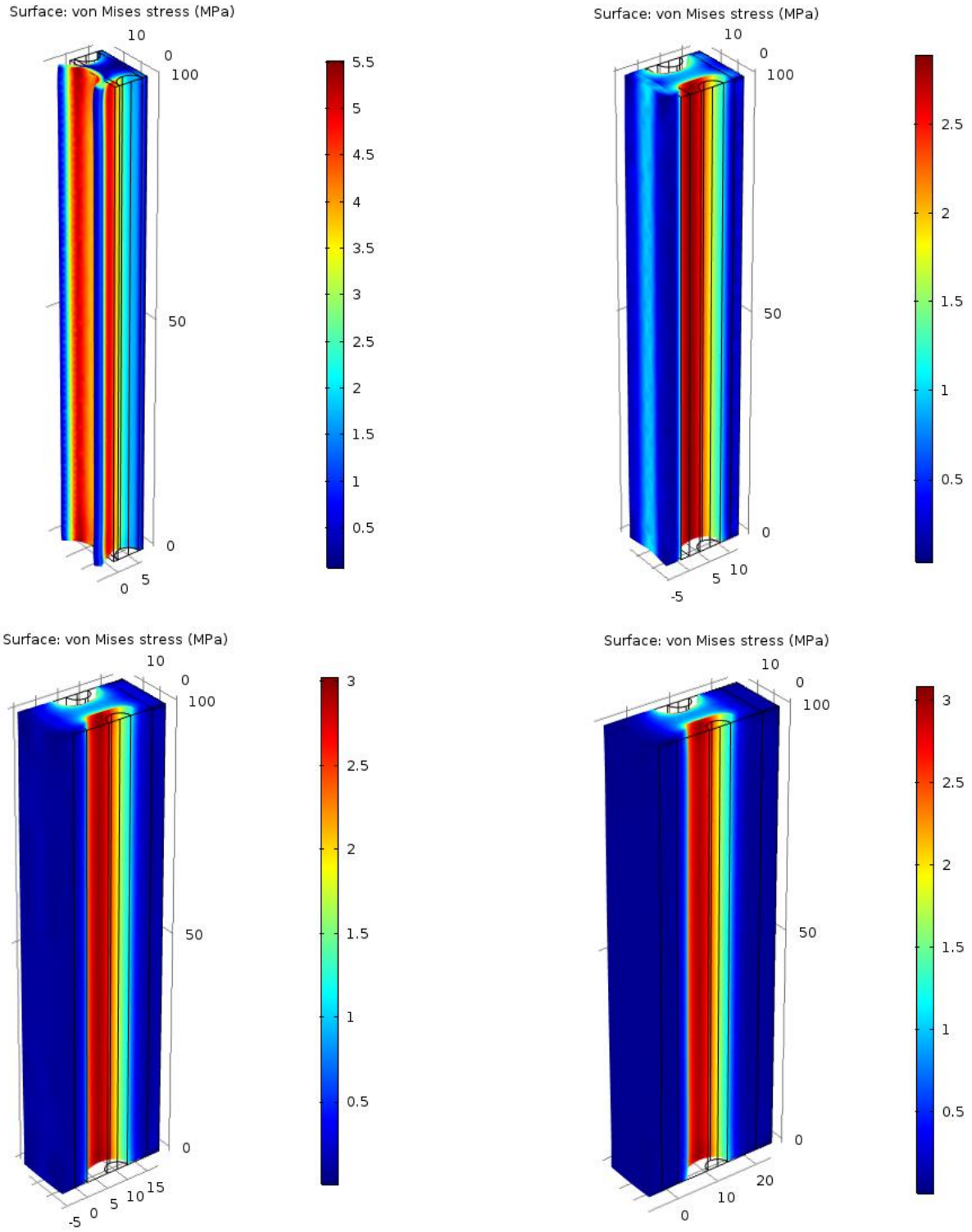

Figure A- 9. Von Mises stresses in the construction at different depths

Results from additional simulations

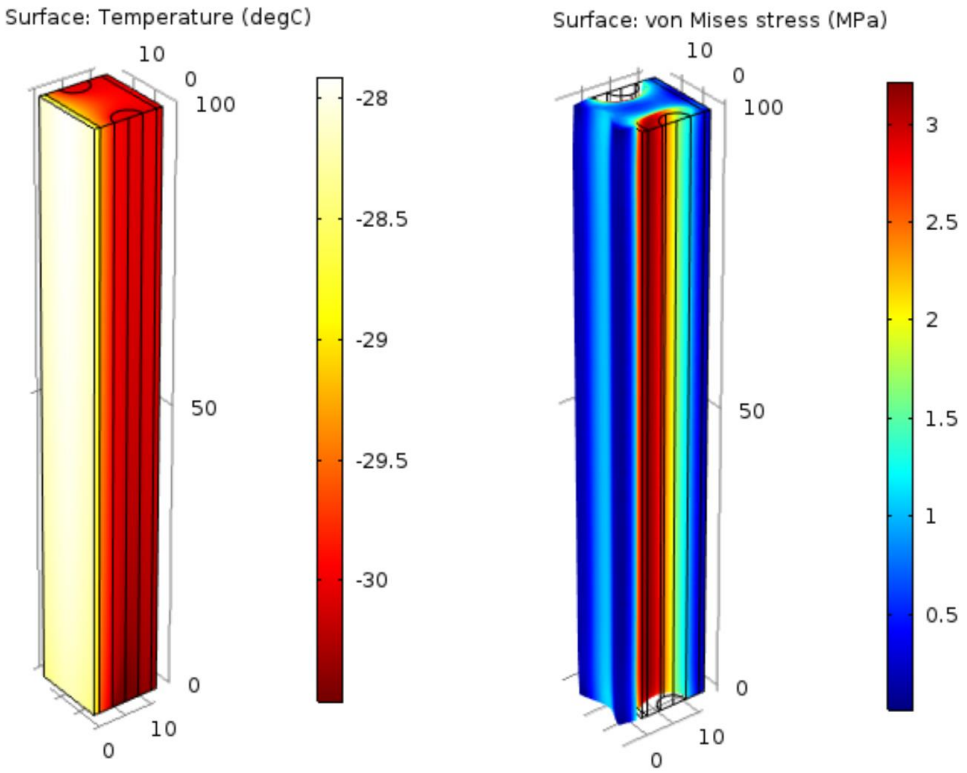

Figure A- 10. Additional simulation with 20 % stainless steel in the drum wall and depth 10 mm

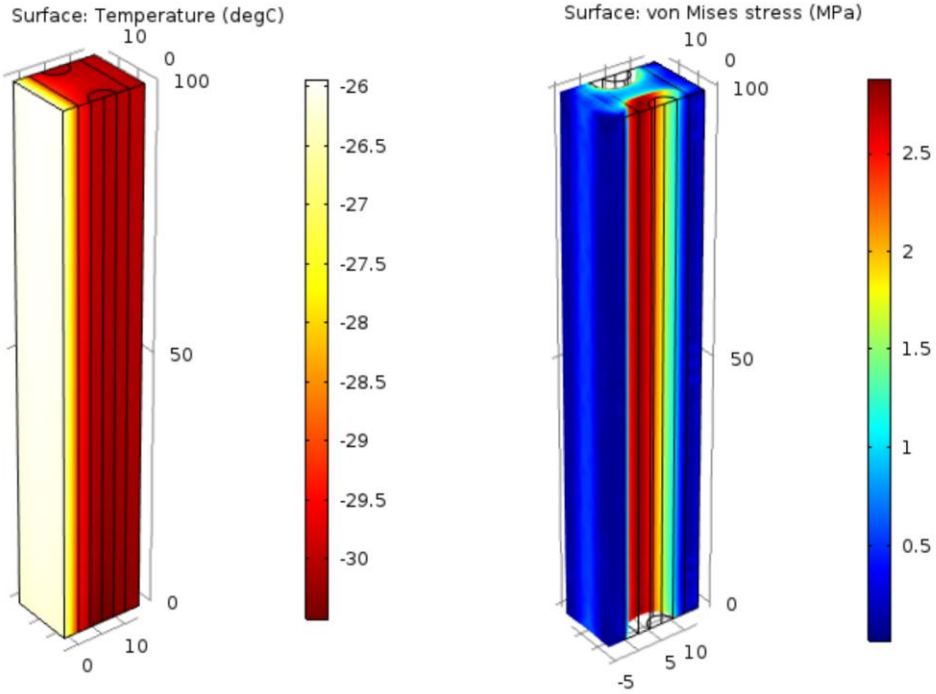

Figure A- 11. Additional simulation with 60 % stainless steel in the drum wall and depth 10 mm

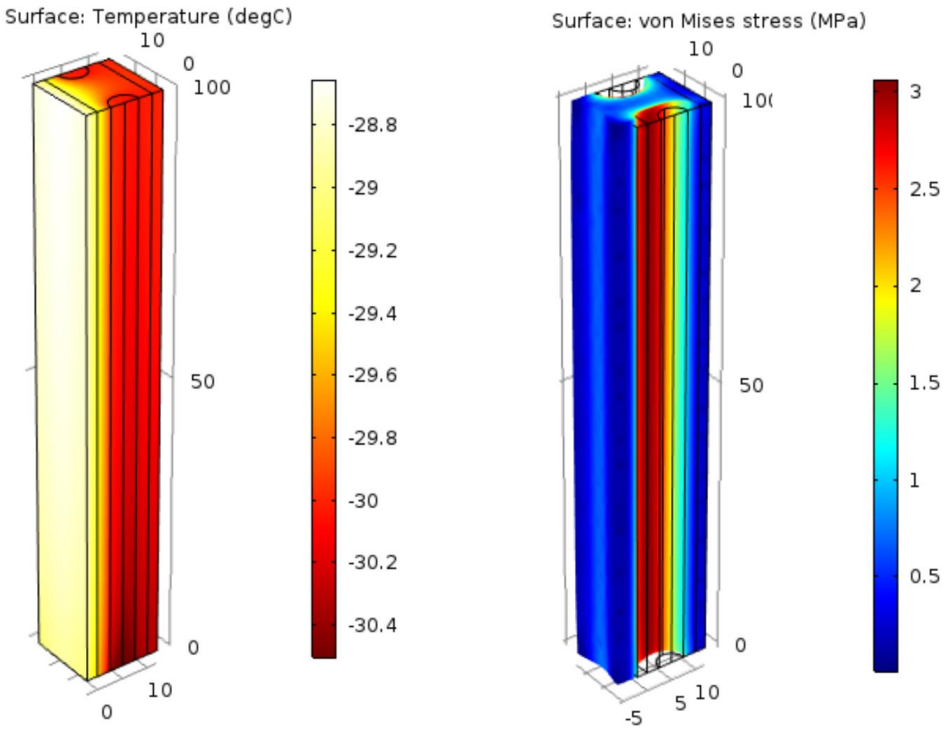

Figure A- 12. Additional simulation with aluminium both in the core and the outer layers, where each of the outer layers is set to 20 % of the depth of 10 mm

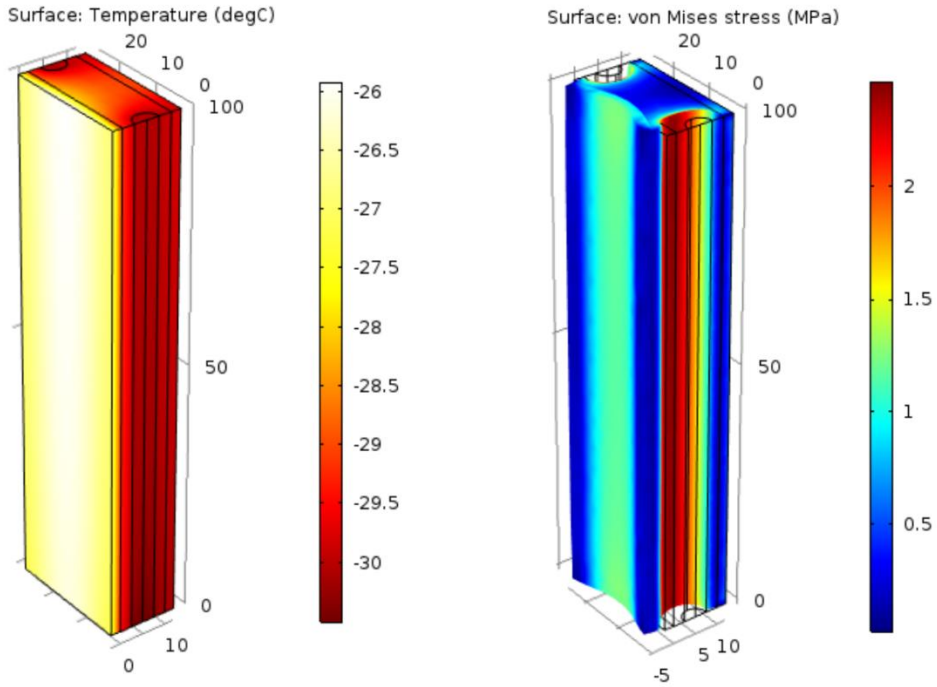

Figure A- 13. Additional simulation with 300 refrigerant pipes and depth 10 mm

I. Air cycle refrigeration system

Table A- 6. State points of the air refrigeration cycle for indoor snow production

State point	Pressure [kPa]	Temperature [°C]	RH [%]	Enthalpy [kJ/kg]	Entropy [kJ/kgK]	Abs. humidity [kg/kg]
1	98	10.00	23.97	15.34	0.06693	0.001937
2	139	55.75	2.56	63.34	0.06768	0.001937
3	137	13.00	27.48	18.49	-0.02172	0.001937
4	135	-4.00	92.71	0.64	-0.08164	0.001937
5	101.325	-14.00	33.66	-13.69	-0.0972	0.000387
6	101.325	-7.00	90	-2.51	-0.00801	0.001938

Table A- 7. State points of PAS30-R

State point	Pressure [kPa]	Temperature [°C]
1	98	35
2	172	90
3	170	40
4	168	-55
5	101.325	-80
6	101.325	-60

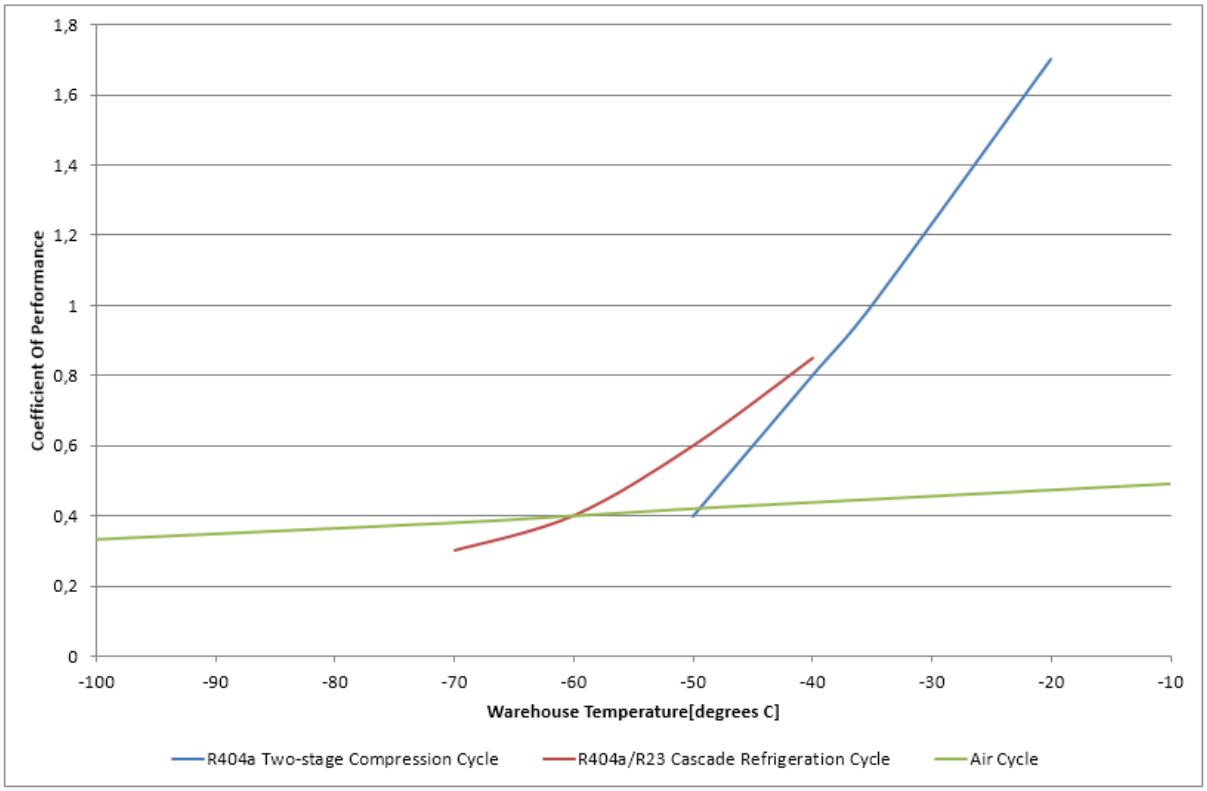

Figure A- 14. Comparison of COP

J. Transcritical CO_2 cycle for indoor snow production

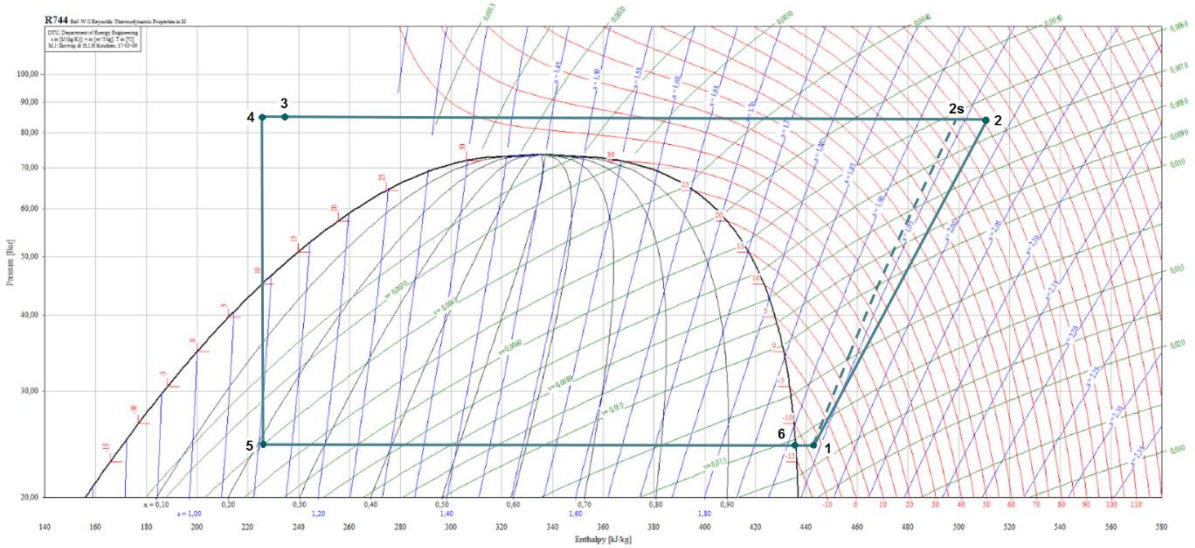

Figure A- 15. Log P-h diagram for the CO_2 refrigeration cycle for indoor snow production

Table A- 8. Results from simulation in Excel

	Transcritical CO_2 cycle
$COP_{cooling}$	3.2
$COP_{heating}$	4.2
Q_{evap}	470 kW
Q_{gc}	617 kW
W_{comp}	147 kW
$\dot{m}_{co2}$	2.171 kg/s

K. Ejector recirculation cycle for the flake ice model

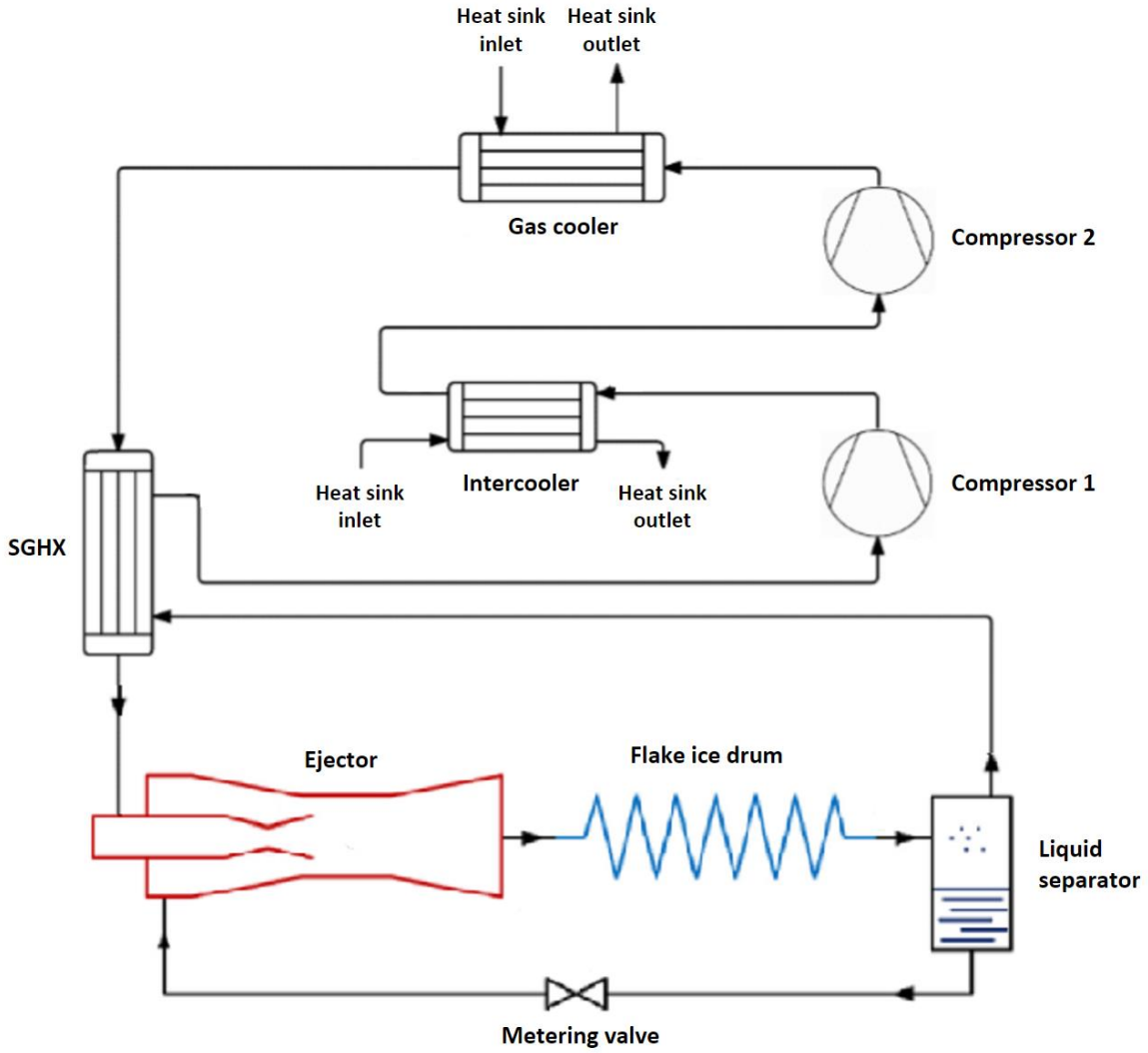

Figure A- 16. Schematic diagram of the FID integrated with an ejector recirculation cycle

L. Scientific paper

Energy Efficient and Environmental Friendly Snow Production by Refrigeration systems

Kaja Wright Bergwitz-Larsen
(*) Norwegian university of Science and Technology, Department of Energy and Process Engineering, Kolbjørn Heies vei 1B, Trondheim, 7491, Norway
kaja.wbl@gmail.com

ABSTRACT

An outdoor flake ice system with a production of 100 tons/day is modelled in EES and implemented with a transcritical CO_2 process for heat recovery. By optimizing the gas cooler pressure, the excess heat from the system is increased. Integration of a coaxial heat exchanger yields the best thermodynamic performance; with maximized COP and close temperature approach, that offers the possibility of reduced demand of the intercooler and suction gas heat exchanger. Implementing heat recovery by DHW heating raises the required power input, but does not hamper the efficiency of the snowmaking process. The simulations in COMSOL validate the calculations in EES. The efficiency of the FID is highly dependent on production rate and design of the drum, which points to the need of an optimization process. The overall system is seen to be both energy efficient and environmental friendly; highlighted by the use of CO_2 as refrigerant.

1. INTRODUCTION

In the light of increasing global temperatures, the winters tend to be shorter and milder, with the periods of natural snow being drastically reduced. In order to counter the challenges of climate change and maintaining good skiing conditions in winters to come, snow production equipment in temperatures above 0 °C will be important for future applications. Such technology exists today, but it is expensive and highly energy-intensive; with an excessive amount of surplus heat that is released to the surroundings and thus wasted. Methods to increase the energy efficiency of the snow producing equipment will therefore be important. This can be achieved by interrelating the snowmaking process with a combined refrigeration and heat recovery system. If the surplus heat from the production process can be utilized, the overall energy efficiency of the system will increase; while the operational costs are reduced. This might justify the extensive investment costs of such technology.

1.1. Flake ice machine

Flake ice machines are widely utilized in industry; and have recently been applied as snow producing equipment (TechnoAlpin, 2016). This type of machine forms ice on the surface of a cooled cylindrical heat exchanger, and the ice is harvested as dry subcooled flakes, usually 2-3 mm thick, and collected by a rotating scraper on the inner surface (Graham et al., 1993). The water enters at the top of the cylindrical drum, which acts as an evaporator, and it is sprinkled onto the inner surface through a series of distribution tubes where it is rapidly cooled to form ice (Cao et al., 2015). The ice is further processed by utilizing an ice crusher and a distribution system to obtain snow of smaller particle sizes and optimal quality. The flake ice machine requires a refrigeration system, with a refrigerant temperature of about -30 °C. This low temperature is needed to ensure high production rate. It will keep the machine small and compact, but extra power is needed to run the machine at such low temperatures.

1.2. CO_2 refrigeration system with integrated heat recovery

In light of the increased awareness of the stratospheric ozone depletion and the atmospheric greenhouse effect, it is important to choose a refrigerant that does not harm the environment. Furthermore, it needs to comply with legal regulations. In this respect, CO_2 will be a good candidate; it is neither toxic nor flammable, widely available, inexpensive, and with ODP and GWP values close to zero. Since the critical temperature of CO_2 is low (31 °C), it is especially well suited for transcritical system configurations; where the heat rejection occurs at gliding temperature and supercritical pressure, while evaporation occurs at constant temperature and subcritical pressure. Such a cycle is efficient in applications where cooling can be combined with heat

recovery, and where good temperature match is obtained when heat rejection causes a significant temperature rise in the heat receiving fluid. DHW heating is a suitable application area in this respect.

With critical pressure at 73.8 bar, the required pressure level on the heat rejection side will be high, and it will pose some restrictions on the equipment. It is necessary to install equipment that can handle such high pressures, and measures should be implemented to ensure that the discharge temperature out of the compressor does not exceed 130 °C (which is regarded as the operational limit for commercial piston compressors). The transcritical cycle suffers from higher throttling losses compared to conventional subcritical systems, and it is important to keep these to a minimum. Some commonly used methods to improve the cycle efficiency are: (1) use of internal heat transfer in terms of a suction gas heat exchanger (SGHX) or a subcooler, (2) use of two-stage compression or expansion, and (3) recovery of expansion work by use of an ejector or expander.

1.3. Gas cooler performance

Knowledge of the optimal gas cooler pressure that yields the best system efficiency is an important factor in the design of a transcritical CO_2 cycle. Due to the thermodynamic properties at supercritical pressures, the COP will vary non-monotonically (Liao et al., 2000). The optimal pressure is to a great extent determined as a function of the gas cooler outlet temperature; where there is a trade-off between the highest possible enthalpy difference in the gas cooler and simultaneous minimum compressor work. Accordingly, in a combined heating and refrigeration system, the amount of heat recovery needs to be evaluated continuously against the work input to determine the pressure which maximizes the COP.

2. METHOD

A simulation model of flake ice machine integrated with a transcritical CO_2 process for combined refrigeration and heat recovery is made in Engineering Equation Solver (EES), Figure 1. The model is designed for outdoor snow production at a rate of 100 tons/day. It is based on fundamental thermodynamics which includes energy and mass balances, as well as empirical correlations for heat transfer and pressure drop. The model is combined with an optimization procedure of the gas cooler pressure conducted in Excel, where the results are integrated in EES by developing simplified heat transfer characteristics. The discharge pressure is raised to a level where the available surplus in the gas cooler can be used for DHW heating. Heat transfer, temperature distribution, displacement and stresses within the FID are calculated in COMSOL, and is used to validate the dimensions and assumptions of the dynamic ice growth model in EES. The main objective of the simulations is to investigate how the performance of the combined cycle changes (a) when the gas cooler pressure is optimized, and (b) when the production rate is doubled; without a simultaneous drop in the efficiency of the snow production.

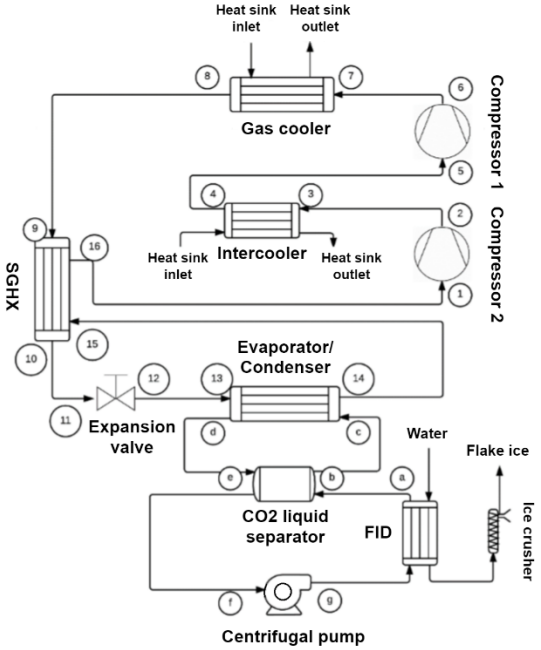

Figure 1. Flake ice system.

2.1. Thermodynamic analysis

Heat transfer coefficients

The overall heat transfer coefficient of a heat exchanger is defined in terms of the total thermal resistance to heat transfer on the warm and cold fluid side, and the plate wall (Incropera et al., 2013c).

$$U = \frac{1}{\frac{1}{\alpha_H} + \frac{\delta}{k_W} + \frac{1}{\alpha_C}} \tag{1}$$

To evaluate the overall heat transfer coefficient of the flake ice drum, the two-phase heat transfer correlation for refrigerant CO_2 flow is applied (Choi et al., 2007).

$$\alpha_{evap,\,CO_2} = S\alpha_{nb} + F\alpha_{evap} \tag{2}$$

The heat transfer coefficient of water is found from eq. (3) (Incropera et al., 2013b).

$$\alpha_w = 0.037 \left(\frac{k_w}{H}\right) \left(\frac{u_w H}{\nu_w} - B\right)^{\frac{4}{5}} Pr_w^{\frac{1}{3}} \tag{3}$$

The condensation heat transfer coefficient of CO_2 (Park and Hrnjak, 2009) and the Martin correlation for one-phase flow in a plate heat exchanger (PHE) (García-Cascales et al., 2007) are applied;

$$\alpha_{cond,CO_2} = \frac{{k_f}^{2/3} {C_{p,f}}^{1/3}}{{\mu_f}^{7/15}} \left[\frac{1-z}{z}\left(\frac{\rho_l}{\rho_g}\right)^{\frac{1}{2}} + 1\right] \tag{4}$$

$$Nu = 0.122 Pr^{\frac{1}{3}} \left(\frac{\mu_f}{\mu_W}\right)^{\frac{1}{6}} (f Re^2 \sin(2\beta))^{0.374} \tag{5}$$

For a coaxial heat exchanger; with inner pipe diameter d and average diameter of the curvature of the coil D, the CO_2 heat transfer coefficient is approximated by a correlation for flow through coils, which was developed by Schmidt and Gnielinski (VDI, 1993). It depends on whether the flow is laminar, turbulent or transitional; with m being an empirical constant. The water heat transfer coefficient is approximated graphically with basis in the Nusselt number for fully developed laminar flow to a bank of circular tubes (Kays and Crawford, 1980). The corresponding equations are:

$$Nu = \begin{cases} \left(3.66 + 0.08\left[1 + 0.8\left(\frac{d}{D}\right)^{0.9}\right] Re^m Pr^{\frac{1}{3}}\right)\left(\frac{Pr}{Pr_W}\right)^{0.14}, & \text{laminar} \\ \frac{\left(\frac{\xi}{8}\right) Re\, Pr}{1+12.7\sqrt{\xi/8}\left(Pr^{\frac{2}{3}}-1\right)}\left(\frac{Pr}{Pr_W}\right)^{0.14}, & \text{turbulent} \\ \gamma Nu_{laminar}(Re_{crit}) + (1-\gamma) Nu_{turbulent}(Re = 2.2 \cdot 10^{-4}), & \text{transitional} \end{cases} \tag{6}$$

$$Nu = \begin{cases} -12.608\left(\frac{s}{r_0}\right)^2 + 50.408\left(\frac{s}{r_0}\right) - 36.097, & \left(\frac{s}{r_0}\right) < 2 \\ 6.4949\left(\frac{s}{r_0}\right)^{1.1941}, & \left(\frac{s}{r_0}\right) \geq 2 \end{cases} \tag{7}$$

The SGHX is modelled as a counter-flow PHE. To obtain a numerical solution of the heat transfer coefficients and pressure drops, built-in functionality in EES is applied; where state equations are integrated numerically through the heat exchanger by use of an integral command and an optimization algorithm in EES (Nellis and Klein, 2009).

Pressure drops

The total pressure drop in the PHEs is the sum of smaller pressure drops; in terms of friction, gravitation, acceleration and manifold loss, eq. (8) (Shah and Sekulić, 2007). The two latter contributions are negative for condensation, and positive for evaporation.

$$\Delta P_{tot} = \Delta P_{fric} + \Delta P_{man} \pm \Delta P_{acc} \pm \Delta P_{grav} \quad (8)$$

Only the frictional term is considered for the coaxial heat exchanger; approximated by the Darcy Weisbach Equation, with a friction factor applicable for bended ducts (Cengel and Cimbala, 2010, Hewitt, 2008). The flake ice drum is modelled with the same correlation for frictional pressure drop, but with a friction factor valid for straight ducts. Acceleration and gravitational pressure drops are defined by Cengel and Cimbala (2010). The pressure drops in the pipelines are calculated using a built-in function in EES.

Dynamic model of the snowmaking process

In order to determine how often the inner surface must be scraped; defined by the time required to produce an ice layer of 3 mm, the dynamic ice growth process is modelled by applying heat and mass conservation. There are two boundary equations: energy conservation and temperature continuity at the inner drum wall boundary between the solid and liquid refrigerant phase (Incropera et al., 2013a);

$$q_{ice} - q_w = (\rho uh)_{ice} - (\rho uh)_w = 0 \quad (9)$$

$$T_b = T_W \quad (10)$$

The ice thickness and the ice growth rate are calculated by rearrangement of the governing equations, where i accounts for the different materials used in the drum wall (Cao et al., 2015).

$$\frac{dx}{dt} = \frac{\frac{T_{ice} - T_{ref}}{\frac{1}{\alpha_{CO2}} + \sum_i \frac{\delta_i}{k_{W,i}} + \frac{x}{k_{ice}} + \frac{1}{\alpha_w}} - \alpha_w (T_W - T_{ice})}{\rho_w h_{fusion,w}} \quad (11)$$

2.2. Optimization procedure

In order to find an optimal operating condition for the gas cooler and to assess the performance at different gas cooler pressures and water flow rates, a heat balance is established where the heat absorbed by the tap water/heat released from the CO_2, $\dot{Q}_{co2}$, is set equal to the heat released in the gas cooler, $\dot{Q}_{trans}$. The gas cooler is divided into 15 sections of equal heat transfer area. The temperature of the fluid, pinch point, heat transfer and U-values are calculated for each part. Two different gas cooler models are assessed; a plate heat exchanger with chevron angles and a coaxial heat exchanger.

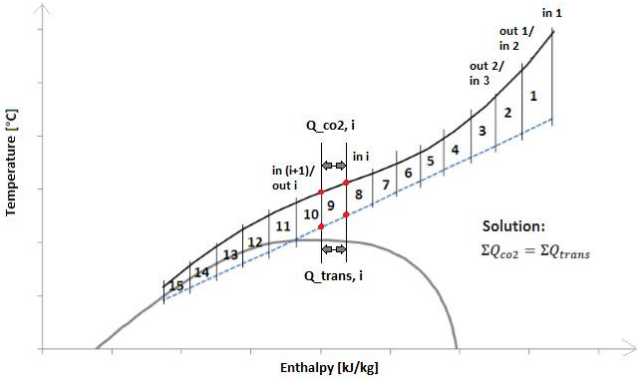

Figure 2. Modelling the gas cooler performance by heat balance.

The inlet CO_2 temperature to the gas cooler is estimated by using a routine library for working fluids in Excel (RnLib) and the input parameters from the model in EES, which must be updated constantly with varying gas cooler pressure during optimization. The outlet CO_2 temperature at each section of the gas cooler is the variable that balances the heat balance. Enthalpy in and out of each section of the gas cooler is calculated by RnLib and the parameters temperature and pressure. The enthalpy difference and the mass flow are used to estimate the amount of heat transferred;

$$\dot{Q}_{co2} = \dot{m}_{co2} (h_{in,co2} - h_{out,co2}) \quad (12)$$

The incoming water temperature is set to 8 °C and will remain constant, while the outlet enthalpy of water for

each section is calculated by eq. (13).

$$h_{out,w} = h_{in,w} + \frac{\dot{Q}_{co2}}{\dot{m}_w} \quad (13)$$

The heat transfer between the two fluids is calculated by eq. (14), where the heat transfer coefficients are found from eq. (5), (6) and (7). By using an iterative procedure and solving the system of equations by the problem solver algorithm in Excel, the heat transfer is balanced when setting the sum of $\dot{Q}_{diff}$ equal to zero by changing the outlet CO_2 temperature at each section of the gas cooler.

$$\dot{Q}_{trans} = U_{tot} A \Delta T \quad (14)$$

$$\dot{Q}_{diff} = \left(\dot{Q}_{co2} - \dot{Q}_{trans}\right)^2 \quad (15)$$

To find the optimal pressure for the heat exchanger models evaluated, the gas cooler pressure is varied between 85 and 115 bar. A simultaneous pinch point analysis is conducted at the different pressure levels, in order to maximize COP by locating the pinch point at the gas cooler outlet. The target temperature of the hot tap water is set to 80 °C at the outlet of the gas cooler, and the mass flow rate of water is adapted accordingly.

3. RESULTS

The results from the optimization process are presented in Table 1. The coaxial heat exchanger has the best thermodynamic performance; it obtains the highest COP and the largest heat duty regardless of the pressure level. The average heat transfer coefficient is considerably higher than for the PHE, and with a closer temperature approach and a lower temperature of the CO_2 gas at the outlet. The difference in performance is lowered when taking into account the pump work on the water side of the gas cooler; which is included in the parameter COP_system.

Table 1. Gas cooler performance at optimal pressure.

	PHE: C202HP3 (Kaori Heat Treatment Co., Ltd.)	Coaxial heat exchanger: WVCI serie 22 (Frigomec)
Optimal pressure [bar]	105	102.5
Gas cooler [kW]	622.4	629.4
Compressor [kW]	267.6	266.1
Water pump [kW]	0.015	2.5
Total work [kW]	267.6	268.6
COP [-]	2.326	2.365
COP_system [-]	2.326	2.343
Average α [W/m^{2}K]	4272	8655
CO_2 outlet temperature [°C]	10.5	8.8
Pinch point at outlet [°C]	2.5	0.8

The main results from simulation of the combined refrigeration and heat recovery system in EES are provided in Table 2. The system yields an energy saving of 453,168 kWh/year. The corresponding economic saving potential is approximately 240,000 NOK/year at an energy price at 0.80 NOK/kWh when compared to electric heating.

Table 2.
Performance of the combined CO_2 refrigeration and heat recovery system.

$COP_{heating}$ [-]	2.37
$COP_{cooling}$ [-]	1.66
$Q_{gas\ cooler}$ [kW]	629.4
Q_{evap} [kW]	442.4
W_{tot} [kW]	266.1
$Q_{intercooler}$ [kW]	79
Q_{SGHX} [kW]	21
$\dot{m}_{co_2}$ [kg/s]	1.911

Figure 3 shows the ice growth rate as a function of production time. In Figure 4, the corresponding ice thickness as a function of time is shown. These figures compare the use of different construction materials in the drum wall; carbon steel, stainless steel and aluminium.

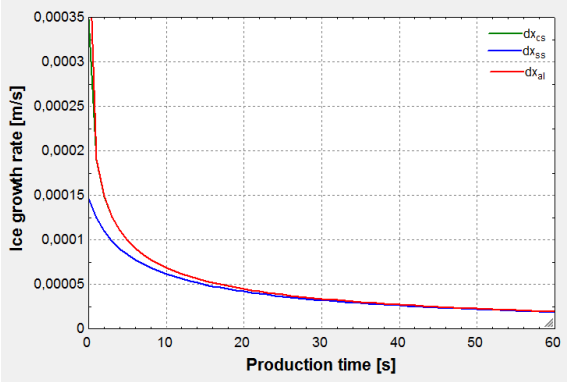

Figure 3. Change of ice growth rate with production time.

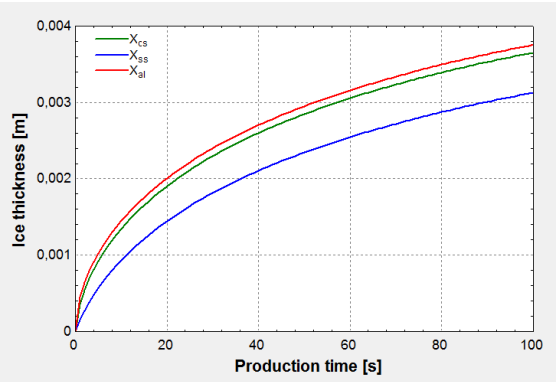

Figure 4. Change of ice thickness with production time.

Table 3 shows the required time to produce an ice layer of 3 mm for different drum wall materials and at varying production capacities. The increase in the production time is not linear when doubling the production rate, and a strong dependency on the material selection is found.

Table 3. Comparison of the required production time.

	Construction material		
Ice production rate	Carbon steel	Stainless steel	Aluminium
50 tons/day	33 s	44 s	31 s
100 tons/day	58 s	90 s	53 s
Percentage increase	76 %	101 %	71 %

The temperature distributions for varying thickness of the drum wall are simulated in COMSOL and presented in Figure 5. The drum wall is modelled as a sandwich construction composed of two steel layers and an inner aluminium profile with refrigerant pipes. The thickness of the aluminium profile referred to as the depth. 600 refrigerant pipes are required to ensure that the pressure drop does not exceed the maximum allowable limit of 2 bar. The displacement of the inner drum wall is small for depths between 5 and 20 mm. The maximum von Mises stresses within the structure are 5.7 MPa, at a depth of 5 mm. The stresses are kept within the ultimate tensile strength (UTS) of the materials with good margin.

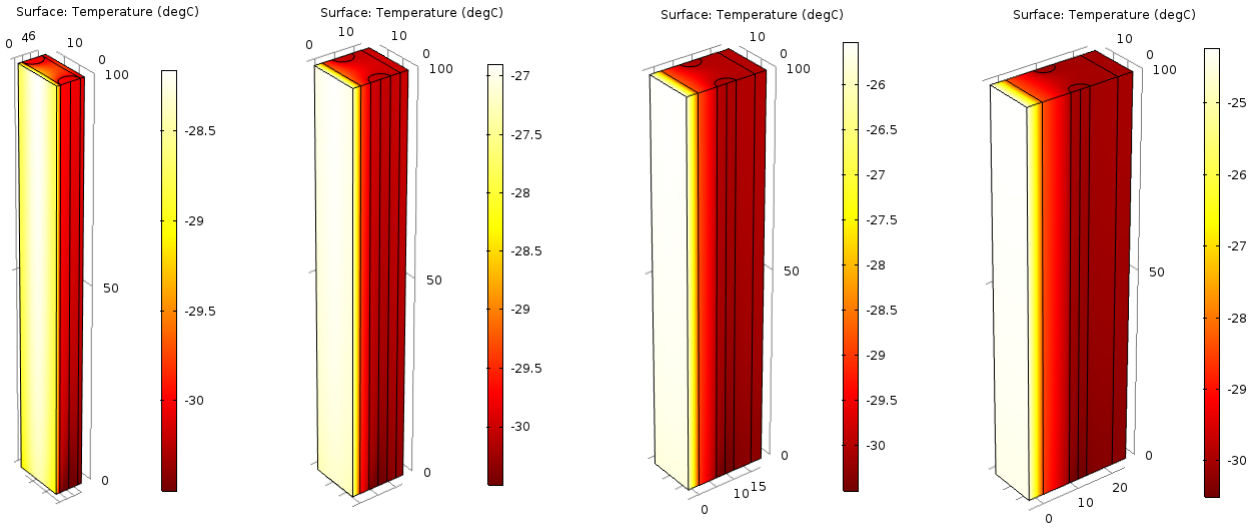

Figure 5. Temperature distribution between the refrigerant pipes at varying depth.

4. DISCUSSION

The analyses show that both heat exchanger types achieve good thermodynamic performance. Both models could be chosen with satisfactory results. The coaxial heat exchanger is however integrated in EES; due to the slightly better heat transfer characteristics. Since the models are relatively small and compact compared to conventional shell-and-tube heat exchangers, differences in outer dimensions and volume will not be crucial for the selection. The same accounts for the investment costs; which are seen to be in the same range. In a future perspective; it is recommended to choose a gas cooler that can handle off-design operation without a drastic reduction in performance when the production time of the snow machine is adjusted to non-constant operation. The coaxial heat exchanger is superior in this respect.

The duty of the gas cooler is seen to be extensive. The available surplus, when integrated with DHW heating, is 42.3 % larger than the required refrigeration load from snowmaking. Integration of heat recovery raises the required energy consumption of the refrigeration system; as the lifting height of the compressor must be elevated to a level suitable for heating of hot tap water. However, the overall energy efficiency of such a system is improved when heat can be utilized both on the hot and cold side; with the accessible gain from the system more than doubled. Implementing the required refrigeration system for the snow machine with heat recovery would make implementation more reasonable; as the operating costs are reduced. Use of CO_2 as refrigerant in a transcritical cycle contributes to obtain a system that is both energy efficient, environmental friendly and viable for the future.

Due to the low evaporation temperature of the FID, two-stage compression with intermediate cooling is necessary in order to prevent the discharge temperature from exceeding the operational limit. As CO_2-systems are affected by relatively large throttling losses, it is essential to obtain low outlet temperatures and good temperature approach in the gas cooler. This is achieved by integration of the coaxial heat exchanger, and the good heat transfer characteristics make it possible to reduce the demand of the intercooler and SGHX. The power consumption of the system is seen to be 16.3 % higher than commercially available models with the same production capacity. While the surplus heat from these machines is released to the surroundings and thus wasted, the EES model is adapted to operations where all excess heat can be recovered. The total energy performance would therefore be equally good, or even better, considering the benefits of both refrigeration and heating from the system.

Integration of heat recovery will not be at the expense of the efficiency of the snowmaking. The dimensioning point is preserved for the snow machine, while heat recovery is designed accordingly. Due to the indirect coupling provided by the heat cascade configuration, refrigeration and heat recovery are interrelated without influencing the thermodynamics of the flake ice machine.

The ice growth rate and the U-value are highest when aluminium is used in the drum wall. This means that the time needed to produce an ice layer of 3 mm is the shortest. The efficiency of the flake ice machine is seen to be highly dependent on the production rate. The ice growth rate drops rapidly at a production of 100 tons/day when compared to a rate of 50 tons/day (Dieseth, 2016). The ice thickness as a function of time will be lower at elevated production rates, thus providing poorer efficiency of the drum since the rotating period of the scraper is decreased. This emphasizes the importance of adapted design of the FID; pointing to the need of an optimization process and a prototype model. As the increase in production time is seen to be non-linear, attention should be directed to find the optimal thickness and material choice of the drum wall which maximizes the water-to-snow conversion. It should be in combination with simultaneous investments, UTS and displacements.

Simulations in COMSOL show that there is a trade-off between increased surface temperature and simultaneous even temperature at the freezing surface. A low surface temperature is important to provide efficient water-to-snow conversion, while a low temperature variation at the freezing surface is desirable in order to avoid an uneven ice layer and possibly hamper the production capacity. In the range considered, all depths will provide performance within acceptable limits. It is more a question of efficiency and costs. The corresponding displacements and stresses are low, which is important to avoid the freezing surface to become rough and bumpy. This may in turn lead to wear or failure of the scraper during harvesting. The thermodynamic analyses points to an optimal depth of the aluminium core between 10 and 20 mm.

Measures to increase the efficiency and flexibility of the system could be explored further; such as integration of an ejector in the bottom cycle, an intermediate tank between the compressor stages or heat recovery in the intercooler. Extending the simulation model to include melting losses, would raise the power consumption and amount of available excess heat. The production time must be increased to provide the same snow volume; thus highlighting the importance of heat recovery from such systems.

5. CONCLUSIONS

Integrating the flake ice machine with a transcritical CO_2 process for combined refrigeration and heat recovery improves the overall energy efficiency; as heat can be utilized both on the hot and cold side of the system. Heat recovery makes the snow producing equipment more reasonable as the operating costs are reduced. Use of CO_2 as refrigerant contributes to obtaining a thermodynamic cycle that is both highly energy efficient; when used in transcritical mode, as well as being environmental friendly.

By optimizing the gas cooler pressure, the excess heat from the snow machine is increased. Integration of the coaxial heat exchanger yields the best thermodynamic performance; and it offers the possibility of reduced demand of the intercooler and SGHX. Integration of heat recovery raises the required power input; however, it will not hamper the efficiency of the snowmaking process featured by the indirect heat cascade configuration, and by fixing the dimensioning point to the flake ice drum. The efficiency of the FID will be highly dependent on production rate and design, and this points to the need of an optimization process.

NOMENCLATURE

Latin letters and abbreviations

A	Area, m^2
B	Constant, water heat transfer
c_p	Specific heat capacity, kJ/kgK
COP	Coefficient of performance
DHW	Domestic hot water
f	Friction factor
F	Correction factor for evaporating CO_2
FID	Flake ice drum
GWP	Global warming potential
h	Enthalpy, kJ/kg
H	Height, m
k	Thermal conductivity, W/mK
$\dot{m}$	Mass flow rate, kg/s
Nu	Nusselt number
ODP	Ozone depletion potential
P	Pressure, Pa
PHE	Plate heat exchanger
Pr	Prandtl number
q	Heat flux, kW/m^2
Q	Heat transfer, kW
r_0	Radius of tubes inside the outer shell, m
Re	Reynolds number
s	Centre-to-centre distance of inner tubes, m
S	Nucleate boiling suppression factor
SGHX	Suction gas heat exchanger
T	Temperature, K
u	Velocity, m/s
U	Overall heat transfer coefficient, W/m^2K
UTS	Ultimate tensile strength
x	Distance, m
z	Gas quality

Greek letters

α	Heat transfer coefficient, W/m^2K
β	Chevron angle
γ	Empirical constant
δ	Wall thickness, m
μ	Dynamic viscosity, kg/ms
ν	Kinematic viscosity, m^2/s
ξ	Empirical parameter
ρ	Density, kg/m^3

Subscripts

acc	Acceleration
al	Aluminium
b	Boundary
C	Cold
cond	Condensation
cs	Carbon steel
diff	Difference
evap	Evaporation
f	Fluid
fric	Friction
g	Saturated gas
grav	Gravitation
H	Hot
l	Saturated liquid
man	Manifold
nb	Nucleate boiling
ref	Refrigeration
ss	Stainless steel
tot	Total
trans	Transmission
w	Water
W	Wall

REFERENCES

CAO, W., BEGGS, C. & MUJTABA, I. M. 2015. Theoretical approach of freeze seawater desalination on flake ice maker utilizing LNG cold energy. *Desalination,* 355**,** 22-32.

CENGEL, Y. A. & CIMBALA, J. M. 2010. Internal flow. *Fluid Mechanics Fundamentals and Applications.* Second edition in SI units ed.: Mc Graw Hill Higher Education pp. 337-417.

CHOI, K.-I., PAMITRAN, A. S. & OH, J.-T. 2007. Two-phase flow heat transfer of CO 2 vaporization in smooth horizontal minichannels. *International Journal of Refrigeration,* 30**,** 767-777.

DIESETH, J.-B. R. 2016. *Snow Production Equipment at Ambient Temperatures Above Zero Degrees Celcius.* Master thesis, Department of Energy and Process Engineering. Norwegian University of Science and Technology.

GARCÍA-CASCALES, J. R., VERA-GARCÍA, F., CORBERÁN-SALVADOR, J. M. & GONZÁLVEZ-MACIÁ, J. 2007. Assessment of boiling and condensation heat transfer correlations in the modelling of plate heat exchangers. *International Journal of Refrigeration,* 30**,** 1029-1041.

GRAHAM, J., JOHNSTON, W. A. & NICHOLSON, F. J. 1993. Ice in fisheries. *Ice in fisheries*.

HEWITT, G. F. 2008. Single-phase fluid flow. *In:* HEWITT, G. F., BARBOSA, J., CELATA, G. P., MUELLER-STEINHAGEN, H., POSKAS, P., CHUDNOVSKY, Y., KANDLIKAR, S., PALEN, J. & TABOREK, J. (eds.) *Heat exchanger design handbook 2008.* Connecticut: Begell House, Inc. pp. 16-17.

INCROPERA, F. P., DEWITT, D. P., BERGMAN, T. L. & LAVINE, A. S. 2013a. Boundary and Initial Conditions. *Principles of heat and mass transfer.* 7th ed.: John Wiley & Sons, Inc. pp. 90-93.

INCROPERA, F. P., DEWITT, D. P., BERGMAN, T. L. & LAVINE, A. S. 2013b. Mixed Boundary Layer Conditions. *Principles of heat and mass transfer.* 7th ed.: John Wiley & Sons, Inc. pp. 444-445.

INCROPERA, F. P., DEWITT, D. P., BERGMAN, T. L. & LAVINE, A. S. 2013c. The Overall Heat Transfer Coefficient. *Principles of heat and mass transfer.* 7th ed.: John Wiley & Sons, Inc. pp. 708-711.

KAYS, W. M. & CRAWFORD, M. E. 1980. Laminar flow inside tubes. *In:* CERRA, F. J. & MAISEL, J. W. (eds.) *Convective heat and mass transfer.* 2nd ed.: McGraw-Hill pp. 103-105.

LIAO, S., ZHAO, T. & JAKOBSEN, A. 2000. A correlation of optimal heat rejection pressures in transcritical carbon dioxide cycles. 20**,** 831-841.

NELLIS, G. & KLEIN, S. 2009. Numerical Model of Parallel- and Counter-Flow Heat Exchangers. *Heat transfer.* 1st ed. New York: Cambridge University Press pp. 888-903.

PARK, C. Y. & HRNJAK, P. 2009. CO 2 flow condensation heat transfer and pressure drop in multi-port microchannels at low temperatures. *International Journal of Refrigeration,* 32**,** 1129-1139.

SHAH, R. K. & SEKULIĆ, D. P. 2007. Heat Exchanger Pressure Drop Analysis. *Fundamentals of Heat Exchanger Design.* Hoboken, NJ, USA: John Wiley & Sons, Inc. pp. 397-399.

TECHNOALPIN 2016. Snowfactory in Northern Europe. *Snow experts magazine.* 01/2016 ed.

VDI 1993. Heat transfer in flow through coils. *In:* ASSOCIATION OF GERMAN ENGINEERS / VDI SOCIETY FOR CHEMICAL AND PROCESS ENGINEERING (ed.) *VDI Heat Atlas.* 1st. ed. Düsseldorf: VDI pp. Gc1-Gc2.

M. Risk assessment

NTNU HSE	Hazardous activity identification process	Prepared by	Number	Date
		HSE section	HMSRV2601E	09.01.2013
		Approved by		Replaces
		The Rector		01.12.2006

Unit: Energy and Process Engineering **Date:** 18.01.2017

Line manager: Olav Bolland

Participants in the identification process (including their function)**: -**

Short description of the main activity/main process: Master project for student EPT-M-2017-11.
Energy Efficient and Environmental Friendly Snow Production by Refrigeration systems

Is the project work purely theoretical? (YES/NO): YES *Answer "YES" implies that supervisor is assured that no activities requiring risk assessment are involved in the work. If NO, briefly describe the activities below. The risk assessment form need not be filled out.*

Signatures: *Responsible supervisor:* *Student:* Kaja Bergwitz-Larsen

ID nr.	Activity/process	Responsible person	Existing documentation	Existing safety measures	Laws, regulations etc.	Comment